Sharifah Salwa Mohd Zuki
Shahrul Niza Mokhatar
Shahiron Shahidan
Mohd Haziman Bin Wan Ibrahim   *Editors*

Proceedings of the Sustainable Concrete Materials and Structures in Construction 2020

Towards Sustainable Green Concrete

Springer

Lecture Notes in Civil Engineering

Volume 157

Lecture Notes in Civil Engineering (LNCE) publishes the latest developments in Civil Engineering - quickly, informally and in top quality. Though original research reported in proceedings and post-proceedings represents the core of LNCE, edited volumes of exceptionally high quality and interest may also be considered for publication. Volumes published in LNCE embrace all aspects and subfields of, as well as new challenges in, Civil Engineering. Topics in the series include:

- Construction and Structural Mechanics
- Building Materials
- Concrete, Steel and Timber Structures
- Geotechnical Engineering
- Earthquake Engineering
- Coastal Engineering
- Ocean and Offshore Engineering; Ships and Floating Structures
- Hydraulics, Hydrology and Water Resources Engineering
- Environmental Engineering and Sustainability
- Structural Health and Monitoring
- Surveying and Geographical Information Systems
- Indoor Environments
- Transportation and Traffic
- Risk Analysis
- Safety and Security

To submit a proposal or request further information, please contact the appropriate Springer Editor:

- Pierpaolo Riva at pierpaolo.riva@springer.com (Europe and Americas);
- Swati Meherishi at swati.meherishi@springer.com (Asia - except China, and Australia, New Zealand);
- Wayne Hu at wayne.hu@springer.com (China).

All books in the series now indexed by Scopus and EI Compendex database!

More information about this series at http://www.springer.com/series/15087

Sharifah Salwa Mohd Zuki ·
Shahrul Niza Mokhatar ·
Shahiron Shahidan ·
Mohd Haziman Bin Wan Ibrahim
Editors

Proceedings of the Sustainable Concrete Materials and Structures in Construction 2020

Towards Sustainable Green Concrete

Editors
Sharifah Salwa Mohd Zuki
Faculty of Civil Engineering
and Built Environment
Universiti Tun Hussein Onn Malaysia
Johor, Johor, Malaysia

Shahiron Shahidan
Faculty of Civil Engineering
and Built Environment
Universiti Tun Hussein Onn Malaysia
Johor, Johor, Malaysia

Shahrul Niza Mokhatar
Faculty of Civil Engineering
and Built Environment
Universiti Tun Hussein Onn Malaysia
Johor, Johor, Malaysia

Mohd Haziman Bin Wan Ibrahim
Faculty of Civil Engineering
and Built Environment
Universiti Tun Hussein Onn Malaysia
Johor, Malaysia

Preface

Seminar on Sustainable Concrete Materials and Structures in Concrete Construction 2020 was held virtually for the first time on 24 August 2020. This event was organized by the Faculty of Civil Engineering and Built Environment (FKAAB), Universiti Tun Hussein Onn Malaysia (UTHM) in collaboration with Concrete Society of Malaysia (CSM) and Civil Engineering and Built Environment Postgraduate Society, FKAAB (CiBPS). The theme of this seminar is Toward Sustainable Green Concrete. This seminar marks the first collaboration between these three organizations.

A total number of 23 papers were presented from researchers, postgraduate students and practitioners from Malaysia and Indonesia. Despite being held virtually, the participants were allowed to exchange ideas via question and answer session provided at the end of the presentation as well as live chat during the presentation.

The editorial team would like to express our heartfelt gratitude to all parties that work hard to make sure this seminar a success. Special acknowledgement goes to the Concrete Society of Malaysia (CSM) for its full support of the seminar. Acknowledgement with gratitude goes to all CiBPS and UTHM-CSM members. We also would like to thank all reviewers for their invaluable efforts. Last but not least, special thanks to co-editors (Nur Anis Najwa Abdul Mutalib, Luqmannul Haqim Mohamad, Wenish Anak Maynet, Mariana Dina Anak Malong and Anis Ayuni Sueid) for their invaluable works.

<div align="right">

Sharifah Salwa Mohd Zuki
Shahrul Niza Mokhatar
Shahiron Shahidan
Mohd Haziman Wan Ibrahim

</div>

Contents

Development of Self-compacting Concrete Incorporating Palm Oil Fuel Ash and Eggshell Powder as Partial Cement Replacement

Sufian Kamaruddin, Wan Inn Goh, Noridah Mohamad, and Ashfaque Ahmed Jhatial

Abstract Self-Compacting Concrete (SCC) is a type of concrete that can flow under its own weight and completely fill the formwork, even in the presence of congested reinforcement. Therefore, raw materials and natural resources are required in large quantities for SCC production. In order, to minimize the usage of the cement in the SCC, the use of agricultural wastes such as palm oil fuel ash (POFA) and eggshell powder (ESP) as partial cement replacement materials for an alternative preventive solution is suggested. In this research, 0, 2.5 and 5% ESP were combined with 5, 10 and 15% POFA as cement replacement in SCC. The influence of POFA and ESP on characteristics of SCC were examined by observation and comparison of the test outcomes with a control sample. Furthermore, the tests are conducted to study the modulus of elasticity (MOE), Poisson's ratio, flexural strength and failure mode of SCC. The maximum modulus of elasticity of 5% POFA along with 2.5% ESP (5P 2.5E) was 31689 N/mm^2, meanwhile, the highest flexural strength was 5.7 MPa with water-cement ratio of 0.4 at the 28 days water curing. Based on the outcomes, optimum replacement percentage of POFA and ESP was 5% POFA and 2.5% ESP exhibitions better behavior which is higher to the outcomes of a control sample of SCC.

Keywords Failure mode · Flexural strength · Modulus of elasticity · Self-compacting concrete · Supplementary cementitious materials · Sustainable concrete

S. Kamaruddin · W. I. Goh (✉) · N. Mohamad
Jamilus Research Centre, Faculty of Civil Engineering and Built Environment, Universiti Tun Hussein Onn Malaysia, 86400 Batu Pahat, Johor, Malaysia
e-mail: wigoh@uthm.edu.my

A. A. Jhatial
Department of Civil Engineering, Mehran University of Engineering and Technology, Shaheed Zulfiqar Ali Bhutto Campus, Khairpur Mirs', Sindh, Pakistan

1 Introduction

Self-compacting concrete (SCC) is described as a highly flowable kind of concrete that is laid into form without any mechanical efforts. SCC is a non-segregating concrete that is flowing by means of its own weight [11]. The significance of SCC is that it preserves all concrete's durability and features, meeting anticipated behavior necessities. Moreover, SCC is perfect for utilization in areas with dense rebar and pipes. Utilizing SCC will give numerous benefits over conventional concrete. Some of those benefits are enhanced workability, decreases manpower, decreases equipment wear, permit for easier pumping process and reduce voids on dense reinforced areas [16, 17].

Malaysia is considered as the second palm oil producer and exporter in the world after Indonesia (Mujah 2016). As enclosed in the Tenth Malaysian Plan (RMK-10), palm oil is recorded as one of the supplies to be exported internationally due to the high need for crude palm oil in the world. Moreover, Malaysia Palm Oil Board (MPOB) assessed that the total oil palm planted area in Malaysia is 5.77 million hectares, creating our country the second-largest manufacturer of palm oil in the world [3]. Over 400 palm oil mills are working and manufacturing a great quantity of solid waste in the form of fibers, kernels, and empty fruit bunches annually. The burning of palm oil husk and palm kernel shells in the steam boiler develops approximately 5% of palm oil fuel ash [2, 10, 15, 19]. Though, solid waste from agricultural industries such as palm oil fuel ash has not been managed correctly. The productive adoption of solid waste material is the greatest method to solve the complications related to their disposal. There exists a great potential for the adoption of solid waste materials as construction material in industrial construction [25]. According to Clean Malaysia [6], Malaysians yield an average of 30,000 tons of waste every day. These wastes were often disposed of at landfills and a small amount of them was recycled [13].

According to Ministry of Agriculture and Agro-Based Industry Malaysia [14], Malaysia consumes 2.8 million poultry eggs daily, and this figure has been increasing over the years as shown in Fig. 1. The higher consumption of eggs leads to increase in eggshell waste which is extremely harmful to the environment. The chemical composition of POFA has high silica oxide [18] but a minimum amount of calcium oxide associated with eggshell powder (ESP) which has a high of calcium oxide and less content of silica oxide [9, 11, 20, 22]. Therefore, the mixture of supplementary material of POFA and ESP provides a good composition of chemical properties as cement replacement.

Based upon their characteristics, the solid waste materials can either be used as a building material in the context of supplementary cementitious materials (SCMs), filler concrete [24]. Therefore, reprocessing POFA and eggshells into the beneficial invention stretches great potential for the agricultural industry, food manufactured and much wider construction industry. It is because utilizing waste can decrease the
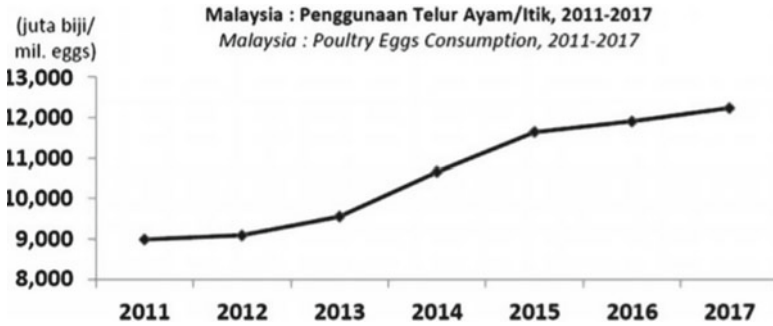
Fig. 1 Poultry eggs consumption in Malaysia from year 2011 to 2017 [7, 21]

emission of carbon dioxide (CO_2) of cement during manufacturing, saves the natural resources of lime but also has decreased the landfill area and decrease environmental pollution [24].

2 Materials and Methods

2.1 Materials

2.1.1 Palm Oil Fuel Ash (POFA)

The POFA which was used in this study was collected from Ban Dung Palm Oil Mill Sdn. Bhd. at Parit Sulong, Batu Pahat, Malaysia. POFA is a solid waste, in the form of ash and is the by-product of the burning of palm oil husk and palm kernel shell processed in a palm oil mill's steam boiler. The collected POFA was first sieved using 300 μm in order to remove bigger particles and other materials, afterwards the sieved POFA was dried in an oven at a temperature of 105 °C for 24 h to remove any moisture that it may contain as it was dumped in open air [12]. Once the POFA was oven-dried, the POFA was grinded into fine particles using the Los Angeles Abrasion Machine and was sieved again using 75 μm sieve in order to collect the fine ashes, passing the same size as cement particle. The fineness of SCMs significantly influences the properties of the concrete [1]. After the sieving process, POFA was kept into the container to maintain the moisture content. Figure 2 illustrates the preparation process of POFA.

Fig. 2 Preparation of POFA

2.1.2 Eggshell Powder (ESP)

Eggshells were collected from Federal Agricultural Marketing Authorities (FAMA), Rengit and local bakeries as well as food stalls around Parit Raja. The eggshells were washed in order to remove the protein-membrane that may be stuck on the eggshells. The eggshells were dried under the sun initially and afterwards in an oven at a temperature of 105 °C $\pm$ 5 °C for 24 h to remove the moisture that may have been absorbed during the initial washing [23].

After drying stage, the eggshells were crushed into small pieces and sieved through 300 μm in order to remove any coarse particles. Afterwards the eggshell was grinded into powder form using the Los Angles Abrasion Machine and the ESP was sieved through 75 μm to ensure that the eggshell particles have a size like the cement particles. After the process of blending and sieving, the ESP was kept in the container in order to maintain the moisture content. The whole preparation of ESP is illustrated in Fig. 3.

Fig. 3 Preparation of eggshell

2.2 Proportion and Mixing of Constituents

The European Guidelines for Self-Compacting Concrete EFNARC [8] were used in this study to design the M35 grade of SCC mixes. The mixing amount method for 28-days water curing with the water-binder ratio is 0.4 and superplasticizer ratio with cement was 2%. The design strength was 35 N/mm^2 for conventional concrete. The mixing proportions of all ingredients are presented in Table 1.

Table 1 Mix proportions and amount of quantities to produce 1 m^3 of SCC

Mix Proportion	% of POFA	% of ESP	Cement (kg/m^3)	POFA (kg/m^3)	ESP (kg/m^3)	Sand (kg/m^3)	Coarse aggregate (kg/m^3)
M0	0%	0%	451	0	0	902	767
M1	5%	0%	428.45	22.55	0	902	767
M2	5%	2.5%	417.17	22.55	11.28	902	767
M3	5%	5%	405.90	22.55	22.55	902	767
M4	10%	0%	405.9	45.10	0	902	767
M5	10%	2.5%	394.62	45.10	11.28	902	767
M6	10%	5%	383.35	45.10	22.55	902	767
M7	15%	0%	383.35	67.65	0	902	767
M8	15%	2.5%	372.07	67.65	11.28	902	767
M9	15%	5%	360.80	67.65	22.55	902	767

2.3 Testing Procedures

2.3.1 Modulus of Elasticity Poisson's Ratio Testing

The elastic modulus is the ratio between stress and strain that was conducted for the cylinder specimens following BS EN 12390-13:2013 [5]. A total of 30 cylinders were utilized to investigate the performance of POFA and ESP on SCC after 28 days of the curing process. The cylindrical samples in diameter 100 mm with height 200 mm were applied an axial load with a specific rate until failure using compression universal testing machine (UTM) with strain gauge attached on the surface of the specimen. Deformation was noted using the strain gauge for every load increment. Figure 4 shows the modulus of elasticity test that was conducted on the cylinder specimens.

2.3.2 Flexural Strength

The flexural strength, also known as the modulus of rupture, or bend strength, or transverse rupture strength is a characteristic property of a material, it's the stress at which a material yields in a flexure experiment. In this experimental study, the wet mixes were poured into $100 \times 100 \times 500$ mm prismatic moulds. A total of 30 prisms were utilized to investigate the performance of POFA and ESP on SCC. In light of BS EN 12390-5:2009 [4], the test samples remained in the moulds for 24 h. Afterwards, the samples were unmoulded and immersed in water for the curing process. Flexural strength test was conducted after 28 days of water curing.

Fig. 4 Poisson's ratio and modulus of elasticity testing of cylinder

Fig. 5 4-points flexure test on the prismatic specimen

Figure 5 shows the 4-point flexural test on $100 \times 100 \times 500$ mm SCC prismatic specimen and the strength can be determined by using Eq. 1.

$$Fct,fl = \frac{Fxl}{d_1 x d_2} \tag{1}$$

3 Results and Discussions

3.1 Modulus of Elasticity and Poisson's Ratio

The modulus of elasticity (MOE) is the ability of a material to resist the deformation that may occur when a load is applied vertically on the 30 cylindrical samples. The MOE was determined using a compression load on the cylindrical samples and

Table 2 Results of modulus of elasticity and Poisson's ratio

Specimen	Average modulus of elasticity (N/mm^2)	Poisson's ratio
M0	26,490	0.17
M1	28,982	0.16
M2	31,689	0.19
M3	25,296	0.16
M4	26,365	0.17
M5	24,697	0.15
M6	23,182	0.14
M7	24,002	0.15
M8	23,112	0.14
M9	21,615	0.12

the deformation was measured using strain gauges and achieved the result by using the stress–strain graph. The outcomes found from the MOE and Poisson's ratio testing of the samples are organized in Table 2.

From the results shown in Table 2, it can be observed that the MOE of SCC reduces significantly when an increased percentage of cement is replaced by POFA and ESP. As seen in Table 2, the MOE of the control sample was recorded to be 26,490 N/mm^2 while the 5% POFA sample (M1) recorded 28,982 N/mm^2. With the addition of 2.5% ESP along with 5% POFA (M2), the MOE increased slightly to 31,689 N/mm^2. But with further increase in ESP, the MOE kept on reducing. The Poisons ratio also decreased with the addition of ESP along with POFA. Thus, it can be said that the enhancement in pozzolanic reaction with the addition of ESP also increased the MOE. As seen in the Table 2, the MOE drops beyond 12.5% to 20% of cement replacement content. This dropin MOE beyond 20% cement replacement can be attributed to lower cement content also causing lesser hydration process in the concrete.

3.2 Flexural Strength

In this study, the flexural strength test was conducted according to BS EN 12390-5 [4] by using a 4-points flexural bending machine. The results obtained from the 4-point bending test of the samples are tabulated in Table 3. As shown in Fig. 6, the flexural strength of SCC incorporating POFA and ESP was slightly increased with the increasing portion of cement replacement with POFA.

The replacement of POFA and ESP increases the flexural strength of M1and M2. The presence of highly reactive silica in POFA itself is the main reason behind the increase in the flexural strength. It can be explained that when pozzolanic materials are combined with Portland cement, it will react to form cementitious properties.

Table 3 Flexure strength of SCC incorporating POFA and ESP

Mix proportion	Flexural strength (MPa)	Difference in strength compared to control (%)
M0	5.0	–
M1	5.5	10.0
M2	5.7	14.0
M3	4.5	−10.0
M4	4.8	−4.0
M5	4.1	−8.0
M6	4.2	−16.0
M7	4.7	−6.0
M8	4.4	−12.0
M9	4.0	−20.0
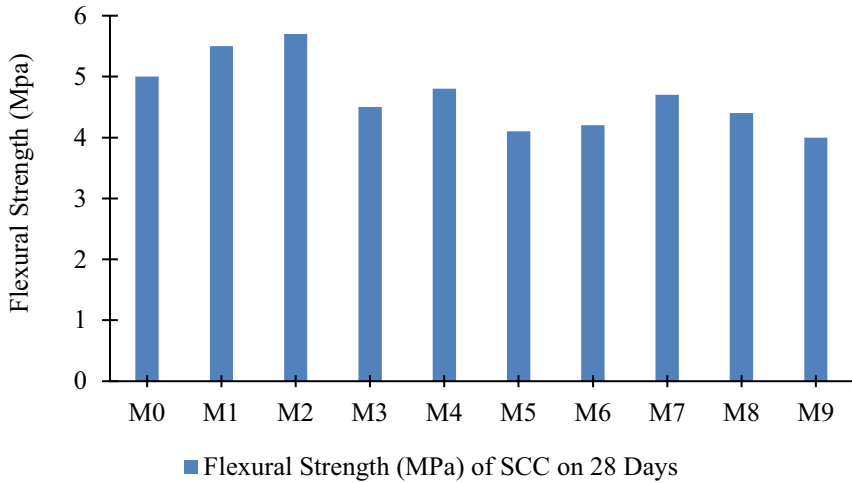
Fig. 6 Average flexural strength of SCC
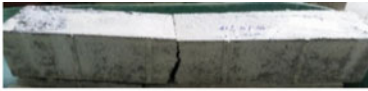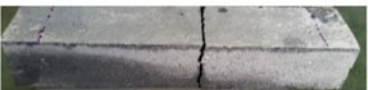
Therefore, a cementitious material can exhibit a self-cementitious (hydraulic activity) react with H_2O from water and CaO from ESP to form calium hydroxide, Ca$(OH)_2$. The SiO_2 of the POFA reacts chemically with the Ca$(OH)_2$ to form a secondary calcium silicate hydrate (C-S-H) gels, which improves the interfacial bonds between the paste and the aggregate, resulting in a compact microstructure. It also fills in the capillary pores to improve the microstructure of the SCC resulting in an enhancement in flexural strength. The content of POFA and ESP showed that it can be used as a replacement with improvement in the flexural strength of the concrete.

The reduction in flexural strength can be due to the decrease in Ca$(OH)_2$ provided with the addition of a higher percentage of ESP (5%) such that the reducing Ca$(OH)_2$ is not fully consumed during the pozzolanic reaction and a higher percentage of POFA content means reduced cement content. Thus, C-S-H gel is not produced due to the reduction of a hydration agent. The trends in Fig. 6 clearly reveal that the sample with the highest POFA and ESP content (M9) obtained flexural strength of 4.0 MPa at 28 days of curing which was approximately 20% less than the control sample (M0).

3.3   Failure Mode

The failure mode appeared in all the SCC prism specimens. The failure mode was recorded from the flexural test (four-points loading test) on every prism. All the prisms tested in the experiment were simply supported. The failure cracks of all tested prisms are illustrated in Table 4. Based on the physical observation, generally, the prisms specimens show the same flexural cracks between each of the

Table 4 Failure mode of the prism

SCC mix proportion	Physical observation
M0	
M1	
M2	
M3	
M4	
M5	
M6	
M7	

SCC mix proportion	**Physical observation**
M8	
M9	

specimens and all specimen prisms had the same failure. All the prisms starting failure with flexural failure was initiated at the middle span of the lower part (tension zone) of the prism and propagated to the upper part (compressive zone).

4 Conclusions

From the outcomes of the modulus of elasticity, flexural strength and failure pattern, the following conclusions can be concluded:

1. The maximum MOE and Poisson's ratio achieved were 31,689 MPa and 0.19 by 5P 2.5E mix, which was higher compared to the control sample.
2. Similar behavior as in flexural strength was seen in a 4-point load test. The results show that the flexural strength achieved was 5.7 MPa by 5P 2.5E mix, which was approximately 14% higher compared to the control sample.
3. Though a further increase in the content of POFA ad ESP decreased the flexural strength, yet it was slightly higher than the control sample. However, a further increase in cement replacement resulted in a reduction in flexural strengths.
4. Furthermore, the inclusion of POFA and ESP more than 10% and 2.5% caused the SCC to be more brittleness because the POFA and ESP have high water absorption.
5. Significantly reduced cement content also causes reduced hydration process in the concrete resulting in a lower production of $Ca(OH)_2$ which is required for the pozzolanic activity to develop secondary C-S-H layers. The hydration process in concrete is incomplete because more water is absorbed by the POFA and ESP.
6. For the future study, the researcher can focus more on the experimental and Finite Element Analysis investigation of SCC slab to evaluate the structural behavior.

References

1. Alsubari B, Shafigh P, Jumaat M (2015) Development of self-consolidating high strength concrete incorporating treated palm oil fuel ash. J Mater 8(5):2154–2173
2. Amran YHM, Farzadnia N, Ali AAA (2015) Properties and applications of foamed concrete: a review. Constr Build Mater 101:990–1005. https://doi.org/10.1016/j.conbuildmat.2015.10.112
3. Yusof A (2019). Malaysia to cap 6.5 m ha of oil palm plantations by 2023. New Straits Times
4. British Standard Institution, Testing hardened concrete (2017). Part 5: Flexural strength of test specimens. London, BS EN 12350-5
5. British Standard Institution, Testing hardened concrete (2013). Part 13: Determination of secant modulus of elasticity in compression. London, BS EN 12390-13
6. Clean Malaysia (2015). Malaysia's First Environmental Magazine on November 21, 2015. https://cleanmalaysia.com/2015/11/21/malaysias-first-environmentalmagazine/

7. Department Veterinary Service (2016). Consumption of Livestock Products, 2011–2017 Report. DVS, Kuala Lumpur. http://www.dvs.gov.my/dvs/resources/user_1/DVS%20pdf/perancangan/2018/Perangkaan%202016%202017/3.Muka_Surat_1-15_.pdf

8. EFNARC (2005). The European Guidelines for Self-Compacting Concrete. The European Guidelines for Self Compacting Concrete, (May) 63. https://www.efnarc.org/pdf/SCCGuidelinesMay2005.pdf

9. Jhatial AA, Goh WI, Mohamad N, Sohu S, Lakhiar MT (2018) Utilization of palm oil fuel ash and eggshell powder as partial cement replacement-a review. Civil Eng J 4(8):1977–1984

10. Juenger MCG, Siddique R (2015) Recent advances in understanding the role of supplementary cementitious materials in concrete. Cem Concr Res 78:71–80

11. Kamaruddin, S., Goh, W. I., Jhatial, A. A., & Lakhiar, M. T. (2018). Chemical and Fresh State Properties of Foamed Concrete Incorporating Palm Oil Fuel Ash and Eggshell Ash as Cement Replacement. *International Journal of Engineering & Technology*, 7(4.30), 350–354.

12. Khankhaje E, Hussin MW, Mirza J, Rafieizonooz M, Salim MR, Siong HC, Warid MNM (2016) On blended cement and geopolymer concretes containing palm oil fuel ash. Mater Des 89:385–398

13. Lim SK, Tan CS, Lim OY, Lee YL (2013) Fresh and hardened properties of lightweight foamed concrete with palm oil fuel ash as filler. Constr Build Mater 46:39–47

14. Ministry of Agriculture and Agro-based Industry Malaysia (2019). Hala tuju Kementerian Per Tanian & Industri Asas Tani, Prioriti & Strategi 2019–2020. Putrajaya https://www.moa.gov.my/documents/20182/139717/Hala+Tuju+2019-2020_LowVer.pdf/1ca7c2b3-f4fb-460a-8e04-1fdd051360cb

15. Mohamad ME, et al (2018) Palm oil fuel ash (POFA) and eggshell powder (ESP) as partial replacement for cement in concrete, vol 1004, pp 1–8

16. Mohamad N, Samad AAA, Lakhiar MT, Mydin MAO, Jusoh S, Sofia A, Efendi SA (2019) Effects of incorporating banana skin powder (BSP) and palm oil fuel ash (POFA) on mechanical properties of lightweight foamed concrete. Int J Integrated Eng 10(9)

17. Munir A, Abdullah H, Sofyan I, Safwan (2015) Utilization of palm oil fuel ash (POFA) in producing lightweight foamed concrete for non-structural building material. Procedia Eng 125:739–746

18. Narendra A, Pathrose C (2017) Development of thermally efficient fibre-based eco-friendly brick reusing locally available waste materials. Constr Build Mater 133:275–284

19. Sata V, Jaturapitakkul C, Chaiyanunt R (2010) Compressive strength and heat evolution of concretes containing palm oil fuel ash. J Mater Civ Eng 22(10):1033–1038

20. Snellings R, Mertens G, Elsen J (2012) Supplementary cementitious materials. Rev Mineral Geochem 74(1):211–278

21. Tiong HY, Lim SK, Lee YL, Ong CF, Yew MK (2020) Environmental impact and quality assessment of using eggshell powder incorporated in lightweight foamed concrete. Constr Build Mater 244:118341

22. Yerramala A (2014) Properties of concrete with eggshell powder as cement replacement. Indian Concr J 88(10):94–102

23. Yu TY, Ing DS, Choo CS (2017) The effect of different curing methods on the compressive strength of eggshell concrete. Indian J Sci Technol 10(6):1–4. https://doi.org/10.17485/ijst/2017/v10i6/111210

24. Jhatial AA, Goh WI, Mastoi AK, Rahman AF, Kamaruddin S (2021) Thermo-mechanical properties and sustainability analysis of newly developed eco-friendly structural foamed concrete by reusing palm oil fuel ash and eggshell powder as supplementary cementitious materials. Environ Sci Pollut Res. https://doi.org/10.1007/s11356-021-13435-2

25. Memon MJ, Jhatial AA, Murtaza A, Raza MS, Phulphoto KB (2021) Production of eco-friendly concrete incorporating rice husk ash and polypropylene fibres. Environ Sci Pollut Res. https://doi.org/10.1007/s11356-021-13418-3

Utilization of Ground Granulated Blast Furnace Slag (GGBS) and Mussel Shell Ash (MSA) as Partial Cement Replacement in Concrete

N. A. A. Hamid, N. S. A. Mutalib, Z. Jamellodin, N. Salleh, K. N. M. Yunus, S. H. Adnan, H. Tami, N. Ali, and S. R. Abdullah

Abstract Mussel shell ash (MSA) and ground granulated blast furnace slag (GGBS) has similar chemical and physical properties as ordinary Portland cement (OPC) which makes it applicable to replace cement in concrete. Currently, the research on combination of GGBS and MSA as partial cement replacement in concrete mix is still limited. In this study, the use of various percentages of GGBS in range of 40 to 60% with combination of 5% of MSA in concrete was investigated. As total, 36 cube concrete samples with size of 100 mm × 100 mm × 100 mm were cast for testing. The concrete samples were tested for density and compressive strength on 28 days, 60 days and 90 days. The test results were compared with control concrete sample contains 100% of OPC. From experimental results, concrete containing GGBS and MSA was obtained higher compressive strength than control concrete up to 90 days. The optimum percentage of GGBS as partial cement replacement is 40% with combination 5% of MSA. The concrete also has less density due to different specific gravity between GGBS and OPC. Hence, the replacement of cement with alternative construction materials of GGBS and MSA can increase the performance of concrete, reducing carbon emission problem then leads to sustainable development of construction industry.

N. A. A. Hamid (✉) · N. S. A. Mutalib · Z. Jamellodin · N. Salleh ·
K. N. M.Yunus · H. Tami · N. Ali · S. R. Abdullah
Department of Civil Engineering, Faculty of Civil Engineering and Built Environment,
University Tun Hussein Onn Malaysia, 86400 Parit Raja, Batu Pahat, Johor, Malaysia
e-mail: azlinah@uthm.edu.my

S. H. Adnan
Department of Civil Engineering Technology, Faculty of Engineering Technology,
University Tun Hussein Onn Malaysia, KM 1, Jalan Panchor, 84600 Panchor, Johor,
Malaysia

1   Introduction

Cement is a binder agent in concrete mix which commonly used in construction industry. In concrete production, cement is mixed with fine and coarse aggregate with sufficient amount of water. However, high production of cement can cause carbon dioxide (CO_2) emission that lead to global warming issues. In order to reduce the use of cement such as ordinary Portland cement (OPC), an alternative of cementitious material of mussel shell ash (MSA) and ground granulated blast-furnace slag (GGBS) are introduced.

The GGBS is a product from blast furnace used to make iron. The chemical composition of GGBS consists about 40% silicon dioxide (SiO_2), 40% calcium oxide (CaO) and 10% Alumina oxide (Al_2O_3) which are the same chemical content in cement, but not in the same percentage (Oner and Akyuz 2020). Many previous studies [1, 3, 6] have found that the used of GGBS can increase the workability of concrete and reduce the risk of early-age thermal cracking due to slow hardening process. Thus, longer curing time is required for analyzing the strength performance of concrete containing GGBS. The GGBS can also reduce the risk of damaging concrete internal reactions and risk of reinforcement corrosion because of high resistance to chloride ingress and provide great shield to be attacked by sulphate and other chemicals [10].

Mussel or also known as Bivalve Mollusc is an aquatic species with shell. The mussel shell consists of similar chemical properties as OPC such as limestone dust that acts as calcium carbonate ($CaCO_3$). It was found that 90% of $CaCO_3$ is similar with mussel shell [12]. Hence, this waste material is suitable to be used as cement replacement. Nevertheless, the crystal structures of the MSA contain high amount of calcite and aragonite which produce high strength and density compared to the limestone [7, 8].

The OPC is normally used in construction, however, the production of cement affect the environment as it releases a greenhouse gaseous by emissions of carbon dioxide (CO_2) then cause global warming. The increased percentage of CO_2 gaseous can cause a lot of problems such as suffocation of living organism and ozone depletion. Therefore, a replacement of cement in concrete by using waste materials of GGBS and MSA can reduce up to 20% of carbon emission then can lead to sustainable development in construction industries and at the same time can decrease the waste dumping problems [9]. This study was conducted to investigate the strength performance of concrete with the use of GGBS and MSA as partial cement replacement.

2 Ground Granulated Blast-Furnace Slag (GGBS)

GGBS is an industrial waste from iron production. Various chemical composition of slag may produce during the iron production process which depends on the consumption of raw material. The combination between chemical composition of silicate and aluminate from the iron ore and coke with a flux considerably can reduce the viscosity of slag.

In cement production, there is one of the processes namely carbonate oxidation that contributes to the greenhouse gaseous emission of carbon dioxide (CO_2). It was found that 4.8% of carbon emission was caused by industrial cement production. Moreover, the cement production and fuel combustion are about on the same level which causes about 9.5% of carbon emission [9].

The usage of GGBS significantly can lead to sustainable construction activity as it would produce about 0.07 tons of carbon dioxide which consume only 1300 MJ of energy rather than OPC which required about 5000 MJ of energy in order to generate 0.95 tons of carbon dioxide [1]. Hence, high reduction of carbon dioxide emission and energy was contributed from using GGBS rather than OPC. This reduction significantly can save the world from global warming issue and also preserving our environment towards sustainable construction development.

According to the previous study, concrete containing GGBS experienced lower compressive strength in an early age compared to conventional concrete. The strength of concrete was increased with increasing of curing period due to pozzolanic reaction and formation of calcium hydroxide. Hence, the compressive strength of concrete which consist of GGBS will increase after 28 days [6]. They also suggested that the optimum percentage of GGBS as cement replacement in concrete about 55 to 59% of binder content. The other researcher has reported also that the optimum percentage of GGBS in concrete was about 40% [4, 6]. Hence, the utilization of waste material of GGBS as cement replacement material is a great idea to preserve our environment from pollution. Moreover, the reuse of GGBS can reduce the effects of improper waste dumping as it caused serious impacts to health and environment.

3 Mussel Shell Ash (MSA)

Mussel shell has the same material characteristics as limestone which composed of high calcium carbonate ($CaCO_3$) as ordinary Portland cement thus makes it suitable to be used as cement replacement and filler [7, 8, 12]. The chemical compositions of mussel shell as shown in Table 1.

All of seashell types will takes longer time to decay [7, 8]. Hence, the use of waste material of mussel shell as replacement material of cement will produce sustainable concrete and solve the issues of global warming by reducing the usage of cement. However, the use of mussel shells is less favourable in application since

Table 1 Chemical composition of mussel shell [5]

Oxide	Percentage (%)
SiO_2	1.6
Al_2O_3	0.92
CaO	51.56
MgO	1.43
Na_2O	0.08
K_2O	0.06
H_2O	0.31
LOI	41.84

the production of shell powder requires intensive energy to burn and grind the shells as fine grain powder. It had been studied that there are other species of waste seashells such as snail, periwinkle and clam shell which can increase the compressive strength of concrete [13]. It was found that the optimum percentage of shell as cement replacement was in range 4–5% [13]. With the presence of high CaO in cockle shell, the strength and workability of concrete was reduced at the early period of curing as the effect from hydration process [7, 8, 13].

4　Materials and Methods

The GGBS in a form of fine particles was sieved with size of 75 µm. As partial cement replacement, about 40, 50 and 60% of GGBS was used in concrete. Only 5% of MSA was used as cement replacement in concrete. Initially, the mussel shell was dried for 7 days in order to make sure it completely clean and dry from any biological substances. Then, the mussel shell was crushed into a fine particles. Mix proportion of control concrete sample containing aggregate, cement and water was designed by using Department of Environment (DOE) method.

As total, 36 cube concrete samples with size of 100 × 100 × 100 mm were cast. The cube concrete samples were cured for 28, 60 and 90 days. All of the concrete samples were kept in mould for 24 h before it being removed for curing process in water. The density and compressive strength test were conducted to all concrete samples on 28, 60 and 90 days by following ASTM C39/C39M [2].

5　Results and Discussions

The density for concrete samples was tested on 28, 60 and 90 days. The experimental results of control concrete sample (CS) and concrete that containing different percentages of GGBS (40–60%) and MSA (5%) as shown in Fig. 1.
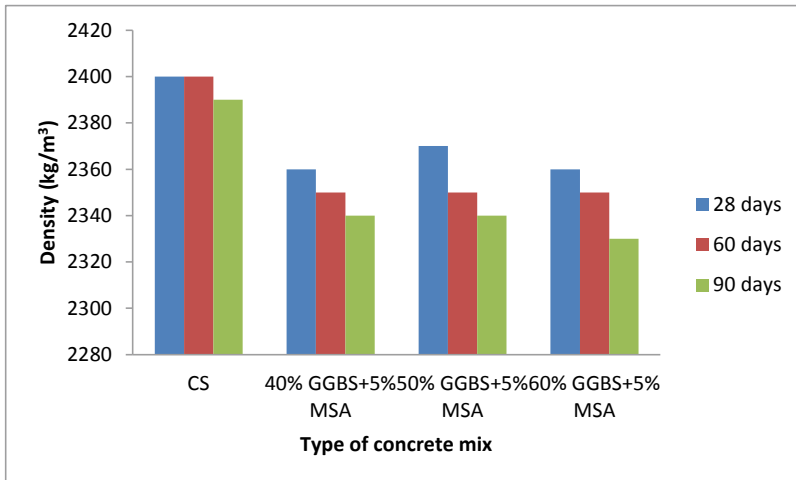
Fig. 1 Density of concrete samples with different percentage of GGBS and MSA

In Fig. 1, it shows that concrete containing GGBS and MSA had lower density than control concrete sample (CS). The density of concrete with partially cement replacement also decreased from 28 to 90 days. It can be seen that the density of concrete sample containing 40% of GGBS and 5% of MSA was reduced from 2360 to 2340 kg/m³ on 28 to 90 days. The similar performance was also found in sample of concrete that containing 50 and 60% of GGBS with 5% of MSA. Hence, the density of concrete containing OPC was denser than the concrete containing GGBS. It can be due to size of OPC which has bigger size of particles about 14.7 μm compared to GGBS that is 9.2 μm [4, 11].

The result of compressive strength tests for all of cube concrete samples as listed in Table 2 and Fig. 2. It shows that the compressive strength of concrete containing 50 and 60% of GGBS with 5% of MSA slightly reduced from 28 to 90 days. As compared, the compressive strength of control concrete sample and concrete containing 40% of GGBS with 5% of MSA were increased gradually from 28 to 90 days. Moreover, the concrete which has 40% of GGBS and 5% of MSA was obtained slightly higher compressive strength than control concrete on 90 days. Meanwhile, the usage of GGBS as partial cement replacement around 50% and above does not significant in increasing the compressive strength of concrete. Similar previous researcher also indicates that the optimum usage of GGBS as cement replacement in concrete around 55%. The additional usage of GGBS will produce more unreacted GGBS and acting as a filler material or fine aggregate in concrete mix [6].

Table 2 Result of compressive strength

Mix	28 days	60 days	90 days
Control concrete	35.4 MPa	39.2 MPa	41.0 Mpa
40% GGBS + 5% mussel shell ash	34.9 MPa	39.7 MPa	42.8 Mpa
50% GGBS + 5% mussel shell ash	34.8 MPa	34.3 MPa	32.2 Mpa
60% GGBS + 5% mussel shell ash	36.8 MPa	39.4 MPa	37.8 Mpa
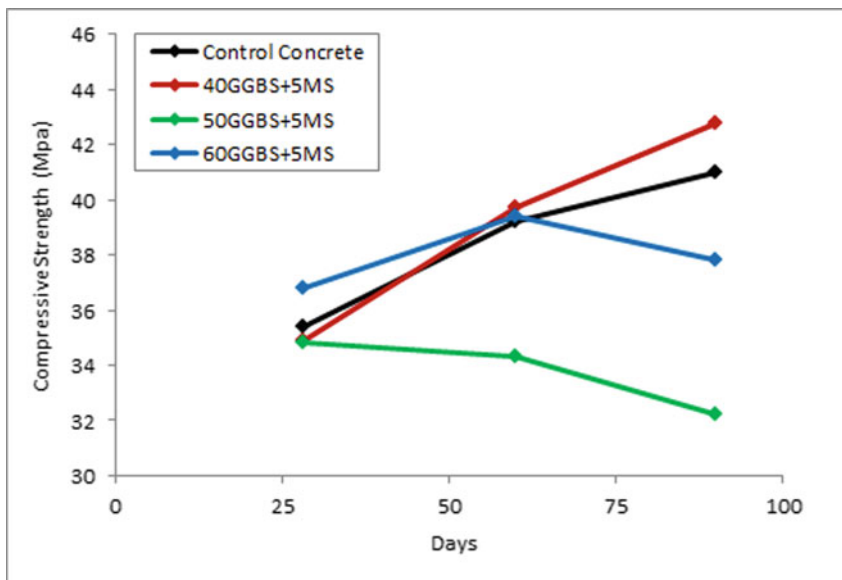
Fig. 2 Compressive strength of concrete with different percentages of GGBS and 5% of MSA

6 Conclusions

This study investigated the performance of GGBS and MSA as partial cement replacement in concrete. From experimental results, the following conclusions are made:

1. The combination usage of GGBS and MSA as partial cement replacement in concrete significantly reduce the density of concrete compared to conventional concrete. It can be due to specific gravity of GGBS which lighter than OPC thus make it less dense than conventional concrete.
2. Higher compressive strength was obtained in concrete sample with 40% of GGBS and 5% of MSA with an increment about 1.8% on 90 days.

3. The usage of GGBS as replacement of cement about 50 to 60% tends to decrease the compressive strength of concrete. The concrete sample with 50% of GGBS and 5% of MSA had the lowest compressive strength test results.

References

1. Arivalagan S (2014) Sustainable studies on concrete with GGBS as a replacement material in cement. Jordan J Civil Eng 8(3):263–270
2. ASTM C39/C39M-20, Standard Test Method for Compressive Strength of Cylindrical Concrete Specimens, 04.02
3. Divsholi BS, Lim TYD, Teng S (2014) Durability properties and microstructure of ground granulated blast furnace slag cement concrete. Int J Concr Struct Mater 8(2):157–164
4. Kumar Karri S, Rao GVR, Raju PM (2015) Strength and durability studies on GGBS concrete. Int J Civil Eng 2(10):34–41
5. Oliviaa M, Mifshellaa AA, Darmayantia L (2015) Mechanical properties of seashell concrete. Procedia Eng 125(2015):760–764
6. Oner A, Akyuz S (2007) An experimental study on optimum usage of GGBS for the compressive strength of concrete. Cem Concr Compos 29(6):505–514
7. Othman H, Hisham B, Bakar A, Don MM, Azmi M, Johari M (2013) Cockle shell ash replacement for cement and filler in concrete. Malays J Civil Eng 25(2):201–211
8. Othman NH, Bakar BHA, Don MM, Johari MAM (2013) Cockle shell ash replacement for cement and filler in concrete. Malays J Civil Eng 25(2):201–211
9. Özbay E, Erdemir M, Durmuş HI (2016) Utilization and efficiency of ground granulated blast furnace slag on concrete properties - a review. Constr Build Mater 105:423–434
10. Suresh D, Nagaraju K (2015) Ground granulated blast slag (GGBS) in concrete – a review. IOSR J Mech Civil Eng 12(4):1684–2278
11. Teng S, Lim TYD, Divsholi BS (2013) Durability and mechanical properties of high strength concrete incorporating ultra fine ground granulated blast-furnace slag. Constr Build Mater 40:875–881
12. Wan Mohammad WASB, Othman NH, Wan Ibrahim MH, Rahim MA, Shahidan S, Rahman RA (2017) A review on seashells ash as partial cement replacement. In: IOP Conference Series: Materials Science and Engineering, vol 271, p 1
13. Yang EI, Yi ST, Leem YM (2005) Effect of oyster shell substituted for fine aggregate on concrete characteristics: part I. Fund Prop Cem Concr Res 35(11):2175–2182

Modal Frequency of Steel and UHPC U-beam Using Finite Element Analysis

Siti Shahirah Saidin, Sakhiah Abdul Kudus, Adiza Jamadin, and Norliyati Mohd Amin

Abstract The high cost of ultra-high performance concrete (UHPC) has discouraged the implementation of the material in Malaysia's construction industry. Thus, this study is to evaluate the UHPC performance on cost-effective of a first-cost basis which are able to provide superior durability and workability to the structure. This superior durability of UHPC could help to reduce the number of maintenances required, thus could minimize the future maintenance cost. A study was conducted on the modal frequency of the superstructure bridge by modelling the concrete bridge deck with two different types of U-beam; steel and UHPC using Finite Element Analysis (FEA). The natural frequencies for both different model materials obtained from the FEA were compared and used to estimate the deflection at the midspan of the bridge structure. The comparison of these two materials indicated the high natural frequencies of UHPC U-beam resulting in a lesser deflection estimation at the mid-span of the structure compared to the steel U-beam. The least deflection value of UHPC showed the material allowing the structure for higher transmissibility and could reduce the risk of structures from failure.

Keywords Ultra-high-performance concrete · Finite element analysis · Structural health monitoring · Natural frequencies · Natural excitation

1 Introduction

Recently, the depletion of natural sources, increasing infrastructure deterioration and high maintenance cost were great challenges experienced by the American Association of State Highway Transportation Officials (AASHTO) [1]. According to the Grand Challenges report issued by AASHTO in 2005, almost a quarter of 590,000 bridges including the substructures and foundations were structurally

S. S. Saidin (✉) · S. A. Kudus · A. Jamadin · N. M. Amin
Faculty of Civil Engineering, Universiti Teknologi Mara (UiTM), 40450 Shah Alam, Selangor, Malaysia
e-mail: shahirahsaidin2011@gmail.com

deficient with regard to the material deterioration. Regarding this issue, the USA spent more than $1 billion annually for bridges maintenances, repairing and retrofit the pile foundations from chloride attack, corrosion and marine borer attack on the timber [11]. In early 2005, the study on the new materials such ultra-high-performance concrete (UHPC) all over the world, began with the aim to extend the service life of the bridges in reducing the maintenance required [2, 15, 20].

The use of UHPC has been widely spread and considered by many researchers and engineers for rehabilitation and strengthening of reinforced concrete beam [8, 9]. The advanced cementitious material with high tensile and compressive strength, ductility and durability of UHPC materials offers practical solution to improve the sustainability of structures which attracted many engineering structures field's attention especially for bridge engineering [17]. In Malaysia, Dura Technology Sdn. Bhd. was the first company that took the opportunities on these UHPC benefits by commercialising the UHPC into the market since 2007 with compressive and flexural strength in between 160 and 30 MPa. Thus, the finite element analysis (FEA) was used to study the dynamic characteristics such as the natural frequencies of UHPC to determine the effectiveness of UHPC as great as, or even much better than steel.

These dynamic parameters are the most important characteristic of bridges' structures that have been frequently used for long-term bridge's monitoring throughout their service life. According to previous researches on the Structural Health Monitoring (SHM), these dynamic parameters could be obtained from finite element method (FEM) and experimental method including ambient and force vibration testing [4, 5, 10, 13, 19, 22]. The experimental testing was required for the SHM purpose in order to validate the result from finite element (FE) model to ensure the accuracy of assumptions made including material properties, boundary condition and analysis option from the analytical modelling. Friswell and Mottershead (1995), validated the FE model using the results obtained from the experimental to determine the uncertainty parameters of the initial model to produce valid FE model.

Vibration based damage detection is one of the techniques used to implement the SHM. Vibration based method is a method that help to monitor the changes of structural condition by monitoring the changes of the dynamic parameters as example natural frequency [12]. Farrar and Jauregui [7], studied on the changes of natural frequencies of I-40 bridge in New Mexico that cross Grande. From this report, they found the changes of natural frequencies were related to the daily operation and temperatures. Wahab and Roeck [18], found the natural frequencies of two concrete bridges have changes up to 5–6% in a year due to the thermal effect which varies in temperature. Similarly, the pattern changes in natural frequencies in a day was reported by Farrar et al. [6]. All these studies highlighted the importance of the dynamic parameters in determining the performance level of the structure. This paper will discuss and analyze the natural frequencies of two model of 3D bridge deck with different U-beam materials using FEA. Five (5) modes of natural frequencies were obtained for each model and the first mode obtained was validated with the analytical theory for simply supported bridge. The validated frequency value of UHPC and steel beam was then used to estimate and compare the deflection at the midspan of the bridge structure.

2 Finite Element Analysis

Three-dimensional (3D) bridge deck with steel U-beam and bridge deck with UHPC U-beam were modelled by using finite element analysis (FEA). The software used for both models is ABAQUS 6.14. The 3D solid-type element was used to model the bridge deck and U-beam. The bridge deck was connected to the U-beam through the nodes conforming each element, by applying the tie constraint. The following geometry details, material properties and boundary condition are discussed in this section.

2.1 Modelling Geometry

The 0.225 m thick, 50 m length and 11.5 m width of concrete deck was featured with three pieces of 50 m UBG1750 U-beam with a spacing of 3.5 m in between the U-beam as shown in Fig. 1. The U-beam cross-sectional dimension is illustrated in Fig. 2. The complete mesh for the whole model is shown in Fig. 3 with 89,488 number of nodes and 72,402 number of elements.
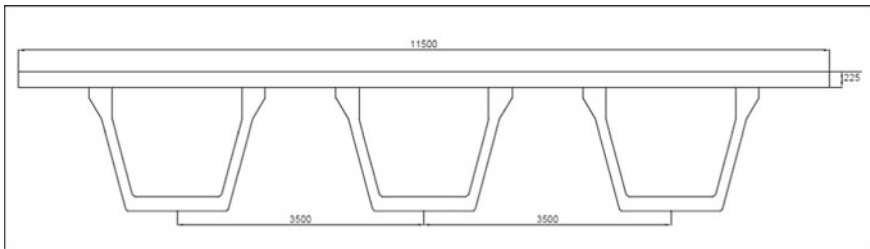
Fig. 1 Concrete deck with U-beam section (mm)

Fig. 2 UBG1750 U-beam (mm)
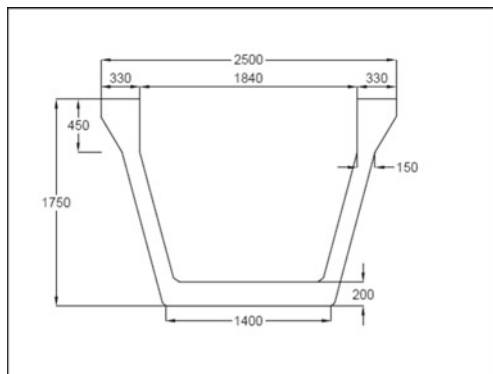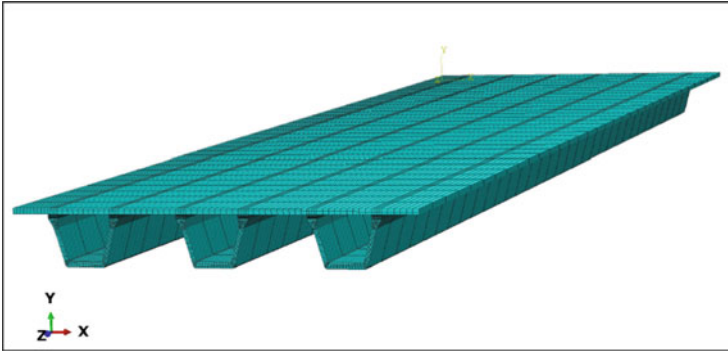
Fig. 3 Abaqus model of bridge

2.2 Material Properties

2.2.1 Reinforced Concrete Bridge Deck

The 250 mm thick and 50 m length of reinforced concrete deck material properties for both model (Steel and UHPC U-beam) was extracted from Chang et al. [3] as illustrated in Table 1.

2.2.2 Steel and UHPC U-Beam

The 50 m of steel U-beam were defined accordingly by Chang et al. [3], meanwhile the UHPC U-beam was according to the UBG1750-UHPC from Yen et al. [21] specification as summarised in Table 2.

Table 1 Material properties [3]

Components	Modulus of elasticity	Mass density (kg/m^3)	Poisson's ratio
Concrete	35 GPa	2500	0.2

Table 2 Material Properties [3] and [22]

Components	Modulus of elasticity	Mass density (kg/m^3)	Poisson's ratios
Steel (Q345)	200 GPa	7850	0.3
UHPC (UBG1750)	45 GPa	2500	0.2

2.3 Boundary Condition

The bridge was modelled as simply supporting both the concrete bridge deck with steel and UHPC U-beam models. One of the end spans was assigned as pinned support which restrained translation movement in all directions (x, y, and z axis) but it allowed rotation movement in all directions (x, y, and z axis). On the other end, the span was a roller support which only restrained translation and rotation movement in vertical directions (y-axis). The boundary condition was assigned at each node of the elements for both the end span of the bridge deck.

3 Beam Analogy for Simply Supported Bridge Superstructure

The dynamic characteristic such natural frequency is relay on the mass and stiffness of the structure. The stiffer structure with lower mass increases the natural frequency and the other way around. These natural frequencies can be determined by simple harmonic equation where the simply supported bridge superstructure is subjected to small vertical deflection. Memory et al. [14], indicated the natural frequencies of the structure could be estimated as per the following equation:

$$n = \frac{1}{2\pi} \sqrt{\frac{k}{m}} \tag{1}$$

where n is the natural frequency (Hz), k is the stiffness of the simply supported beam (kN/m), and m is the mass of the beam (m).

Equation (1) was used to calculate the natural frequency theoretically in order to validate the natural frequencies from FEM results. Hence, for UHPC U-beam, the natural frequency calculated was 3.618 Hz compared to the 1st mode of frequency obtained from FEM. Therefore, according to Eurocodes EN 1991-2:2003 (6.4.4), the natural frequencies value obtained from the Eq. (1) for simply supported bridge that subjected to the bending could be used to estimate the deflection value as specified in Eq. (2);

$$n_o = \frac{17.75}{\sqrt{\delta_0}} \tag{2}$$

Where n_o is the natural frequency (Hz) and the δ_0(mm) is the deflection at mid-span permanent actions.

4   Comparison of Finite Element Analysis and Theoretical

From the simulation, it showed the mass of the bridge deck with UHPC U-beam was 674,063 kg which was lesser compared to the bridge deck with steel U-beam which was 674,136 kg. From this finding, it indicated the UHPC materials provided lightweight structures compared to steel structures as Fehling et al. [8], claimed that UHPC without reinforcement could reduce the weight of structures. Table 3 shows the natural frequencies obtained from the analytical for both steel and UHPC U-beam material. The results obtained showed the natural frequencies of UHPC U-beam were higher than the steel U-beam.

The natural frequencies obtained were then validated with the theoretical calculation based on the Eq. (1), to determine the first mode natural frequency value. A small percentage difference ($<10\%$) shown in Table 4 indicated the result from the analytical FEA was acceptable and reasonable [23]. The smaller the percentage difference between the two sets of data indicated the more precise the result obtained.

Meanwhile, the value of natural frequencies obtained from the Eq. (1) was used to estimate the deflection (mm) at mid-span of the structures by applying Eq. (2). Hence, the deflection value of concrete bridge deck with UHPC U-beam was lesser compared to the bridge deck with steel U-beam as shown in Table 5. According to Ren et al. [16], their studies reported the use of UHPC in long span cable stayed bridge showed the estimated deflection was lesser than the allowable values. From this, it could be concluded the high natural frequencies of UHPC material allowed for higher transmissibility that resulted in low displacement and low strain which may reduce the risk of structures from collapsing.

Table 3 Comparison of frequencies for composite and UHPC bridge deck and girder section

Mode	Frequency (cycles/time)	
	Steel	UHPC
1	2.8784	3.118
2	3.0148	3.421
3	6.677	6.901
4	11.158	12.118
4	13.111	13.546
5		

Table 4 Percentage difference between FEM and theoretical calculation

Components	FEM (cycles/time)	Theoretical (cycles/time)	Percentage difference (%)
Steel U-beam	2.8784	2.978	3.40
UHPC U-beam	3.118	3.324	6.39

Table 5 Deflection value estimation (mm)

Components	Theoretical natural frequencies (Hz)	Estimation deflection (mm)
Steel U-beam	2.978	35.5
UHPC U-beam	3.118	32.41

5   Conclusion

The dynamic characteristics of two different materials of steel and UHPC beams were studied based on the result obtained from finite element analysis and theoretical finding. These results showed acceptable correlation in terms of the natural frequencies. The five modes natural frequencies of steel and UHPC beam obtained were compared. The first mode natural frequency obtained was compared to the theoretical value where the percentage difference ranging between 3–7%. Generally, the finite element analysis was more detailed but the result produced was not so accurate since the model was constructed based on the as built design drawings. Hence, the theoretical calculation was one of the valuable sources of information to validate the accuracy of the FE model. These discrepancies were may come from the finite element modelling such boundary condition and material properties assigned. In a companion paper, the writers will attempt to validate the FE model with the field measurement result and finite element modelling updating in order to minimize the discrepancies. In conclusion, this study has achieved its objective where modal parameters obtained from UHPC material showed it was more stiffened compared to steel material thus could provide more efficiency in workability and even the weight of the structures was less.

References

1. AASHTO (2005) Highway subcommittee on bridges and structures. Grand challenges: a strategic plan for bridge engineering. Washington (DC)
2. Behloul M, Ductal R (2006) Prestressed girders for a traffic bridge in Mayenne, France. In: 7th International conference on short & medium span bridges. Quebac, Canada
3. Chang C, Chang T, Zhang Q (2001) Ambient vibration of long-span cable-stayed bridge. J Bridge Eng 6(1):46–53
4. Chiewanichakorn M, Aref AJ, Alampalli S (2007) Dynamic and fatigue response of a truss bridge with fiber reinforced polymer deck. Int J Fatigue 29:1475–1489
5. Farhey DN (2006) Integrated virtual instrumentation and wireless monitoring for infrastructure diagnostics. Struct Health Monit 5(1):29–43

6. Farrar CR, Doebling S, Cornwell P, Straser E (1997) Variability of modal parameters measured on the Alamos Canyon Bridge. In: Proceedings 15th International Modal Analysis Conference, Orlando, FL, pp 257–263

7. Farrar CR, Jauregui D (1996) Damage detection algorithms applied to experimental and Numerical modal data from the I-40 bridge. Los Alamos National Library Report, LA-13074 MS

8. Fehling E, Bunje K, Leutbecher T (2004) Design relevant properties of hardened ultra high performance concrete. In: Proceedings of the International Symposium on Ultra High Performance Concrete, Kassel University Press, Kassel, Germany, pp 327–338

9. Habel K, Denari E, Brühwiler E (2007) Experimental investigation of composite ultra-high-performance fiber reinforced concrete and conventional concrete members. ACI Struct J 104:93–101

10. Kwasniewskia L, Lib H, Wekezerb J, Malachowskic J (2006) Finite element analysis of vehicle–bridge interaction. Finite Elem Anal Des 42(11):950–959

11. Lampo R, Maher A, Busel JP, Odello R (1997) Design and development of FRP composite piling systems. In: Proceedings of the international composite expo, Nashville, TN

12. Laxmikant K (2008) Damage Detection in Structures using Natural Frequency Measurements. PhD Thesis, University of New South Wales Australian Defence Force Academy, Australia

13. Li H, Wekezer JF, Kwasniewski L (2008) Dynamic response of a highway bridge subjected to moving vehicles. J Bridge Eng 13(5):439–448

14. Memory T, Brameld GH, Thambiratnam D (1991) A simplified method for estimating the natural frequency of bridge superstructures. In: Heywood RI (ed) AUSTROADS conference Brisbane, Bridges—Part of the Transport System, pp 539–550

15. Ozyildirim C (2011) Evaluation of ultra high performance fiber reinforced concrete. Final Report. Virginia Center for Transportation Innovation & Research. Charlottesville, VA

16. Ren L, Fang Z, Wang K (2018) Design and behavior of super-long span cable-stayed bridge with CFRP cables and UHPC members. Compos Part B Eng 164:72–81

17. Schmidt M, Fehling V (2005) Ultra-High performance concrete: research development and application in Europe. In: The 7th international symposium on the utilization of high-strength/high- performance concrete, pp 51–78

18. Wahab MA, De Roeck G (1997) Effect of temperature on dynamic system parameters of a highway bridge. Struct Eng Int 7(4):266–270

19. Wang Y, Loh KJ, Lynch JP, Fraser M, La K, Elgamal A (2007) Vibration monitoring of Voigt Bridge using wired and wireless monitoring systems. In: The processing of 4th China–Japan–US symposium on structural control and monitoring, Hangzhou, pp 16–17

20. Wipf TJ, Phares BM, Sritharan S, Degen BE, Giesmann MT (2009) Design and evaluation of single span bridge using ultra high-performance concrete. Final report. Center for Transportation Research and Education, Iowa State University

21. Yen LV, Behzad N, Abu Bakar MS, Balamurugan AG, Tet SY (2012) Application of ultra high-performance fiber reinforced concrete–the Malaysia perspective. Int J Sustain Constr Eng Technol 3(1):26–44. (ISSN: 2180–3242)

22. Yun CB, Min J (2011) Smart sensing, monitoring, and damage detection for civil infrastructures. KSCE J Civil Eng 15(1):1–14

23. Zhang Z, Zhang W, Zhai ZJ, Chen QY (2007) Evaluation of various turbulence models in predicting airflow and turbulence in enclosed environments by CFD: part 2—comparison with experimental data from literature. Am Soc Heating Refrigerating Air-Conditioning Eng Inc 13 (6):871–886

The Potential of Glued Laminated Timber Sleepers Made from Malaysian Tropical Heavy Hardwood

Mohamad Bhkari Norshariza, Wei Chen Lum, Zakiah Ahmad, Mohammad Soffi Md Noh, and Mahsuri Mat Dris

Abstract This paper discussed the potential of glued laminated timber (glulam) sleepers made from Malaysian tropical heavy hardwood. First, the prospect of using timber as railway sleepers is discussed. Technical, environmental and economical perspectives are also discussed. Challenges and shortcomings due to serviceability life span, cost, timber supply and preservative treatment for non-durable species are explained. Next, the alternative solution of using glulam to replace solid timber sleepers is explored. The advantages of using glulam as sleepers are highlighted. Although studies on glulam sleeper made from softwood and hardwood in temperate country show promising results, the performance of glulam made from tropical timber especially heavy hardwood is still less known. Thus, it is important to discuss the development of glulam sleeper prototype made of Malaysian heavy hardwood, namely Kekatong. Standard sized railway sleepers are manufactured according to MS758. Compliance test was conducted according to American Railway Engineering and Maintenance-of-Way Association (AREMA). Finally, the strength performance and behaviour of Kekatong glulam sleeper assessed through laboratory and field study are discussed. According to the observation and previous studies by the authors, it can be concluded that Kekatong glulam sleepers display promising potential as the alternative solution for the conventional solid timber sleeper.

M. B. Norshariza (✉) · W. C. Lum
Institute for Infrastructure Engineering and Sustainable Management (IIESM), Universiti Teknologi MARA, 40450 Shah Alam, Selangor, Malaysia
e-mail: nshariza@uitm.edu.my

M. B. Norshariza · Z. Ahmad
School of Civil Engineering, College of Engineering, Universiti Teknologi MARA, 40450 Shah Alam, Selangor, Malaysia

M. S. M. Noh
Faculty of Civil and Environment Engineering, Universiti Tun Hussein Onn Malaysia, 86400 Parit Raja, Batu Pahat, Johor, Malaysia

M. M. Dris
Malaysian Timber Industry Board (MTIB), Menara PGRM, Jalan Pudu Ulu, 56100 Cheras, Kuala Lumpur, Malaysia

1 Introduction

Sleepers are identified as one of the most crucial elements of a railway track system. They serve as a support beam for the loading on the track and also transfer and distribute the oncoming load to the ballast [26]. Moreover, glulam serve as an elastic medium between the rails and the ballast and thus providing secure and even support for the track system [18]. Furthermore, sleepers are also able to sustain and withstand oncoming load therefore preventing them from moving from the rail system in the lateral and longitudinal direction [20, 21].

The utilisation of timber as railway sleepers started in the 1900s [31]. To date, railway sleepers made from timber are still wide used to build railway track due to their effectiveness and reliable performance. Globally, approximately 2.5 billion railway sleepers made from hardwood has been installed in the railway track [8]. In United States (US) alone, 13 million of sleepers made from timber are still being used and the demand remains high [1]. Outside of the US, the countries in the Europe, Asia and Australia still use timber as sleepers but usage of timber sleepers are lower compared to sleepers made from other materials.

In Malaysia (based on KTMB record in year 2012), the number of timber sleepers installed on the railway track has decrease. Of the total track length of 1724.50 km, only 26.4% is covered by timber sleepers (approximately 750 thousand timber sleepers). Owing to the lack of large diameter logs from naturally durable heavy hardwood species namely Chengal, Balau and Bitis, most of the timber sleepers were replaced by pre-stressed concrete (PSC) sleepers [18]. This scenario causes the timber log of the required hardwood timber species price to increase. Nonetheless, the utilisation of untreated timber from non-durable species will results in the decrease of the in-service life span of the timber sleepers used. Therefore, non-durable timber sleepers often need to be treated with creosote. However, the use of creosote as a preservative raised the concern about environmental impact as it will leach into the environment [17].

Although the KTMB has initiated to shift to PSC sleepers due to the above reasons, this solution does not provide the answer to the overall problem. The usage of PSC also has limitation where at certain location in railway track the timber sleepers are most preferable. Those locations are areas which contribute to extreme shock and excessive force to the sleepers such as at railway bridges, tunnels, stations, yards and industrial lines ([17], 23], Engineer in Permanent Way KTMB, in *personal communication*). The ability of PSC to absorb impact is low [20, 21] compared to timber sleepers which resulted in cracked problems in the PSC sleepers. Hence, timber sleepers are the best choice in those locations.

Therefore, it is necessary to find an alternative material to substitute solid timbers while still retain the ability of timber. This has promoted the use of sleepers

made of engineered timber, such as glued laminated timber (glulam). It is possible to design and engineered Glulam to suit the needs of the construction industry. The scale of the utilization of glulam as railway sleepers, however, is still small [12]. Generally, previous studies mostly focus on the performance of glulam sleepers from softwood timber [11, 39], low grade hardwood [12] and Brazilian hardwood [7] are good. The study on the glulam timber sleepers made from Malaysian tropical heavy hardwood timber is still limited. Thus, this paper discussed the perspective and challenges of using timber sleepers in Malaysia, alternative the existing solid timber sleepers, past research on the performance and behaviour of glulam timber sleepers, and development and potential of glulam sleepers.

2   The Prospects of Timber Railway Sleepers and the Challenges

Red and white oaks, beech, the birches, gums, maples and hickories are the species of hardwood timber commonly used for timber sleepers in Europe [11]. While, in Malaysia, timber species such as Chengal, Balau and Bitis which come from heavy hardwood and naturally durable categories are commonly utilised since in the early days by the Malayan Railways [35]. However, increased demand and insufficient timber supply led the shift by Malaysian Forest Department in utilising medium hardwoods of Keruing and Kempas. But in order to be used for exterior purposes, these timber species need to undergo chemical treatment and the chemical used are known to cause environment and health impacts. Therefore, this section is discussed the issues of timber sleepers in terms of technical, economic and environmental perspectives as well as their advantages and disadvantages of their usage in railway track. Despite timber sleepers installed at mainline track in certain required locations (e.g. station, bridges industrial line, etc.), they are also suitable to install at railway turnout as in Fig. 1 and at the side track [17, 20, 21]. Technically, their adaptability and the ease of manufacturing and handling make these timber sleepers are more suitable to install in this particular railway section [14, 32]. At these locations, the sleepers are mounted at various lengths and fastening locations with different sleepers dimensions in order to manage the complicated loads generated by the train crossing [20, 21].

In the locations such railway station, yard and industrial line of the railway track, timbers sleepers are generally preferable compared to PSC sleepers due to the elastic nature of the material. At the locations mentioned above, the sleepers have to endure high vibration produced by the weight of the locomotive as a result of the resistance of the brakes as the heavy haul train slows down before coming to a stop. The abilities of timber sleepers to absorb the energy and resist the impact load [32, 14] have become the deciding factors for the railway operators to select timber
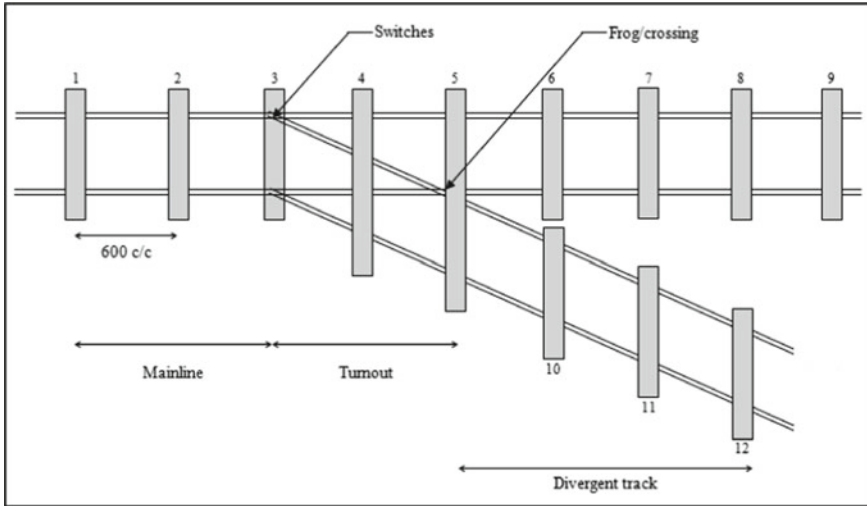
Fig. 1 Standard right-hand railway turnout

sleepers as the preferable material where such excessive force and shocks will smash the PSC sleepers and lead to flexural cracks [13].

Furthermore, timber sleepers are relatively easy to install and also easy to be replaced afterwards for maintenance purposes. The transportation and installation of the renewal timber sleepers is also efficient and economical viable. There is no heavy and special machinery required and more labour efficient. In comparison, timber sleepers have a lower weight compared to sleepers made of other materials (PSC and steel sleepers), with a weight range from 60 to 70 kg for regular mainline sleepers. [20, 21]. The inherent insulating properties that timber possesses are another advantage of timber sleepers, which is a critical feature for track signalling.

The replacement of the timber sleeper with the PSC sleeper is challenging and costly from an economic perspective. [17] claimed that a complete renewal process is necessary and inevitable, such as upgrading secondary or low traffic routes and replacing and modifying existing bridge and tunnel substructures. These all add up and further increase the cost of replacing and maintaining the railway sleepers. In addition, during the replacement process, problems occur because the mechanical properties of PSC sleepers are incompatible with current timber sleepers [19].

PSC sleepers create high noise emissions from an environmental point of view, creating sound pollution. However the ability of timber sleepers to withstand impact loads and absorb energy can mitigate the effects of track noise [32]. In terms of sustainability concerns, timber is a green and renewable material, through re-planting and sustainable forest management, timber will always be available in the market. Concrete and steel are non-renewable material which have a higher carbon footprint during manufacturing process. Taking all factors into consideration, the decision to select timber sleepers is clear and strongly justified.

However, one aspect that needs to take into consideration for choosing timber as sleepers is the serviceable life span of timber. Due to higher axle loads and trip frequency, speed and other detrimental environmental effects, timber sleeper is normally susceptible to degradation and decay. [15, 31] which lower its structural strength. It has been reported that fungal decay (as in Fig. 2(a)), end splitting (as in Fig. 2(b)) and termite attacks are the most prevalent railway track failure modes that increase the cost of maintenance and decrease its serviceable life span [10]. For several decades, the targeted life span of timber sleepers varied from 20 to 30 years [19]. However, nowadays the serviceable life span of timber sleepers is approximately 15 years or less due to the decline in the availability of high quality timber for railway sleepers [14, 15].

Creosote treatment is normally used for medium and light grade hardwood timber as well as softwood timber in order to extend their life span due to deterioration from termite attacks. However, the replacement and renewal operation generate an abundant timber sleeper and increase the overall cost for disposal since these sleepers have to be disposed properly in order to avoid contribute to toxic hazard environment. Creosote is a controlled substance in European countries and only approved industries such as railways, harbours and waterways are authorised by the European Commission to use it until 2018 [17]. Other creosote-treated structures such as any building interiors, that are exposed to regular skin contact with the general public are limited [2]. There are some alternatives outlined by the [17] owing to the limitation imposes on the usage of creosote such as:

(a) to use naturally durable timber species without the requirement of treatment
(b) to use green and environmentally friendly preservative; and
(c) to use of composite and steel sleepers.

(a) Fungal decay   (b) Splitting at ends
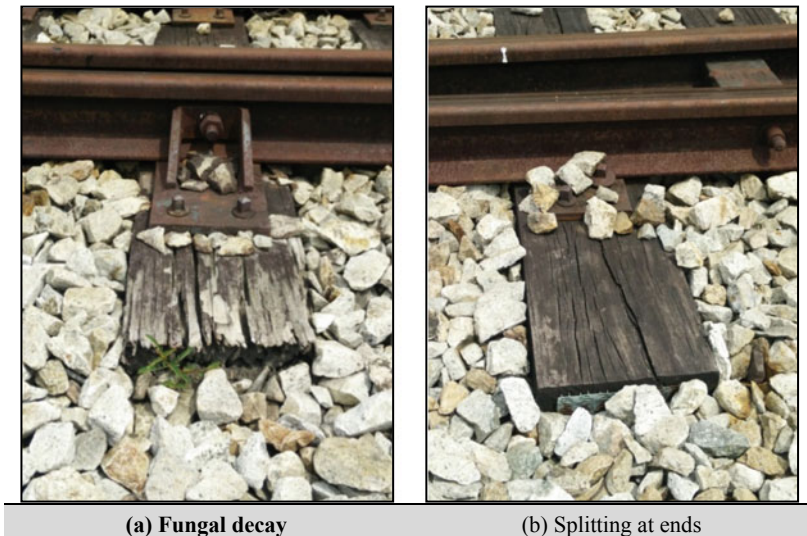
Fig. 2 Common type of failure modes in timber sleepers

It is clear that there is a need for a substitute for solid hardwood sleepers as its market availability has become scarce. The substitute materials need to satisfy the performance requirement while being environmentally friendly at the same time. This is where glulam sleepers come into the picture. Glulam sleepers can even be manufactured using discharged solid timber sleepers which further contribute to its sustainability and feasibility [6]. However, in this preliminary study, naturally durable Malaysian hardwood timber was selected because it is more advantageous as these timbers do not have to undergone preservative treatment.

3   Glued Laminated Timber Railway Sleepers as an Alternative

In Malaysia, the application of solid timber sleepers has decrease. This is chiefly cause by the inconsistency in timber supply since there are inadequate resources of high-grade hardwood timber with large diameter which is required for the production of solid timber sleepers. Large sections that are free of defects are needed for the current production of solid hardwood timber sleepers. The timber pieces must also be of *select and better* grade for naturally durable hardwood and *standard and better* grade for non-durable hardwood [34]. These days, one smaller diameter timber log can only be used to produce a few good quality timber sleepers and this resulted in very low recovery rate per timber log and produces a lot of wastages. Consequently, the cost for the production of timber sleepers will transfer to the end products thus make it very expensive. The necessity to find an alternative material to solid timbers has initiated the development and utilisation of engineered timber product (ETP) particularly glued laminated timber (glulam) in this case. Glulam is one of the first engineered timber products introduced in the early 1900s and is still commonly used in the modern construction industry because it has a very competitive edge compared to other materials. Glulam is produce by gluing individual sawn timber pieces together under meticulous manufacturing conditions [36]. The application of glulam as building structures and bridges is rather common compared to the application as railway sleepers. In the case where glulam is utilised as sleepers, the timber species selected are mostly limited to European and Brazilian hardwood or softwood.

According to MS 758: 2001, glulam is fabricated using thin pieces of sawn timber and the thickness shall be less than 40 mm [24]. The timber can be sawn in any of the cutting pattern as illustrated in Fig. 3. In addition, glulam timber sleepers can be produced in any desired dimension and can be used in conjunction with existing timber sleepers whose mainline track dimensions are different compared to turnout sleepers. Glulam timber sleeper strength and stiffness can be designed and

(a) Normal quarter sawing	(b) True radial sawing
(c) True quarter sawing	(d) Commercial quarter sawing
(e) Plain sawing	(f) Billet sawing
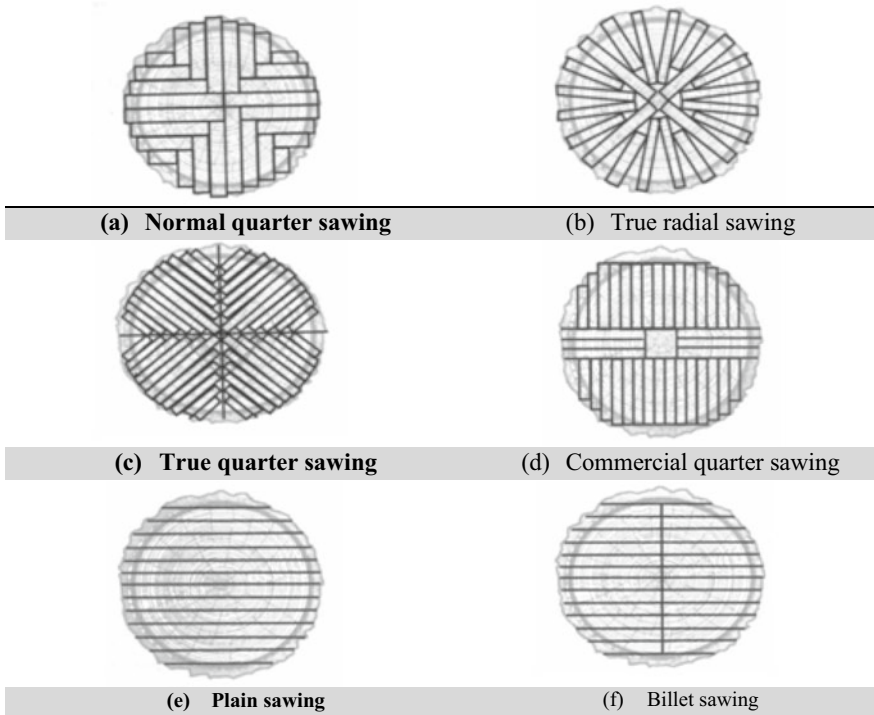
Fig. 3 Types of timber cutting [22]

controlled by extracting or dispersing timber knots inside the layers or lamellas. Therefore, glulam timber sleepers with stronger and more homogeneous properties compared to solid timber sleepers can be manufactured. Moreover, glulam sleepers also have excellent dynamic performance characteristics and has ability to withstand repetitive dynamic loads caused by train loading which make it extremely ideal to carry the heavy axle load [33].

Glulam timber sleepers are produced from kiln dried sawn timber which dries at relatively low moisture content of 12% [33]. Therefore, its propensity to exhibit surface regulation and splitting is much less than that of solid timber sleepers. Moreover, its dimensions and cross-sections are stable. In comparison to green sawn timber, Glulam timber sleepers also have a higher fastener design values and less tendency of fastener to work out from the member. Table 1 present the advantages using the glulam sleepers compared to the existing solid timber sleepers.

Table 1 Advantages using the Glulam sleepers

Existing solid timber sleepers	Glulam timber sleepers
The present timber sleepers are manufactured from naturally durable timber log with large diameter	Utilisation of cross section of timbers
Existing of timber defects (knots) reducing the strength of timber. The strength of timbers varies	Enhancing the properties of timber
The depleting supply of natural durable timber in required sleeper's size	Sustainability of product
	Still maintain the use of natural durable timber

4 Past Research on Strength Performance and Structural Behaviour of Glued Laminated Timber Railway Sleepers

Past research were conducted a study on strength performance based on field works [11, 39, 40] and laboratory works [7, 12]. In the field work, physical observation has been made and discovered the field-performance of glulam sleeper has been reasonably acceptable [40]. At the top lamination and inside glue lines, there was minimal surface checking observed [11, 39].

According to Carrasco et al. [7], through their laboratory works concluded that the advantages obtained from glulam technology contributed to the high mechanical performance of glulam timber sleepers. The dimensional stability of glulam timber sleepers and the lower variability of mechanical properties initiated the railway industry shifted to utilize the glulam sleepers [2]. The strength capacity of the sleepers can be designed due to configuration of lamellas where the higher stresses distributed throughout the depth of member [7]. Furthermore, defects in timber parts can be eliminated and knotted timber pieces can be used in the lower stress area, which led to greater strength capacity.

Moisture content of timber pieces for glulam should normally dried, resulted the stability of glulam dimension. According to Malaysian Standard, MS 758 [24], timber pieces for non-treated timber should be dried in the range of 8 to 15% during the assembly and for treated timber the range is in between 11 to 18% through kiln-drying. This requirement minimise the issue of end splitting as this type of deterioration occurred as second principal cause of failure at in-service solid timber sleepers due to fluctuations and variation in relative humidity and temperature [10, 12]. Therefore, at the point of end splitting, the capacity of glulam sleepers to resist transverse shear loading is decreased. Glulam sleepers which required in dried conditions also provide lower variability in mechanical properties thus increased the strength. However, a major investment in kiln drying equipment is required to dry the timber pieces for glulam manufacturing and thus raised the energy cost and consequently increase the products price [38].

Glulam was stated to be stronger compared to solid sawn timber in terms of strength characteristics [11]. [7] detailed the strength and behaviour of glulam timber sleepers made from Brazilian hardwood timber (*Eucalyptus citriodora*) bonded by a water-resistant resorcinol formaldehyde adhesive. The design of the experimental programme was to simulate the actual situation on the railway track. The ultimate load of the glulam timber sleeper was 110% higher from the experimental work compared to expected values, suggesting that the glulam timber sleeper has high performance.

[9] were studied the physical and mechanical properties of selected timber and observed the suitability of the timber species to be utilised as railway sleepers. In this study, softwood timber from *Oocarpapinus* was used as glulam timber sleepers. The average MOR and MOE values were far closer to the limit stipulated in the Brazilian standard for Class II timber sleepers from the static bending-centre negative tests.

Besides the desirable performance of glulam sleepers as mentioned above, the information of the strength performance and behaviour of glulam sleepers made from tropical hardwood is still lacking. In order to use hardwood glulam sleepers as an alternative or replacement to conventional solid timber sleeper particularly from Malaysian tropical timber, investigation on its performance and behaviour is required. Some studies on heavy hardwood glulam sleepers made from Kekatong species were carried out by [27–30]. The studies show promising results for Kekatong glulam as sleepers. Detailed discussion on the development and potential of Kekatong timber to be used as glulam sleepers are discussed in following section.

5 Development of Glued Laminated Timber Railway Sleepers Using Malaysian Tropical Hardwood Timber

Glulam sleepers were produced for this preliminary work at glulam factory in Pasir Gudang, Johor, Malaysia. The production of glulam sleepers were taken from the standard and regulated production process accordance with MS 758: 2001 [24]. Figure 4 present the manufacturing processes of glulam sleepers.

In this study, Kekatong (*Cynometra* spp.*)* having a strength group 2 (SG2) was selected as glulam sleepers. This species was selected based on the market availability among the several species listed in KTMB Technical Specifications 2005 [18] and the required grade which is *Select and Better*. The density of this timber species ranges between $880-1155$ kg/m^3. This species is classified as naturally durable heavy hardwood where treatment with preservative is not needed [35]. Glulam sleepers were prepared for a standard mainline track for a meter-gauge of $127 \times 254 \times 2000$ mm length [18]. The Kekatong glulam sleeper had five laminations with average thickness of 26 mm. The sleepers were suitable for outdoor exposure by using the Phenol-resorcinol formaldehyde (PRF) adhesive as
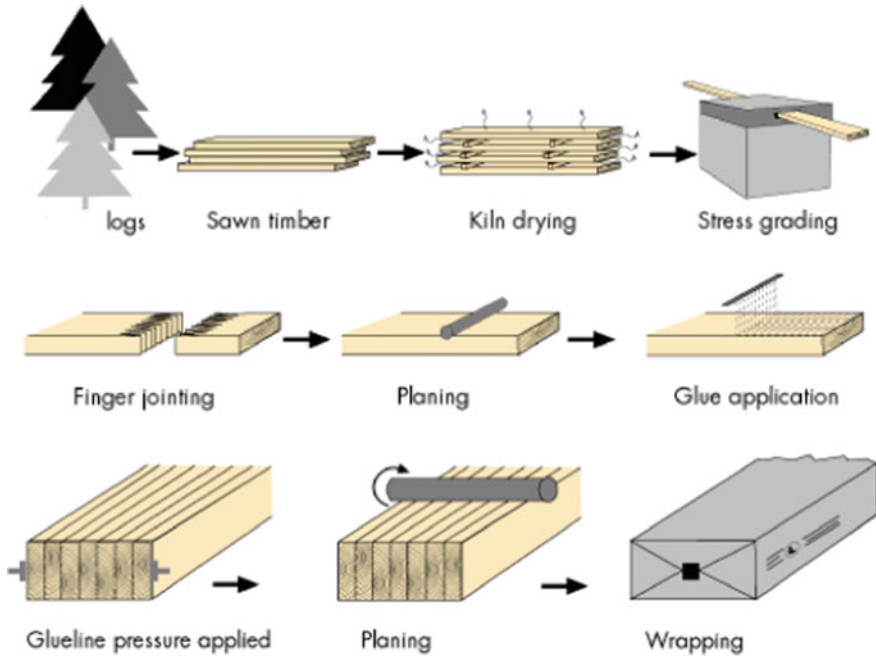
Fig. 4 Manufacturing process of glulam sleepers (Source: www.glulam.co.uk)

recommended in MS758 [24]. The four phases of the manufacturing processes were shown in Fig. 4. Control measures are addressed herein, such as the necessary moisture content, wood grading, glue curing and clamping time. The production processes of glulam sleepers are also detailed.

5.1 Timber Drying and Timber Grading

As proposed in the kiln drying schedule by MTIB, Kekatong hardwood sawn timber was kiln-dried for a few days [25]. The timber specimens were dried until the desirable moisture content (12 to 15%) was reached. All timber samples were visually graded according to strength grading rules for Hardwood Structural Grade (HSG) as stipulated in MS 1714:2003 after the timber specimens was dried to the required MC. The grading process was conducted by qualified graders registered with Malaysian Timber Council (MTC). For the production of high-quality glulam timber sleepers, only timbers graded as *Select and Better* were selected.

5.2 Finger Jointing

Prior to finger the jointing process, timber pieces were planned to make sure that the surface is smooth and even. Next, finger joint profile was made by passing both ends of timber pieces through the cutting heads. The finger joint length required for this study was 20 mm. Saw dust was cleaned from the surface of finger joint before structural adhesive was applied. Phenol Resorcinol Formaldehyde (PRF) (Akzo Nobel Synteko 1734) was used as the binding agent. The liquid adhesive system used was supplied by Casco Adhesive Pte. Limited which is weatherproof and durable liquid and appropriate to be used in Service Class 3 structure. This adhesive was used to bind the finger joint together and was also applied on the surfaces of timber pieces during glulam sleepers fabrication process. This adhesive was a mixture of liquid resin and powder hardener by the ratio of 4:1 as recommended by the supplier. The adhesive system was stirred until a homogenous state and was maintained at room temperature. Figure 5 (a) and (b) display the liquid resin and powder hardener and the mixture of the adhesive system in the homogeneous state after stirring.

Timber pieces were finger jointed and then composed to the required sleeper length with a pressure of 250 to 300 kg/cm^2 for about three seconds by the finger composer. In order to stop the resin from coming out of the timber pieces, the process from planing to finger jointing the timber pieces must be accomplished within four hours. After adhesive has cured, the moisture content was determined and maintained at 15% [37]. Next, the finger jointed timber pieces were planed again to obtain clean, parallel and glueable surfaces prior the edge and face gluing.

(a)   (b)
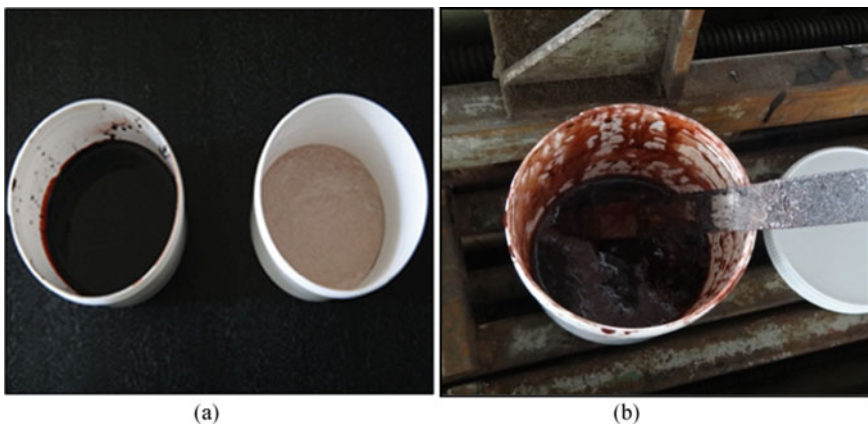
Fig. 5 The adhesive **a** liquid resin and powder hardener; **b** After stirred up and in homogeneous state

5.3 Gluing and Clamping

During the gluing stage, the finger jointed timber pieces were assembled into a standard sleeper size with the dimension of 254 × 127 × 2000 mm (width × thickness × length) as detailed by KTMB [18]. In this step, two kinds of gluing process were involved, namely edge gluing and face gluing. The edge gluing was carried out in order to obtain a wider-width of timber lamella. After applying the PRF at edge of timber piece as shown in Fig. 6(a), the timber piece was then assembled together. To ensure the proper bonding between these two timber pieces, the lamella was hammered. Later, this lamella was clamped without the application of pressure as damage might occur in the thin lamella. The lamella was left for a minimum of 6 h but not exceeding 24 h for the adhesive to properly cure.

The lamella was planned again after the adhesive for edge gluing had cured in order to get the smooth surface. Next, as shown in Fig. 6(b), the PRF was applied to the face for each lamella and this procedure must be performed completely within four hours in order to prevent unnecessary resin. Then all lamellas were placed closely to each other and were assembled at the clamping bed (Fig. 6(c)). The suitable pressure applied from the clamping bed ensure that each lamella remain attached in close contact. The adhesive was allowed to cure within 6 to 24 h in room temperature under clamping pressure. After the sleeper was released from the bed, it was then conditioned at room temperature for several days to make sure that it has cured completely. The moisture content of the sleeper was determined and maintained in the desirable range (12 to 15%). Finally, the glulam sleepers were trimmed and planed for final finishing.
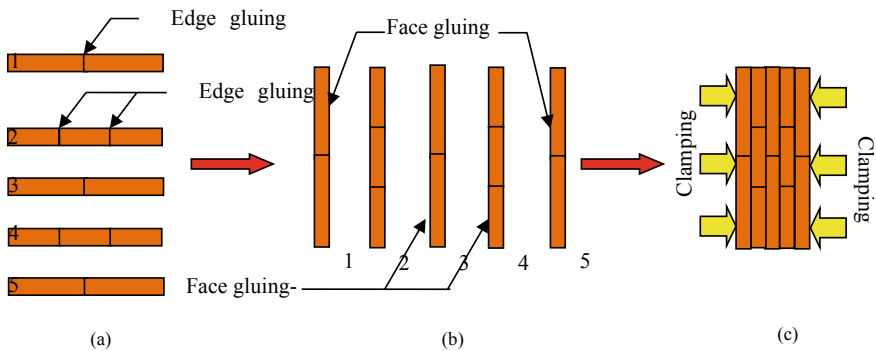
Fig. 6 The gluing and clamping process

5.4 Planing and Packaging

The last step in the production process of glulam sleeper was surface planing and trimming. At this point, surface planing was carried out to smooth the surfaces from adhesive beads that had been squeezed out of laminations during the gluing and clamping process. Next, glulam sleepers were cut into required dimension. Lastly, all glulam sleepers were wrapped (Fig. 7) with plastic cover to protect them against moisture and dust before being shipped for performance testing.

6 The Potential of Glulam Timber Sleepers from Malaysian Tropical Hardwood Timber

The key requirements to be met before any timber products can be deemed sufficient to be used as railway sleepers are strength characteristics. The American Railway Engineering and Maintenance-of-Way Association (AREMA) has established a set of requirements used to verify the suitability of the timber species used for railway sleepers through *compliance tests*. Based on the results obtained from *compliance tests*, it can be concluded that Kekatong timber glulams display excellent performance as railway sleepers since the all the glulams sleepers passed all the requirements stated in the AREMA [28].

Under laboratory condition, static and fatigue test which simulates the actual loading on-site was conducted at the Heavy Structural Laboratory, Universiti Teknologi MARA as in Fig. 8. The result shows that the strength performance of Kekatong glulam timber sleepers under static load condition is almost at par with the Kekatong solid timber and this indicates that these sleepers can be used as an alternative to the existing solid timber sleepers. The behaviour of Kekatong glulam

Fig. 7 Packaging of glulam timber sleepers

Fig. 8 Laboratory testing under static and fatigue loading

timber sleepers under the design train wheel load also demonstrated the safe margin value of displacement and can sustained more energy before failure occurred [27]. Under fatigue condition, these sleepers were able to resist fatigue resistance with adequate remaining residual strength after these sleepers were imposed with two million cycles of train simulation load [29].

Further investigation of field measurement on the performance and condition of Kekatong glulam sleepers was conducted at the track line in between Sentul and Batu Cave. The total length of this track is about 10 km with double line operation. This line was chosen due to heavy trains traffic by commuters, inter-city passengers and freight trains with estimated load cycles of 375,440 cycles per year. Based on field observations, these Kekatong glulam sleepers are still in good condition even after the sleepers have been installed at the respective track line for two years [30]. Early results from laboratory and field tests on the Kekatong glulam sleepers show that the glulam sleepers display promising potential as the alternative solution for solid timber or even PSC sleepers.

References

1. Anon (2006) International federation for structural concrete. fib bulletin 37: Precast concrete railway track systems, state-of-art report. Stuttgart
2. Silva A, Martins AC, Feio AO, Machado JS (2014) 'Feasibility of creosote treatment for glued-laminated Pine-timber railway sleepers J. Mater. Civ. Eng 1–11
3. AREMA (2012) Chapter 30, Volume 1 - Ties, The American railway engineering and maintenance-of-way association (AREMA) Manual Rail Eng
4. Bodig J, Jayne BA (1982) Mechanics of wood and wood composites. Van Nostrand Reinhold Company Inc., New York, USA

5. Buchanan A.H (1990) Bending strength of lumber. J Struct Eng 116(5):1213–1229
6. Carrasco EVM, Passos LB, Amorim STA, Ramos FM, Rodrigues FC, Mantilla JNR (2019) Glulam wood sleepers manufacturing from recycling discharge sleepers: an engineering recycling project. BioResources 14(3):5059–5070
7. Carrasco EVM, Passos LB, Mantilla JNR (2012) Structural behavior evaluation of Brazilian glulam wood sleepers when submitted to static load. Constr Build Mater 26(1):334–343. https://doi.org/10.1016/j.conbuildmat.2011.06.031
8. Ets Rothlisberger SA (2008) History and development of the wooden sleeper. www.corbat-holding.ch
9. Icimoto FH, et al. (2013) Glulam ties manufactured with Oocarpa pinus and polyurethane adhesive. In: Forest product society (ed.) international conference on wood adhesives 2013. Madison, WI: Curran Associates, Inc., pp. 600–607
10. Ferdous W, Manalo A (2014) Failures of mainline railway sleepers and suggested remedies - review of current practice. Eng Fail Anal 44:17–35. https://doi.org/10.1016/j.engfailanal.2014.04.020
11. Gallery D, Gauntt JC, Webb DA (1999) Progressively engineered hybrid wood crossties for the next century. In: The Roadmaster's conference proceedings of american railway engineering & maintenance-of-way association. Lanham, MD: American railway engineering and maintenance-of-way association (AREMA)
12. Gong M et al (2013) Use of low grade hardwoods for fabricating laminated railway ties. Constr Build Mater 41:73–78. https://doi.org/10.1016/j.conbuildmat.2012.11.114
13. González-Nicieza C et al (2008) Failure analysis of concrete sleepers in heavy haul railway tracks. Eng Fail Anal 15(1–2):90–117. https://doi.org/10.1016/j.engfailanal.2006.11.021
14. Gupta BL, Gupta A (2010) Railway engineering. Standard Publishers Distributors, New Delhi
15. Hamzah SH, Din K (2008) Appraisal of used wooden railway sleeper. J Eng Sci Technol 3 (3):224–233
16. International Federation for Structural Concrete (2006) fib bulletin 37: Precast concrete railway track systems, state-of-art report Stuttgart
17. International Union of Railways (UIC) (2013) Sustainable wooden railway sleepers France
18. KTMB (2005) Technical specifications. KTMB, Malaysia
19. Manalo AC et al (2010) A review of alternative materials for replacing existing timber sleepers. J Composite Struct 92:603–611
20. Manalo A.C (2011) Behaviour of fibre composite sandwich structures: a case study on railway sleeper application. University of Southern Queensland
21. Manalo A.C. et al. (2011) The effect of modulus of elasticity on the behaviour of railway turnout. In: Setunge S, et al. (eds) Incorporating sustainable practice in mechanics and structures of materials. London: Taylor& Francis Group London, pp 427–432. https://doi.org/10.1201/b10571-76.
22. McKenzie WMC (2004) Design of Structural Elements. Palgrave Macmillan, New York, USA
23. Mohamed AR (2012) 'Engineer of Permanent Way, KTMB in personal communication
24. MS 758 (2001) Glued laminated timber - performance requirements and minimum production requirements (First revision). Malaysia: Department of Standards Malaysia
25. MTIB (2010) 100 Malaysian timbers. 2010 Editi. Kuala Lumpur: Malaysian Timber Industry Board (MTIB)
26. Mundrey JS (2010) Railway track engineering, 4th edn. Tata Mc Graw Hill Education Private Limited, New Delhi
27. Norshariza MB, et al. (2013) Ultimate strength of Kekatong glued laminated timber railway sleepers. In: Hassan R. et al. (eds) The international civil and infrastructure egineering conference Springer, pp 97–105
28. Norshariza MB et al (2014) Structural behaviour of Kekatong glued laminated timber railway sleepers under sleepers static performance test. In: Kao JCM, Sung W-P, Chen R (eds) The 4th international conference on green building, materials and civil engineering (GBMCE) 2014. Taylor & Francis Group London, Hong Kong, pp 45–49

29. Norshariza MB, et al. (2016) Post-fatigue behaviour of Kekatong glued laminated timber railway sleepers. In: Yusoff M, Hamid NHA, Arshad MF, Arshad AK, Ridzua ARM, Awang H, (ed.) Proceedings of the international civil and infrastructure engineering conference (InCIEC 2015). Singapore: Springer, pp 819–832
30. Norshariza MB, et al. (2018) 'Performance study of laboratory and in-service kekatong glued laminated timber railway sleepers, WCTE 2018 - World Conference on Timber Engineering
31. Sadeghi J, Barati P (2012) Comparisons of the mechanical properties of timber, steel and concrete sleepers. Struct Infrastruct Eng Maintenance Manage Life-Cycle Des Perform 8 (12):1151–1159
32. Sonti SS et al (1995) A review of wood crosstie performance. Forest Products J 45(9):55–58. https://doi.org/10.1108/17506200710779521
33. The Engineered Wood Association (1999) Glulam in Railroad Construction. Washington
34. The Malaysian Timber Industry Board (2009) The Malaysian grading rules for Sawn Hardwood Timber. Kuala Lumpur: Malaysian Timber Industry Board (MTIB)
35. The Malaysian Timber Industry Board (no date) Malaysian Wooden Railway Sleepers. Kuala Lumpur: MTIB
36. Thelandersson S, Larsen HJ (2003) Timber engineering. John Wiley & Sons Ltd., England
37. Tiew J (2012) Operation manager, woodsfield Glulam manufacturing Sdn Bhd in personal communication
38. Webb DA (1998) The tie guide. handbook for commercial timbers used by the crosstie industry. Edited by Gauntt JC, Corallo DL, Fayetteville GA: Railway Tie Association.
39. Sanchez O (2009) Inspection of the Advanced Engineered Lumber Railroad Ties at the New Meadows Bridge. Maine
40. Qiao P, Julio FD, Michael GZ (1998) Modeling and optimal design of composite-reinforced wood railroad crosstie. J Compos Struct 41:87–96

Cement Stabilisation of Subgrade Soil for Sustainable Pavement Structure

Ahmad Kamil Arshad, Ekarizan Shaffie, Khairil Azman Masri, Ramadhansyah Putra Jaya, and Yulinar Ismail

Abstract Unsuitable or poor quality subgrade material requires proper treatment in order to make the subgrade suitable for overlying top layers of pavement for road construction. Stabilisation of the subgrade layer using cement is a method to improve the strength and stiffness of the subgrade, minimising the risk of road damage such as permanent deformation and improve the long-term performance of the pavement. This paper details a study on the soil–cement stabilisation method for a low-volume road in Malaysia. The scope of this study involved mix design in the laboratory and site verification. The laboratory tests involved soil classification, compaction test, unconfined compressive strength and California Bearing Ratio (CBR) tests while site verification tests comprised of field density test and unconfined compressive strength tests. From the laboratory tests, it was determined that the type of soil for the study area (silty clay) was suitable to be stabilised using cement based on the results obtained from soil classification test and unconfined compressive strength achieved of more than 0.8 MPa obtained after the addition of 5% cement by weight. Field density test achieved more than 95% laboratory com paction density and unconfined compressive strength of 1.01 MPa, indicating that the method was successfully implemented as site. It is recommended that future research should be carried out on more sites and on different types of soil to determine the suitability of cement as additive for subgrade stabilization in Malaysia.

Keywords Subgrade soil · Subgrade stabilisation · Cement stabilisation · Subgrade improvement · Sustainable material

A. K. Arshad (✉) · E. Shaffie
Institute for Infrastructure Engineering and Sustainable Management (IIESM)/Faculty of Civil Engineering, Universiti Teknologi MARA, 40450 Shah Alam, Selangor, Malaysia
e-mail: drahmadkamil@salam.uitm.edu.my

K. A. Masri · R. P. Jaya
Faculty of Civil Engineering and Earth Resources, Universiti Malaysia Pahang, Gambang, Malaysia

Y. Ismail
Public Works Department of Malaysia, Kuala Lumpur, Malaysia

1   Introduction

Subgrade is defined as the existing ground or that part of the embankment or cutting which is immediately beneath the subbase layer of the road pavement and shoulders [1]. In order to provide a good foundation for the road pavement structure, the type and condition of soil for the subgrade layer must be taken into consideration. Unsuitable or poor quality subgrade material requires proper treatment in order to make the subgrade suitable for overlying top layers of pavement for road construction. The higher strength and stiffness of the subgrade materials will minimize or avoid the risk of road damage such as permanent deformation and improve the long-term performance of the pavement. Hence, the design of pavements should include the improvement of existing subgrade materials to optimise their performance.

Soil stabilisation is one of the methods for subgrade improvement and can provide benefits such as reduction in pavement thickness, economic use of available materials, provides a stronger and more uniform platform for pavement construction and reduction in erosion and environmental problems [2]. Soil stabilisation is the process of blending and mixing additional materials with an existing soil to improve certain properties of the soil to meet the specified engineering requirements [3]. The process may include blending of soils and additives to achieve a desired gradation or the mixing of commercially available additives that may alter the plasticity, or act as a binder for cementation of the soil [3].

Types of soil stabilization include cementitious (using cement or lime) and bituminous stabilization (using foamed bitumen or emulsion) [4, 5]. Supplementary cementitious materials such as the use of fly ash, a pozzolanic material mixed with lime are also used to stabilise soils [5, 6]. In addition, proprietary chemical binders using polymer additives are also available for soil stabilization [5]. Stabilisation using cement is one of the most common techniques for stabilising existing material on site. Kamruzzaman et al. and Uddin et al. suggested that a minimum percentage of cement is required to improve the strength of the untreated clay [7, 8]. Chemical reaction by the presence of cement effect will increase in stiffness of the stabilised layer and would provide better load transfer to the pavement foundation underneath [9].

Particle size distribution and Atterberg limits are commonly used for preliminary assessment on the type of stabilization required for pavement subgrade. Figure 1 provides guidance on the form of stabilization required based on percentage of materials passing the 75 µm sieve and plasticity index [2]. It could be seen that cement stabilization is generally suitable for soils with less than 25% passing the 75 µm sieve. Table 1 shows typical cement contents for various types of soil for subgrade stabilization [2].

In Malaysia, soil stabilisation using cement is not commonly used for subgrade improvement of poor subgrade soils. One of the advantages of stabilising the soil is the possible reduction in the thickness of the road pavement, due to the higher stiffness achieved for the subgrade after the stabilisation. Presently, although there is a specification for road works [10], there is no specific guideline in Malaysia

	MORE THAN 25% PASSING 75μm			LESS THAN 25% PASSING 75μm		
Plasticity Index	PI ≤ 10	10 < PI <20	PI ≥ 20	PI ≤ 6 PI x % passing 75μm ≤ 60	PI ≤ 10	PI > 10
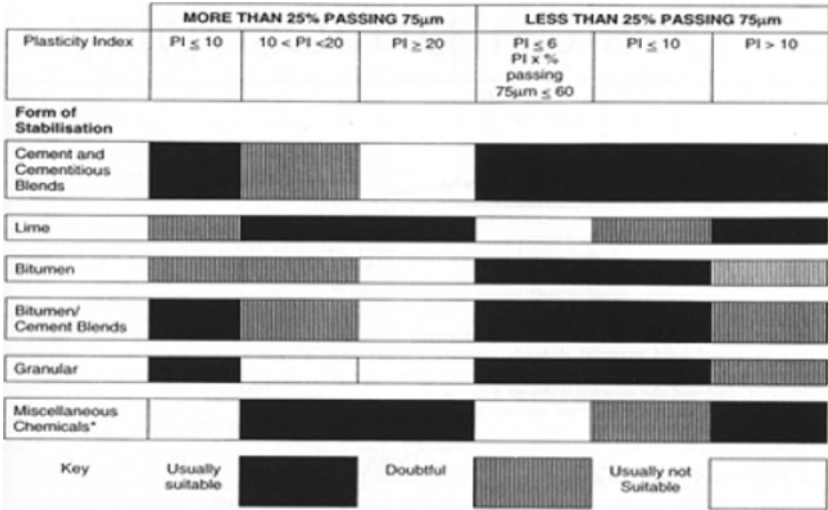
Fig. 1 Guide to selecting method of stabilisation [2]

Table 1 Typical cement content for various soil types in pavement construction [2]

Soil type	Cement requirement (% by mass)
Fine crushed rock	0.5–2
Well-graded sandy clay gravels	2–4
Well-graded sand	2–4
Poorly-graded sand	4–6
Sandy clay	4–6
Silty clay	6–8
Heavy clay	8–12
Very heavy clay	12–15
Organic soils	10–15

regarding the use of cement to stabilise the subgrade soil. However, the Public Works Department of Malaysia (PWD Malaysia) requires a minimum unconfined compressive strength of at least 0.8 MPa for stabilised subgrade [11].

A study on the soil–cement stabilisation method for a low-volume road located in a housing scheme known as Rimbunan Kasih in Dungun, Terengganu was carried out by PWD Malaysia. The objectives of this study are to determine the optimum percentage of ordinary portland cement to increase the strength of the soil; to evaluate optimum moisture content and maximum dry density of the soil cement mix; and to verify the strength and degree of compaction of the soil–cement on site.

2   Methodology

2.1   Laboratory Tests

Laboratory tests were carried out to determine the suitability of the soil to be
stabilised with cement and the amount of cement to be added to the soil. Field tests
were then carried out to verify the soil achieving the required properties after
construction.

Soil sample was obtained from the proposed site. The laboratory tests conducted
include soil classification (sieving and hydrometer analysis), Atterberg limits
(plastic and liquid limit), moisture content, standard Proctor compaction test and
California Bearing Ratio (CBR) test as per BS 1377:1990 [12].

Samples with different cement percentages by weight (3, 4 and 5%) were then
prepared. The maximum dry density (MDD) and optimum moisture content
(OMC) for the samples were determined. Samples were then prepared for uncon-
fined compressive strength test for the determination of the strength achieved at 3
and 7 days.

2.2   Construction Site Verification

For site verification two tests was conducted; field density test to verify that the
stabilized subgrade achieved more than 95% of the laboratory compaction density
and unconfined compressive strength test to verify that a minimum unconfined
compressive strength of at least 0.8 MPa was achieved for the stabilized subgrade
as required by PWD Malaysia [11].

Construction of Stabilized Subgrade. Mix in-place method was used in the
construction of the stabilised subgrade. The cement was first spread uniformly on
the subgrade at the designed dosage target of 5% cement by weight using a
mechanical spreader which automatically spread the required dosage on the surface
of the subgrade (Fig. 2). The dosage amount was checked by weighing the amount
of cement spread on a one square metre of canvas which was laid on the surface of
the subgrade before the dosage was applied. After the spreading was completed, dry
mixing of the cement and subgrade was carried out to a depth of 275 mm using a
stabiliser machine (Fig. 3). This machine has a row of paddles which blend the soil
and cement together in the mixing chamber. The mixing depth is manually checked
by manually measuring in a trench at the edge of the spreading area. The layer was
then trimmed with a grader (Fig. 4). After the dry mixing was completed, water was
then added on the surface of the mixed layer using a water spray distributor con-
nected to the water tanker. Immediately after water is sprayed on the surface, the
stabilizer machine was again used to pulverize the soil, for wet mixing throughout
the 275 mm depth of the soil layer. Steel drum roller was then used to compact the
soil layer (Fig. 5). An initial rolling was carried out without vibration to trim the

Fig. 2 Spreading of the cement using mechanical spreader

Fig. 3 Dry mixing process using stabiliser machine

Fig. 4 Trimming of the surface using grader

Fig. 5 Compaction using steel drum roller

surface level. This is then followed by final rolling to further compact and level the surface of the stabilised subgrade. The curing period for the stabilised subgrade is 7 days for the soil–cement mix to develop its strength.

3 Results and Discussion

3.1 Laboratory Tests

Laboratory tests were carried out to determine the suitability of the subgrade soil to be stabilised with cement and to determine the amount of cement to be added to the soil.

a) **Moisture Content**

The moisture content obtained for three samples tested are 17.18, 15.89 and 16.50%. The average moisture content obtained was 16.52%. The natural moisture content is to be compared with the optimum moisture content and the field moisture content during construction for moisture adjustments during field compaction stage.

b) **Particle Size Distribution**

The soil sample consists of 0.9% gravel, 20.51% sand and 78.6% fines (29.76% clay and 48.83% silt). The sample was classified as a fine grained soil based on the Unified Soil Classification System (USCS). The results for the particle size distribution are as shown in Fig. 6. Further classification using Atterberg limits is required for the determination of suitability to be stabilised with cement additive.
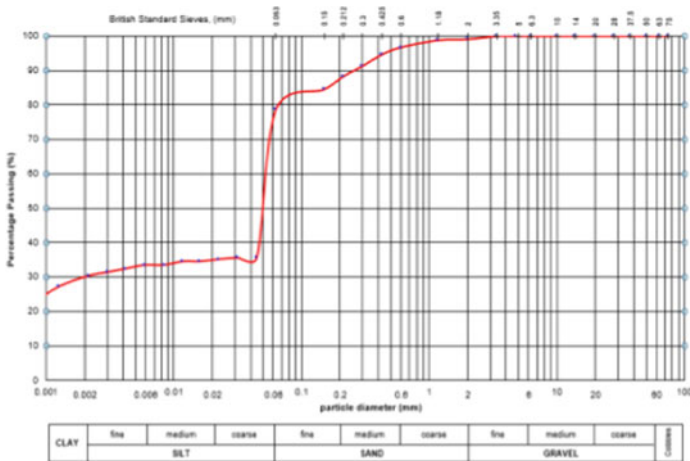
Fig. 6 Particle size distribution of soil

c) **Atterberg Limits**

The Liquid Limit (LL) of the soil sample is 11 while the Plastic Limit (PL) is 21. Therefore the Plastic Index (PI) is 10. Based on Unified Soil Classification System (USCS), the sample was classified as low plasticity. According to Austroads, for soils with plasticity index of less than or equal to 10, the suitable additive is cement [2, 5].

d) **Results for particle density of soil**

This test was performed to determine the specific gravity of soil by using a pycnometer. The specific gravity (Gs) was determined based on the procedures according to BS 1377- Part 2: 1990 [12]. The test was carried by preparing three samples. The average Particle Density obtained for samples was 2.68 Mg/m^3.

e) **California Bearing Ratio (CBR) Test**

Laboratory test was conducted to determine the CBR of soil samples. The CBR tests were conducted as per BS 1377: 1990 [12]. The CBR value for the samples tested at 2.50 mm penetration was 3.49% while at 5.00 mm penetration was 3.62% as shown in Table 2. As the CBR value of soil sample is less than 5%, PWD Malaysia requires that the soil be stabilised or treated to improve its stiffness [11].

f) **Unconfined Compressive Strength (UCS)**

From Table 3, it could be seen that the unconfined compressive strength of the soil increased progressively with the increase in the amount of cement added. The strength for the subgrade soil with 5% cement achieved the highest value of 0.76 MPa after 3 days curing and 0.80 MPa after 7 days curing. PWD Malaysia requires a minimum UCS of 0.80 MPa [11].

Table 2 CBR value at 2.50 mm and 5.00 mm penetration

Penetration (mm)	2.50	5.00
Load (kN)	0.46	0.72
Standard load (kN)	13.20	20.0
CBR (%)	3.49	3.62

Table 3 UCS after 3 days and 7 days curing

Cement contents	3%	4%	5%
UCS at 3 days (MPa)	0.30	0.46	0.76
UCS at 7 days (MPa)	0.40	0.51	0.80

g) **Selection of the additive**

The assessment for type of stabilisation was based on particle size distribution and Atterberg limits. According to Austroads, for soil samples with percentage passing 75 µm more than 25% and plasticity index of less than or equal to 10, the suitable additive is a cement [5]. It is also recommended by the Joint Departments of Army and Navy, USA that Portland cement is used and mixed intimately with fines fraction (<0.075 mm) for low plastic soil [13].

h) **Mix Design Parameter**

Based on the results obtained from the soil classification, which the percentage of particles passing 0.075 mm is more than 25%, plasticity Index (PI) less than or equal to 10 and UCS strength equal or more than 0.8 MPa, it was decided that 5% cement content is the required dosage/amount of cement for the existing soil on chosen site.

i) **Compaction Characteristics**

Standard Proctor tests were performed for the subgrade soil added with 5% cement content by weight to determine the maximum dry density and optimum moisture content. From the tests as shown in Fig. 7, the optimum moisture content for the soil with 5% cement mix is 12.50% and the maximum dry density is 1.987 Mg/m^3. For construction of the stabilised subgrade, field density test should achieve at least 95% of the laboratory compaction maximum dry density.

3.2 Site Tests for Verification of Specification Requirements

Field density tests and unconfined compressive strength tests were carried out to verify that the requirements of the specifications were achieved during the construction of the stabilised layers.

a) **Field Density Test and Moisture Content**

After compaction work was completed, the field density tests were carried out at two randomly selected locations along the stabilised area to measure the degree of the compaction. The percentage of compaction is defined as the ratio of in-place dry density of soil to the laboratory maximum dry density that was obtained from the Proctor test. The dry densities achieved were 1.929 Mg/m^3 and 1.900 Mg/m^3. The degrees of the compaction achieved are 97 and 95.6% which is higher than specification requirement of 95% as required in PWD Malaysia's Standard Specification for Road Works [10]. The corresponding moisture contents were determined by Calcium Carbide Gas Pressure Moisture
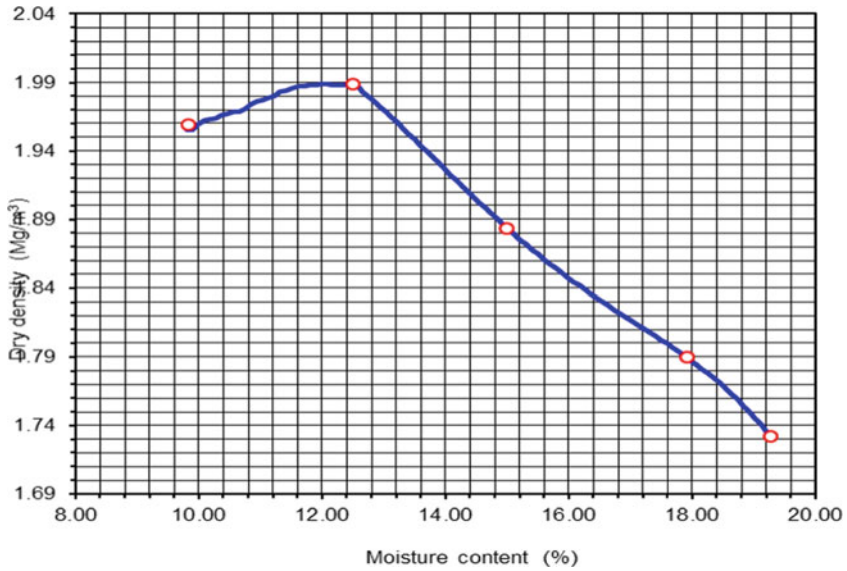
Fig. 7 OMC and MDD for soil with 5% cement added

Tester (Speedy Moisture Tester) on site. The moisture content determined on site is lower than moisture content that obtained from the laboratory test by 12.5%.

b) **Unconfined Compressive Strength**
The compressive strength is indicative of the degree of reaction in the soil–cement-water mixture based on the rate of hardening of the mixture. Table 4 shows the results of the UCS test at 7 days. The average result obtained for the Unconfined Compressive Strength (UCS) test of soil cement mix sample is 1.01 MPa, which is higher than the minimum 0.8 MPa required by PWD Malaysia [11].

Table 4 The result of UCS test at 7 days

	Compressive strength (MPa)				Average (MPa)
Samples	1	2	3	4	
UCS (MPa)	1.09	0.97	0.98	0.98	1.01

4   Conclusion

Stabilisation of the subgrade layer using cement is a method to improve the strength and stiffness of the subgrade, minimising the risk of road damage such as permanent deformation and improve the long-term performance of the pavement. The silty clay soil for the study area with plasticity index value of less than 10 and fine material of more than 25% is suitable for cement stabilisation. The results from unconfined compressive strength during mix design stage showed that the strength of soil cement mix increases proportionally with increasing cement content. The amount of cement content (5%) added to soil sample obtained (0.8 MPa) complied with the minimum UCS value requirement by PWD Malaysia for stabilised subgrade. The average unconfined compressive strength (UCS) for site samples carried out after 7 days curing is 1.01 MPa, which is higher than the strength obtained from laboratory test (0.8 MPa) and complies with PWD Malaysia's requirement. The subgrade stabilised was compacted to a minimum of 95% of maximum dry density as required in the specification. The degree of compaction obtained at site is 97 and 95.6%, higher than the minimum 95% required in the specification. It can be concluded that cement stabilisation was successfully carried out for the study area based on the results obtained.

References

1. PWD Malaysia (2013) Standard Specification For Road Works - Section 2: Earthworks (JKR/SPJ/2013-S2). Kuala Lumpur: PWD Malaysia
2. Austroads (2009) Guide To Pavement Technology Part 4I: Earthworks Materials. Austroads, Sydney
3. Sherwood P (1993) Soil Stabilisation with Cement and Lime: State of the Art Review. TRL, London
4. Jones D, Rahim A, Saadeh S, Harvey JT (2010) Guidelines for the Stabilization of Subgrade Soils in California. University of California, Davis
5. Austroads (2019) Guide To Pavement Technology Part 4D: Stabilised Materials. Austroads, Sydney
6. Fauzi A, Nazmi WM, Fauzi UJ (2010) Subgrade Stabilisation of kuantan clay using fly ash and bottom ash. In: Proceedings of the 8th international conference on geotechnical and transportation engineering geotropika 2010, Kota Kinabalu, Malaysia
7. Kamaruzzaman AHM, Chew SH, Lee FH (2001) Behaviour of soft Singapore marine clay treated with cement. ASCE Geotech Special Publication No. 113, 472–485
8. Uddin K, Balasubramaniam AS, Bergado DT (1997) Engineering behaviour of cement-treated Bangkok soft clay. J Geotech Eng 2891:89–119
9. Abdulhussein SK, Kassim KA, Nur H (2014) Physicochemical characterisation of cement treated kaolin clay. J Croatian Assoc Civil Eng 6(2014):513–521
10. PWD Malaysia (2008) Standard Specification For Road Works - Section 4: Flexible Pavement (JKR/SPJ/2008-S4). PWD Malaysia, Kuala Lumpur

11. PWD Malaysia (2013) Design Guide for Alternative Pavement Structures: Low-Volume Roads (JKR 21300-0025-12). PWD Malaysia, Kuala Lumpur
12. British Standards Institution (1990) Methods of Test for Soils for Civil Engineering Purposes (BS1377:1990). BSI, London
13. Joint Dept. of the Army and the Air Force (1994) Soil Stabilisation for Pavements. (TM 5–822–14/AFJMAN 32–1019). Washington D.C.: Joint Departments of the Army and the Air Force, U.S.A.

Inclusion of Palm Oil Fuel Ash (POFA) as Micro Engineered Material (MEM) in Ultra High Performance Concrete (UHPC)

M. S. Muhd Norhasri, A. R. Muhammad Faiz, I. Shafienaz, H. Mohd Shafee, M. A. M. Fauzi, and J. Nurliza

Abstract This study is to determine the workability and strength properties of Ultra-High-Performance Concrete (UHPC) with the incorporation of Palm Oil Fuel Ash (POFA) as Micro Engineered Material (MEM), which relates to the usage of industrial waste for sustainability. In this research, the MEM was assessed in UHPC through 48 numbers of 100 mm cube samples. POFA as MEM is partially used as cement replacement from 2.5, 5.0 and 7.5% by cement weight. The workability of UHPC was assessed by conducting slump test and flow table test whereas compressive strength test was carried out for samples taken at 1, 3, 7, and 28 days of curing. The optimum percentage of POFA was marked at 5% with compressive strength of 139 MPa at day 28. Moreover, the 5% mix of MEM also recorded the optimum fresh properties with slump reading of 265 mm and flow table of 640 mm as compared to the other UHPC samples. In conclusion, POFA as MEM enhanced the fresh and hardened properties of UHPC by producing dispersion particles of cement and enhanced the binder properties with cement.

Keywords Micro engineered material · UHPC · POFA · Slump · Flow · Compressive strength

1 Introduction

In Malaysia, the agriculture sector remains as an important in economy sector by contributing RM55.9 billion to Malaysia 's GDP in 2013 and the sector employing 1.7 million workers [7], Raja [11]. That being said, oil palm is one of the most important products from Malaysia that has helped to shape and change the agriculture and

M. S.M. Norhasri (✉) · H. M. Shafee · M. A. M. Fauzi · J. Nurliza
Institute for Infrastructure Engineering and Sustainable Management (IIESM), Universiti Teknologi MARA, 40450 Shah Alam, Selangor, Malaysia

A. R.M. Faiz · I. Shafienaz
Faculty of Civil Engineering, Universiti Teknologi MARA, 40450 Shah Alam, Selangor, Malaysia

economy landscape in the country. The palm oil industry not only produced a very large amount of crude palm oil for the usage in the country and export, but also equivalent amount of solid waste in the process [5, 14]. These solid wastes include oil palm trunks (OPT), oil palm fronds (OPF), empty fruit bunches (EFB) and palm pressed fibers (PPF), palm shells, palm oil mill effluent palm (POME) and not to forget palm oil fuel ash (POFA). These solid wastes can bring harm to the environment if not disposed properly and possibly bring harm to human health [1, 2, 7, 13].

Eventually, the wastage from palm oil industry will increase. Later, this will become a major problem in this country when the waste is not recyclable and not reusable. By dumping the solid waste improperly, it can cause health problems and environmental issues. To avoid this event from happening, usage of these waste to produce a new potential design concrete mix to optimize the large amount of solid waste from keep piling up at the landfill area.

In recent years, the usage of recycled solid waste materials from the agriculture industry has grown its popularity and its rapid developing as the regulations increasingly concerned with environmental problems. This is a good initiative by the construction industry considering the large amount of solid waste from palm oil industry. There are also a decent number of researches on different materials in cement as supplementary material to enhance the concrete strength such as palm oil fuel ash (POFA), which will eligible to reduce the solid waste produced and ultimately, saving the earth [4, 9]. More than two million tons of solid waste of palm oil residue is produced every year. By utilizing the solid waste produced, we not just only help the mother earth but also create a new mix of concrete that is useful to the construction industry.

As we all know, the common ultra-high performance concrete (UHPC) includes the usage of silica fumes [6, 12]. In the first world country, silica fumes might be easy to obtain and relatively cheap or affordable, but in Malaysia, it is expensive. Other than safety, cost also need to be taken into account in the construction industry. So, replacing silica fumes with palm oil fuel ash (POFA) is not only save the environment, but also to save cost using what already have and it is free [3, 10].

By optimizing POFA into construction industry, we will not only be able to reduce the waste generated from palm oil industry but also can decrease the amount of waste dumped into dumping area. By commercializing POFA, not only the cost of construction can be decrease as the cost of buying POFA is zero as it is a waste but can decrease the amount of dumping area needed for dumbing waste like POFA and finally, promotes better environmental solution. The purpose of this research is to study the workability and strength properties of ultra-high performance concrete with the inclusion of POFA.

2 Methodology

2.1 Procurement of POFA

Palm oil fuel ash (POFA) is one of the industrial by-products from the palm oil industry. By utilizing materials from industry waste, we not only be able to reduce environmental pollution of the surrounding but also cutting the overall cost of the construction by using material that is free instead of buying one. Due to its pozzolanic content, POFA can be safely used in concrete as a partial replacement for cement. For this research, POFA is taken from Nibong Tebal Palm oil factory, which is located in Pulau Pinang.

2.2 Water-Cement Ratio

The design for water to cement ratio in this research is fixed to 0.2. Water supplied from tap water in concrete laboratory. Cement was procured from YTL cement. Cement was used in this research is Ordinary Portland Cement (OPC).

2.3 Mix Proportion

This experiment was used a modified design mix which was originally created by (Norhasri et al. [8]) which utilize the usage of POFA. For this experiment, cement was replaced with POFA with ascending order percentage of cement weight. Table 1 below shows the mix proportion used in this study.

Table 1 Design mix used in this research

Mix	Cement (kg/m^3)	Fine aggregate (kg/m^3)	Coarse aggregate (kg/m^3)	SP (kg/m^3)	Water (kg/m^3)	POFA (kg/m^3)
OPC	800	433	800	16	160	-
P2.5	760	433	800	16	160	40
P5.0	720	433	800	16	160	80
P7.5	680	433	800	16	160	120

Table 2 Number of samples required

Mix	1 day cured	3 day cured	7 day cured	28 day cured
OPC	3	3	3	3
P2.5	3	3	3	3
P5.0	3	3	3	3
P7.5	3	3	3	3

2.4 Number of Sample

Total number of samples that needs to be prepared for this experiment is 48 samples of cubes. Proportion for each day cure is 12 samples of cubes. The sample cured in water and tested at age of 1, 3, 7, and 28 day of curing. Table 2 shows the number of samples for this research.

2.5 Fresh Properties

In this research, two tests were conducted to determine the fresh properties of MEM in UHPC. Slump test and flow table test were conducted for fresh samples of UHPC immediately after mixing and procedure of the test is according to BS EN 12,350–2:2019 and BS EN 12,350–5:2019 respectively.

2.5.1 Slump Test

The strength of concrete of a given mix proportion is seriously affected by the degree of its compaction. It is therefore important that the consistency of the mix is such that concrete can be transported, placed and finished sufficiently easily and without segregation. A concrete satisfying these conditions is said to be workable. Slump test is carried out to represent the workability of fresh concrete. The procedure to carry out slump test is after the fresh concrete finish mixed; the fresh concrete was poured into cone as one layer. The fresh concrete then being tamp 25 times on that first layer using tamping rod. The steps then are repeated for the next layer until fresh concrete is full within the cone. Next, the cone is lifted vertically slowly and the cone is placed beside the free slump. The difference between free slump and cone was recorded. This test is according to BS EN 12,350–2:2019.

2.5.2 Flow Table Test

Flow table test or flow test is a method to determine consistency of fresh concrete. It is used primarily for assessing concrete that is too fluid to be measured using the slump test because the concrete will not retain its shape when the cone is removed. First step of conducting flow table test is wetting the flow table. After the flow table is wet, a cone is later placed in the center of the flow table. Then fresh concrete is filled into the cone. The cone then was let 30 s before it can be lifted. After the cone is lifted, the flow table then lifted vertically. This allows the fresh concrete to flow. The table will give out diameter for X-axis and Y-axis. The final value of flow table diameter is taken by the average value from X-axis and Y-axis measured on the flow table. This test is according to BS EN 12,350–5:2019.

2.6 Mechanical Properties

2.6.1 Compression Test

Compressive strength is the capacity of a material or structure to withstand loads. Compressive strength test is conducted to determine the maximum load that a concrete can withstand. The strength of concrete is depending on the design and material mixing of the concrete itself. To conduct compressive strength test, concrete sample cubes are taken out from cure pond and was let to dry up. Sample cubes must be free from any impurities. The sample cubes later placed inside room temperature to let excessive water to evaporate. After that, the sample cubes placed at the center of the bearing surface inside the compression test machine and set up a constant compression rate of 6.8 kN/sec. The compression was applied at the center of the sample cubes and the machine door is closed before the machine is being run. Data is recorded and tabulated. The procedure to conducting test is accordance to BS EN 12,390–3:2019.

3 Result and Discussion

This sub-topic was presented the results and necessary discussion from the result that was obtained during the laboratory test that has been done on the cube samples. There are two perimeters that been investigated during this experiment which is the use of POFA as the supplementary cementitious material, i.e. the workability of the fresh concrete and the compressive strength of the hardened concrete. For these achieved, a total of 48 UHPC cube samples representing the control sample, 2.5%

POFA, 5.0% POFA and 7.5% POFA in the size of $100 \times 100 \times 100$ mm cube sample at 1, 3, 7 and 28 days curing have been prepared. For every day test, three cubes from each types of sample are required to be tested, so that the average value can be taken in order to reduce the distributing factor and also to get the most accurate value amongst the three samples.

3.1 Workability of Fresh Concrete

3.1.1 Slump Test

Slump test is the number one of the laboratory testing that being carried out on fresh concrete to check for workability. The slump test results for the samples using POFA as cement replacement materials with the additives of superplasticizer are tabulated in Table 3 and drawn in Fig. 1.

Based on the Table 3 and Fig. 1, the slump value for control sample containing zero percentage of POFA is 250 mm. For sample which containing 2.5% of POFA, the slump value is 255, and 5 mm more than control sample. As the percentage of POFA increases to 5.0 and 7.5%, the slump values also increase to 265 and 270 mm respectively. Throughout all four samples, slump value of control sample is the lowest amongst all and increases as the percentage of POFA in the sample increases.

3.1.2 Flow Table Test

Flow table test is another laboratory test that being carried out to fresh concrete on this research to check for workability. The flow table test results are shown in Table 4 and Fig. 1.

Table 3 Slump test results for MEM in UHPC

Percentage of POFA (%)	Slump (mm)	Workability
0	250	Fine
2.5	255	Moderate
5.0	265	Good
7.5	270	Very Good

Table 4 Slump test results for MEM in UHPC

Percentage of POFA (%)	Slump (mm)	Workability
0	250	Fine
2.5	255	Moderate
5.0	265	Good
7.5	270	Very Good
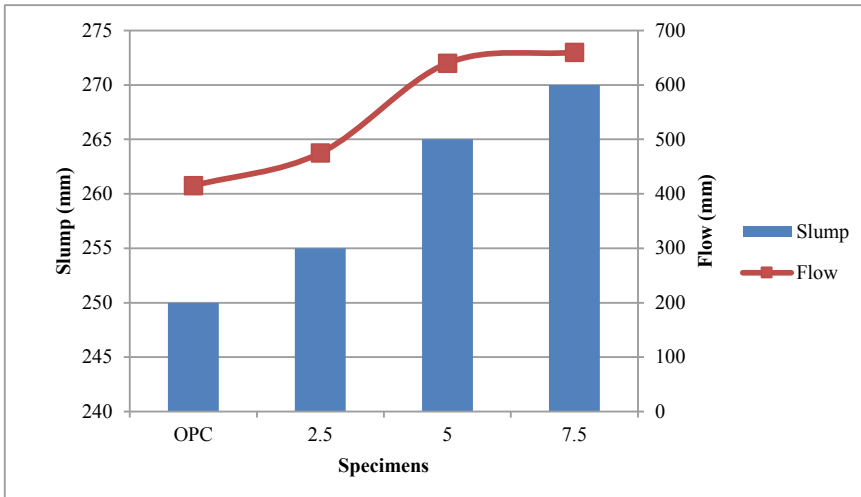
Fig. 1 Fresh properties for POFA as MEM in UHPC

Based on Table 4 and Fig. 1, it clearly shows that control sample of fresh concrete gives out average value of 415 mm diameter on the flow table. For fresh concrete sample containing 2.5% of POFA, average diameter of flow table is 475 mm, there is slight increase diameter in flow table. Next, average diameter for flow table for sample containing 5.0% of POFA is 640 mm. Finally, sample containing 7.5% of POFA recorded value for flow table at 660 mm in diameter.

Workability of fresh concrete improves as percentage of POFA in sample increases. This is majorly because of the mixture of POFA with the help from superplasticiser (Masterglenium Ace 8538) resulting in improvement workability of fresh concrete. Concrete that mixed with POFA produces low water absorption and with the addition of superplasticizer, it improves workability more. POFA improves ability of fresh concrete to flow and make fresh concrete easier for placement and compaction.

In addition, size of POFA used in this research was in micro level which is 4 micron. The action taken by POFA is similar to the normal pozzolanic reaction. It can be concluded that, the inclusion of POFA engineered the action of filler by its micro size. The micro size of POFA disperse the cement particles and resulting in high fluidity which produces high slump and flow of all mix of MEM with the inclusion of POFA. Furthermore, the shape and surface texture of POFA which in rounded formation contributes to the good inhesion between the cement particles and allows water to bind cement easily and faster with the ease of superplasticizers. From Fig. 1 portraits that the optimum replacement for POFA in UHPC is marked at 5% with respect to slump and flow results. This confirms the effectiveness of having POFA in the UHPC mix to enhance the effect of fresh properties. However,

due to its finer particles, it is suspected that beyond 5% of POFA the effect of slump and flow may be reduced due to its ability of POFA to absorb water. Since the higher replacement of POFA can be tailored in normal concrete mix, but in high cement content such as high performance concrete and also UHPC the effect in fresh properties is not successful.

3.2 Compressive Strength of Concrete

For this research, the compressive strength of the concrete was also taken. Figure 2 shows the results of compressive strength test that being carried out on 100 mm^3 cube between control sample and the POFA samples at 1, 3, 7 and 28 days of curing. From the results, sample with highest compressive strength and optimum percentage of POFA was determined.

As shown in Fig. 2, the enhancement of compressive strength is recorded at early age which marked by 5%, OPC, 2.5% and 7.5% with 78, 69, 55 and 48 MPa respectively. This confirms on the early strength effect which is cause by high calcium in the POFA which accelerate the engineered formation of Calcium Silica Hydrate (CSH). This effect is followed by day 3 until day 28 and the optimum compressive strength recorded by 5%, OPC, 7.5% and 2.5% mix with 139, 131, 117 and 109 MPa respectively. The enhancement of strength properties is promoted by engineered action of silica and alumina in POFA when combines with calcium hydroxide in cement at age 3 and 7. Furthermore, the continuous strength is
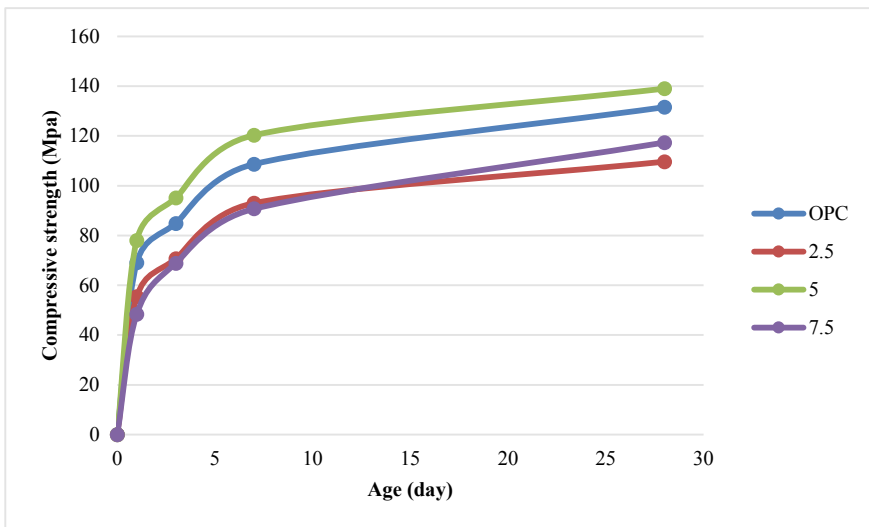
Fig. 2 Compressive strength for NEM POFA in UHPC

contributed by the reaction of pozzolanic action which caused engineered formation of hydration products. This action is the main factor in promoting later strength effect cause by POFA especially at day 28 is the reaction of pozzolanic reaction from POFA itself.

4   Conclusions

From this research, the utilization of POFA as micro engineered material in enhancing UHPC properties. The action engineered by POFA, which is high in silica and calcium, is as filler, promoting hydration product by engineered the transformation of Calcium Hydroxide and finally promoting pozzolanic reaction.

References

1. Alsubari B, Shafigh P, Jumaat MZ (2016) Utilization of high-volume treated palm oil fuel ash to produce sustainable self-compacting concrete. J Cleaner Prod 137:982–996. https://doi.org/10.1016/j.jclepro.2016.07.133
2. Hamada HM, Yahaya FM, Muthusamy K, Jokhio GA, Humada AM (2019) Fresh and hardened properties of palm oil clinker lightweight aggregate concrete incorporating Nano-palm oil fuel ash. Constr Build Mater 214:344–354. https://doi.org/10.1016/j.conbuildmat.2019.04.101
3. Hossain MM, Karim MR, Hasan M, Hossain MK, Zain MFM (2016) Durability of mortar and concrete made up of pozzolans as a partial replacement of cement: a review. Constr Build Mater 116:128–140. https://doi.org/10.1016/j.conbuildmat.2016.04.147
4. Huseien GF, Tahir MM, Mirza J, Ismail M, Shah KW, Asaad MA (2018) Effects of POFA replaced with FA on durability properties of GBFS included alkali activated mortars. Constr Build Mater 175:174–186. https://doi.org/10.1016/j.conbuildmat.2018.04.166
5. Jafer HM, Atherton W, Sadique M, Ruddock F, Loffill E (2018) Development of a new ternary blended cementitious binder produced from waste materials for use in soft soil stabilisation. J Cleaner Prod 172:516–528. https://doi.org/10.1016/j.jclepro.2017.10.233
6. Jin X, Li Z (2003) Effects of Mineral Admixture on Properties of Young Concrete. J Mater Civ Eng ASCE 15:435–442. https://doi.org/10.1061/(ASCE)0899-1561(2003)15:5(435)
7. Lim NHAS, Ismail MA, Lee HS, Hussin MW, Sam ARM, Samadi M (2015) The effects of high volume nano palm oil fuel ash on microstructure properties and hydration temperature of mortar. Constr Build Mater 93:29–34. https://doi.org/10.1016/j.conbuildmat.2015.05.107
8. Muhd Norhasri MS, Hamidah MS, Mohd Fadzil A, Megawati O (2016) Inclusion of nano metakaolin as additive in ultra high performance concrete (UHPC). Constr Build Mater 127:167–175

9. Nik Daud NN, Mohammed AS (2014) Material characterization of palm oil fuel ash (POFA) mixed with granite residual soil. Adv Mater Res vol 955–959. https://doi.org/10.4028/www.scientific.net/AMR.955-959.2093

10. Owaid HM, Hamid R, Taha MR (2014) Influence of thermally activated alum sludge ash on the engineering properties of multiple-blended binders concretes. Constr Build Mater 61:216–229. https://doi.org/10.1016/j.conbuildmat.2014.03.014

11. Raja Zulkefli, RNA, Yaacob H, Putra Jaya R, Warid MNM, Hassan N, Hainin MR, Idham MK (2018) Effect of different sizes of palm oil fuel ash (POFA) towards physical properties of modified bitumen. In: IOP Conference Series: Earth and Environmental Science, vol 140. https://doi.org/10.1088/1755-1315/140/1/012108

12. Sabir B, Wild S, Bai J (2001) Metakaolin and calcined clays as pozzolans for concrete: A review. Cement Concr Compos 23(6):441–454. https://doi.org/10.1016/S0958-9465(00)00092-5

13. Usman J, Rahman A, Sam M, Hussin MW (2017) Behavior of palm oil fuel ash and metakaolin ternary blend cement mortar at elevated temperatures. J Mater Civil Eng 29(2):1–8. https://doi.org/10.1061/(ASCE)MT.1943-5533.0001722

14. Zarina Y, Mustafa Al Bakri AM, Kamarudin H, Nizar IK, Rafiza AR (2013) Review on the various ash from palm oil waste as geopolymer material. Rev Adv Mater Sci **34**(1):37–43

Earthquake Fuse Bar as Smart Material in Improving Seismic Performance of Beam-Column Joint During Earthquakes

N. H. Hamid, N. F. D. Hadi, and I. F. Azmi

Abstract Earthquake fuse bar with 600 mm long and reduce diameter of 12 mm at the center with 200 mm long is designed using Eurocode 8 to cater earthquake excitation with Peak Ground Acceleration (PGA = 0.3 g) under Ductility Class Medium (DCM). It is placed at corners, exteriors and interiors beam-column joints of RC buildings. Lateral strength capacity, stiffness and ductility are increases while equivalent viscous damping reduces when installing fuse bars in corner beam-column joint. Experimental results show that fuse bar can perform better as compare with beam-column joint without fuse bars. Therefore, it is recommended that earthquake fuse bar should be installed in beam-column joint of RC buildings that exposed to moderate and severe earthquake excitations.

Keywords Seismic performance · Lateral strength capacity · Fuse bar · Ductility · Stiffness · Equivalent viscous damping

1 Introduction

West Malaysia is exposes to far-field earthquakes while East Malaysia affected by near-field earthquakes. Far-field earthquake threats to West Malaysia usually come from neighboring countries such as North Sumatera, Nias Island and Jawa Island. Whereas, the near-field earthquake in Sabah comes from two active fault lines known as Mensaban fault and Lobou-lobou fault. Furthermore, most of the RC buildings in Malaysia were designed using BS8110 (non-seismic code of practice) [1] where there is no provision for earthquakes at all especially for RC

N. H. Hamid (✉) · I. F. Azmi
Institute For Infrastructure Engineering Sustainable and Management (IIESM),
Universiti Teknologi MARA, 40450 Shah Alam, Selangor, Malaysia
e-mail: norha454@uitm.edu.my

N. F. D. Hadi
Faculty of Civil Engineering, Universiti Teknologi MARA, 40450 Selangor, Shah Alam,
Malaysia

buildings. There were many structural damages occurred during the 2015 Ranau Earthquake to the school buildings, hospitals, mosques, homestays and houses. Subsequently, the future buildings need to be designed using Eurocode 8 to cater for seismic load in Sabah regions. Hence, one of the innovate method to reduce the structural damages of RC buildings is to incorporate fuse bars in the beam-column joints by using high yield threaded rods and trimmed at the middle rod to a small diameter which reacts as fuse when earthquake strike.

Earthquake fuse bar is one of the earthquake protective systems that aids in improving seismic response of a structure under earthquake excitation without over designing it. It is also can consider as passive damper because it can absorb the extra seismic energy and reduce the energy dissipation on primary structural members [15]. Furthermore, many researchers had proved the concept of designing some sacrificial members dissipating the seismic energy while preserving the integrity of other main components is known as the earthquake fuse bars [5, 6]. There are many types of earthquake fuse bars can be applied to different types of structures such as wall, RC frame, steel frame, and beam-column joint [12]. The most common earthquake fuse bars used in frame or connections are steel plates [2, 18] and wall panels [10, 13, 16]. These fuse bars are varying in terms of capacity, condition, application and materials. The use of steel bars as energy dissipating fuse in walls are quite popular. Marriott et al. 2008 incorporated four walls with an alternative dissipation solution and experimentally tested them under in-plane lateral cyclic loading.

The performance of full-scale of six precast hollow core walls with longitudinal unbounded pre-stressing tendons and a pair of fuse bar located at the middle of the wall tested under in-plane quasi-static reverse cyclic loading [7–9]. Rahman and Restrepo [16] implemented a similar concept where they studied the performance of cantilever wall with prestressed unbonded tendons and equipped with energy dissipators. Christopoulos et al. [4] incorporated the usage of fuse bar as energy dissipator in Post Tension Energy Dissipator of steel joint and providing a self-centering response along with 22 mm diameter No. 7 Dywidag bars. Palermo et al. [13] applied the concept of structural fuse of energy dissipator in a hybrid Laminated Veneer Lumber (LVL) beam-column joint. The LVL external joint is equipped with unbonded post-tensioned tendon along the beam. The mild steel bars with a reduced section located at the critical beam-column interface as energy dissipators. It was found that the method of incorporating fuse bars in the structure is the most effective and appropriate method to reduce structural damages to the buildings especially in achieving the medium class ductility. However, the idea of using unbonded fuse bars as energy dissipator by embedded it inside the reinforced beam-column joint need to consider for the purpose of aesthetic values. The concept of using mild steel or high yield steel as fuse bars give more economical and sustainable approach in Malaysian construction industries. However, in this paper only corner beam-column joint with fuse bars will be presented, discussed and elaborated because this joint is considered as the most critical joint as compared to exterior and interior beam-column joints.

2 Design Earthquake Fuse Bar for Corner Beam-Column Joint

The concept of capacity design approach is uses in designing the earthquake fuse bar corner beam-column joint. Capacity Design is a design process in which it is decided which objects within a structural system will be permitted to yield (ductile components) and which objects will remain elastic (brittle components). Paulay and Priestley [14] illustrate the principle of capacity design as ductile chain as shown in Fig. 1. The idea is that the ductile link yields at a load that is well below the failure load of brittle links. In this paper, the ductile link is refers to the earthquake fuse bars allows to dissipate energy and the brittle link is beam in the RC frame which designed using Eurocode 8.

The earthquake fuse bar is designed to be ductile and yield earlier than the brittle link is refers to the beam. It is also the designed based on the lateral strength capacity of the structures to resist earthquake excitations. The Monolithic Beam Analogy (MBA) and the procedure of moment-rotation analysis for ductile structures was adopted for determining the lateral capacity of structures associates with the diameter of earthquake fuse bars. All the calculations regarding the moments, lateral forces, lateral displacements and diameters of fuse bars were performed using Microsoft Excel Spreadsheet. Figure 2 shows the simulation of lateral load versus displacement for different sizes of fuse bars. Previous study by Kay Dora and Hamid [11] found that the maximum lateral capacity of the corner beam-column joint under in-plane lateral cyclic loading is 85 kN. Hence, the appropriate size of fuse bars to suit with 85 kN lateral load is 12 mm in diameter as shown in Fig. 2. Subsequent, the high yield reinforcement bar with 16 mm diameter was trimmed into 12 mm at the center with 200 mm long as shown in Fig. 3. It is important to determine the physical and mechanical properties of the earthquake fuse bars before testing in the laboratory. Table 1 tabulates the overall dimension of 600 mm, 200 long with reduced diameter of 12 mm and mechanical properties of the fuse bars. A total numbers of 8 fuse bars will be placed inside the corner beam-column joint before testing them under in-plane lateral cyclic loading. The super-assemblage of corner beam-column joint consists of foundation beam, column, one in-plane beam and one out-of-plane beam will be constructed in Heavy Structural Laboratory,
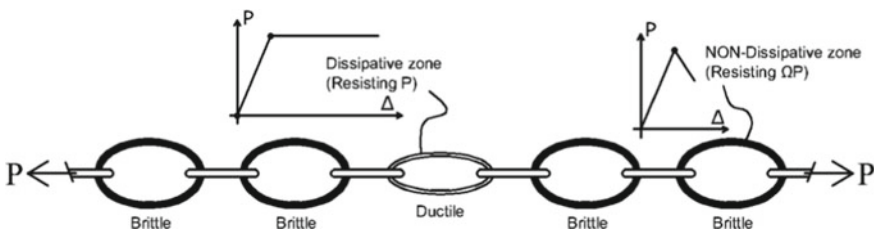
Fig. 1 Capacity design by ensuring the ductile links weaker that brittle links [14]
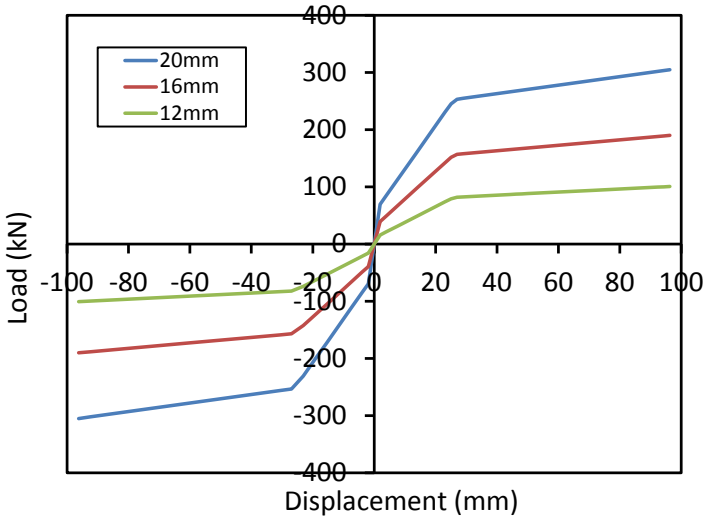
Fig. 2 Simulation of Spreadsheet Excel for different size of fuse bars
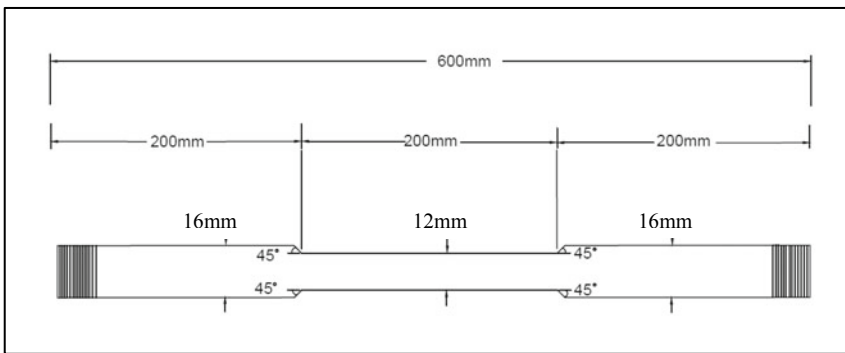
Fig. 3 Dimension of fuse bar with 16 mm diameter with a reduced section of 12 mm.

Table 1 Dimensions and properties of earthquake fuse bar

Total fuse bars	Length of fuse bars (mm)	Diameter of fuse bar (mm)	Reduced diameter (mm)	Young's Modulus (GPa)	Yield Stress (MPa)	Yield strain
8	600	16	12	200	533	0.00265

Faculty of Civil Engineering, Universiti Teknologi MARA, Shah Alam, Selangor. Figure 4 shows the column, in-plane beam and out-of-plane beam was labeled as Column 1, Beam 1 and Beam 2. All the structural elements were designed using
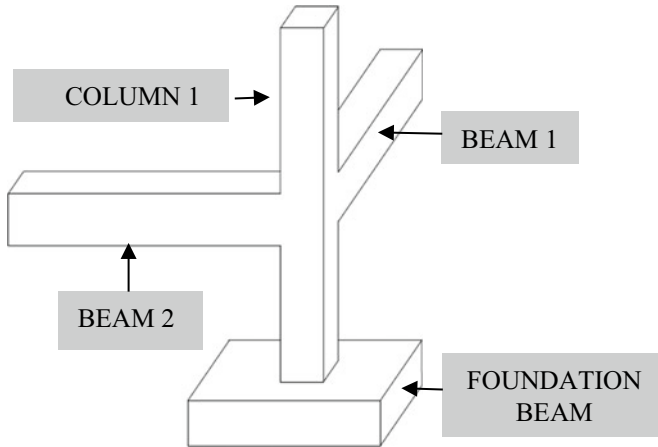
Fig. 4 Three dimensions of corner beam-column joint

Eurocode 8 with concrete Grade 50 and high yield strength steel reinforcement bar. The dimension of the foundation beam is $1800 \times 900 \times 500$ mm, beam is $400 \times 400 \times 3500$ mm and column is $400 \times 400 \times 3500$ mm.

3 Construction of Corner Beam-Column Joint

The construction processes of full-scale two beams and one column were started by preparing the reinforcement bar caging for Beam 1 and Beam 2. Earthquake fuse bars and transverse rebar were securely tied together at the corner beam-column joint of RC building as shown in Fig. 3. Figure 3(a) demonstrates on how to locate eight numbers mechanical couplers at each end of longitudinal reinforcement bars which located inside the beam's formwork. Meanwhile, Fig. 3(b) shows the installation of eight numbers of fuse bars at the end of mechanical coupler before attached back to end of steel plate. The mechanical couplers were welded to the steel plate before screwed them with earthquake fuse bars (Figs. 4 and 5).

Upon the completion of construction corner beam-column joint with earthquake fuse bars on the strong floor, the specimen was needed to paint with white color for easy marking of hairline cracks during testing. Before conducting the experimental work, all the instrument and equipment need to be serviced and calibrated for accurate measurement of data. Figure 6 shows a total number of five LVDTs were placed along one side of the column, one LVDT on Beam 1 and two LVDTs on the foundation beam. The labeled LVDT 1, LVDT 2, LVDT3, LVDT4 and LVDT 5 were positioned on right hand side of the column to record the in-plane lateral displacement when applying the in-plane lateral load at top of the column. The lateral load was supplied by the 500 kN of load cell which located at the top end of
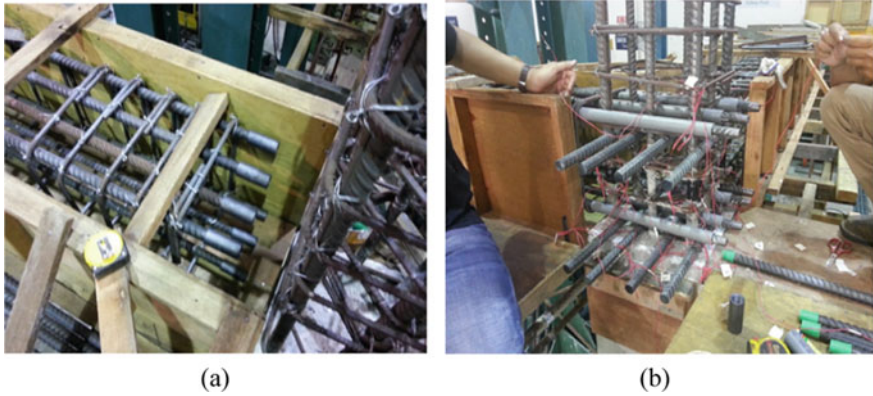
Fig. 5 Placing the fuse bars inside the joint (**a**) locate the mechanical couplers at the end of main bars; (**b**) install the fuse bars and screw them to the mechanical couplers
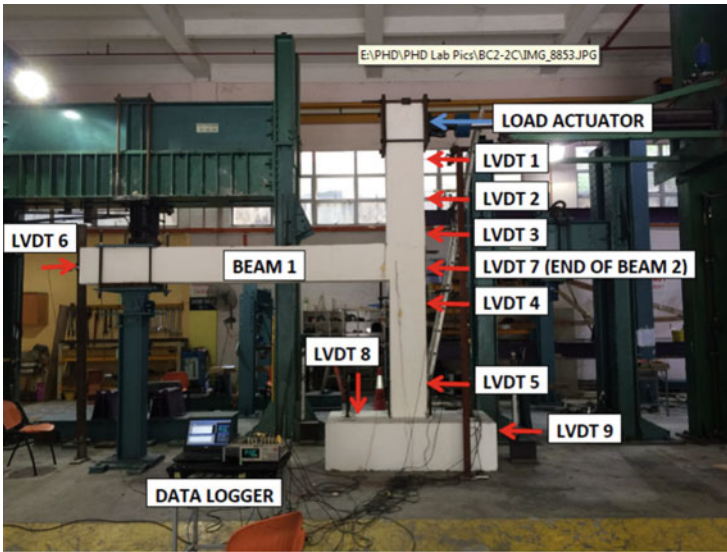
Fig. 6 Schematic locations of LVDTs and load cell in double actuator

the column. LVDT 6 was placed at the end of Beam 1 and LVDT 7 at the end of Beam 2 in order to observe the lateral movement of the beams in x-direction and y-direction (out-of-plane), respectively. LVDT 8 was positioned vertically and LVDT 9 horizontally to the foundation beam for monitoring sliding and uplift of the foundation beam during testing because it was designated as fixed support.

Figure 7 shows the loading regime of testing for corner beam-column joint using the displacement control method. Initially, the specimen was tested ±0.01%,

Number of Cycles
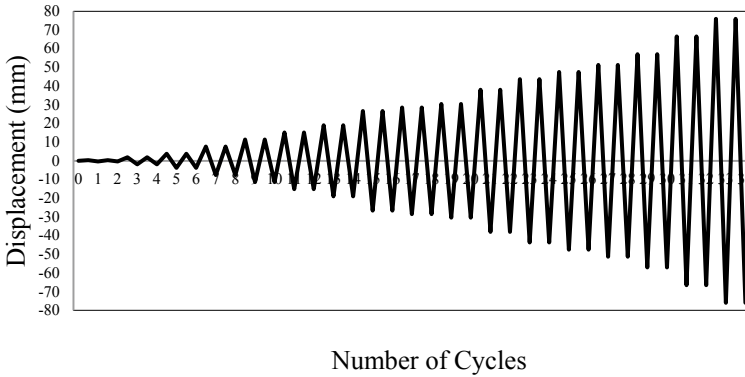
Fig. 7 Loading regime used for testing corner beam-column joint

±0.05% and ±0.10% drifts to make sure that all the LVDTs, load cell and strain gauges were able to measure lateral displacement, lateral load and strains of reinforcement bars. Following by other drifts such as ±0.20, ±0.50, ±0.75, ±1.00, ±.15, ±1.25, ±1.35, ±1.50, ±1.75 and ±2.00% drifts. For each drift, two cycles of experimental work will be repeated in order to get the accurate and precise results. After completed testing each drift, red and blue markers were used to mark the cracks in pushing and pulling direction.

4 Data Analysis And Interpretation of Results

The experimental data needs to be measured, calculated, analyzed, evaluated and interpreted under earthquake engineering contents in order to suit with the current situation which occurred in and around Malaysia. Initially, the visual observation of damage can be used to classify the Damage States according to Performance Based Earthquake Engineering (PBEE). From the plotted hysteresis loops, the seismic performance parameters such as lateral strength capacity, stiffness, ductility and equivalent viscous damping were evaluated. The experimental values of these parameters can be applied to model and validate the hysteresis loops using HYSTERES program in RUAUMOKO 2D folder.

4.1 Visual Observation of Damages

Figure 8 shows the overall comparison of visual observation of damages to the corner beam-column joint with and without fuse bars. Figure 8(a) shows the vertical cracks beam at +1.35% drift and Fig. 8(b) shows the overall cracks on beams,
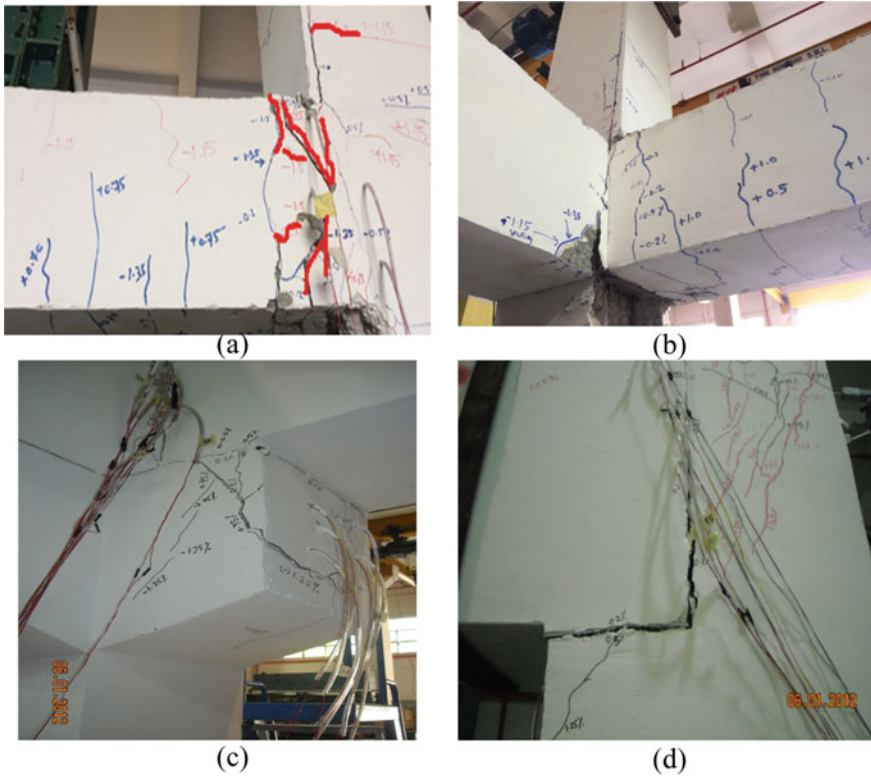
Fig. 8 Comparison of overall visual observation of damages on corner beam-column joint with and without fuse bars; (**a**) vertical cracks on beam-column interface with fuse bars; and (**b**) vertical cracks on beams +1.75% drift, (**c**) diagonal cracks at corbels without fuse bars, and (**d**) vertical and horizontal gaps of 25 mm at beam-column interface without fuse bars.

columns and beam-column interfaces up to ±2.00% drift with fuse bars. Even though fuse bars were used inside the corner beam-column joint but there are still some minor structural damages occurred at the joints and some cracks in beam. Moreover, the ductile link which has fuse bars yielded earlier followed by cracks in beams classified as brittle link under capacity design. Despite of this minor damages, it is also allows under Damage Limit States as long as the buildings standstill without collapse in any moderate or severe earthquakes. Contradictory, Fig. 8(c) shows severe damages with diagonal cracks occurred at corbel at beam-column joint without fuse bars. Similar, Fig. 8(d) shows the vertical and horizontal gaps of 25 mm at beam-column interface without fuse bars. It is observed that beam-column without fuse bars suffered severe damage as compared to beam-column joint with fuse bars.

4.2   Lateral Strength Capacity

The experimental hysteresis loops of corner beam-column joint can be plotted the load versus displacement measured by load cell and linear potentiometer labeled as LVDT 1. These hysteresis loops were used to determine the lateral strength capacity, stiffness, ductility and equivalent viscous damping. Figure 9(a) shows hysteresis loops of corner beam-column joint with fuse bars whereas Fig. 9(b) shows the hysteresis loops without fuse bars. The hysteresis loops with fuse bars have higher drifts up ±2.00% as compared without fuse bars up to ±1.35% drift. The ultimate lateral strength capacity is 90.38 kN and lateral displacement is 60 mm beam-column joint with fuse bars is higher than without fuse bars of 44 kN and 43.46 mm, respectively. Figure 10 demonstrates the comparison of skeleton curve of lateral strength capacity for hysteresis loops with and without fuse bars. Figure 10(a) shows the maximum lateral strength capacity in pushing direction is 90.39 kN and the pulling direction is −102.66 kN for beam-column joint with fuse bars. Meanwhile, the lateral yield force is 67.79 kN in pushing direction and −38 kN in pulling direction. Figure 10(b) shows the skeleton curve of lateral strength capacity without fuse bars. The maximum lateral capacity in pushing direction is 44 kN and pulling direction is −77.92 kN. Moreover, the lateral yield force is 33 kN in pushing direction and −58.44 kN in pulling direction.

(a)   (b)
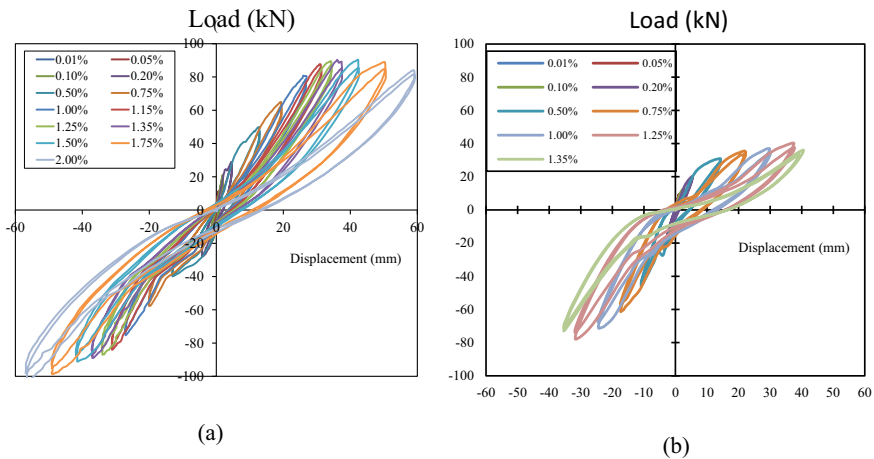
Fig. 9 Comparison of hysteresis loops of corner beam-column joint measured by LVDT 1 (**a**) with fuse bars; and (**b**) without fuse bars [11]
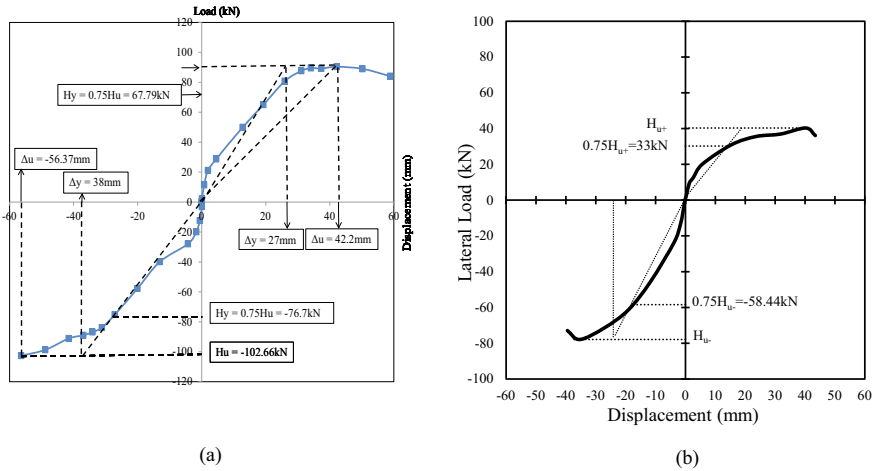
Fig. 10 Skeleton curve of lateral load versus displacement for the joints (**a**) with fuse bars; and (**b**) without fuse bars (Kay Dora, 2015)

4.3 Stiffness

Stiffness is calculated by taking the ratio of lateral load over lateral displacement and it is related to the rigidity of the structures. Figure 11 shows the comparison of stiffness with and without fuse bars for Cycle 1 and Cycle 2 in pushing and pulling directions based on the data given in Table 2. The slope of stiffness versus drift is bigger with fuse bars than without fuse-bars. The beam-column joint with fuse-bars has higher strength because more reinforcement bars are occupied in the joint as compared without fuse bars. Furthermore, the elastic and secant stiffness of joint with fuse bars are also higher than without fuse bars. However, the elastic stiffness reduces by half starting from 0.2 until 0.5%. The secant stiffness started to decrease from 0.75 to 2.00% drift with fuse bars and 0.75 to 1.25% without fuse bars as tabulated in Table 2. This is due to the formation of cracks in concrete could reduce the stiffness of corner beam-column joint and it occurred at load much smaller than the yielding of reinforcement and lateral strength capacity of beam-column joint.

4.4 Ductility

Displacement ductility is calculated by taking the ratio of applied displacement over the yield displacement based on the hysteresis loops as shown in Fig. 9. Ductility is one of the most important factor in designed the structures or buildings under earthquake excitations. This type of corner beam-column joint supplemented with earthquake fuse bars was designed using Eurocode 8 under Ductility Class medium
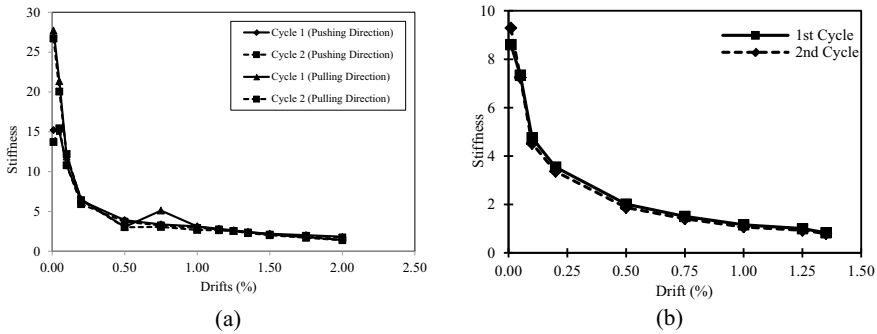
Fig. 11 Comparison of stiffness beam-column joint with and without fuse bars, (**a**) with fuse bars and, (**b**) without fuse bars [11]

Table 2 Comparison of stiffness with and without fuse bars in pushing and pulling direction

Target drift (%)	Pushing direction				Pulling direction			
	Cycle 1 (with fuse bars)		Cycle 1 (without fuse bars)		Cycle 2 (with fuse bars)		Cycle 2 (without fuse bars)	
	K_e	K_{sec}	K_e	K_{sec}	K_e	K_{sec}	K_e	K_{sec}
0.01	15.21		–		26.70		–	
0.05	15.03		–		20.05		–	
0.10	10.78		1.51		12.19		1.45	
0.20	6.35		1.13		6.41		1.09	
0.50	3.90		1.28		3.01		1.02	
0.75		3.37		1.02		3.05		0.98
1.00		3.11		0.83		2.67		0.75
1.15		2.82		0.53		2.63		0.49
1.25		2.62		0.28		2.55		0.21
1.35		2.39		0.15		2.36		0.11
1.50		2.14		–		2.09		–
1.75		1.77		–		1.94		–
2.00		1.43		–		1.72		–

(DCM) with Peak Ground Acceleration (PGA = 0.3 g). Table 3 shows the comparison of ductility values for corner beam-column joint with and without fuse bars in the pushing and pulling directions for both cycles of loading. Under Cycle 1 and Cycle 2 for corner beam-column joint with fuse bars have the maximum displacement ductility in the pushing and pulling direction are μ = 2.69 and μ = 2.03 respectively. Whereas, the maximum displacement ductility for Cycle 1 and Cycle 2 without fuse bars are 1.85 and 1.51, respectively. It is clearly shown that beam-column joint with fuse bars has higher displacement ductility as compare without fuse bars. It is expected that this type of joint will survive under moderate

Table 3 Comparison of ductility with and without fuse bars in pushing and pulling directions.

Target drift (%)	Pushing direction		Pulling direction	
	Cycle 1 (with fuse bars)	Cycle 1 (without fuse bars)	Cycle 2 (with fuse bars)	Cycle 2 (without fuse bars)
	Ductility, μ	Ductility, μ	Ductility, μ	Ductility, μ
0.01	0.00	–	0.00	–
0.05	0.03	–	0.02	–
0.10	0.09	0.12	0.06	0.03
0.20	0.21	0.24	0.15	0.07
0.50	0.58	0.65	0.47	0.29
0.75	0.88	1.00	0.72	0.44
1.00	1.18	1.36	0.97	0.62
1.15	1.42	1.55	1.12	0.81
1.25	1.56	1.70	1.22	1.20
1.35	1.71	1.85	1.33	1.51
1.50	1.93	–	1.50	–
1.75	2.29	–	1.75	–
2.00	2.69	–	2.03	–

earthquake due to their ductility more than 2.0. For non-ductile structures without fuse bars and designed using BS8110 (non-seismic code of practice), the displacement ductility of the structures is less than 2.0 which categorized as brittle structures.

4.5 Equivalent Viscous Damping

When the structure gets into the elastic–plastic state, its seismic performance mainly depends on the energy dissipation capacity. Energy dissipation and equivalent viscous damping are the two main factors that affect the seismic performance of a building [17]. Equivalent viscous damping is a way for measuring response of a system to harmonic force at exciting frequency. Higher value of equivalent viscous damping factor indicates that more energy is required to dissipate through the system and cause a lot of structural damages. The energy dissipated in a vibration cycle of the structure was determined by calculating the equivalent viscous system. An equivalent viscous damping factor can be calculated using Eq. 1 [3] as follow,

$$\xi_{eq} = \frac{E_D}{4\pi E_{so}} \tag{1}$$

(a)   (b)
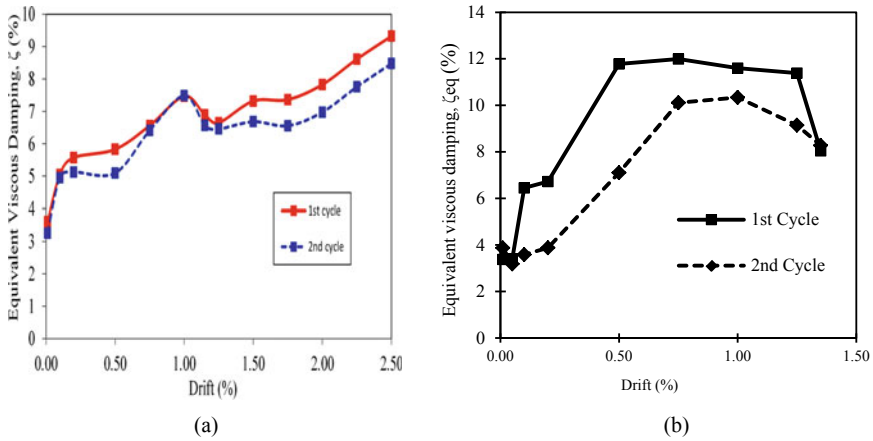
Fig. 12 Comparison of equivalent viscous damping versus drift for corner beam-column joint, (**a**) with fuse bars, and (**b**) without fuse bars

where E_D is energy dissipation under one complete cycle of hysteresis loops and E_{SO} is strain energy under triangle load versus displacement graph. Figure 12 shows the comparison of equivalent viscous damping for corner beam-column joint with and without fuse bars. Generally, it is notified that there is gradually increase in percentage of equivalent viscous damping as percentage of drift increases. It is also can be observed that the equivalent viscous damping for Cycle 1 is higher than Cycle 2 because more resistance of lateral force is required to push and pull the specimen to achieve the target drift. The maximum percentage equivalent viscous damping for corner beam-column joint with fuse bars is 9.2% for Cycle 1 and 8.5% for Cycle 2 which occurred +2.5% drift. While, the values of equivalent viscous damping without fuse bars is 12% for Cycle 1 occurred at +0.5% drift and 10% for Cycle 2 at +1.00% drift. Therefore, the conclusion is that by installation of fuse bars inside the corner beam-column joint can reduce the equivalent viscous damping and reduce the structural damage during earthquake or vice versa. It is because the hysteresis loops are smaller and slimmer when installed the fuse bars inside the joint rather than joints without fuse bars.

5   Discussions

Based on the data analysis and interpretation of results, it shows that by installing fuse bars at corner beam-column joints can improve the seismic performance parameters and simultaneously, increase the structural stability and integrity under earthquakes excitations. It is observed that by incorporating fuse bars in the beam-column joints can reduce the structural damages tremendously and minor

Table 4 Comparison of seismic parameters for beam-column joint with and without fuse bars

Seismic parameters	Beam-column joint with fuse Bars	Beam-column joint without fuse bars	Percentage different (%)
Lateral strength capacity Pushing direction (kN) Pulling direction (kN)	90.39 −102.66	44 −77.92	51.32% 24.10%
Elastic and secant stiffness Ke-1 cycle (kN/mm) Ke-2 cycle (kN/mm) Ksec – 1 cycle (kN/mm) Ksec – 2 cycle (kN/mm)	3.90 3.01 3.37 3.05	1.28 1.02 1.02 0.98	67.18% 66.11% 69.73% 67.87%
Displacement ductility Pushing direction (1 Cycle) Pulling direction (2 Cycle)	2.69 2.03	1.85 1.51	31.23% 25.61%
Equivalent viscous damping 1 Cycle (%) 2 Cycle (%)	9.2% 8.5%	12% 10%	−30.43% −17.65%

damage occurred in the beams instead in the columns which fulfill the requirement of capacity design as specified in Eurocode 8. Table 4 shows the comparison of seismic parameters for beam-column joint with and without fuse bars. The lateral strength capacity increases by 51.32% in pushing direction and 24.10% in pulling direction after mounting fuse bars in beam-column joint. The elastic and secant stiffness increases with an average of 67.72% when fixing earthquake fuse bars in the beam-column joint. Displacement ductility increases by 31.23% in pushing direction and 25.61% in pulling direction. Finally, the equivalent viscous damping reduces by 30.43% in 1 Cycle and 17.65% in 2 Cycle after installing fuse bars in the corner beam-column joint. Generally, it is concludes that fuse bars in corner beam-column joint can improve the seismic parameter and performed better under moderate and strong earthquake excitations.

6   Conclusions and Recommendations

Based on the experimental data, results and its interpretation, it can be concluded that earthquake fuse bars which install inside the corner beam-column joint can improve the seismic performance of the RC buildings. The seismic performance's parameters can be calculated from experimental hysteresis loops such as lateral strength capacity, stiffness, ductility and equivalent viscous damping. From the experimental data, the ultimate maximum load is 90.39 kN and yield load is 67.79 kN in pushing direction. Whereas in pulling direction, the maximum load is −120.66 kN and yield load is −38 kN. Furthermore, the stiffness of the corner

beam-column joint decrease as the percentage of drift increases. Contradictory, the values of ductility increases as the percentage of drift increases and it has been proven that by installing fuse bars inside the corner joint. The maximum value of ductility is 2.69 which is acceptable to be designed for moderate earthquake regions. Lastly, the percentage of equivalent viscous damping is linearly increases as the percentage of drift increases. Therefore, it is recommended that earthquake fuse bars should be installed inside beam-column joint for the construction of reinforced concrete buildings especially in Sabah which had been categorized as moderate seismic regions.

References

1. BS 8110–1:1997, British Standard , Structural use of concrete, Part 1: Code of Practice for design and sonstruction , ISBN No: 0 580 262081, United Kingdom
2. Calado L, Proenca JM, Espinha M, Castiglioni CA (2013) Hysteretic behavior of dissipative welded fuses for earthquake resistant composite steel and concrete frames. Steel Compos Struct J 14(6):547–569
3. Chopra AK (1995) Dynamics of structures: theory and applications to earthquake engineering. Prentice-Hall, New Jersey
4. Christopoulos C, Filiatrault A, Uang C, Folz B (2002) posttensioned energy dissipating connections for moment-resisting steel frames ASCE, Technical Paper. J Struct Eng 128 (9):1111–1120
5. Connor JJ, Wada A, Iwata M, Huang YH (1997) Damage-controlled sstructures. I: preliminary design methodology for seismically active regions, ASCE. J. Struct. Eng. **123** (4):423–431
6. El-Bahey S, Bruneau M (2010) Structural fuse concept for bridges. Transp Res Rec J 2202 (1):167–172
7. Hamid NH, Mander JB (2016) Experimental study on bi-lateral seismic performance of precast hollow core wall using shaking table. In: Proceedings of 10th east asia-pacific conference on structural engineering and construction (EASEC-10), Thailand
8. Hamid NH, Mander JB (2010) Lateral seismic performance of multipanel precast hollowcore walls ASCE. J Struct Eng 136(7):795–804
9. Hamid NH, Mander JB (2014) Damage avoidance design for buildings. KSCE J Civil Eng 18 (2):541–548
10. Kam WY, Pampanin S, Palermo A, Carr A (2010) Self-centering structural systems with combination of hysteretic and viscous energy dissipations. Earthquake Eng Struct Dyn 39 (10):1083–1108
11. Kay Dora AG, Hamid NH (2012) Seismic performance of SFRC beam-column joint with corbel under reversible lateral cyclic loading. IACSIT Int J Eng Technol 4(1):76–80
12. Marriot D, Pampanin S, Bull D, Palermo A (2008) Dynamic testing of precast, post-tensioned rocking wall systems with alternative dissipating solutions. Bull New Zealand Soc Earthquake Eng 41(2):90–103

13. Palermo A, Pampanin S, Calvi GM (2005) Concept and development of hybrid systems for seismic-resistant bridges. J Earthquake Eng Imperial College Press 9(6):899–921
14. Paulay T, Priestley MJN (1992) Seismic design of reinforced concrete and masonry buildings. Wiley Online Library
15. Priya DS, Cinitha A, Umesha PK, Nagesh RI (2014) Enhancing the seismic response of buildings with energy dissipation methods – an overview. J Civil Eng Res 4(2A):17–22
16. Rahman A, Restrepo JI (2000) Earthquake Resistant Precast Concrete Buildings: Seismic Performance of Cantilever Walls Prestressed using Unbonded Tendons, Research Report 2000–5. University of Canterbury, Christchurch, New Zealand, Department of Civil Engineering
17. Rodrigues H, Varum H, Arede A, Costa A (2012) A comparative analysis of energy dissipation and equivalent viscous damping of RC columns subjected to uniaxial and biaxial loading. Eng Struct 35(2012):149–164
18. Stanton JF, Stone WC, Cheok GS (1997) A hybridreinforced precast frame for seismic regions. PCI J 42(2):20–32

Load Bearing Capacity Analysis for RC Slab Strengthened Externally with CFRP Plates

N. M. Amin, N. E. Naha, S. A. Kudus, and A. Jamadin

Abstract This research is focused on the investigation of the effectiveness of Carbon Fiber Reinforced Polymer (CFRP) plate to strengthen the slab in Sekolah Kebangsaan Chengal Lempong which is located in Kuantan. The school project had been abandoned for five years due to construction contract termination. The compressive strength and conditions of existing Reinforced Concrete (RC) slab were investigated using destructive and non-destructive tests. The result of the investigation showed a reduction in the value of concrete compressive strength in several slabs. The authorities have decided to repair the particular slab by using the CFRP plate strengthening method. In this study, the critical slab was identified and redesign according to the data obtained from the investigation of the existing structure. The slab was modeled using Orion software according to BS8110. The critical slab was re-analyzed using the Finite Element method to investigate the behavior of slab strengthened with CFRP in accordance to load-carrying capacity.

Keywords CFRP · Reinforced Concrete (RC) slab · Strengthening · Service performance · Finite element analysis

1 Introduction

Rehabilitation of an old building is more economical than the reconstruction of a new building. The rehabilitation of buildings can be understood as the set of operations that aim to increase the level of quality of building systems, so as to achieve compliance with functional requirement standards which are stricter than those planned (Linhares [3]). The decision of strengthening techniques as one of the rehabilitation processes should be decided in order to save time and cost. The strengthening of reinforced concrete structures using fiber-reinforced polymer

N. M. Amin (✉) · N. E. Naha · S. A. Kudus · A. Jamadin
School of Civil Engineering, College of Engineering, Universiti Teknologi MARA, 40450 Shah Alam, Selangor, Malaysia
e-mail: norli830@uitm.edu.my

(FRP) has become an alternative method in recent years due to the need for building maintenance and upgrade essential infrastructure. The advantages of FRP such as good corrosion resistance, excellent strength, high stiffness, and ease for site handling. Moreover, the reduced cost of FRP composites material has increased the demand for FRP strengthening method. Carbon fiber reinforced polymers (CFRPs) have been widely used as a strengthening method of RC structures such as beams, columns, slabs, bridge girders, structural joints as well as masonry structures (Durucan et al. [2]).

2 Background of the Project

The construction works for Sekolah Kebangsaan Chengal Lempong which is located at Kuantan, Pahang has started in 2010 under the authority of the Ministry of Education Malaysia (KPM). This building is situated approximately two kilometers away from the sea. The school project had been abandoned for five years due to construction contract termination.

An inspection and assessment work for the existing structure has been done before executing the construction works. The assessments were executed through visual observations, destructive testing and non-destructive testing (NDT) in accordance with the prescribed rules. The strengthening and reparation works were proposed based on the results of the assessment and site testing. The quality of material and building integrity are supposed to comply with the specified specification to ensure the design requirement and structural integrity are met during and after the construction. Non-compliance with this specification may cause building structure failure and pose a substantial risk to the occupants.

The Forensic Division of Public Work Department (JKR) has also done additional testing on-site to ensure all the data collected was accurate. The result of the investigation shows that there was a reduction in the values of concrete compressive strength for column, beam and slab in all of the five (5) building blocks. Figure 1 show the FE model of the building. All the affected structures had been identified to be strengthened with a suitable approach to increase their load-carrying capacity and service performance.

The study investigated the behavior of slabs structure of Academic Building Block C. The behavior of RC slab before and after externally strengthened with CFRP was investigated. In this study, a non-linear finite element analysis model of RC slab strengthened with CFRP will be conducted using finite element analysis which is ABAQUS software in order to study the performance of the slab in terms of load-bearing capacity and possible failure modes.
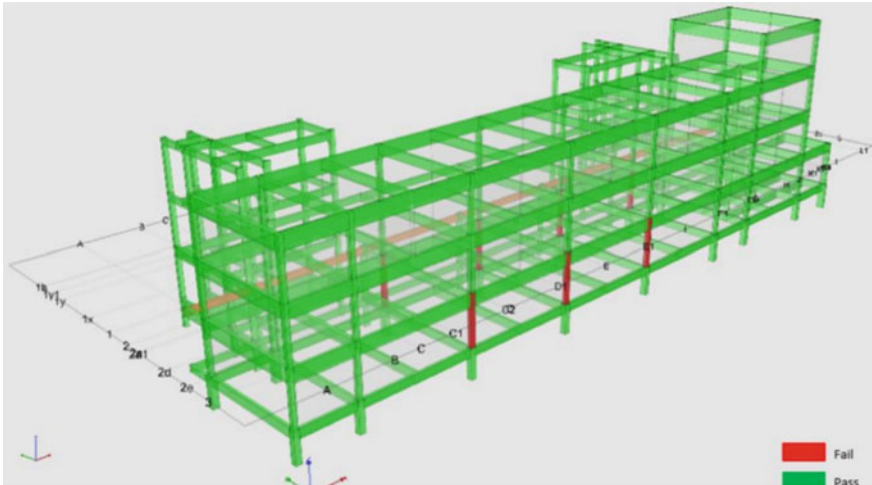
Fig. 1 Design analysis for Block C, academic building using Orion 18 (Amin et al. [6])
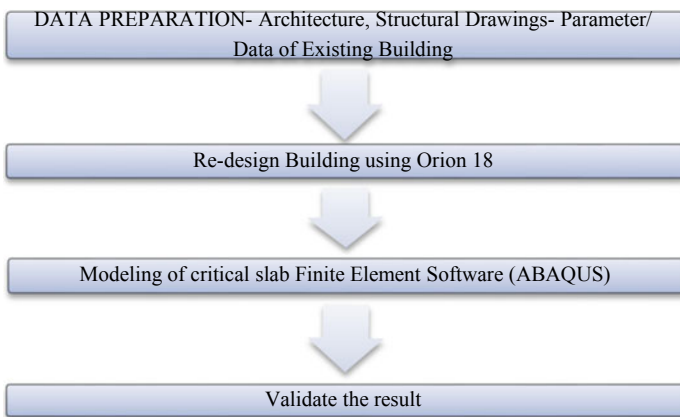
Fig. 2 Process of analysis

3 Methodology

In this study, Block C of Sekolah Kebangsaan Chengal Lempung has been chosen as the structure to be analyzed. This research will involve the design and analysis of the overall building structure using the data and parameter collected through testing and investigations at the site. The design will be modeled using ORION software Version 18 to examine the structural integrity of the overall building. The critical slab from the design will be reanalyzed using Finite Element software, ABAQUS with the application of CFRP plate below the slab as a strengthening method. Figure 2 shows the process of analysis in this study.

3.1 Data and Parameter of Existing Building

The assessment was executed through visual observations, destructive testing and non-destructive testing (NDT) in accordance with the prescribed rules by an appointed consultant.

There were five types of testing conducted on-site to assess the condition of the existing structure. However, only Coring Test, Rebound Hammer and Ferro Scan result will be adopted for this study. Additional testing of Rebound Hammer and inspection for verification of steel reinforcement were executed by The Forensic Division of Public Work Department (JKR) was given a responsibility to ensure all the data collected were comprehensive in representing the performance of Block C. Table 1 shows the type of tests and results.

3.2 Setting Properties for Modeling Slab Using Orion

The most critical slab was identified based on the largest panel size and the lowest value of concrete compressive strength from site investigation. Hence, the whole slab area was modeled using ORION to ensure the accuracy of the design. Based on the Coring Test result, the lowest value of concrete compressive strength was 20.8 kN/m^2 which is observed at the First-Floor level. Thus, only the floor slab at the First Floor level will be redesigned using the existing parameter obtained including the concrete compressive strength and concrete cover value. The result of ORION determined whether the slab was sufficient in design according to the deflection of the slab within limitation and the required steel area was less than provided on-site. The provided steel area was obtained from Ferro Scan Test and

Table 1 Type of site test and results

Nos.	Type of Test	Result	
1	Coring Test (DT)	Concrete Compressive Strength	20.8kN/m²(rounded to 20 kN/m²)
2	Rebound Hammer (NDT)	Concrete Compressive Strength	20.8kN/m²(rounded to 20 kN/m²)
3	Ferro Scan (NDT) And Inspection (DT)	Rebar saiz	10mm
		Rebar spacing	200 (x -direction) 220 (y-direction)
		Concrete cover	50mm

inspection result did on site. Table 1 shows the type of tests executed and the results obtained that will be adopted in the modeling.

The structural properties of the First-Floor frame were assigned in accordance with BS8110:1997. The overall slab for the First Floor level was modeled in order to obtain an accurate results of continuous slab design.

3.3 Model of Project Case Study

The selection of RC slab panel to be investigated is based on the size of the slab itself and the lowest value of concrete compressive strength according to the testing result. The specimen was a continuous solid slab panel with a size of $8.0 \times 4.25 \times 0.15$ m. The modeling of this critical slab was using the same verification model of the slab that has been amended to suit the current parameter data (sizing, concrete strength, etc.). The material properties and imposed load in Orion software are shown in Table 2.

Table 2 Material Properties and Imposed load adopted in structure modeling

Design Parameters	Values of Parameters
Compressive strength concrete, f_{cu} (N/mm^2) (According to coring test result)	20
Characteristics strength of high yield strength, f_y (N/mm^2) (According to structural drawing)	460
Nominal concrete cover , mm (According to steel verification result)	50
Density of concrete, ρ_c (kN/m^3)	24
Live Load (kN/m^2) (According to BS 6399-1:1996) Classroom Toilet Corridor	3.0 2.5 4.0

However, in the analysis, the symmetry of slabs is used to reduce calculation time and only half of a slab is considered for modeling purposes. The size of modeling of the slab panel is $4.0 \times 4.25 \times 0.15$ m as shown in Fig. 3.

The consultant of this school project has issued a Structural Rectification drawing for a method of strengthening for reparation works on a particular structure. Figure 4 shows the floor slab strengthening at soffit using CFRP plate at the First Floor level. The CFRP strips named S1014 was arranged with spacing 0.75 m center to center. Figure 5 shows the fixed boundary condition assigned in the model.

The geometrical and material parameters assigned in the modeling of the slab are tabulated in Tables 3, 4 and 5.

Fig. 3 Specimen of RC Slab
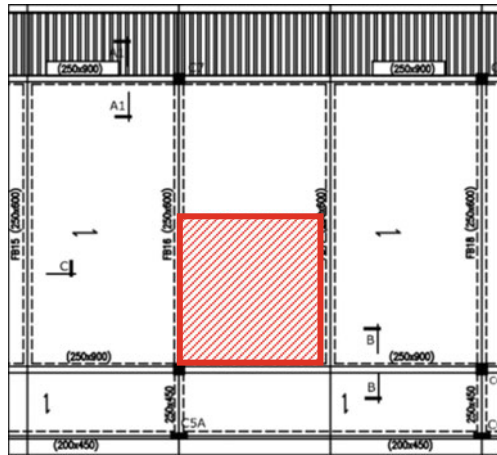
Fig. 4 Slab with CFRP Strips Modelling in ABAQUS
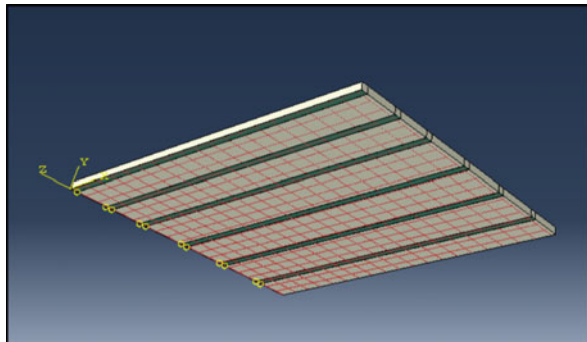
Fig. 5 Fixed boundary condition
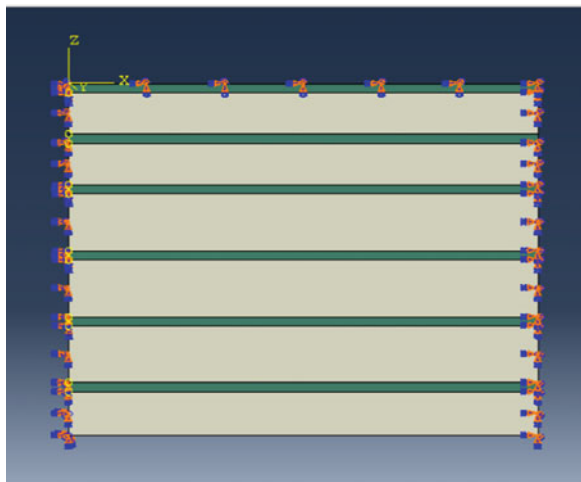
Table 3 Properties of CFRP and Resin (Sika Product Data Sheet)

Properties of CFRP	Remarks of CFRP
Size of each strip (mm)	8000 × 100 × 0.0014
Tensile strength (MPa)	3100
Elastic modulus (MPa)	165000
Ultimate tensile strain (%)	1.8

Table 4 Properties of Reinforcement (Anil [1])

Mechanical properties of reinforcement	
Reinforcement size (mm)	10ϕ @ 200
Yield strength (MPa)	480
Ultimate tensile strength (MPa)	627
Poisson's ratio, υ	0.3
Young Modulus, Es (MPa)	209000

4   Results and Discussion

4.1   Model of Project Case Study

This study was conducted to investigate the performance of the critical RC slab of an abandoned school project situated in Kuantan. The deterioration of concrete compressive strength was observed in RC slab according to coring and rebound hammer test result due to the reduction value of concrete compressive strength.

Firstly, the critical slab was identified based on the lowest concrete compressive strength and the largest size of slab panel. The performance of critical slab before it was strengthened with CFRP is investigated. Thus, the identified slab was redesign using ORION software to determine whether it is sufficient in design to resist the vertical load applied according to the testing result obtained. The slab is sufficient in design if the actual deflection is less than allowable deflection and the design steel area is less or equal to the steel bar area provided on-site (size and spacing). The result shows whether the slab is required to be strengthened or leave it as it is, as shown in the construction drawing.

Figures 6 and 7 show for elevation view and plan view of slab reinforcement respectively. The result shows the required bar is T10-250 both ways.

The result shows that the provided area of steel bar in ORION design is 314 mm^2/m (T10-250) which less than the provided steel bar area in the existing slab equal to 393 mm^2/m (T10-200). Thus, the provided steel bar in the existing slab is sufficient to carry the current and future load during its service life.

Table 5 Simulation parameters for concrete (Enochsson et al. [4])

Denotation	Parameter
Plasticity parameters	Dilation angle, $\psi = 12°$ Eccentricity, E = 0.1
	Ratio of biaxial to uniaxial compressive strength, $\sigma b0/\sigma c0 = 1.16$
	Second stress invariant ratio, K = 2/3
	Viscosity parameter = 0 (default)
Poisson's ratio, υ	0.2
Young Modulus, Ec (MPa)	21019
Compressive strength, fcm (MPa)	20
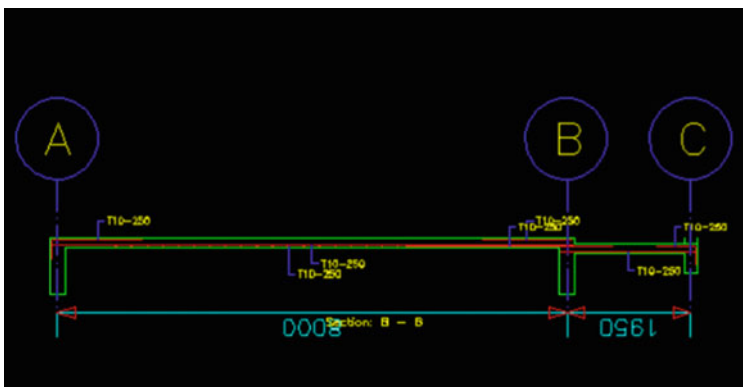
Fig. 6 Elevation view of slab reinforcement

Fig. 7 Plan view of slab reinforcement
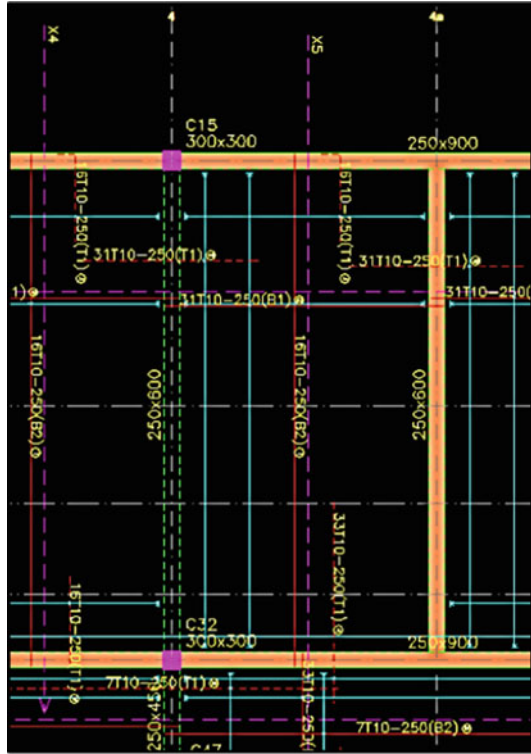
4.2 The Load-Displacement Curve of Abandoned RC Slab Strengthened with CFRP Plates

Figure 8 shows the Load-Displacement graph of two slabs with concrete compressive strength 20 N/mm². The red line indicates the result of the slab modeled with CFRP plate while the blue indicates slab without the CFRP. The graph shows the curve of the result divided into three different regions, where the first region is the initial linear region or elastic behavior stage, at mid curve is a transition region or non-linear stage and lastly is a third linear region.

The yield point for the slab with CFRP was 12 kN/m² with a deflection of 24 mm, while the yield point for the slab without CFRP plates was 9.2 at kN/m² with a deflection of 26 mm. The difference percentage of load between these two curves is approximately 41.3%. Hence, it shows that the carrying load capacity of the slab with CFRP plate increases approximately 41.3% at non-linear state. Lokman [5] stated that through the experimental results of the initial linear region, concrete behavior is dominant where-as FRP characteristic is dominant for the third linear region. However, the second region is a non-linear stage owing to the
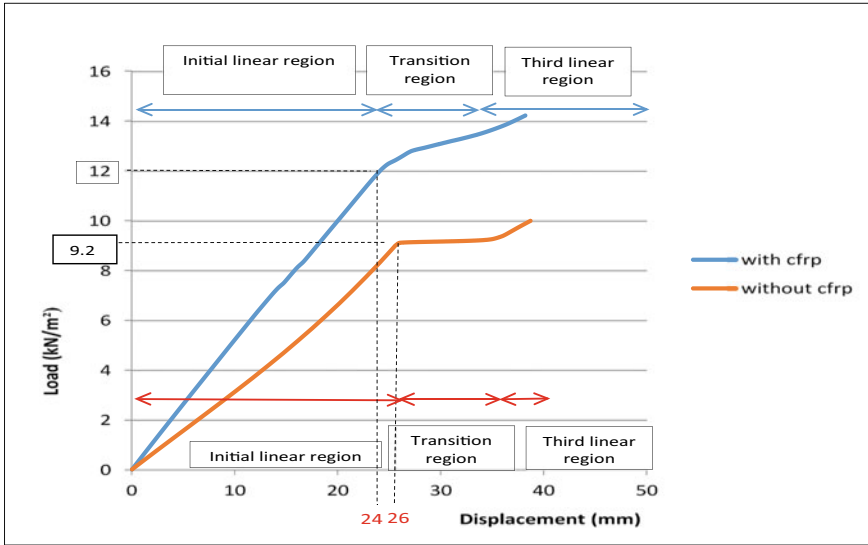
Fig. 8 The load versus displacement
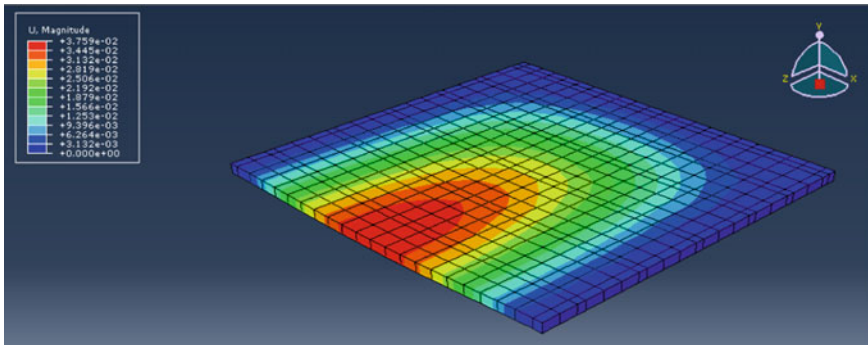
Fig. 9 Displacement contour for CFRP strengthened slab

intensive cracks on concrete. Hence, the study of load-carrying capacity of RC slab is made on the stage of concrete starts to crack in a transition region.

Figures 9 and 10 show the visualization of slab displacement and their magnitude for both strengthened with CFRP and without CFRP slab, respectively. The maximum value of displacement is taken at mid-span of the slab. The maximum displacement for a strengthened slab with CFRP was 37.59 mm while for slab without CFRP the maximum displacement is 38.46 mm. The strengthened slab starts transforming from linear to non-linear state at 12 kN/m^2 compare to without CFRP slab 8 kN/m^2. The slab continues to deflect to maximum displacement. The slabs deflection is within the allowable limit.
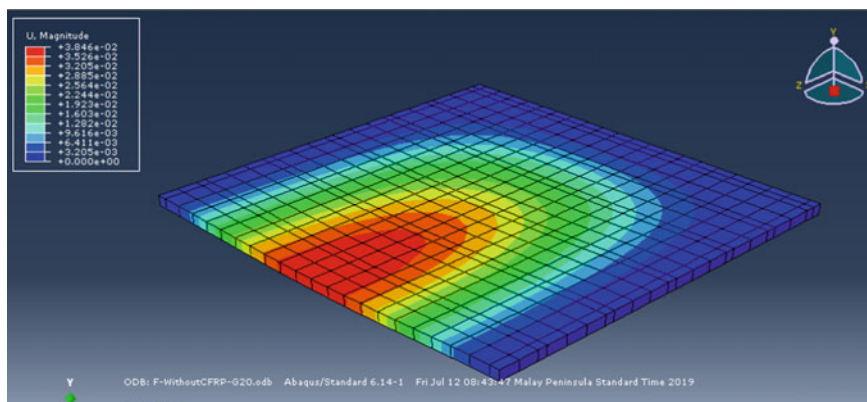
Fig. 10 Displacement contour for without CFRP slab

The result shows that steel required for the main direction was T10-250 (314 mm^2/m area) while provided on-site was T10-200 (393 mm^2/m area). On the other hand, steel required for secondary direction was T10-250 (314 mm^2/m area) while provided on-site was T10-220 (356 mm^2/m area). However, to maintain the durability of slab performance the slab has strengthened with CFRP plate to ensure the slab is able to withstand safely and reliably the loading through its expected lifetime.

5　Conclusions

The analysis was carried out to measure the effectiveness of CFRP plates as a strengthened material on RC slab for a school project. The results can be summarized as follow:

- The redesign of the critical slab of Block C in accordance with BS8110:1997 shows that it is sufficient in design due to deflection and provided steel reinforcement. Thus, the slab still capable to withstand the vertical load during its service life without CFRP plate strengthening.
- The yield point for the slab with CFRP was 12 kN/m^2 with deflection of 24 mm, while the yield point for the slab without CFRP plates was 9.2 at kN/m^2 with deflection of 26 mm.
- The carrying load capacity of the strengthened slab with CFRP increases approximately 41.3% than the slab without CFRP strengthening in a non-linear state. The method of strengthening project slabs by using CFRP plates increased the load-carrying capacity of specimens. In addition, this technique is applied easily in a short time with minimum cost.

References

1. Anil Ö, Kaya N, Arslan O (2013) Strengthening of one way RC slab with opening using CFRP strips. Constr Build Mater 48:883–893
2. Durucan C, Anıl Ö (2017) Nonlinear 3D finite element simulation of reinforced concrete flat plates retrofitted with externally bonded CFRP strips. Struct Infrastruct Eng 13(9):1198–1211
3. Qualharini EL, Oscar LHC, Ramos M, da Silva (2019) Rehabilitation of buildings as an alternative to sustainability in Brazilian constructions. Open Eng 9(1):139–143
4. Enochsson O, Lundqvist J, Täljsten B, Rusinowski P, Olofsson T (2007) CFRP strengthened openings in two-way concrete slabs – an experimental and numerical study. Constr Build Mater 21(4):810–826
5. Gemi L, Madenci E, Özkılıç YO (2019) Investigation of reinforced concrete-filled pultruded beams strengthened by GFRP composite. In: Proceeding International Earthquake Symposium, IESKO 2019, Kocaeli, pp 651–656
6. Amin NM, Ahmad NA (2020) Performance of reinforced concrete columns strengthened with carbon fiber reinforced polymer (CFRP) - case study of an abandoned school project. IOP Conf Ser Mater Sci Eng 933:012014

Impact of Meteorological Factors on Air Pollution Trends in West Peninsular Malaysia

R. S. Hussin, M. Maskin, and A. Amir

Abstract This study investigates the impact of meteorological factors on air pollution trends in West Peninsular Malaysia. This study was conducted at three (3) industrial area, which are (1) Perai, Penang, (2) Ipoh, Perak, and (3) Petaling Jaya, Selangor. Data on air pollutants (particulate matter (PM_{10}), carbon monoxide (CO), nitrogen dioxide (NO_2), sulfur dioxide (SO_2) and ozone (O_3)) and meteorology (rainfall, humidity and temperature) were obtained from the Meteorology Department of Malaysia. This study used five (5) years (2013–2017) data to investigate the impact of meteorological factors on the air pollution trends at industrial area located at west peninsular Malaysia. Annual average concentration of each air pollutant was analyzed and compared with the Recommended Malaysia Ambient Air Quality Guideline (RMAAQG). Interestingly, all air pollutants were complianced with the RMAAQG within 2013 to 2017. PM_{10} was the predominant air pollutant that contributes to Air Pollutant Index (API) that probably released from the industrial activities, transportation and peatland fires. A significant correlation between the air pollutants and meteorological parameters was identified. Correlation between PM_{10} and rainfall (Perai, r = −0.39; Ipoh, r = −0.43; and Petaling Jaya, r = −0.34) was significant and consistent at these industrial areas within 2013 to 2017. Another significant correlation (Perai, r = 0.44; Ipoh, r = 0.45 and Petaling Jaya, r = 0.38) was also observed between air pollutant and temperature at these areas. This correlation finding revealed that these industrial areas at the West Peninsular Malaysia significantly contributed to the global warming issue and mitigation measures to control increment of temperature is urgently required. This study provides significant finding on the impact of the meteorological factors on air pollution trends and global warming phenomena in West Peninsular Malaysia.

R. S. Hussin · A. Amir (✉)
Faculty of Civil Engineering, Universiti Teknologi Mara Malaysia, 40300 Shah Alam, Malaysia
e-mail: amnorzahira@uitm.edu.my

M. Maskin
Agensi Nuklear Malaysia (Nuklear Malaysia), Bangi, 43000 Kajang, Selangor, Malaysia

1 Introduction

Air pollution is not a new phenomenon and it has been a current issue in many countries in the region of South East Asia. It first recorded in 1982 when regional haze from the burning of biomass has disrupted everyday life in Malaysia (Sham [17]). In 2015, South East Asian experienced severe haze due to illegal burning forest in Indonesia that has caused critical health impact and environment deterioration. According to the Department of Environment (DOE) [5], the haze considered as one of the worst episodes since 1997 as the air quality recorded unhealthy levels with Air Pollutant Index (API) more than 100. This literature indicates that air pollution issues in Malaysia are crucial to preserve the ecosystem as well as to maintain human health (DOE [5]). Air pollution can be described as the presence of air pollutants such as dust, fumes, gas, and others that are in immoderate quantities delivered into earth's environment resulted in unsafe results to the human health, material damage, harm dwelling sources and ecosystem (Afroz et al. [1]). Hence, it additionally affects the economic system and contributes to global warming and climate change because of massive greenhouse gas emissions and different pyrogenic products (Huang et al. [10]).

Nowadays, air pollution becomes one of the predominant environmental concerns. The air pollution is normally induced by natural or anthropogenic activities. The main anthropogenic activities consist of motor vehicles, power generation and industrial activities that are also known as primary pollutants as the main source of air pollution (e.g., PM_{10}, CO, NO_2 and SO_2) (Fernandez et al. [9]). Secondary air pollutants also can be formed in the atmosphere due to the interactions between the primary pollutants and other chemicals that present in the atmosphere (e.g., O_3) (Fernandez et al. [9]). In Malaysia, the Recommended Malaysia Ambient Air Quality Guidelines (RMAAQG) is the guideline used for monitoring the air quality which stated by the Department of Environment (DOE) under the Ministry of Energy, Science, Technology, Environment & Climate Change (MESTECC). The RMAAQG must be complied with to ensure the concentration of air pollutants in acceptable limits for human and environment exposure.

The urban-industrial emission is the main source of the deterioration of air quality problems (Ismail et al. [11]). This is due to the atmosphere surrounding that area is polluted with several common air pollutants which may include particulate matter (PM_{10}), carbon monoxide (CO), nitrogen dioxide (NO_2), sulphur dioxide (SO_2) and ozone (O_3). However, PM_{10} and O_3 are the crucial air pollutants concerned due to their high concentration released from uncontrolled sources (Amir [4]; DOE [5]). The O_3 was formed in the existence of the sunlight where the reaction of chemical between volatile organic compounds (VOCs) and nitrogen oxides (NO_x) and can increased more O_3 production during dry days (Amir [4]).

The VOC and NO_x may come from the emission of industries and motor vehicles exhaust especially in urban areas (DOE [5]). Besides that, PM_{10} was the predominant pollutant that caused unhealthy situations particularly during the dry season in the late Northeast Monsoon (February to March) and Southwest Monsoon (May to October) (DOE [5]). According to Enger and Smith [8], the PM_{10} and O_3 pollutants mainly come from emissions of NO_x and VOCs that can destroy people's sensitive tissues and impair respiratory functions. Besides, more than 60,000 people die prematurely in the United States over two years due to excessive exposure to the PM_{10} (American Lung Association [3]). Hence, it shows that PM_{10} and O_3 are very harmful to human health. Besides that, air pollutants (e.g., PM_{10}, CO, NO_2, SO_2 and O_3) emissions into the atmosphere may significantly increase the atmospheric temperature and cause global warming (Patrick et al. [16]). Hence, this study is important to investigate the impact of air pollutions on global warming in the urban-industrial area.

2 Study Area

Figure 1 shows the location area of this study that located at three (3) main industrial areas in West Coast Peninsular Malaysia. These selected areas are (1) Perai, Penang, (2) Ipoh, Perak, and (3) Petaling Jaya, Selangor. Literature has reported that these areas are highly developed area in Malaysia that experience crucial air quality due to the emission of air pollutants from the industrial activities (DOE [5]). According to Ismail et al. [11], the industrial expansion, rapid urbanization and increment of high volume vehicles significantly cause serious air pollution and threats to both the natural environment and public health. Perai is located in the state of Penang, the Northern region of Peninsular Malaysia (coordinate of 5°22′40.263″ N and 100°23′56.989″ E) (Google Maps [14]). Department of Statistics Malaysia (DOSM [6]) reported that Perai is an industrial city that has population approximately 14,433 people. Perai has strategic location due to its location near to Butterworth City, logistic facilities between Perai River and the Penang Bridge, and rapid development of residential area (e.g., township of Seberang Jaya) (DOSM [6]). Due to these factors, Perai is experiencing rapid urbanization and industrialization development. The second area is Ipoh that located in the state Perak, the Northern Region of Peninsular Malaysia (coordinate 4°35′50″ N and 101°04′30″ E) (Google Maps [14]. It covers 64,300 ha area of mainly former tins mining industry (DOSM [6]). There are many heavy industrial activities in Ipoh city that lead to serious air pollution problem in Ipoh (DOE [5]). For example, Tasek, Bercham and IGB industrial areas (DOE [5]). Tasek Industrial area has various industries such as plastics, non-metal, rubber bases, food, printing and wood bases ((Ismail et al. [11]). The third area is Petaling Jaya that located in the Klang Valley (coordinate 3°05′50″ N and 101°38′40″ E) (Google Maps [14]). It covers 9,720 ha area and the capacity of the population is very dense with 197,949 people (DOSM [6]). This area is mainly former rubber estates in the 1950s. Now, the area is mostly surround
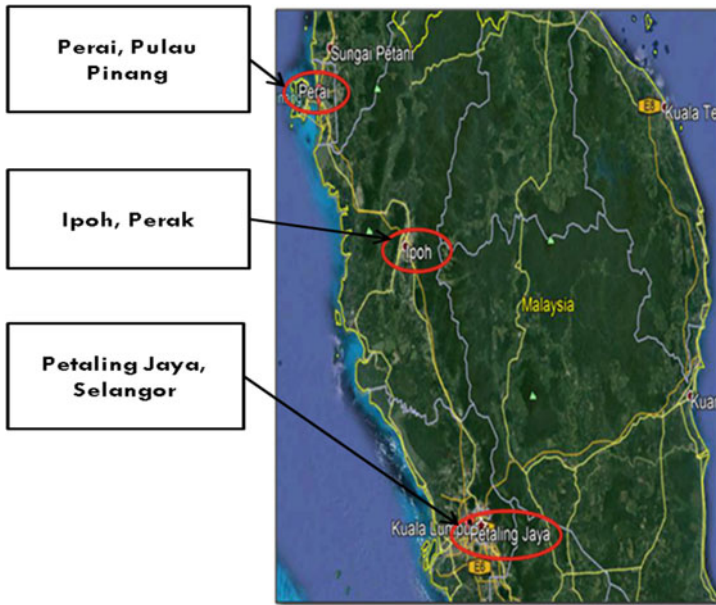
Fig. 1 Locations of study areas

by residential, commercial (e.g., PJ21 Commercial Centre), light industrial (e.g., Mayang Industrial Park and Bandar Sunway Light Industrial Park) and green areas (e.g., Tropicana Golf and Country Resort). DOE has reported that air quality level in Petaling Jaya is one the main environmental issue in Klang Valley (DOE [5]).

3 Air Quality and Meteorological Data

3.1 Data Collection

This study focus on the data collection of air pollutants and meteorological from DOE and Meteorological Department of Malaysia (MMD), respectively. DOE provided five (5) years (2013–2017) data of PM_{10}, CO, NO_2, SO_2, and O_3 at (1) Perai, Penang, (2) Ipoh, Perak, and (3) Petaling Jaya, Selangor. While, MMD provided 5 years data of rainfall, temperature and relative humidity at these industrial areas. DOE and MMD are using Continuous Air Quality Monitoring (CAQM) Station and Automatic Weather Stations (AWS) for air quality monitoring at these areas. Collected data from the DOE and MMD were analyzed using statistical analysis (as described in Sect. 3.1). There were three (3) main analysis were involved in this study (1) trends of air pollutants in compliance with the RMAAQG,

(2) correlation between the air pollutants and the influence of meteorological conditions and (3) the impact of air pollutant on the global warming.

3.2 Statistical Analysis

The descriptive statistics were carried out using SPSS Statistics statistical software. SPSS statistic is a software package used for statistical analysis that is interactive or batched. IBM acquired it in 2009 for a long time by SPSS Inc. IBM SPSS Statistics is name for the current versions (2015). The descriptive assessment carried out to evaluate the form, dispersion and allocation of information for the research fields. The most vital information to obtain out of a data set is the measurement tendency and the measurement of variability. SPSS Statistics 22 has been used in this study to analyze the descriptive statistics for each data set (e.g., concentration of air pollutants and meteorological data). The Pearson correlation was carried out in this study to evaluate correlation between various air pollutants (e.g., PM_{10}, CO, NO_2, SO_2 and O_3) and meteorological parameter (e.g., temperature, humidity and rainfall) at the selected study areas (e.g., Perai, Ipoh and Petaling Jaya). Examples of the correlation output are regression analysis (e.g., r-value) and p-value where it is correlated at 95% significant level ($\alpha = 0.05$).

4 Result and Discussion

4.1 Air Pollution Index (API) Analysis

The trend of air pollution was determined by the Air Pollutant Index (API) analysis. The API calculation was based on the average daily air pollutant concentration that involved PM_{10}, CO, NO_2, SO_2 and O_3. Figure 2 shows the annual API at Perai, Ipoh and Petaling Jaya in the year 2013 to 2017. The API result indicates that these industrial areas were in good condition (API: 0–50) except for 2015, where the API was slightly moderate (API: 50–100) at Ipoh and Petaling Jaya. The API value was contributed by PM_{10} for all areas in these five years. This analysis shows that API measurement for Perai was predominantly "good", where the API was in the range of 30.00–47.00. The highest API at Perai was 47 measured in 2015. While in Ipoh and Petaling Jaya, the air quality was predominantly "good" in all years except for 2015 and the range of API was 37.00–49.00 and 35.00–55.00, respectively. The highest API at Ipoh and Petaling Jaya were 53.00 and 55.00, respectively. The API measurement at Petaling Jaya was 4 and 15% higher compared to Ipoh and Perai respectively. The air quality status for Perai, Ipoh and Petaling Jaya constantly increased from 2013 to 2015 and constantly decreased from 2015 to 2017. The constant increased at Perai, Ipoh and Petaling Jaya was probably due to the haze
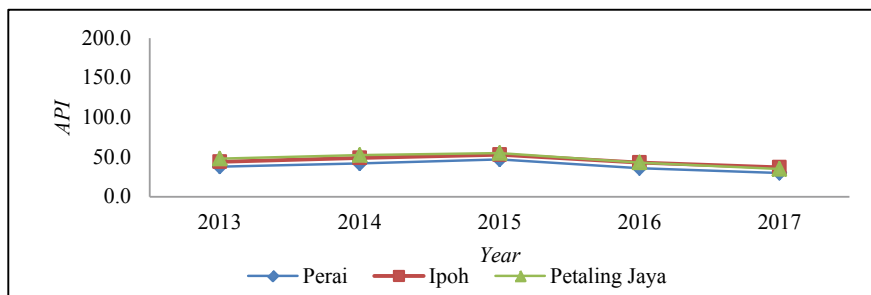
Fig. 2 Annual API at Perai, Ipoh and Petaling Jaya

event from the biomass burning in Southern Sumatera and Kalimantan in Indonesia, which had caused severe haze events in Malaysia (DOE [5]). Based on the MMD, the wind was moving from the Sumatera towards West Peninsular Malaysia during the southwest monsoon season in September and October (MMD [13]). West Peninsular Malaysia experienced a dried season with minimum rainfall during this season, except for Sabah and East Malaysia (MMD [13]). Due to this reason, PM_{10} was not significantly washout by rainfall and remained in the atmosphere at high concentration (<150 $\mu g/m^3$).

4.2 Trends of Air Pollutants in Compliance with RMAAQG

Figure 3(a) shows the annual average trend of PM_{10} concentration at Perai, Ipoh and Petaling Jaya from 2013 to 2017. The annual trend for these areas indicates that the trend with an average of about 74, 69 and 68% at Perai, Ipoh and Petaling Jaya, respectively were below the RMAAQG limit (150 $\mu g/m^3$). Besides, there was an acute increased of PM_{10} in 2015 than that in 2014, where the concentration of PM_{10} at Perai, Ipoh and Petaling Jaya was increased 11 (47), 13 (56), and 8% (60 $\mu g/m^3$), respectively. The API reading for 2015 was significantly contributed by PM_{10} due to the drastic increment of PM_{10} concentration that caused by the severe haze from the Indonesia. Therefore, it shows that the haze problem is one of the main problem that increased THE PM_{10} concentration. Other than that, the increased of PM_{10} concentration also may come from the industrial activities and combustion of fuels in the study areas (Vasudevan [19]).

Figure 3(b) shows the annual average trend of CO concentration at Perai, Ipoh and Petaling Jaya from 2013 to 2017. The annual trend of CO concentration for these areas indicates that the trend with an average of about 91, 94 and 86.6% at Perai, Ipoh and Petaling Jaya, respectively were below the RMAAQG limit (9 ppm). Although the concentration of CO not achieving the RMAAQG limit, there was a slight increase of CO in 2017 where the concentration of CO at Perai, Ipoh and Petaling Jaya was 0.86, 0.77 and 1.26 ppm, respectively. According to the
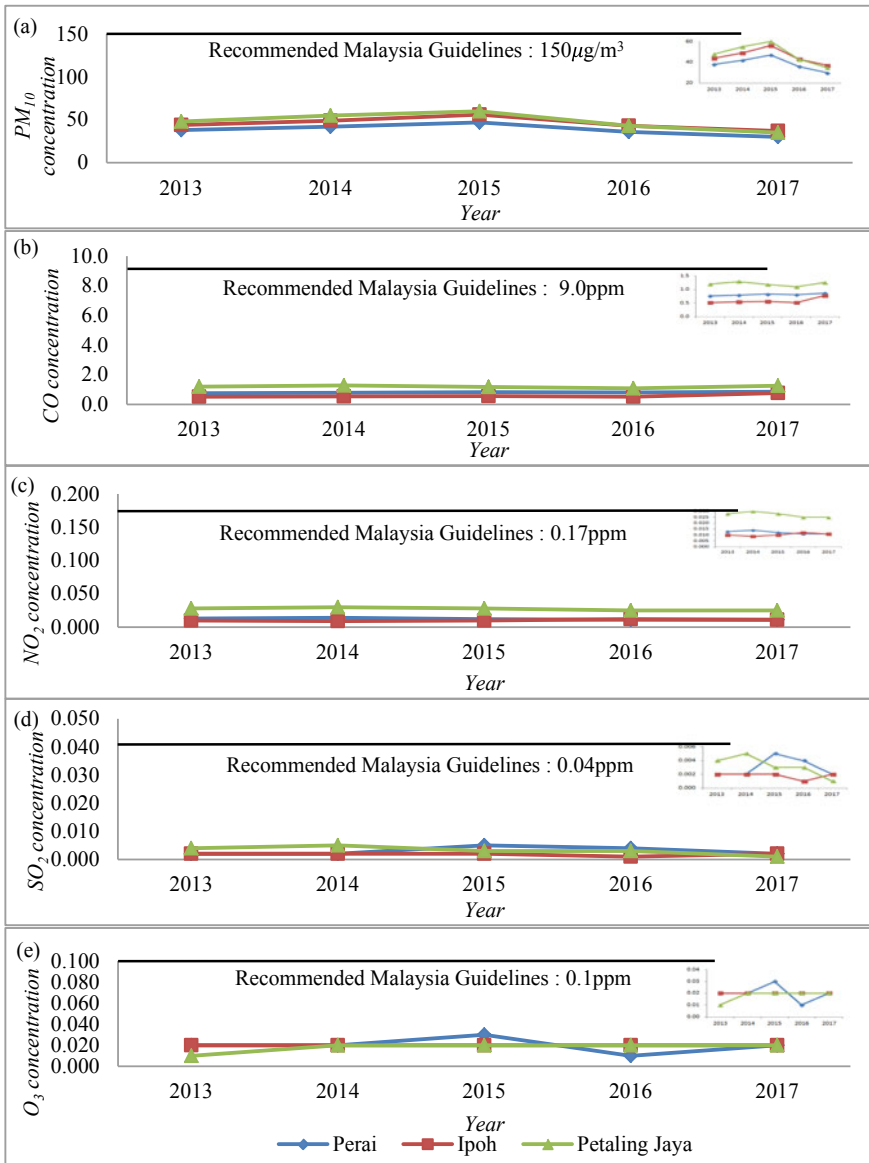
Fig. 3 Annual Average Concentration of (a) PM_{10} (b) CO (c) NO_2 (d) SO_2 and (e) O_3 at Perai, Ipoh and Petaling Jaya, 2013–2017

Ministry of Transport Malaysia [15], it stated that the average daily traffic in Petaling Jaya for 2017 was 153,545 vehicles compared to 2016 which only 138,711 vehicles. Hence, it shows an increase of average daily traffic in Petaling Jaya by 9.7% from 2016 to 2017. Therefore, the high increased of daily traffic significantly

increased the emission of CO from the motor vehicles that can contribute to the increased of CO concentration in 2017 at Petaling Jaya.

Figure 3(c) shows the annual average trend of NO_2 concentration at Perai, Ipoh and Petaling Jaya from 2013 to 2017. The annual trend of NO_2 concentration for these areas indicates that the NO_2 concentration was below the RMAAQG limit value, which is 0.17 ppm. This finding indicates that the NO_2 concentration at Perai, Ipoh and Petaling Jaya were averaging at 92.82, 93.88 and 84%, respectively below the RMAAQG limit value. There was no significant change in NO_2 concentration within the years 2013 to 2017. However, concentration of NO_2 in Petaling Jaya was slightly higher compared to Perai and Ipoh. This may due to a significant increased in the number of motor vehicles in the urban area and other sources of NO_2 (e.g., manufacturing industries and processing).

Figure 3(d) shows the annual average trend of SO_2 concentration at Perai, Ipoh and Petaling Jaya from 2013 to 2017. The annual trend of SO_2 concentration for these areas indicates that the SO_2 concentration was below the RMAAQG limit value (0.04 ppm). This finding indicates that the SO_2 concentration at Perai, Ipoh and Petaling Jaya were averaging at 92.5, 95.5 and 92%, respectively below the RMAAQG limit value. This finding shows that SO_2 concentration may not be harmful to human health because the reading is below than RMAAQG limit value. However, SO_2 still one of the dangerous pollutants to human health that needs to be controlled and concerned where the main sources of SO_2 come from industrial activity processes material that contains sulphur, such as the generation of electricity from coal, oil or gas that contains sulphur (Fernandez et al. [9]).

Figure 3(e) shows the annual average trend of O_3 concentration at Perai, Ipoh and Petaling Jaya from 2013 to 2017. The annual trend of O_3 concentration for these areas illustrates that the O_3 concentration was below the RMAAQG limit value (0.1 ppm). This finding indicates that the O_3 concentration at Perai, Ipoh and Petaling Jaya were averaging at 80, 80 and 82%, respectively below the RMAAQG limit value. Hence, this pollutant is still in control since the reading still below the RMAAQG limit value. This finding also reveals that the highest O_3 concentration was at Perai (0.03 ppm) in 201. This may probably due to the haze episode from September to October (DOE [5]). The O_3 also can be formed from the reaction of VOCs and NO_X in the presence of sunlight and heat (Amir [4]).

4.3 Correlation Between Air Pollutants and Meteorological Factors

Table 1 shows the correlation coefficients (r-value) and significant value ($p < 0.05$) between air pollutants (PM_{10}, CO, NO_2, SO_2, and O_3) and meteorological parameters (Rainfall, temperature, and humidity) at Perai, Ipoh and Petaling Jaya in 2013 to 2017. Statistical analysis reveals that there have significant correlations between air pollutants and meteorological parameters at Perai, Ipoh and Petaling Jaya where

Table 1 Correlation between air pollutant and meteorological parameter

Location	Pollutants	Meteorological parameter		
		Rainfall	Temperature	Humidity
Perai	PM_{10}	−0.387[*] (0.002)	0.438[*] (0.000)	−0.416[*] (0.001)
	CO	0.114 (0.386)	−0.059 (0.652)	0.122 (0.352)
	NO_2	−0.146 (0.266)	−0.040 (0.759)	−0.253 (0.051)
	SO_2	0.050 (0.702)	−0.354[*] (0.006)	−0.019 (0.884)
	O_3	0.087 (0.510)	−0.036 (0.787)	0.189 (0.149)
Ipoh	PM_{10}	−0.432[*] (0.001)	0.451[*] (0.000)	−0.451[*] (0.000)
	CO	−0.007 (0.958)	0.052 (0.692)	−0.090 (0.492)
	NO_2	−0.242 (0.062)	0.200 (0.125)	−0.044 (0.741)
	SO_2	−0.051 (0.696)	0.028 (0.831)	−0.029 (0.827)
	O_3	−0.409[*] (0.001)	0.306[*] (0.017)	−0.419[*] (0.001)
Petaling Jaya	PM_{10}	−0.335[*] (0.009)	0.382[*] (0.003)	−0.310[*] (0.016)
	CO	0.100 (0.446)	−0.123 (0.351)	0.226 (0.083)
	NO_2	0.269[*] (0.037)	−0.077 (0.557)	0.164 (0.211)
	SO_2	−0.118 (0.369)	0.022 (0.866)	0.091 (0.490)
	O_3	−0.189 (0.149)	0.432[*] (0.001)	−0.436[*] (0.000)

Note: [*]Significant at $\alpha = 0.05$. Value in parenthesis = p-value.

the p-value is compared at 95% significant level ($\alpha = 0.05$). From Table 1, it shows that PM_{10} is significantly correlated with rainfall, temperature and humidity. The correlation PM_{10}-Rainfall significantly correlated at Perai ($r = -0.39$), Ipoh ($r = -0.43$) and Petaling Jaya ($r = -0.34$). This result indicates that PM_{10} significantly removed during rainfall. A similar finding reported by previous studies, where the associations between meteorological parameters and particulates were found that the increased of rainfall established a negative correlation with PM_{10} (Dominick et al. [7]). PM_{10} also significantly correlated between temperature in Perai ($r = 0.44$), Ipoh ($r = 0.45$) and Petaling Jaya ($r = 0.38$). This positive significant correlation indicates that increased of the temperature increased the concentration of PM_{10} in

Perai, Ipoh and Petaling Jaya. Generally, the trends show that there was increased of PM_{10} concentration from June to July, indicating that relationship between PM_{10} and temperature are consistent. During June to July (southwest monsoon), West Peninsular Malaysia experienced a dried season with minimum rainfall during this season. Due to this reason, PM_{10} significantly increased with increased in the temperature and may remain in the atmosphere. PM_{10} also shows significant correlation between humidity at Perai (r = −0.42), Ipoh (r = −0.45) and Petaling Jaya (r = −0.31). This significant negative correlation indicates that PM_{10} may trap or dissolve in water droplets in the atmosphere. A similar finding was reported from the previous studies by Jayamurugan et al. [12], where the PM_{10} (r = −0.71) was negatively correlated with humidity. Moreover, during April and October to November (transitional period), West Peninsular Malaysia received a high amount of rainfall and winds from various directions. Due to this reason, the percentage of humidity during this period was also high and PM_{10} was significantly dissolved in water droplets in the atmosphere (Amir [4]). Theoretically, the rate of dissolution of particulates in the atmosphere increases with the increase of humidity (Jayamurugan et al. [12]). Moreover, the humidity value in Ipoh (88.5%) was higher than the humidity value in Perai (86.5%) and Petaling Jaya (82.5%). Due to this reason, PM_{10} may significantly dissolve in water droplets in the atmosphere at Ipoh compared to Perai and Petaling Jaya.

O_3 has a significant correlation between rainfall (r = −0.41) at Ipoh. A similar finding reported by the previous study indicates that O_3 was significantly removed by the rainfall (Yoo et al. [20]). Rainy weather is typically associated with low O_3 concentration because O_3 can significantly dissolved in the water droplets in the atmosphere (Yoo et al. [20]). In the meantime, Ipoh is in the valley area compared to Perai and Petaling Jaya where O_3 can be trapped in the valley area. Literature has reported that valley area has significant potential to trap more pollutants compared to a flat surface or hilly area (Airgo [2]). Table 1 also shows that there is significant positive correlation between NO_2-Rainfall (r = 0.27) at Petaling Jaya. This result indicates that NO_2 has no significant effect on the washout or scavenging effect from the rainfall event. This is probably due to the haze episode that occurred from September to October that prolonged the dry season (South West Monsoon) and the emission of NO_2 from the transportation and industrial activities in Petaling Jaya. Meanwhile, Perai has a significant negative correlation between SO_2-Temperature (r = −0.35). This result indicates that SO_2 has no significant effect on the temperature in Perai. This is probably due to the SO_2 concentration in Perai was lower compared to the SO_2 concentration in Ipoh and Petaling Jaya. Due to this reason, there is no significant reaction occurred between SO_2 and temperature at Perai.

4.4 Impact of Air Pollutant Related to Meteorological Factor on Climate Change

Figure 4 shows the annual temperature at Perai, Ipoh and Petaling Jaya from 2013 to 2017. The annual temperature shows that temperature for Perai, Ipoh and Petaling Jaya was increased except for 2017. There was a slight increased in temperature in 2016 than that in 2015 at Perai, Ipoh and Petaling Jaya where the temperature was raised to 28.94 °C (2.1%), 28.21 °C (2.5%) and 28.95 °C (1.8%), respectively. This is due to the effect of the biomass burning in Southern Sumatera, Indonesia that occurred in August 2016. According to MMD [13], West Peninsular Malaysia experienced a dried season with minimum rainfall during Southwest Monsoon (May–Sept). Moreover, the wind was moving from the Sumatera towards West Peninsular Malaysia and transported more pollutants (e.g., PM_{10} and O_3) that can increase the temperature. Other than that, the industrial processes also contribute to the high emission of air pollutants at the study area. According to Huang et al. [10], the burning of fossil fuels from industrial areas is a major source of both air pollutants and greenhouse gases. Air pollution also has a short-term regional climate effect-pollutant like black particles, ozone, and its precursors contribute to warming and consequently recognized as short-lived climate pollutants. Therefore, due to this reason, it shows that air pollution affects the significant increase in the temperature reading (related global warming) at Perai, Ipoh and Petaling Jaya in 2016. Similar findings reported by previous study, where the association between global warming and air pollutant such as PM_{10} that adversely affects human health directly or indirectly (Tagaris and Liao [18]). According to Patrick et al. [16], global warming or climate change adversely affects the ecosystem, economic and human health. Generally, global warming and climate change can cause drought, flooding, deforestation, homelessness and extinction of animal and plant species resulting in famine and disease.
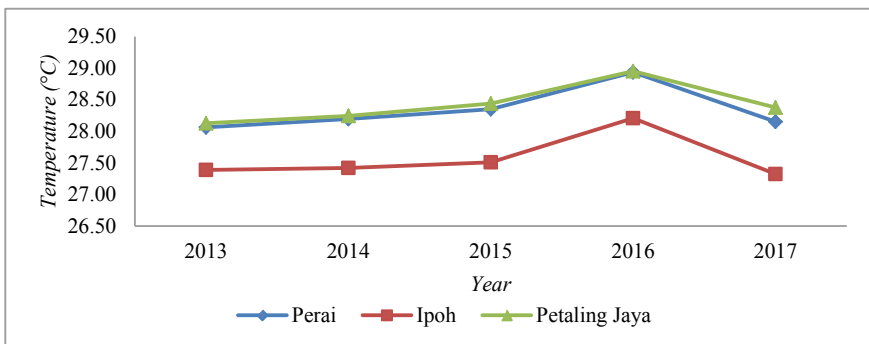
Fig. 4 Annual Temperature at Perai, Ipoh and Petaling Jaya from 2013–2017

5   Conclusions

A comprehensive study on the impact of meteorological factors on air pollution trends at the industrial area in West Peninsular Malaysia. This study reveals significant correlation between air pollutants (e.g., PM_{10}, CO, NO_2, SO_2, and O_3) and meteorological data (e.g., rainfall, temperature and humidity). The API analysis shows that API for Petaling Jaya was higher compared to Ipoh and Perai. This finding indicates that these areas were in good condition except for 2015, where the API was slightly moderate at Ipoh and Perai. The API value was contributed by PM_{10} for all areas in these years. The concentration of five (5) main air pollutants monitored by the DOE (e.g., PM_{10}, CO, NO_2, SO_2, and O_3) were well below the RMAAQG limit. Evaluation of the correlation between the air pollutants and the meteorological conditions reveals that there was significant correlation between air pollutants and meteorological parameters at Perai, Ipoh and Petaling Jaya. Interestingly, PM_{10} shows a significant correlation between meteorological parameters namely rainfall, temperature and humidity at Perai, Ipoh and Petaling Jaya. The temperature analysis indicates that air pollutants released significantly influenced the increment of temperature that leads to global warming issue. It is important to understand the impact of global warming to human health, climate change, environments (e.g., flora and fauna) and economy. In conclusion, meteorological factors play an important role in influencing air pollutants concentration in the atmosphere that may related to global warming phenomena.

References

1. Afroz R, Hassan MN, Ibrahim NA (2003) Review of Air pollution and health impacts in Malaysia. Environ Res 92:71–77
2. Airgo (2018) Air Pollution. https://www.airgo2.com/air-pollution/. Accessed 6 Nov 2018
3. American Lung Association (2013) American Lung Association State of the Air 2013 - Health Effects of Ozone and Particle Pollution. https://www.stateoftheair.org/2013/health-risks/. Accessed 26 Nov 2018
4. Amir A (2007) Air Pollution Trends in Petaling Jaya, Selangor, Malaysia. (Master of Science). UPM
5. Department of Environment (2015) Malaysia Environmental Quality Report
6. Department of Statistics Malaysia (2013) Compendium of Environment Statistic (Department of Statistics Malaysia, Trans), Malaysia, p 278
7. Dominick D, Latif MT, Juahir H, Aris AZ, Zain SM (2012) An Assessment of influence of meteorological factors on PM10 and NO_2 at selected stations in Malaysia. Sustain Environ Res 22(5):305–315
8. Enger ED, Smith BF (2000) Environmental Science: A study of Interrelationships, 7th edn. McGraw-Hill, Boston

9. Fernandez A, Frampton W, Holgate ST, Janssen N, Ito KN, Schlesinger R (2005) Air Quality Guidelined Global Update 2005. Europe: World Health Organization Europe
10. Huang K, Fu JS, Hsu NC, Gao Y, Dong X, Tsay SC, Lam YF (2013) Impact assessment of biomass burning on air quality in South East and East Asia during BASE-ASIA. Atmos Environ 78:291–302
11. Ismail AS, Abdullah AM, Samah MAA (2017) Environmetric Study on Air Quality Pattern for Assessment in Northern Region of Peninsular Malaysia
12. Jayamurugan R, Kumaravel B, Palanivelraja S, Chockalingan MP (2013) Influence of temperature, relative humidity and seasonal variability on ambient air quality in a coastal urban area. Int J Atmos Sci 2013:7
13. Malaysian Meteorological Department (2016) Malaysian Meteorological Department Annual Report.
14. Google Maps (2019) Google. https://maps.google.com.my/
15. Ministry of Transport Malaysia (2017) Transport Statistics Malaysia 2017
16. Patrick DL, Murray TP, Sullivan RK, Kimmell KL (2018) Health and Environmental Effects of Air Pollution. Commonwealth of Massachusetts
17. Sham S (1984) Suspended particulate air pollution over Petaling Jaya during the september 1982 Haze. Ilmu Alam 12(13):83–90
18. Tagaris E, Liao KJ (2009) Potential impact of climate change on air pollution-related human health effects. Environ Sci Technol 43:4979–4988
19. Vasudevan N (2006) Essentials of Environmental Science. Alpha Science International Ltd., Oxford
20. Yoo JM, Lee YR, Kim D, Jeong MJ et al (2014) New indices for wet scavenging of air pollutants by summertime rain. Atmos Environ 82:226–237

The Effect of Curing Conditions on the Strength of Masonry Blocks Incorporating Palm Oil Fuel Ash

Zalipah Jamellodin, Hairu Azila Abd Hamid, Noor Azlina Abdul Hamid, Norhafizah Salleh, and Suraya Hani Adnan

Abstract Palm Oil Fuel Ash (POFA) is a by-product of the palm oil industry that is often disposed at landfills. In oil palm-producing countries such as Malaysia, Indonesia and Thailand, the high amount of POFA waste disposal is undoubtedly an environmental problem that needs to be overcome to contribute towards zero-carbon emissions by 2050. This paper presents the incorporation of POFA as a partial cement replacement in the production of concrete masonry blocks – a common building material in developing countries. In this study, the cement content by weight of a conventional concrete masonry block was replaced incrementally at 10% interval until 30% with ground POFA. The specimens were either cured in water or left dry and tested after 28 days of curing for density, compressive strength and water absorption rate based on standard testing requirements. A general observation has been taken note on the superior results of water-cured masonry blocks with up to 20% POFA content. The results of this study is anticipated to add value to the present knowledge bank on incorporating waste material into sustainable building material research and development. In general, POFA is a highly potential replacement for cement, but further studies need to be done to ensure consistency in performance and for industrial application.

Keywords Cement replacement · Masonry block · POFA · Pozzolanic · Soaked and Unsoaked

Z. Jamellodin (✉) · H. A. A. Hamid · N. A. A. Hamid · N. Salleh
Faculty of Civil Engineering and Buit Environment, Universiti Tun Hussein Onn Malayia, Batu Pahat, 86400 Parit Raja, Johor, Malaysia
e-mail: zalipah@uthm.edu.my

S. H. Adnan
Faculty of Engineering Technology, Universiti Tun Hussein Onn Malayia, Pagoh Higher Education Hub, KM 1 Jln Panchor, 84600 Panchor, Johor, Malaysia

1   Introduction

Masonry is a building material with its usage dated back to the very beginning of human civilization. It is favoured for its low maintenance requirement and good durability (Sousa et al., 2011). In Malaysia, concrete masonry blocks commonly made from cement, sand and water (Rahman et al. 2014) are used in almost all construction projects. However, the conventional production method utilizing fossil fuel combustion is undoubtedly a contributor to global warming and a hindrance to achieve net zero-carbon emissions by 2050.

Cement is still the major ingredient for masonry block production, and thus, to address the global warming effect brought upon by its usage, efforts have been continuously made in the research and development of alternative material. A notable development is in study of pozzolanic material such as Palm Oil Fuel Ash (POFA) that contain chemical properties similar to cement. POFA is a waste material mostly disposed at landfills. As a palm oil-producing country, Malaysia is undeniably at the advantage in the advancement of sustainable material for the future. Aside from a reduction in pollution-related issues (Safiuddin et al. 2011), replacement of cement with POFA, even only partially, is able to reduce construction cost significantly (Rahman et al. 2014).

This paper intends to present the results of a study conducted on POFA as a cement replacement based on three important characteristics of a series of masonry units produced in a laboratory environment – density, water absorption rate, and compressive strength. In all tested units, 10 to 30% of the cement by weight were replaced with POFA. The results of this study is anticipated to add value to the present knowledge bank on incorporating waste material into sustainable building material research and development.

1.1   *Unconventional Masonry Block*

The study on masonry blocks containing various waste material is not entirely a new venture. Mutohar and Rahman (2014) studied the use of oil palm shell (OPS) waste as a masonry block material and concluded that a mixing ratio of 1:1:1 for cement, sand and OPS would produce the masonry unit with highest compressive strength.

Study using POFA, on the other hand, can be dated back to 2009 when Awal and Hussin (2009) performed compressive tests on Ordinary Portland Cement (OPC) concrete that had been partially replaced with POFA. However, the results were not favourable; the modulus of elasticity and compressive strength of the tested units were found lower that those of OPC concrete. In addtion, the POFA concrete's shrinkage strain was also higher than OPC concrete.

The study of Weerachart and Chai (2010) reached a completely different conclusion. Their study found that the compressive strength of OPC concrete had

increased with increased fineness of the POFA. This was not the first time where POFA had been regarded highly. In 1997, Awal and Hussin (1997) had already highlighted that POFA could potentially suppress expansion due to alkaliesilica reaction. Subsequent studies had also emphasized on a variety of other potential. For instance, Abdul Awal and Shehu (2013) found that POFA could control the hydration heat of concrete formation and Chai et al. (2007) noted an increased durability and sulphate resistance of concrete incorporated with POFA. Johari et al. (2012) studied the strength and durability properties of high-strength green concrete (HSGC) containing up to 60% ultrafine POFA and also obtained favourable results.

Rahman et al. (2014) attempted to replace OPC with POFA in an increment of 20 until 60% by binder weight. Each masonry block was 200 mm long, 100 mm wide and 70 mm thick. The masonry blocks were cured and tested after 28 days for strength and 65 days for long term effects. All tests were carried out according to (ASTM 2011), which were comprised of compressive strength test, breaking load test, water absorption test and efflorescence teset. The notable finding of this study was a significant decrease in masonry's density with increasing POFA content. In the study of (Ling and Teo 2011) whereby similar tests were conducted, it was found that all water absorption values were below the maximum water absorption capacity defined in ASTM C55-11 (2011). Based on the standard, the water aborption should be 208 kg/m^3 for normal weight masonry block, 240 kg/m^3 for medium weight masonry block and 320 kg/m^3 for light weight masonry block.

1.2 Palm Oil Fuel Ash (POFA)

The studies aforementioned clearly showed that Palm Oil Fuel Ash has been a material of research interest since two decades ago. POFA is a by-product of the oil palm industry, generated from the burning of oil palm shell and empty fruit bunches. Fundamentally, it has been proven that the calcium hydroxide (Ca $(OH)_2$) produced during the hydration process of concrete can react with the silica oxide content in POFA. This pozzolanic reaction increases the formation of a gel compound called "calcium silicate hydrate" (C-S–H) and reduces the $Ca(OH)_2$ content at the same time (Sooraj 2013).

The production and disposal of POFA is not expected to drop over the years, particularly in oil palm-producing countries such as Malaysia, Thailand and Indonesia. This phenomena presents an untapped potential to produce sustainable material from the waste for the construction industry.

The major challenge to overcome is the alteration of the POFA characteristics due to the combustion process (Safiuddin et al. 2011). Not only that, the particle size of the POFA has also been found to significantly affect the quality of the final product – the finer the particles, the better the compressive strength, in general (Mohamad 2016). Another unfavourable property lies in its high organic and alkali content.

2 Experimental Program

2.1 Material

The main material used in the production of masonry blocks are cement, fine sand, water and POFA. All were sourced locally with the POFA obtained free from a local palm oil mill owned by the Ban Dung Palm Oil Industries Sdn. Bhd. In Kangkar Senangar, Parit Sulong, Johor. The POFA was dried in an oven for 24 h to remove the moisture. Then, the POFA material were grinded using a grinder machine with only 1 to 3% retained at a sieve size of 75 μm.

The OPC used was grade 42.5, following the requirement of ASTM:C150/C150M – 12. The fine sand particle size was less than 1.18 mm, achieved by sieving the sand particles through the relevant sieve size.

2.2 Masonry Block Mix Design Proportion

Sizes of all masonry blocks were fixed at 215 × 105 × 65 mm (length x breadth x thickness). Five batches of masonry block were made. The OPC content was replaced by weight with POFA at an increment rate of 10 until 30%. The mixing ratio of cement and sand (C:S) was fixed at 1:3. The water binder ratio was set at 0.5. Table 1 shows the masonry block mix ratios for all series. The masonry blocks were tested after 28 days of curing in a wet and dry condition.

2.3 Preparation of Masonry Blocks

The masonry blocks were produced manually using hand compaction method. The OPC and fine sand were first weighed, mixed and blended well before POFA was added into the mixture. During mixing, water was added gradually until a homogeneous mixture was obtained. The whole mixing process took about 15–20 min. After that, the mixture was poured into an iron block mold. The specimens were then compacted manually, left for 24 h, and demoulded for curing.

Table 1 Masonry brick ratio for all series of masonry blocks

Series	Symbol	Ratio
1	C100	C: S = 1:3 (Control)
2	C90P10	C + POFA (10%): S = 1:3
3	C80P20	C + POFA (20%): S = 1:3
4	C70P30	C + POFA (30%): S = 1:3

Fig. 1 Masonry block specimens cured in wet condition

Fig. 2 Masonry block specimens cured in dry condition
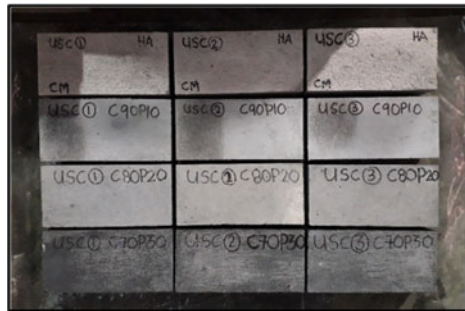
Two curing conditions were set in this experiment. The first batch of specimens were soaked as shown in Fig. 1 for 28 days. The second batch were cured in dry condition as shown in Fig. 2.

2.4 Testing Methods

Compressive strength test and water absorption test were conducted based on the requirements stipulated in ASTM C55-11 (2011) for masonry blocks and structural clay tiles. For the first batch of specimens cured in wet condition, compressive strength test was conducted immediately after 28 days of curing. For the second batch, the water absoprtion test was conducted first after 28 days of curing, followed by the same compressive strength test.

2.4.1. Compression Test

The compressive strength test of the masonry blocks was done on the 28[th]day after curing, using the Universal Testing Machine (UTM) that complied to BS EN 196–1 (BS 2016). Load was applied onto the masonry block until failure at a constant loading rate of 1.25 mm/min. The compressive strength of each specimen was calculated in MPa (N/mm^2) following Eq. (1) below:

$$C = P/A \tag{1}$$

where C is the compressive strength, P is the maximum load (kN) and A is the average surface are (mm^2).

2.4.2. Water Absorption Test

The water absorption rate test was conducted based on the requirement stipulated in BS EN 772–21 (2011). This test was conducted on both sets of specimens, regardless of the curing condition. Specimens which had been cured in wet condition was oven-dried for 24 h at 105 °C. The dry weight after oven-drying was taken W_d. After that, the specimens were cooled down to room temperature (approximately 25 °C) as shown in Fig. 3, and then re-immersed in water at 25 °C for another 24 h.

After 24 h of immersion, the surface of the specimens were wiped dry with a damp cloth and the weight recorded after that was recorded as the saturated weight, W_s. The water absorption of each specimen in percentage was calculated as:

$$\text{Water Absorption, } \% = 100\,(W_s - W_d)/W_d \tag{2}$$

3 Results and Discussions

3.1 Density of Masonry Block

The density of the masonry block specimen was calculated and as illustrated in Fig. 4. In general, the graph showed that the density of the soaked specimens were consistently higher than that of unsoaked specimens. In addition, other than a significant increase in density when 10% of cement was replaced with POFA, further replacement did not seem to remarkably affect the density of the masonry block.

Fig. 3 Specimen cooling process after 24 h oven-drying to reach room temperature
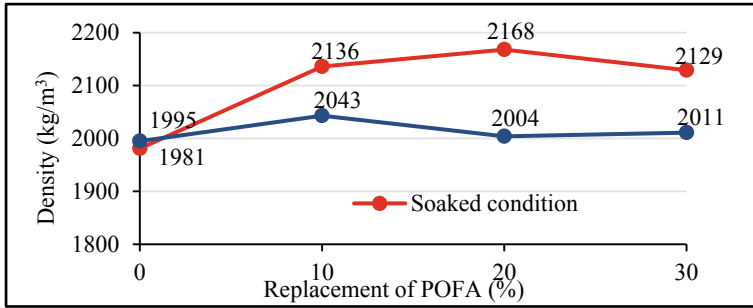
Fig. 4 Average densities of all masonry block specimens

The average density of the control specimen cured in wet condition was 1981 kg/m^3. When the cement weight was replaced with 10% POFA, this increased 7.80% to 2136 kg/m^3. Although this had further increased another 1.5% to 2168 kg/m^3 when the POFA increased to 20%, it had dropped to 2129 kg/m^3 when 30% POFA was incorporated.

In the case of unsoaked specimens, the density had increased from 1995 kg/m^3 for control specimen to 2043 kg/m^3 (2.41%) for the specimen with 10% POFA content. However, when the POFA content increased to 20%, the density had dropped to 2004 kg/m^3. At 30% POFA content, the density was 2011 kg/m^3, which was just 0.8% higher than the control specimen.

The results of density had generally showed that the optimal replacement rate of cement with POFA was 20% for the soaked specimens. For the dry specimens, the optimal replacement rate was 10%. However, in both cases, 10% replacement rate would cause the most significant increment in density.

3.2 Compressive Strength of Masonry Block

Figure 5 shows the results of compressive strength test for all specimens. Generally, an increase in POFA content up to 20% had caused an increase in compressive strength. The compressive strength for the control specimen (C100), for both soaked and dry specimens, were 24.9 MPa and 23.2 MPa, respectively. At an optimal cement replacement rate of 20% with POFA, the compressive strength of soaked specimens (C80P20) had increased 12.4% to 28 MPa and the compressive strength of dry specimens had increased 7.33% to 24.9 MPa. Beyond that, both specimens portrayed a significant drop in compressive strength even below the control specimen's. For the soaked specimens, the compressive strength was 24.8 MPa. For the dry specimens, the compressive strength was only 22.3 MPa.

The significant drop was attributed to the POFA particle size of 75 μm that was bigger than the cement's average size of 45 μm. When the POFA content increases,
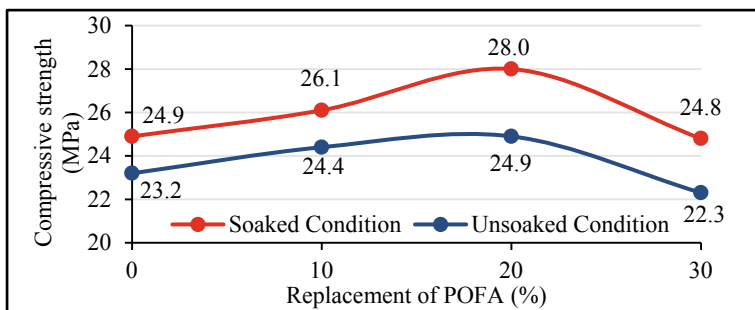
Fig. 5 Compressive strength results of masonry block specimens

Table 2 Average compressive strength of masonry block specimens

Mix Design	Average compressive strength (MPa)		Percentage difference between soaked and unsoaked curing conditions
	Soaked condition (water curing)	Unsoaked condition (air curing)	
C100	24.9	23.2	6.8
C90P10	26.1	24.4	6.5
C80P20	28.0	24.9	11.1
C70P30	24.8	22.3	10.1

more gaps were created between cement particles, causing a drop in microfilling ability and thus, a drop in compressive strength. The ability of higher microfilling to increase compressive strength had been previously discussed by Awal et al. (2010).

A further comparison was made between soaked and dry specimens in terms of the compressive strength, as shown in Table 2. In all cases, the compressive strength of soaked specimens were at least 6.5% higher than its dry counterpart. This difference was attributed to the hydration process which had facilitated in strength development. The highest difference was 11.1% for the specimens with 20% POFA. It is also worth highlighting that the compressive strength of dry specimens in this sense was also the strength of the control specimens cured in water.

3.3 Water Absorption of Masonry Block

The water absorption results are presented in Fig. 6. The water absorption rates of the control set were 7.04% for the soaked specimens and 6.29% for the dry specimens. masonry block specimen which was C100 specimen obtained average water absorption of 7.04% for soaked masonry block and 6.29% for unsoaked
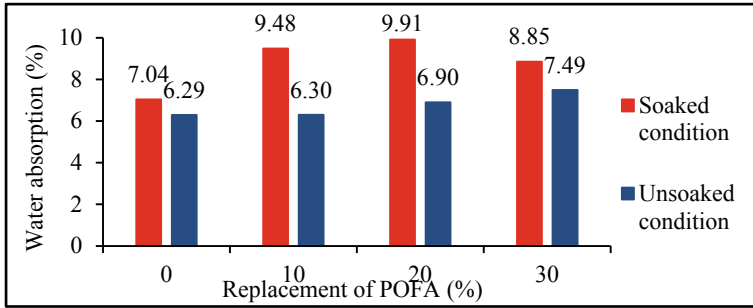
Fig. 6 Water absorption of masonry block specimens

masonry block. When 10% of the cement weight was replaced with POFA, the water absorption rates for the dry specimen maintained while that of soaked specimens increased 34.70 to 9.48%. The highest water absorption for the soaked masonry block was 9.91% when the POFA content was 20%, which then decreased to 8.85% when the POFA content increased to 30%. For the dry specimens, the increment in water absorption was generally insignificant. From 0 to 30% POFA content, the rate had merely increased 19% from 6.29 to 7.49%.

The results clearly showed that, in terms of water absorption rate, 20% cement replacement with POFA was the optimal rate to produce the highest water absorption rate. Soaked specimens also depicted higher water absorption rate than dry specimens (Safiuddin et al. 2011) attributed the higher water absorption rate to greater porosity of POFA, but the results of this study have pointed the inconsistency of this statement. If higher POFA content would increase the water absorption rate, then regardless of the curing condition, the specimens should consistently show incremental water absorption rate. This was not the case in this study.

In consideration of the overall results on density, compressive strength and water absorption rate, the optimal replacement rate of cement weight with POFA for the soaked specimens would be 20%. The results have also clearly showed that the masonry units need to be cured in water to improve its qualilty.

4 Conclusion

This study on the potential of POFA to partially replace cement in the production of masonry units have reached the following conclusions:

1. Regardless of the POFA content, water-curing would increase the overall quality of the masonry blocks compared to dry-curing.
2. Under wet-curing condition, a replacement of cement with 20% POFA by weight was the optimal rate to produce masonry blocks with the highest density, compressive strength and water absorption rate.

3. In general, POFA is a highly potential replacement for cement, but further studies need to be done to ensure consistency in performance and for industrial application.

References

ASTM C55-11 (2011) Standard Specification for Concrete Building Brick, *ASTM* International, West Conshohocken, PA

BS EN 196-1 (2016) Methods of Testing Ccement Part 1: Determination of Strength. British Standard. BSI Standards Publication

BS EN 772-21 (2011). Methods of Test for Masonry Units: Determination of Water Absorption of Clay and Calcium Silicate Masonry by Cold Water Absorption. British Standard. BSI Standards Publication

Ismail M, Ismail MA, Lau SK, Muhammad B, Majid Z (2010) Fabrication of Bricks from Paper Sludge and Palm Oil Fuel Ash. Concrete Res Lett 1(2):60–66

Ling IH, Teo DCL (2011) Properties of EPS RHA lightweight concrete bricks under different curing conditions. Constr Build Mater 25(8):3648–3655

Kubica, J. and Gąsiorowski, S. (2010). Mortar Selection in Design Practice Description of the Problems. *Solutions and Requirements, Architecture Civil Engineering Environment* 53–62.

McLellan BC, Williams RP, Lay J, Riessen AV (2011) Costs and carbon emissions for geopolymer pastes in comparison to ordinary portland cement. J. Clean Prod 19(9–10):1080–1090

Mohamad, M. E., Mahmood, A.A., Min, A.Y.Y., and Khalid, N.H.A. (2016). A Review of the Mechanical Properties of Concrete Containing Biofillers. *IOP Conference Series: Materials Science and Engineering,* 160(1).

Rahman ME, Boon AL, Muntohar AS, Hashem Tanim MN, Pakrashi V (2014) Performance of masonry blocks incorporating palm oil fuel ash. J Clean Prod 8:195–201

Rahman ME, Ong P, Nabinejad O, Islam S, Khandoker N, Pakrashi V, Shorowodi K (2018) Utilization of blended waste materials in bricks. Technologies 6(1):20

Ramli M, Dawood ET (2011) Comparative study between flowable high strength mortar and flowing high strength concrete. Concrete Res Lett 2(2):249–261

Safiuddin M, Abdus SM, Jumaat MZ (2011) Utilization of palm oil fuel ash in concrete: a review. J Civil Eng Manage 17(2):234–247

Sooraj VM (2013) Effect of palm oil fuel ash (POFA) on strength properties of concrete. Int J Sci Res Publ 3(6):2250–3153

Sousa LC, Sousa H, Castro CF, Antonio CC, Sousa R (2014) A new lightweight masonry block: thermal and mechanical performance. Arch Civil Mech Eng 14(1):160–169

Fracture Energy of Foamed Concrete Using Compression Test and Splitting Tensile Test

Norashidah Abd Rahman, Siti Amirah Azra Khairuddin, and Zainorizuan Mohd Jaini

Abstract Nowadays, foamed concrete has been renewed in its own structural characteristics, such as lightweight materials. Foamed concrete has received attention due to its potential as a building construction material. However, given its brittleness, the crack length highly depends on the strength and fracture properties of foamed concrete. Therefore, the fracture energy and crack length characteristic of foamed concrete are analysed. This study focuses on a cube sample size of $150 \times 150 \times 150$ mm and a cylinder specimen size of 150×300 mm with various densities of foamed concrete from 1000 to 1700 kg/m^3. The cube samples were tested under a compression test, while cylinder specimens underwent a splitting tensile test. Furthermore, the fracture energy were calculated using Bazant, CEB and Oh model. The experimental result shows that the fracture energy was significantly increased by the density of the concrete with a range under the compression test.

Keywords Crack length · Foam concrete · Fracture energy

1 Introduction

Foamed concrete, also known as cellular lightweight concrete, is one of the innovations that stem from normal concrete. Foamed concrete is now accepted as a structural material for construction. Thus, such acknowledgement leads to an increased confidence in its usage. Many researchers have provided a solid result, in which the strength of foamed concrete is influenced by the density, testing technique, water content, curing age and physical and chemical properties. Foamed concrete has dry densities, which range from 400 to 1600 kg/m^3, whilst the

N. A. Rahman (✉) · S. A. A. Khairuddin · Z. M. Jaini
Department of Civil Engineering, Faculty of Civil Engineering and Built Environment, Universiti Tun Hussein Onn Malaysia, Batu Pahat, 86400 Parit Raja, Johor, Malaysia
e-mail: nrashida@uthm.edu.my

compressive strength can withstand up to 15 MPa; the tensile strength achieves 10% of its compressive strength [7].

Bazant [3] has proposed that the fracture energy G_f may be uniquely defined as the energy required for crack growth in an infinitely large specimen. The fracture energy provides a great deal of insight to the failure process of brittle material, such as foamed concrete. Therefore, a great deal of attention should be paid to the fracture energy of foamed concrete. In addition to the fracture energy, the softening behaviour is important for the realistic description of the fracture formation in concrete. The fracture energy is a required value to perform the fracture analysis of concrete structure. A simple and prediction formula for fracture energy of concrete is proposed. In order to analyses the fracture energy, several of mathematical models is used to predict the values. Based on a few previous researches, it has proven that a few empirical equations have been used in order to predict the fracture energy. Compressive strength of concrete reflects the fracture energy as strength play the important role in ability to sustain loading and resist the crack.

The resistance to crack growth in foamed concrete is an important material property which needs to be investigated because the crack grows as the applied load increases. Furthermore, measuring the crack length is difficult, as the crack in the concrete is small in the microcracking zone. The crack length characteristic of foamed concrete depqqends on the value of fracture energy, tensile strength, compressive strength and Young's modulus of elasticity. The fracture energy is essentially a measure of the extent of plastic deformation associated with cracks. However, this study focuses on using a few empirical formulas that have been proposed by previous researchers to analyse the fracture energy and crack length characteristics.

2 Fracture Energy

The fracture behaviour of concrete has received considerable attention in recent years. Fracture energy is defined as the energy required for a crack to grow in a specimen. It is the most important parameter that governs the crack and failure of the structure. This energy is materially constant, and it is dependent on the material, type and geometry of the structure. A recent study by Rahman et al. [13], Jaini et al. [9] and Zamri et al. [14] have also found that the fracture energy of foamed concrete from the Hillerborg model falls within 10% of the prediction by the models of Bazant and the Comité Euro-International du Béton (CEB). Compressive strength is one of the fundamental properties used to ensure the quality of lightweight concrete. The value of compressive strength for densities from 400 to 1600 kg/m^3 range from 0.5 to 10.0 MPa [4]. The empirical equation used to predict the value of fracture energy using the value of compressive strength proposed by Bazant and Becq-Giraudon [2] is

$$G_f = 2.5\alpha_0 \left(\frac{f_c}{0.058}\right)^{0.40} \left(1 + \frac{D_{max}}{1.94}\right)^{0.43} \left(\frac{w}{c}\right)^{-0.18} \quad (N/m),\tag{1}$$

and the equation by the CEB [5] is

$$G_f = \left[0.0469(D_{max})^2 - 0.5D_{max} + 26 \times \left(\frac{f_c}{10}\right)^{0.7}\right] \quad (N/m).\tag{2}$$

Tensile strength is also one of the important properties of concrete that must be considered due to its high vulnerability to tensile cracking. Moreover, foamed concrete is known for its brittle tension but tougher compression. Given its low brittle nature, foamed concrete is not usually expected to resist direct tension. The previously-published good experimental data for the fracture energy of concrete have been used to determine the fracture energy equation proposed by Oh et al. [12]. Previous studies have proven that the fracture energy varies linearly with tensile strength. The prediction equation for the fracture energy of concrete is found from the test data [12]:

$$G_f = 58.4 f_t d_a / E_c \quad (N/m).\tag{3}$$

Oh et al. [11] have simplified the equation in Eq. (4):

$$G_f = 56.24 f_t d_a / E_c \quad (N/m).\tag{4}$$

Simple formula has been proposed by Bazant and Oh [3] by using tensile strength and Young's modulus of elasticity:

$$G_f = (15.53 + 17.72 f_t) f_t^2 \left(\frac{d_a}{E_c}\right) \quad (N/m),\tag{5}$$

where G_f is in N/mm, f_t is in N/mm^2 (or MPa), and d_a is the diameter of the aggregate in mm.

In Young's modulus of elasticity, E_c is the ratio between stress and strain, which depends on the stiffness of the constituents and their relative proportions in the mix. The stress strain relationship in any material is of vital interest in any structural design to establish the behaviour, deformation types, elasticity and elastic limit. The elastic limit represents the maximum allowable stress before the material undergoes permanent deformation. This concept is applied to foamed concrete to determine the value of Young's modulus of elasticity. However, the range value for the densities from 400 to 1600 kg/m^3 is 0.8 to 12 kN/mm^2 [4]. E_c is Young's modulus of elasticity in GPa. The value of elastic modulus, E_c, of foamed concrete is not measured directly through the experiment. Instead, the usual relations suggested by Byun et al. (1998) [15], Jones and McCarthy [8], Ramamurthy and Nambiar (2009) [16] and Jaini et al. (2015) [18] may be used.

$$E_c = 0.42 f_c^{1.18} \quad \text{(GPa)}, \tag{6}$$

where f_c is the compression strength of concrete in N/mm^2 (or MPa).

3 Experimental Work

Experimental studies on fracture energy of foamed concrete and crack length characteristics were conducted. For the preparation of foamed concrete, 3 mm sand size, Portland cement, water and form were used. The design mix of foamed concrete in this study was based on the Ultimate Study Manual (USM) method. The concentration of the foam agent used was 1/20, which was the ratio of 1 foam agent to 20 of water. The mix proportion used to produce foamed concrete with various densities is shown in Table 1.

A total of 15 cube samples with the size of $150 \times 150 \times 150$ mm and 15 cylinder specimens with the size of 150×300 mm were prepared with various densities of foamed concrete from 1000 to 1700 kg/m^3. A compression test was conducted on cube samples, whilst cylinder specimens underwent a splitting tensile test Fig. 1. The tests were conducted at 7, 14 and 28 days.

Table 1 Mix proportion

Material	Cement	Sand	W/C	F/C	Foam concentration
Ratio	1	2	0.55	0.7	1/20

*W/C = Water–Cement Ratio
*F/C = Foam–Concrete Ratio.
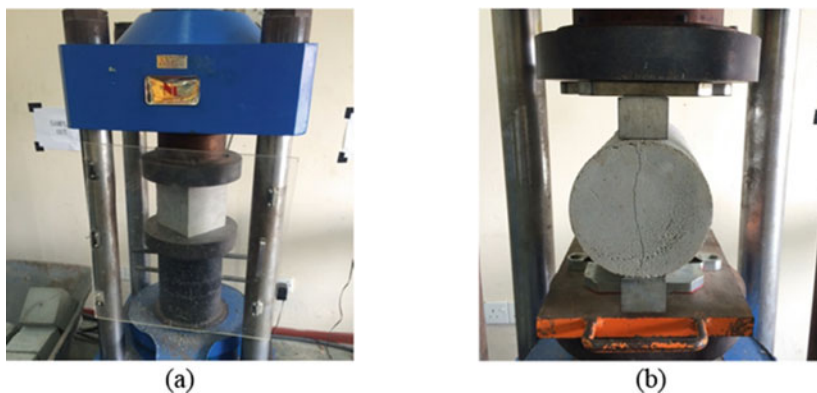
Fig. 1 Experimental test **a** Compression test **b** Spilitting test test

4 Results and Discussion

4.1 Compressive Strength and Tensile Strength of Foamed Concrete

Table 2 and Fig. 2 shows the result of compression strength and tensile strength of foamed concrete. From the result, it is show, the compressive strength of densities of 1700, 1600 and 1300 kg/m^3 is not acceptable, according to the British Cement Association [4]. However, the result obtained from experimental work for the densities of 1100 and 1000 kg/m^3 are not in the acceptable range because foamed concrete is brittle. Moreover, the strength may be affected by the weather and the temperature of the environment. Kearsley [10] has stated that increased temperature curing increases the compressive strength of foamed concrete. According to Jaini et al. [7], the tensile strength of foamed concrete is directly proportional of its compressive strength and is lowered approximately ten times. This result shows that the value of tensile strength is within an unacceptable range.

Table 2 Compression and splitting tensile test results on the 28th day

Density (kg/m^3)	Compression test			Splitting tensile test			
	Specimen	Compressive strength, f_c (MPa)	Average f_c (MPa)	Specimen	Tensile strength, f_t (MPa)	Average f_t (MPa)	Young modulus E_c (kN/mm^2)
1000	C10-1	1.0	0.93	T10-1	0.24	0.22	0.385
	C10-2	0.9		T10-2	0.23		
	C10-3	0.9		T10-3	0.20		
1100	C11-1	1.5	1.5	T11-1	0.29	0.29	0.368
	C11-2	1.6		T11-2	0.30		
	C11-3	1.4		T11-3	0.28		
1300	C13-1	5.7	5.57	T13-1	0.61	0.58	3.186
	C13-2	5.5		T13-2	0.55		
	C13-3	5.5		T13-3	0.58		
1600	C16-1	11.1	10.6	T16-1	1.25	1.20	6.809
	C16-2	10.5		T16-2	1.23		
	C16-3	10.2		T16-3	1.13		
1700	C17-1	15.3	15.87	T16-1	1.41	1.40	10.963
	C17-2	15.9		T16-2	1.40		
	C17-3	16.4		T16-3	1.39		
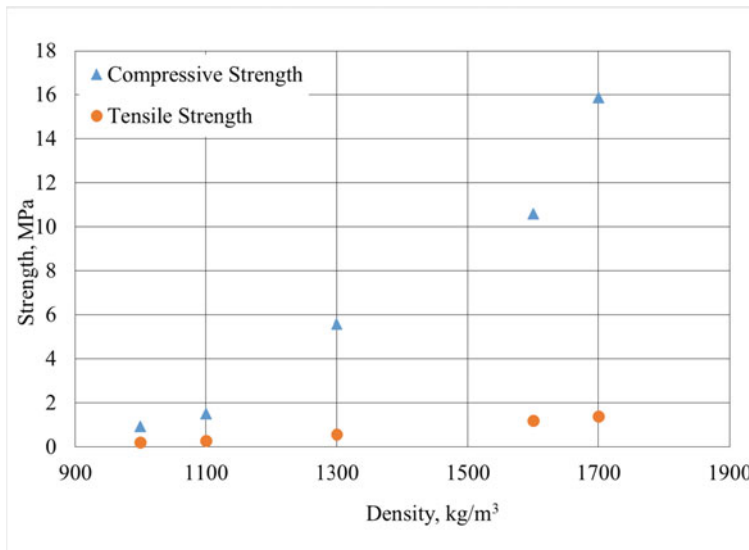
Fig. 2 Result of compressive strength and tensile strength

4.2 Fracture Energy of Foamed Concrete

The determination of fracture energy using the models by Bazant [1] and CEB [5] include an important parameter: the compressive strength of foamed concrete. The models proposed by Bazant and Oh [3] require tensile strength obtained from experimental work and Young's modulus, which is calculated using empirical formula. The results of tensile strength and compressive strength Table 2 obtained from experimental work are used to analyse fracture energy and Young's modulus of foamed concrete.

A few models are used to analyse the fracture energy of foamed concrete. These models have been used to calculate fracture energy for normal concrete. However, the parameters used in analysing various models of fracture energy are compressive strength, tensile strength, diameter of aggregate, water–cement ratio and Young's modulus. On the basis of the empirical formula proposed by the Bazant-Becq [2] and CEB models [5], it focuses on using compressive strength. The results show that the value of fracture energy is acceptable because the value of the compressive strength of foamed concrete is within an acceptable range [4].

Table 3 Fracture energy of foamed concrete using the Bazant-Becq model

Density (kg/m^3)	Fracture energy, G_f (N/m)				
	Compressive test		Splitting tensile test		
	Bazant-Becq	CEB	Oh [12]	Oh [11]	Bazant
1000	8.45	4.93	99.98	96.28	7.32
1100	10.23	6.89	77.56	74.69	8.31
1300	17.30	17.26	31.89	30.73	8.17
1600	22.37	27.08	30.87	29.73	23.34
1700	26.29	35.92	22.37	21.55	21.64

Under the splitting tensile test, the value of the fracture energy of foamed concrete is analysed using the models in the studies of Oh [12] and Oh [11]. The results from Table 3 shows instability. The value of the fracture energy for the density of 1000 kg/m^3 is 99.98 N/m, which is higher than that of the density of 1700 kg/m^3 at 22.37 N/m. The Oh [11] model shows the same result, where the value for density of 1000 kg/m^3 at 96.28 N/m is larger than that of the density of 1700 kg/m^3 at 21.55 N/m. A different result of fracture energy is obtained using the Bazant model [1], as shown in Table 3. Table 3 also shows the value of fracture energy using the Bazant model [1]. The table reveals that the value does not increase linearly. All models are unsuitable for foamed concrete because it requires a parameter of tensile strength and Young's modulus in the equation. Foamed concrete is fragile within tension. As the tensile load is applied, the foamed concrete can easily fracture. Rahman et al. [13] have proven that the empirical formula of the Bazant-Becq [2] and CEB models [5] can be used to calculate the fracture energy of the foamed concrete, mortar and normal concrete. Furthermore, the Bazant-Becq model [2] provides results that are almost exactly the same as the Hillerborg model [6] for the densities of 1400 and 1600 kg/m^3 [13]. The result for the prediction of fracture energy using tensile strength is unsuitable for foamed concrete because it is more fitting for normal concrete. The value of the fracture energy for normal concrete increases linearly with density analyses using the Oh [11] model Fig. 3. Rahman et al. [13] have also reported that the value of fracture energy using the Oh model is unsuitable for analysing foamed concrete and mortar because the value obtained is inconsistent.
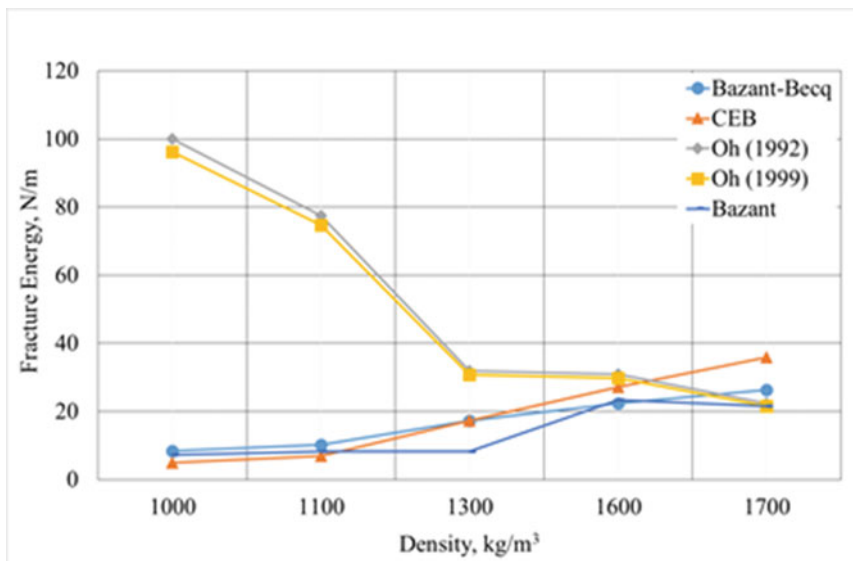
Fig. 3 Relationship graph of fracture energy with the density of foam concrete

4.3 Crack Pattern

Figure 4 shows that the fracture process zone starts when the load is subjected to the specimens and the crack starts to propagate through the specimen. Hillerborg (1976) [6] has stated that the crack propagation in the fracture process zone starts when the critical stress is equal to the tensile strength of the concrete. Even as the crack starts propagating, the stress does not become zero. Failure of concrete structures typically involves stable growth of large cracking zones and the formation of large fractures before the maximum load is reached (Bazant 1992) [17].

a)   Pattern of crack on cylinder specimen   b)   Pattern of crack on cube sample

Fig. 4 Crack pattern

5   Conclusion

An experimental study was conducted on the fracture energy of foamed concrete using various mathematical models. The results were compared with that of the Bazant, CEB and Oh models. The value of fracture energy analyse using both models increase as the density of foamed concrete increase. Although the fracture energy of foamed concrete was a fraction of normal concrete, it was relatively high for compressive strength of approximately 0.93 to 15.87 MPa. Whilst the value of tensile strength was approximately 0.22 to 1.4 MPa, the fracture energy significantly increased the density and compressive strength. Therefore, it can be conclude that, the fracture energy decreased by density and tensile strength.

References

1. Bazant ZP (2002) Concrete fracture model: testing and practice. Eng Fract Mech 69:165–205
2. Bazant ZP, Becq-Giraudon E (2002) Statistical prediction of fracture parameters of concrete and implications for choice of testing standard. Cem Concr Res 32:529–556
3. Bazant ZP, Oh BH (1983) Crack band theory for fracture of concrete. Mater Struct 16:155–177
4. British cement association (1994) Foamed concrete-composition and properties, Camberley, UK
5. Comité Euro-International du Béton (1990) CEB-FIP model code, p 437. Thomas Telford, London
6. Hillerborg A, Modéer M, Petersson PE (1976) Analysis of crack formation and crack growth by means of fracture mechanics and finite elements. Cem Concr Res 6:773–782

7. Jaini ZM, Mokhatar SN, Yusof ASM, Zulkiply S, Abd Rahman MH (2016) effect of pelletized coconut fibre on the compressive strength of foamed concrete. In: MATEC Web of Conference, vol. 47

8. Jones MR, McCarthy A (2005) Preliminary views on the potential of foamed concrete as a structural material. Mag Concr Res 57(1):21–31

9. Jaini ZM, Abd Rahman N, Rum RHM, Haurula MM (2017) Fracture energy of foamed concrete: numerical modelling using the combined finite-discrete element method. MATEC Web Conf 103:02030

10. Kearsley EP (1999) Just foamed concrete – an overview, Specialist techniques and materials for concrete construction. In: Dhir RK, Henderson (ed) Proceedings of the international conference 'creating with concrete', University of Dundee, Scotland, Thomas Telford, 8–10 September 1999, pp 227–237

11. Oh BH, Jang SY, Byun HK (1999) Prediction of fracture energy of concrete. KCI Concr J 11 (3):211–221

12. Oh BH (1992) Fracture energy of concrete and equivalent crack length. In: Bazant ZP (ed) Fracture mechanics of concrete structure, chapter 4, pp 419–423. Taylor & Francis, London

13. Rahman NA, Jaini ZM, Zahir NNM (2015) Fracture energy of foamed concrete by means of the three-point bending tests on notched beam specimens ARPN J Eng Appl Sci 10(15):6562–6570

14. Zamri MN, Rahman NA, Jaini ZM, Kozłowski M (2019) Fracture energy of fibrous-foamed concrete using V-notched beam specimens. Int Rev Civ Eng 10(1):8–14

15. Byun KJ , Song HW, Park SS (1998) Development of structural lightweight foamed concrete using plymer foam agent. In: Proceeding of the 9th International Congress on Polymers in Concrete, Bologna, Italy

16. Ramamurthy K, Kunhanandan Nambiar EK, Indu Siva Ranjani G (2009) A classification of studies on properties of foam concrete. Cem Concr Compos 31(6):388–396

17. Bazant ZP (1992) Fracture mechanic of concrete structures. In: Proceedings. FRaMCoS1. Internatonal Conference on Fracture Mechanic of Concrete Structures, Breckenridge, Colorado, June

18. Jaini ZM, Mokhatar SN, Feng Y, Seman MA (2015) 2D multi-scale simulation and homogenization of foamed concrete containing rubber bars. In: InCIEC 2014. Springer, Singapore

Review of Carbon Dioxide (CO$_2$) Sequestration in Bio-Concrete

M. F. M. Arif, J. M. Irwan, N. Othman, and A. F. Alshalif

Abstract Recently bio-concrete is one of carbon dioxide (CO$_2$) sequestration process which has suitability to ensure the biggest problem on global warming can be solved and this technology also has been discussed widely by researches. The application of this technology could provide a new sustainable product of building material in several kinds of product. In bio-concrete its synonym with the various type of bacteria and the most famous is *Bacillus* species. Thus, the mechanism of self-healing of bacterial concrete occurs through the metabolic conversion of calcium lactate to calcium carbonate in crack sealing. Encouragement by this technology it brings in parallel the green technologies which potential to adsorb CO$_2$ to reduction of emission CO$_2$ that main contributor on global warming. Besides that, CO$_2$ that fills the atmosphere through the natural conversion and capturing which is biological, chemical and physical processes. The potential bio-concrete to sequestrate CO$_2$ use concept carbonic anhydrase (CA) through the carbonation process and bacterial species is highlighted. The main objective of this paper is to review on carbon dioxide sequestration in bio-concrete and self-healing.

Keywords Bio-concrete · Carbon dioxide (CO$_2$) sequestration · Bacteria · Carbonic anhydrase (CA)

M. F. M. Arif · J. M. Irwan (✉) · A. F. Alshalif
Jamilus Research Centre for Sustainable Construction (JRC), Faculty of Civil Engineering and Built Environment, University Tun Hussein Onn Malaysia, 86400 Parit Raja, Johor, Malaysia
e-mail: irwan@uthm.edu.my

N. Othman
Micro-Pollutant Research Centre (MPRC), Faculty of Civil Engineering and Built Environment, University Tun Hussein Onn Malaysia, 86400 Parit Raja, Johor, Malaysia

1 Introduction

Intensive phenomena such as climate changes, global warming and the rise of sea level are the impact of increasing of CO_2. Anthropogenic activities are the main contributor that increasing the concentration of carbon dioxide and other gasses on atmosphere [16]. Industrial processes, transportation and combustion of fossil fuels used in power generation is some kind of sources that can contribute CO_2 emissions on our atmosphere. Through that kind of sources cement manufacturing is the industrial processes is higher responsible for anthropogenic CO_2 emissions which are 88% and the others of 12% are from deforestation [24].

Bio-concrete is the successful green technologies and development of technology microbial-based strategy which an emerging field in self-healing concrete cracks. Autogenous healing, encapsulation of polymeric material and microbial production of calcium carbonate are three main way to established self-healing mechanism in concrete [36]. The process of carbonate precipitation depends on microbial influence. The formation of calcium carbonate is produced or induced by most of the bacteria under suitable conditions [6]. Bio-concrete technology is the product from natural additive material to concrete by using various types of bacteria like *Ureolytic, Bacillus Sphaericus, Shewanella, Bacillus pasteurii and Pseudomonas aeruginosa*. The precipitation process of calcium carbonate ($CaCO_3$) in concrete pores is the ability of bio-concrete [3, 4, 12, 13]. The used of urease helps in mineralization of $CaCO_3$ and hydrolyzing urea that present in the environment have been proved by bio-concrete incorporating ureolytic bacteria such as *Bacillus Sphaericus*. Combination of urea and calcium ions will release CO_2 that resulting in deposition of $CaCO_3$ in the form of calcite [33].

The process of repairing concrete cracks which autogenous healing will function when the presence of water. Thus, it fills by carbonation of dissolved calcium hydroxide or hydration of unhydrated cement particles [8, 26]. The presence of carbon dioxide on the atmosphere will react with calcium hydroxide that produces form hydration of calcium. Through that reaction the result in the production of calcium carbonate ($CaCO_3$) have been shown in Eq. (1) and (2) [11]:

$$CaO + H_2O \rightarrow Ca(OH)_2 \tag{1}$$

$$Ca(OH)_2 + CO_2 \rightarrow CaCO_3 + H_2O \tag{2}$$
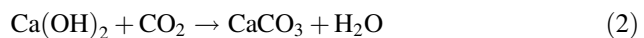
Biomineralization will produce $CaCO_3$ based on the process of biological healing. The result from this development can longer lifespan of concrete in conjunction with a significant reduction in cement [28]. It also might contribute to area of reduction of carbon dioxide. The paper aims is to review the bacteria concrete and the sequestration of carbon dioxide in concrete.

2 Bacteria Concrete

On the preparation of bacteria concrete (bio-concrete) it consists of the healing agent which is bacteria that can be inserted in concrete by various type of methods such as directly mixed in concrete preparation or vascular network. On the method of the vascular network, it already embedded during concrete preparation and the healing agent will supply from outside of the structure. Since the crack occurs, the pressure gradient between agent source and crack will move healing agent through the vessel. For simulated vascular networks with cylindrical concrete which its core and outer parts were porous and compact, respectively [27]. To make sure the concrete performance in under control condition healing agent must have constant viscosity during the whole of the concrete service life to make going easily [32]. If the amount of released healing agent is more than the crack capacity, it causes aesthetic issues. Secondly, it would be difficult to distribute vessels homogenously throughout the structure. Thirdly, incorporation of the vascular system in concrete may decrease the bond between concrete compositions and consequently leads to structural delamination as shown in Fig. 1a.

During the concrete preparation and casting bacteria also can be embedded directly in the concrete matrix as shown in Fig. 1b. Healing agents dissolve in water, and then the mixture is added to cement and sand during this process. In bio self-healing concrete there are most attractive species of bacteria like *Bacillusas* as shown in Table 1 because it can tolerate extremely with the concrete environment. On the other hand, for dormant endospores can handle environmental changes or chemicals including ultraviolet radiations and mechanical stresses [15, 30, 32]. Microbial metabolic activity depends on direct incorporation of microorganism into materials like concrete. Bacteria cannot survive in dry condition of concrete and also at pH reading more than 11 [34]. In this area there are several most popular
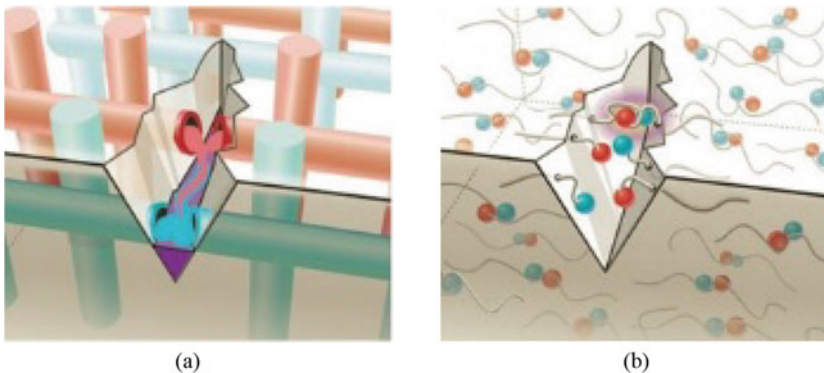

(a)   (b)

Fig. 1 Self-healing type; **a** vascular **b** mixed to concrete mixture [5]

Table 1 Types of bacteria used in bio-concrete for different applications

Types of bacteria	Role of bacteria	Reference
Bacillus Pasteurii, Pseudomonas Aeruginosa	Microbial concrete as a crack healer	Bang et al. [4]
Shewanella	To increase strength in concrete mixture	Ghosh et al. [10]
Sporosarcina pasteurii	Enhanced urease and calcite production	Achal et al. [1]
Ureolytic, Bacillus	Strength enhancement of sand	Al-Thawadi [2]
Bacillus alkalinitrilicus	Self-healing concrete	Wiktor and Jonkers[35]
Bacillus Sphaericus	Microbial concrete as surface treatment	Pacheco-Torgal and Labrincha [22]
B. subtilis	Enhancement of concrete properties	Nosouhian et al. [21]

bacteria used in concrete as shown in Table 1. Bacteria can play an important role in concrete by microbial mineral precipitation due to metabolic activities of some specific microorganisms.

3 Carbon Dioxide (CO_2) Sequestration

Recently, many studies state that reduces the amount cement used and replace it with others material for example silica fume, fly ash, waste ash of palm oil which produced green concrete at the same time it can reduce the CO_2 emission [31]. According to increasing of CO_2 emissions, sequestration of carbon dioxide is one of the new developments that can reduce CO_2. The most previous case studies focused on sequestration CO_2 geological-based using deep underground rock formation and also using power plants or biological sequestration [14, 19]. Carbonation process can be sequestrate the emission of CO_2 from the atmosphere in concrete. It also occurred on the surface of the concrete by penetration CO_2 into pores inside the concrete. To ensure the penetration of CO_2 it depends on various factor like additional material into cement mixture, CO_2 concentration and relative humidity and the availability of $Ca(OH)_2$ and water. First, the reaction CO_2 with water in pore will produced carbonic acid (H_2CO_3) then react with calcium compounds to form calcium carbonate. The chemical reaction of $Ca(OH)_2$ and calcium-silicate-hydrate (C-S-H) with CO_2 will form calcium carbonate $CaCO_3$ and water H2O is the result from neutralizing process of carbonation [14]. The illustration of that process as shown in Fig. 2. Re-capturing of carbon dioxide production to concrete can be done by chemical reaction to calcination in the form of carbonation [23]. By that process, it can improve the durability of concrete by pore refinement of the cement and also the surface hardness strength. Previously, some
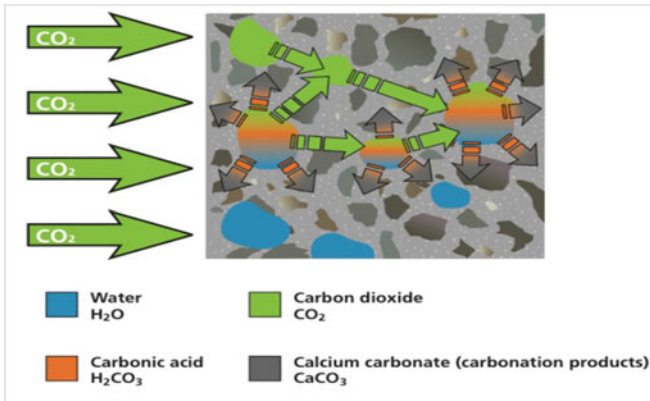
Fig. 2 Illustration the process of carbonation in pore concrete [20]

case study state that especially in normal concrete the carbonation process is generates very slow [23].

On the carbonation depth process of concrete, CO_2 concentration is an important aspect. Besides that, the carbonation of the concrete structure is contributed by the micro climatic condition and different water-cement ratio (W/C). The carbonation in the concrete shows that the concentration of CO_2 increased when high of W/C compared to low W/C [37]. Carbonation in concrete can be categories to three zones which is the fully carbonated, partly carbonated and non-carbonated zone. For fully carbonated zone the degree of carbonation more than 50% with pH less than 9.0. Then, for the partly carbonated zone the degree of carbonation is between 0 to 50% with pH 9.0 to 11.5 and for the non-carbonated zone there is no sign of carbonation. Therefore, the concentration of CO_2 and pH is an important aspect of penetration of carbonation into concrete [7]. Under a suitable surrounding environment, biological sequestration of CO_2 can be accelerated which it progresses through the hydration of CO_2 and the enzyme of carbonic anhydrase is used [9]. In the purpose of CO_2 sequestration, carbonic anhydrase can be extracted from bacteria like; *Ureolytic bacteria, Bovine CA, Bacillus cereus and Citrobacter freundii* [16–18, 25]. From the others study, it mentions that the carbonic anhydrase enzyme is the important thing which can make reaction much faster as well as accelerate the process of CO_2 sequestration [29].

4 Conclusion

The used of bacteria in concrete can widely use in various type of function and many researches have been focused on this kind of technology. In order to tackle the problem of environmental and global warming which to minimize the emissions

of CO_2 in the atmosphere. According to many studies, it showed many bacteria have possible to improve concrete properties especially in compressive strength and tensile strength. The used of bacteria in concrete will ensure the green technologies were applied which are able to significantly reduce high energy consumed, does not lead to environment destruction, or it has high performance with life cycle sustainability. The carbonation process from this method well-chosen as CO_2 sequestration process but it cannot more impact in term of efficiency. Furthermore, advance studied on concrete properties, materials, bacteria enzyme, carbonation process and carbonic anhydrase must be done to accelerate the sequestration process of CO_2 according to bio-concrete.

References

1. Achal V, Mukherjee A, Basu PC, Reddy MS (2009) Lactose mother liquor as an alternative nutrient source for microbial concrete production by sporosarcina pasteurii. J Ind Microbiol Biotechnol 36(3):433–438
2. Al-Thawadi Salwa Mutlaq (2011) Ureolytic bacteria and calcium carbonate formation as a mechanism of strength enhancement of sand. J Adv Sci Eng Res 1:98–114
3. Faisal AA, Irwan JM, Othman N, Anneza LH (2016) Isolation of sulphate reduction bacteria (SRB) to improve compress strength and water penetration of bio-concrete. MATEC Web Conf 47:1–6
4. Bang SS, Galinat JK, Ramakrishnan V (2001) Calcite precipitation induced by polyurethane-immobilized bacillus pasteurii. Enzyme Microbial Technol 28(4–5):404–409
5. Blaiszik B, Kramer SLB, Moore JS, Sottos NR, Olugebefola SC, White SR (2010) Self-healing polymers and composites. Annu Rev Mater Res 40(1):179–211
6. Boquet E, Boronat A, Ramos Cormenzana A (1973) Production of calcite (calcium carbonate) crystals by soil bacteria is a general phenomenon. Nature 246:527–529
7. Chang CF, Chen JW (2006) The experimental investigation of concrete carbonation depth. Cem Concr Res 36(9):1760–1767
8. Edvardsen C (1999) Water permeability and autogenous healing of cracks in concrete. ACI Mater J 96(4):448–454
9. Favre N, Lorraine CM, Alain PC (2009) Biocatalytic capture of CO2 with carbonic anhydrase and its transformation to solid carbonate. J Mol Catal B Enzym 60(3–4):163–170
10. Ghosh P, Mandal S, Chattopadhyay BD, Pal S (2005) Use of microorganism to improve the strength of cement mortar. Cem Concr Res 35(10):1980–1983
11. Hearn N (1998) Self-sealing, autogenous healing and continued hydration: what is the difference? Mater Struct/Materiaux et Constr 31(212):563–567
12. Irwan JM, Anneza LH, Othman N, Faisal AA (2016) Compressive strength and water penetration of concrete with enterococcus faecalis and calcium lactate. Key Eng Mater 705:345–349
13. Irwan JM, Anneza LH, Othman N, Faisal Alshalif A, Zamer MM, Teddy T (2016) Calcium lactate addition in bioconcrete: effect on compressive strength and water penetration. MATEC Web Conf 78:0–5

14. Johannesson B, Utgenannt P (2001) Microstructural changes caused by carbonation of cement mortar. Cem Concr Res 31(6):925–931
15. Jonkers HM (2011) Bacteria based self healing concrete – a review. Mater Environ 56(1):1–12
16. Karthikeyan C, Rajeswari S, Maruthamuthu S, Subramanian K, Rajagopal G (2014) Biogenic ammonia for CO$_2$ capturing and electrochemical conversion into bicarbonate and formate. J CO2 Utilization 6:53–61
17. Kim IG, Jo BH, Kang DG, Kim CS, Choi YS, Cha HJ (2012) Biomineralization-based conversion of carbon dioxide to calcium carbonate using recombinant carbonic anhydrase. Chemosphere 87(10):1091–1096
18. Li W, Chen WS, Zhou PP, Long Jiang Yu (2013) Influence of enzyme concentration on bio-sequestration of CO2 in carbonate form using bacterial carbonic anhydrase. Chem Eng J 232:149–156
19. Liu N, Bond GM, Abel A, McPherson BJ, Stringer J (2005) Biomimetic sequestration of CO2 in carbonate form: role of produced waters and other brines. Fuel Process Technol 86(14–15):1615–1625
20. Monkman S (2016) Technical Note - Types of Concrete Carbonation Early Age Carbonation. CarbonCure Technologies
21. Nosouhian F, Mostofinejad D, Hasheminejad H (2015) Influence of biodeposition treatment on concrete durability in a sulphate environment. Biosys Eng 133:141–152
22. Pacheco Torgal F, Labrincha JA (2013) Biotech cementitious materials: some aspects of an innovative approach for concrete with enhanced durability. Constr Build Mater 40:1136–1141
23. Pade C, Guimaraes M (2007) The CO$_2$ uptake of concrete in a 100 year perspective. Cem Concr Res 37(9):1348–1356
24. Quéré Le, Corinne MR, Raupach JG, Canadell GM, Bopp L, Ciais P, Conway TJ, Doney SC, Feely RA, Foster P, Friedlingstein P, Gurney K, Houghton RA, House JI, Huntingford C, Levy PE, Lomas MR, Majkut J, Metzl N, Ometto JP, Peters GP, Colin PI, Randerson JT, Running SW, Sarmiento JL, Schuster U, Sitch S, Takahashi T, Viovy N, Van Der Werf GR, Ian Woodward F (2009) Trends in the sources and sinks of carbon dioxide. Nat Geosci 2 (12):831–836
25. Ramanan R, Kannan K, Sivanesan SD, Mudliar S, Kaur S, Tripathi AK, Chakrabarti T (2009) Bio-sequestration of carbon dioxide using carbonic anhydrase enzyme purified from citrobacter freundii. World J Microbiol Biotechnol 25(6):981–987
26. Ramm W, Biscoping M (1998) Autogenous healing and reinforcement corrosion of water-penetrated separation cracks in reinforced concrete. Nucl Eng Des 179(2):191–200
27. Sangadji S, Schlangen E (2013) Mimicking bone healing process to self repair concrete structure novel approach using porous network concrete. Procedia Eng 54:315–326
28. Seifan M, Samani AK, Berenjian A (2016) Bioconcrete: next generation of self-healing concrete. Appl Microbiol Biotechnol 100(6):2591–2602
29. Shekh AY, Krishnamurthi K, Mudliar SN, Yadav RR, Fulke AB, Devi SS, Chakrabarti T (2012) Recent advancements in carbonic anhydrase-driven processes for CO$_2$ sequestration: minireview. Crit Rev Environ Sci Technol 42(14):1419–1440
30. Soltmann U, Raff J, Selenska-Pobell S, Matys S, Pompe W, Böttcher H (2003) Biosorption of heavy metals by sol-gel immobilized bacillus sphaericus cells, spores and S-layers. J Sol-Gel Sci Technol 26(1–3):1209–1212
31. Tangchirapat W, Saeting T, Jaturapitakkul C, Kiattikomol K, Siripanichgorn A (2007) Use of waste ash from palm oil industry in concrete. Waste Manag 27(1):81–88
32. Van Tittelboom K, De Belie N (2013) Self-Healing in Cementitious Materials-a Review. Material 6:2182–2217
33. Van Tittelboom K, De Belie N, De Muynck W, Verstraete W (2010) Use of bacteria to repair cracks in concrete. Cem Concr Res 40(1):157–166
34. Wang JY, De Belie N, Verstraete W (2012) Diatomaceous earth as a protective vehicle for bacteria applied for self-healing concrete. J Ind Microbiol Biotechnol 39(4):567–577

35. Wiktor V, Jonkers HM (2011) Quantification of crack-healing in novel bacteria-based self-healing concrete. Cem Concr Compos 33(7):763–770
36. Wu M, Johannesson B, Geiker M (2012) A review: self-healing in cementitious materials and engineered cementitious composite as a self-healing material. Constr Build Mater 28(1):571–583
37. Yoon IS, Çopuroğlu O, Park KB (2007) Effect of global climatic change on carbonation progress of concrete. Atmos Environ 41(34):7274–7285

Evaluation of Cold Mix Patching Materials Along Jalan Persiaran Mokhtar Dahari, Selangor

Ekarizan Shaffie, Ahmad Kamil Arshad, Anizahyati Alisibramulisi, Mohd Amin Shafii, Ramadhansyah Putra Jaya, and Khairil Azman Masri

Abstract The increasing of road accidents and the economic loss due to maintenance operation is becoming an important issue in Malaysia asphalt industry. Potholes are the most common distress occurred in asphalt pavement which require immediate attention to minimise further pavement damage and reduce the opportunity for potential accidents. Hence, a study was conducted to evaluate the performance of six commercially available cold mix asphalt products in Malaysia. Six kinds of patching materials that is nominated as a company sample A, B, C, D, E and F currently used in practice were tested in the laboratory. The laboratory tests included the sieve analysis, density analysis, bitumen content, volumetric properties and moisture susceptibility test. The result of the laboratory tests indicates that the gradation for all the samples are close to the gradation requirements for the AC14 mix as per JKR Malaysia's specification. However, none of the samples fully complied with the gradation envelope. For density, all the samples are lower than the requirements for the AC14 mix and none of the samples fully complied with the compaction requirements due to the compaction method using the plate compactor. Meanwhile, for volumetric properties results, stability values of the various cold mix samples met the standard specification. Based on the ranking performance criteria of six different cold mix patching materials, Sample B and Sample D obtained the highest score of compliance with the requirements of the specification.

E. Shaffie (✉) · A. K. Arshad · A. Alisibramulisi
Institute for Infrastructure Engineering and Sustainability Management (IIESM),
Universiti Teknologi MARA (UiTM), 40450 Shah Alam, Selangor, Malaysia
e-mail: eka@uitm.edu.my

E. Shaffie · A. K. Arshad · A. Alisibramulisi
School of Civil Engineering, College of Engineering, Universiti Teknologi MARA (UiTM),
40450 Shah Alam, Selangor, Malaysia

M. A. Shafii
Centre of Geotechnics, Faculty of Engineering and The Built Environment, SEGi University,
Kota Damansara, 47810 Petaling Jaya, Selangor, Malaysia

R. Putra Jaya · K. A. Masri
Department of Civil Engineering, College of Engineering, Universiit Malaysia Pahang
(UMP), Lebuhraya Tun Razak, 26300 Kuantan, Pahang, Malaysia

Therefore, it is suggested that sample B and sample D are the most suitable cold mix materials to be used in patching maintenance work.

Keywords Cold mix asphalt · Patching · Hot mix asphalt · Strength · Pothole

1 Introduction

The rapid economic development over the last two decades has put tremendous pressure on Malaysia's road networks. Hot-mix asphalt (HMA) pavement is widely practiced in Malaysia for its economic and flexibility. Unfortunately, this HMA mix have deteriorated more rapidly than expected due to the increase in traffic volume, higher tire pressure, moisture, and temperature from our climatic condition. Many attempts have been carried out such as polymer modified bitumen in order to minimize the deterioration of the flexible pavement [2, 12]. Previous research has been conducted using additives/modifier in asphalt bitumen to enhance the engineering properties and performance of the conventional HMA mixes. In these, the various type of additives/modifier polymers and nanopolymers used included polyethylene (PE), polypropylene (PP), ethylene–vinyl acetate (EVA), ethylene–butyl acrylate (EBA), styrene–butadiene–styrene (SBS), nanoclay, nanocarbon, nanopolyacrylate and etc. These materials were reported to lead to some improved properties such as higher stiffness at high temperatures, higher cracking resistance at low temperatures, better moisture resistance or longer fatigue life [6, 9, 13, 14]. However, there are still shortcomings of using polymers in asphalt pavement mixes. Only a few are satisfactory with regards to the performance and costs [5, 16].

Potholes are the most common distress occurred in asphalt pavement. Potholes defined as small, bowl-shaped depressions in the pavement surface that penetrate all the way through the HMA layer down to the base course. They generally have sharp edges and vertical sides near the top of the hole. Potholes are most likely to occur on roads with thin HMA surfaces (25 to 50 mm) [1, 8, 11]. Potholes occurred due to repeated vehicle loads and heavy rainfall especially during a rainy season. These factors contribute small cracks in asphalt surface. When water penetrates into cracks with the repetitive traffic loads, the base layer becomes weak and loss of pavement structural support can be sudden. The asphalt surface layer starts to break up. Potholes are usually the result of alligator cracking. As alligator cracking becomes severe, the interconnected cracks create small chunks of pavement that can be dislodged as vehicles drive over them. Then, various sizes of potholes are created on the pavement surface [3].

Potholes require immediate attention to minimise further pavement damage and reduce the opportunity for vehicle damage potential accidents. Patching potholes in flexible pavements is an important maintenance operation because this activity is expensive and time-consuming. During the rainy season, the patching activity is even more important as pavements deteriorate more in wet weather. The selection of the best materials and patching of deteriorate areas in a road surface to secure

safety and ride ability are important to repair pothole successfully. Conventionally, hot mix asphalt is used to repair pothole permanently. However, hot mix asphalt is only produced at plants and flows while it is hot. The premix asphalt hardens and thus producing a durable surface when it is cools [8]. Therefore, the need to use a new and improved cold mix patching materials are required to produce more economical and long-lasting solutions in pothole repair evaluations.

Presently, there is an increased interest in the use of cold mix asphalt as the primary patching material to be used for potholes in Malaysia. This is because cold mix asphalt offers certain advantages over hot mix asphalt such as no requirement for heating, reduction in the use of energy and lower emissions of gases and pollutants, leading to a more environmental-friendly product [7, 8]. Cold mix asphalt has generally been perceived to be less superior in quality compared to the conventional hot mix asphalt. Furthermore, potholes must be filled repeatedly are expensive to repair. Therefore, the longevity and serviceability of the pothole patching material on the repaired pothole could significantly help to the cost-effectiveness of the repairs [4]. Due to this reason, many studies have been conducted by several agencies to determine the economical, long-lasting materials and techniques [1].

Stability, stickiness, resistance to water action, durability, skid resistance, workability and storage ability are the most important properties requirement in bituminous patching mixture. Stability used to allow the patch to resist displacement by traffic. Aggregate gradation and properties may influence the stability of the mixture. Marshall stability is affected considerably by the cohesion and the internal friction of aggregate. According to [7], the dense-graded cold mix asphalts (CMAs) have higher stability values, indicating more cohesive mixes, as compared with the open-graded CMAs. Stickiness also influenced by the temperature of the mixture and the bitumen. Usually hot mixture materials have satisfactory adhesion when they are still hot, whereas cold-mixtures do not have adequate stickiness. Patching material must be resistance to water action to keep the bitumen from stripping off the aggregate. This property influences by the bitumen and the aggregate types. Durability and workability are required to ensure that the patch has a satisfactory resistance to disintegration and that the material can be easily compacted. Storage stability also important for patching materials so that the mixture can be stockpiled without hardening excessively or having the bitumen drain off the aggregate [15].

The present study aims to evaluate the performance of the commonly used cold mix asphalt used for patching of potholes in Malaysia. Instant Patchmix, Instant Tarmac, Tipco, Carboncor, Global Patch, QP Industries, Ecoinfira, Nescaya Positif and Alloy MTD, are some of the cold asphalt patching products available in Malaysia. In this study, a laboratory study was carried out to evaluate the performance of six commercially available cold mix asphalt products in Malaysia. This report presents the results and analysis of the study.

2 Materials and Method

2.1 Materials

The materials used for the patches were selected according to available cold mix asphalt products in Malaysia. Six products were the major materials for the project and were nominated as company product A, B, C, D, E and F. Each cold mix products having their own advance formulation. The section for the coring process was selected based on the site observation that is nearest to the potholes distress area in order to simulate the pavement condition due to potholes failures. Samples were cored from 2 different points on each location to be brought back to Highway Laboratory for evaluation.

2.2 Methods

The laboratory tests such as sieve analysis, density analysis, bitumen content, strength properties and resilient modulus test were carried out to evaluate the material properties of six commercially available cold mix asphalt products in Malaysia. These products were laid at two different sites located at Persiaran Mokhtar Dahari (Route B49) located in the district of Petaling, Selangor as shown in Fig. 1. For this field assessment, all potholes produced by creating a new pothole in a heavily damaged pavement. Traffic control was provided by the district personnel, while patches and potholes were prepared for patching. Existing patching material has been removed to make potholes and then filled with water. After 1 h, the patch crew swept the water and removed the debris from the holes and immediately installed the patching material. Contractors and district staff made the selection of the patching mixture used to fill the pothole appropriately. Figure 2 show the core samples from road sections.

Fig. 1 Site located along Persiaran Mokhtar Dahari, Selangor

Fig. 2 Core samples

2.2.1 Bitumen Content Test

Bitumen content is important in determining hot mix asphalt (HMA) mixture performance. The ignition test (AASHTO T 308) is the most common method used to determine bitumen content. This method involves the separation of bitumen and all other volatile substances from aggregates. It is an alternative to the conventional solvent extraction method. The remaining aggregates will be used for the determination of aggregate gradation and specific gravity. The test procedure starts by spreading more than 1200 g of loose material into the sample basket (Fig. 3a) to keep the material away from the edges. When the basket is ready, it is inserted inside the chamber, which reaches a temperature of 540 °C, to burn any flammable substance. The toxic fumes emitted during the test are reduced significantly by the afterburner, which has a temperature exceeds 900 °C. The machine monitors the temperature and changes in mass during the test; the test ends when there are no more mass changes. This test measures the bitumen content by subtracting the difference in mass before and after burning (Fig. 3b) in the ignition oven.
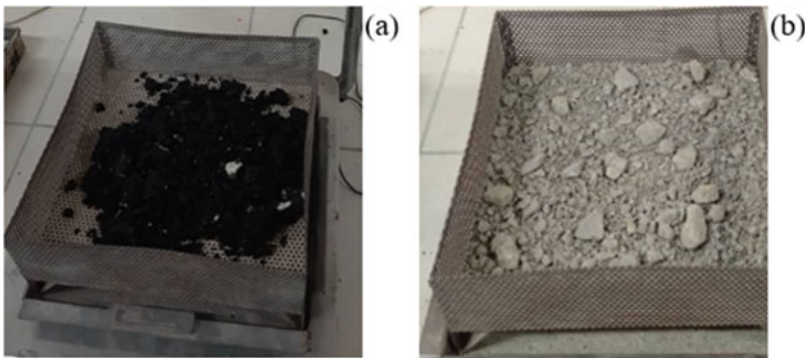

Fig. 3 Material **a** before test **b** after test

2.2.2   Particle Size Distribution Test

The particle size distribution test was performed according to ASTM D 136. This test was used to determine the particle size distribution of the extracted aggregates which obtained using the clean material derived from the ignition test. This method is performed by filtering an aggregate sample through a stack of wire mesh sieves, separating it into different size ranges. A mechanical sieve shaker (Fig. 4) is used to vibrate the sieve stack for a 7 to 15 min. On completion of sieving, the material on each sieve is weighed and the cumulative mass passing through each sieve is calculated as a percentage of the total sample mass. The results of the sieve analysis recorded graphically on a semi-log graph with particle size as abscissa (log scale) and the percentage smaller than the specified diameter as ordinate.

2.2.3   Density Analysis Test

Density analysis test was conducted to compare the level of compaction achieved on the cold mix patching materials from sections of the project according to ASTM D2726 and ASTM D2041 using a sample obtain from the selected site. Density was estimated as mass of the sample divided by the volume (dimensional volume). ASTM D2726 was used for determination of bulk specific gravity while ASTM D2041 was used for determination of theoretical maximum specific gravity. For determination of bulk specific gravity (ASTM D2726), the mass of the sample was tested under three (3) different conditions which include dry mass, mass in water and saturated surface dry mass (water fills the internal air voids). Figure 5 shows the bulk specific gravity test procedures.

For determination of theoretical maximum specific gravity, sample was prepared by heated a coring sample for ±1 h in the oven. After that, the sample immediately spread and loosen on a tray so that the fine aggregate is separated into particles

Fig. 4 Mechanical sieve shaker used for aggregates sieving
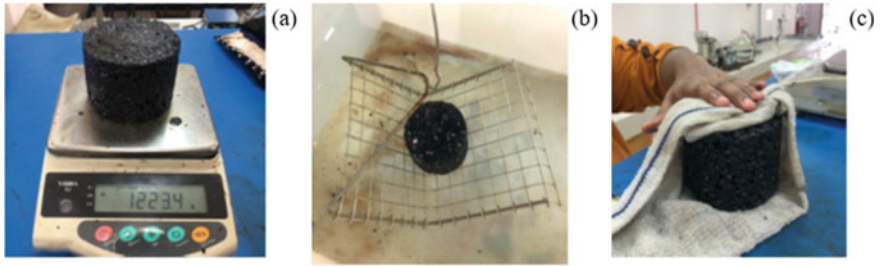
Fig. 5 Bulk specific gravity test procedures **a** Dry condition **b** Wet condition **c** Saturated surface dry (SSD) condition

Fig. 6 Corelok machine

smaller than 0.25 in. (6.25 mm). Further procedure was continued using corelok machine (Fig. 6). In corelok machine, determination of the theoretical maximum specific gravity requires inserting a loose sample inside a specially designed plastic bag, careful placement of the bag in the vacuum chamber and activation of the vacuum pump by closing the door. Internal controls regulate the vacuum pump and ensure proper operation until 99% of the total vacuum. Then, an automatic sealing strip inside the chamber heat seals the bag. At this stage, air will enter a controlled chamber and the bag will form a tight fit and conform to the shape of the loose sample. Then the vacuum chamber door opens, and the sample has been removed and immersed in 25 °C water bath to obtain a constant mass value in water. This mass is used in the calculation of theoretical maximum specific gravity by divided mass of sample in air with mass of water displaced by the sample. The density was therefore obtained by comparing the degree of compaction of each sample. As stipulated by the specification requirements of the Public Work Department (PWD) Malaysia-JKR/SPJ/2008-S4, compaction requirements of 98% of Marshall density at optimum bitumen content (OBC) were used.

2.2.4 Volumetric Properties Test

Marshall stability and flow tests were conducted to determine the volumetric properties of the asphalt mixture, such as stability (kN), flow (mm), stiffness (kN/mm) and air void (percent) to control the quality of the asphalt mixture. The Marshall stability and flow test procedure is in accordance with ASTM D 6927, which began with the immersion of the test samples in the water bath for 30 min at a constant temperature of 60 °C. As shown in Fig. 7, the test samples were then placed inside the loading head of the Marshall stability test machine. The flow meter was set to zero by inserting a 101.6 mm cylindrical metal diameter in the loading head. The test load was applied to the samples at a constant deformation rate of 50.8 mm per minute until the maximum capacity or peak resistance load was reached. The stability value is obtained by determining the maximum load that can be maintained by the samples before reaching its failure point. While the stability test was in progress, the flow metre remained firmly in position over the guide rod and was removed as the load began to decrease. The flow value of the sample is defined by the deformation at the maximum load. The stiffness value for each sample was then calculated as the stability and flow test average. The percentage of air voids was calculated from the bulk specific gravity and theoretical maximum specific gravity of the mixture performed in the density test section.

2.2.5 Moisture Susceptibility Test

Modified Lottman Test (AASHTO T283) and Boiling Water Test (ASTM D3625) were used to verify that the design test mixture formulated was susceptible to moisture damage in the pavement. These test measures the loss of strength or stiffness of an asphalt mix due to moisture induce damage. The modified Lottman

Fig. 7 Marshall stability test

Fig. 8 Indirect tensile strength (ITS) test machine

test (AASHTO T283) is performed by compacting $7 \pm 0.5\%$ air void samples. Three samples were selected for control (tested without moisture conditioning) and another three samples were selected for conditioning by saturation with water at 70–80%, followed by 24-h immersion in water at 60 °C in a water bath. The samples were then tested for indirect tensile strength (ITS) by loading the samples at a constant head rate (50 mm/minute vertical deformation at 25 °C) using ITS machine (Fig. 8).and recording the maximum compressive force required to break the samples. An indication of the potential for moisture damage is the Tensile Strength Ratio (TSR) values in the test. A higher TSR value indicates that the mix is more resistant to moisture damage. Tensile Strength Ratio (TSR) results were determined by comparing the indirect tensile strength (ITS) of unconditioned (dry) samples to the control samples. Retained tensile strength ratio (TSR) was used at 80% as the boundary between moisture-resistant and moisture-sensitive mixtures [10]. The boiling water test (ASTM D3625) is a qualitative test which determines the effect of water on the adhesion between aggregate and asphalt bitumen. A loose mixture (passing a 9.5 mm sieve and retained on a 4.75 mm sieve) was placed in 800 mL distilled boiling water and was allowed to remain in the boiling water for 10 min. Thereafter, the retained coated area was evaluated by visual rating. According to standard specification for boiling water test, the specification limit for retained coated area minimum 95%. Those mixes above 95% retained coating is considered as resistant to moisture susceptibility.

3 Results and Discussions

3.1 Bitumen Content

According to standard Specification for Hot Mix Wearing Course: 4–6%. Table 1 shows that only cold mix asphalt for sample C and D are complied with the JKR specification. The bitumen content for Specimen A, B, E and F were not acceptable as it is exceeding minimum requirements. These excess bitumen content can lead to flushing or bleeding in the pavement thus lead to various type of pavement failure.

3.2 Particle Size Distribution

Table 2 shows the summary for gradations for cold mix asphalt samples of patching materials. The upper and lower gradation limits for all mixes type are shown in Fig. 9 which illustrate the percentage aggregate passing versus sieve size. The gradation for all the samples is close to the gradation requirements for the AC14 mix as per JKR Malaysia's specification requirements. However, none of the samples fully complied with the gradation envelope. It is possible that the gradation of these samples were slightly modified to ensure other requirements such as workability of the cold mix asphalt.

3.3 Density Test

The percentage of compaction for all the samples (Table 3) are lower than the requirements as per JKR Malaysia's specification requirements (compaction requirements of 98% of Marshall density). However, none of the samples fully complied with the compaction requirements. Company sample A achieved the highest compaction of 95.11%. It is possible that the compaction is lower than the

Table 1 Bitumen content results

Samples	Company sample					
	A	B	C	D	E	F
Mass of sample before extraction, g	1200.0	1200.0	1200.0	1200.0	1200.0	1200.0
Mass of sample after extraction, g	1077.6	1117.5	1137.3	1137.8	1106.2	1124.7
Mass loss, g	122.4	82.5	62.7	62.2	93.8	75.3
Bitumen content (%)	10.20	6.88	5.23	5.19	7.82	6.27

Table 2 Gradation for cold mix asphalt

| Sieve size (mm) | Percentage passing | | | | | | | |
	Company sample						Gradation limit	
	A	B	C	D	E	F	Lower	Upper
20.0	100.0	100.0	100.0	100.0	100.0	100	**100.0**	**100.0**
14.0	100.0	100.0	100.0	100.0	98.2	100	**90.0**	**100.0**
10.0	100.0	99.5	100.0	100.0	94.4	100	**76.0**	**86.0**
5	68.4	66.9	54.4	60.0	56.8	43.5	**50.0**	**62.0**
3.35	43.7	54.6	29.1	33.1	44.2	27.8	**40.0**	**54.0**
1.180	22.7	31.2	12.9	16.1	23.1	13.4	**18.0**	**34.0**
0.425	13.6	18.1	8.8	9.4	12.9	8.7	**12.0**	**24.0**
0.15	10.7	3.4	7.9	2.9	7.2	4.0	**6.0**	**14.0**
0.075	3.2	3.4	2.9	2.9	3.9	4.0	**4.0**	**8.0**
Pan	0.0	0.0	0.0	0.0	0.0	0.0		
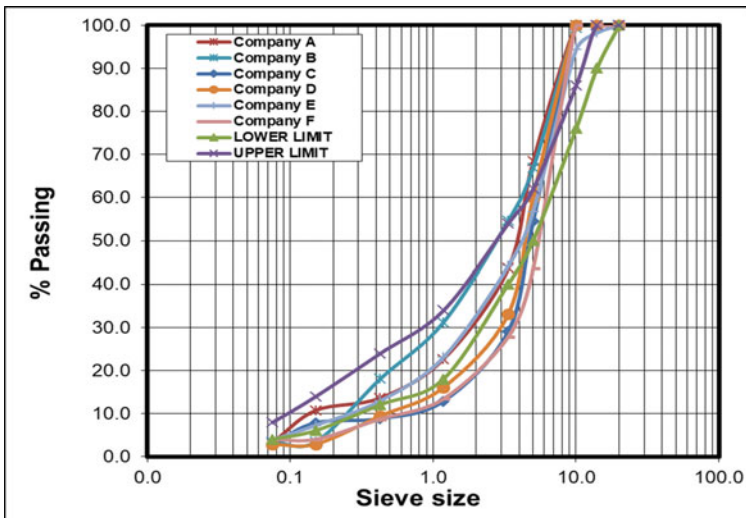
Fig. 9 Gradation Limit for all company sample patching material

requirements due to the compaction method using the plate compactor. These failures may be due to poor quality control during construction work. Insufficient compaction leads to poor performance even if other desirable mixture design characteristics are met.

Table 3 Density results for cold mix asphalt sample

Samples	Company sample					
	A	B	C	D	E	F
Bulk specific gravity	2.215	2.021	2.037	2.021	2.208	2.036
Theoretical maximum specific gravity	2.329	2.331	2.317	2.339	2.327	2.417
% Compaction	95.11	86.69	87.92	86.39	94.87	84.24

3.4 Volumetric Properties

Table 4 shows the strength properties of various samples of cold mix asphalts as compared with standard for hot mix asphalts. The stability values of the various cold mix samples met the standard specification where the samples exhibited high stability values, complying with the requirements of JKR specifications. The flow values of the various cold mix samples show that the Company A, C and D samples had flow value in the range of the hot mix standard specification. However, the company sample B, E and F had flow values slightly above the range for hot mix standard specification. The air voids content of all cold mixes asphalt samples did not comply with the hot mix standard specification except for company B cold mix sample which fall within the limits of the general asphalt specification of 3–4%.

Table 4 Strength Properties result for cold mix asphalt sample

Samples	Company sample						Standard specification for hot mix wearing course JKR/SPJ/2008-S4
	A	B	C	D	E	F	
Stability (KN)	21.4	19.7	15.1	14.1	11.0	12.8	>8 KN
Flow (mm)	3.18	4.17	2.74	3.78	4.59	5.77	2–4 mm
Stiffness (KN/mm)	6.73	4.74	5.53	3.72	2.40	2.21	>2 KN/mm
Air Voids in mix (%)	4.89	2.70	12.08	13.61	5.13	15.76	3–4%

3.5 Moisture Susceptibility

The Indirect Tensile Strength (IDT) results for unconditioned (dry) and conditioned (wet) samples for different types of patching material are shown in Fig. 10. The trend of the bar graph shows that the indirect tensile strength of conditioned (wet) samples values is lower than the unconditioned (dry) indirect tensile strength values. This shows that the moisture (wet conditioned sample) will decrease the value of indirect tensile strength. From the TSR values (Fig. 11), it clearly shows that the ratio unconditioned (dry) and conditioned (wet) samples for all mixes were complied with AASTHO T283 recommendation for hot mix asphalt except for Company sample F. This indicates that all cold mix asphalt except from company F are resistant to moisture damage which could sustain the load from vehicles and exposed to severe condition without large degradation of the structure. Test results from ASTM D3625 testing procedure (Boiling water test) are shown in Table 5. This table indicates that all cold mix samples tested except for sample C and F showed less than five percent coating loss, which showed greater than 95% coating retained or in other words these mixes were resistance to moisture damage. This shows that all the cold mixes are resistant to stripping and can sustain the load from vehicles as well as exposed to severe condition without high degradation of the pavement structure. The company C and F samples are not resistant to stripping as their values are lower than the standard requirements.
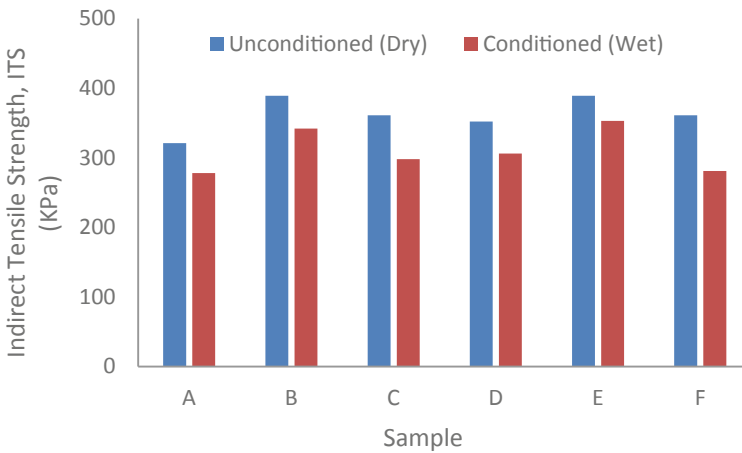

Fig. 10 Indirect tensile strength of conditioned (wet) and unconditioned (dry) samples
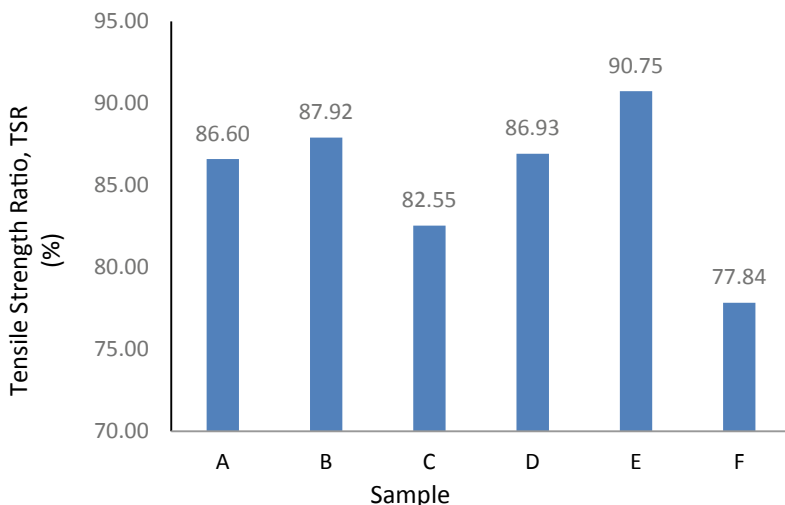
Fig. 11 Tensile strength ratio (TSR) with different cold mix asphalt sample

Table 5 Boiling water index result for cold mix asphalt sample

Samples	A	B	C	D	E	F
Percentage retained coating (%)	96	97	87	96	98	85
Retained coating greater than 95% (Yes/No)	Yes	Yes	No	Yes	Yes	No

3.6 Selection of Cold Mix Patching Materials By Using Grid Analysis

Table 6 tabulated the ranking performance criteria of cold mix patching materials which were conducted and measured in the previous sections. Table 6 presented that sign of $\sqrt{}$ is indicate that the results complied with standard specification and sign of x is indicate that the result did not complied with standard specification.

Based on the laboratory tests carried out on the six different cold mix asphalt used for patching, Sample B and Sample D obtained the highest score of compliance with the requirements of the specification/standard (6 out of 8) followed by Sample A and Sample C (5 out of 8). Next is Sample E which obtained 4 out of 8 score. Sample F has the lowest compliance with the requirements of the specification/standard (2 out of 8). Therefore, based on the ranking, Sample B and sample D are the most suitable cold mix patching materials to be used in patching maintenance work.

Table 6 Ranking performance criteria of cold mix patching materials

Company samples	Bitumen content (%)	Stability (KN)	Flow (mm)	Stiffness (KN/mm)	Air voids in mix (%)	Density (%)	Tensile strength (%)	Boiling water test (%)	Score (out of 7)
A	10.2	21.4	3.18	6.73	4.89	95.11	86.60	85.6	5 of 8
	X	√	√	√	X	X	√	√	
B	6.88	19.7	4.17	4.74	2.7	86.69	87.92	82.6	6 of 8
	√	√	X	√	√	X	√	√	
C	5.23	15.1	2.74	5.53	12.08	87.92	82.55	74.4	5 of 8
	√	√	√	√	X	X	√	X	
D	5.19	14.1	3.78	3.72	13.61	86.39	86.93	83.2	6 of 8
	√	√	√	√	X	X	√	√	
E	7.82	11	4.59	2.4	5.13	94.87	90.75	94.8	4 of 8
	X	√	X	√	X	X	√	√	
F	6.27	12.8	5.77	2.21	15.76	84.24	77.84	45.1	2 of 8
	X	√	X	√	X	X	X	X	
Standard specification for hot mix wearing course	4–6%	>8 KN	2–4 mm	>2 KN/mm	3–4%	>98%	>80%	>75%	

4 Conclusions

Based on the laboratory tests carried out on the six different cold mix asphalt used for patching, Sample B and Sample D obtained the highest score of compliance with the requirements of the specification/standard. All the cold mixes except for sample C and F are resistant to stripping and can sustain the load from vehicles as well as exposed to severe condition without high degradation of the pavement structure. The Boiling water test (ASTM D3625) method is a subjective test; however the results has shown to be consistent in term of identifying stripping quality of HMA mixes. In addition, the stability values of the various cold mix samples met the standard specification where the samples exhibited high stability values, complying with the requirements of JKR specifications. In conclusion, it is suggested that Sample B and sample D are the most suitable cold mix patching materials to be used in patching maintenance work. It is recommended to conduct advance performance testing such as resilient modulus, simple performance testing and rutting testing to validate the results testing of coring sample.

References

1. Abela A (2006) Evaluation of cold asphalt patching mixes by Anna Abela Munyagi Masters in Engineering (MEng) University of Stellenbosch
2. Arshad AK, Shaffie E, Hashim W, Rahman ZA (2020) Evaluation of rutting resistance of dense graded asphaltic concrete with nanosilica modified bitumen. In: AIP conference proceedings 2020, p 020025, October 2018

3. Day D, Lancaster IM, McKay D (2019) Emulsion cold mix asphalt in the UK: a decade of site and laboratory experience. J Traffic Transp Eng (English Ed) 6(4):359–365

4. Diaz LG (2016) Creep performance evaluation of Cold Mix Asphalt patching mixes. Int J Pavement Res Technol 9(2):149–158

5. Fang C, Yu R, Liu S, Li Y (2013) Nanomaterials applied in asphalt modification: a review. J Mater Sci Technol 29(7):589–594

6. Golestani B, Nam BH, Moghadas Nejad F, Fallah S (2015) Nanoclay application to asphalt concrete: characterization of polymer and linear nanocomposite-modified asphalt bitumen and mixture. Constr Build Mater 91:32–38

7. Liao MC, Luo CC, Wang TY, Xie X (2016) Developing effective test methods for evaluating cold-mix asphalt patching materials. J Mater Civ Eng 28(10):1–10

8. Maher A, Gucunski N, Yanko W, Petsi F (2001) Evaluation of pothole patching materials. https://cait.rutgers.edu/files/FHWA-NJ-2001-002.pdf

9. Moghaddam TB, Karim MR, Abdelaziz M (2011) A review on fatigue and rutting performance of asphalt mixes. Acad J 6(4):670–682

10. Lottman RP (1982) Predicting moisture-induced damage to asphaltic concrete field evaluation

11. Roberts FL, Kandhal PS, Brown ER, Lee D-Y, Kennedy TW (2009) Hot mix asphalt materials, mixture design and construction, 3rd edn. NCAT, Alabama

12. Shaffie E, Ahmad J, Arshad AK, Jaya P, Rais NM, Shafii MA (2019) Relationship between rheological properties of nano polymer modified asphalt bitumen and permanent deformation of asphalt mixture. Int J Integr Eng 11(6):244–253

13. Shaffie E, Ahmad J, Arshad AK, Kamarun D, Awang H (2016) Investigation on rutting performance of nanopolyacrylate and natural rubber latex polymer modified asphalt bitumen mixes. Jurnal Teknologi 78(7–3):11–15

14. Shaffie E, Arshad AK, Ahmad J, Hashim W (2018) Effect of mixing variables on physical properties of modified. Int J Civ Eng Technol (IJCIET) 9(7):1812–1821

15. Suda J, Valentin J, Žák J (2016) Cold bituminous emulsion mixtures - laboratory mix design , trial section job site and monitoring. In: E&E Congress 2016, 6th Eurasphalt & Eurobitume Congress, Prague, Czech Republic, 1–3 June 2016

16. Zhu J, Birgisson B, Kringos N (2014) Polymer modification of bitumen: Advances and challenges. Eur Polymer J 54:18–38

Effect of Eggshell Powder on the Mechanical and Durability Properties of Cement Mortar

X. F. Li, S. I. Doh, P. J. Ramadhansyah, M. R. Hainin, and W. I. Mohd Haziman

Abstract Concrete is a civil engineering material and widely used in various constructions. Cement, as major composition in concrete, consumes amounts of energy and generates pollution during production. Thus more research should be conducted to reduce the dependency of cement. In this paper, micro sized eggshell powder is used as a cementitious supplementary material to partially replace cement. Four cement replacement percentages are set with 2.5, 5, 7.5 and 10%. Workability, compressive strength, flexural strength, water absorption and acid attack were tested to analysis the performance of eggshell mortar. The results revealed that 0.4 micron micro size eggshell powder could improve the workability and mechanical properties of mortar while cause negative effect on durability of concrete. Replacement of 5% cement replacement with eggshell powder is the optimum percentage for both of compressive strength and flexural strength. On the basis of mechanical properties, eggshell could be a potential alternative material to replace cement.

Keywords Concrete · Eggshell · Cement · Replacement · Compressive strength

1 Introduction

Cement is an important civil engineering material for the construction industry. The use of cement can provide the strength required by all kinds of buildings and make construction more convenient and efficient, but it causes a large amount of consumption of energy and natural resources. Cement, as a binder in concrete,

X. F. Li · S. I. Doh (✉) · P. J. Ramadhansyah · M. R. Hainin
Department Civil Engineering, College of Engineering, Universiti Malaysia Pahang,
Lebuhraya Tun Razak, 26300 Gambang Kuantan, Pahang, Malaysia
e-mail: dohsi@ump.edu.my

W. I. Mohd Haziman
Faculty of Civil Engineering and Built Environment, Universiti Tun Hussein Onn Malaysia,
Batu Pahat, 86400 Johor Bahru, Malaysia

consumes high non-renewable resources but also produces a large amount of CO_2, which is the main product of greenhouse effect [16]. For a long time, researchers around the world have been trying to find alternative materials cement replacement in order to minimize the dependency on the natural resources. Industrial waste can be used as an alternative cement material to replace the binder material needed in the manufacture of concrete. These waste materials are often stacked in the open air or buried in landfills as industrial by-product, and cause waste of resources and environmental pollution. In the past, researchers have studied the effects of replacing cement with industrial waste, such as steel slag, fly ash and palm oil shells [2, 10]. These materials show a good bonding property when used as a cementitious supplementary material. These industrial wastes can provide substances needed for cement hydration, such as calcium or silicon, which could react with cement hydration products and lead to secondary hydration reactions that produce more C-S-H. This reaction could increase the performance of the concrete. Eggshell is a kind of solid waste which is largely produced in the confectionary industry. The calcium, which forms the main component of eggshell, can be utilized as renewable material for the cement production. Eggshell, which have relatively high CaO make it a potential alternative material to cement production [9, 17]. Some researchers have studied the mechanical properties and durability of concrete made from eggshell instead of cement. In the study of Jhatial et al. [14], partial replacement with cement by eggshell powder could improve the compressive strength of concrete. The optimum compressive strength was the specimen with replacement of 10% eggshell powder. Similar result was achieved by Tan et al. [18], in which the performance of concrete with the addition of eggshell powder increases in two types of curing condition. It is also indicated that eggshell concrete is suitable for strong acid and sulfate environments as its durability would decrease with the addition of eggshell powder. Overall, eggshell powder as cementitious supplementary material is feasible for improving the properties of concrete.

This research studies the effect of micro size eggshell powder as cement replacement on the mechanical and durability of mortar. The workability, mechanical property and durability of mortar were analyzed to evaluate its performance.

2   Experimental Programme

2.1   Materials

2.1.1   Cement

The cement powder used in this research is YTL Cement Orang Kuat, type one. The chemical and physical composition of cement is tabulated in Table 1.

Table 1 Chemical and physical composition of OPC

Tests	Units	Specification MS EN 197-1: 2014 CEM/B-L 32.5 N	Test results
Sulfate content (SO_3)	%	Not more than 3.5	2.1
Chloride (Cl^-)	%	Not more than 0.10	0.01
Fineness (According to Blaine)	m^2/kg	–	440
Setting time: initial	mins	Not less than 75	155
Soundness	mm	Not more than 10	0.8
Compressive strength			
7 days	MPa	Not less than 16	24.0
28 days	MPa	$32.5 \leq x \leq 52.5$	35.2

2.1.2 Eggshell

The waste eggshells were the byproduct of Eggtech Manufacturing Sdn Bhd located in Ijok District of Selangor. Only brown eggshells waste were collected from the factory. The eggshell waste was then cleansed using tap water immediately upon arrival to the laboratory to avoid rotten smell emission. The cleansed eggshells are then sun dried before crushing and grinding it into micro size powder. The particle size of eggshell powder ranges from 190.1 to 396.1 nm. The gradation of micro size eggshell powder is shown in Fig. 1. The comparison of chemical compositions for Ordinary Portland Cement and eggshell powder is tabulated in Table 2.
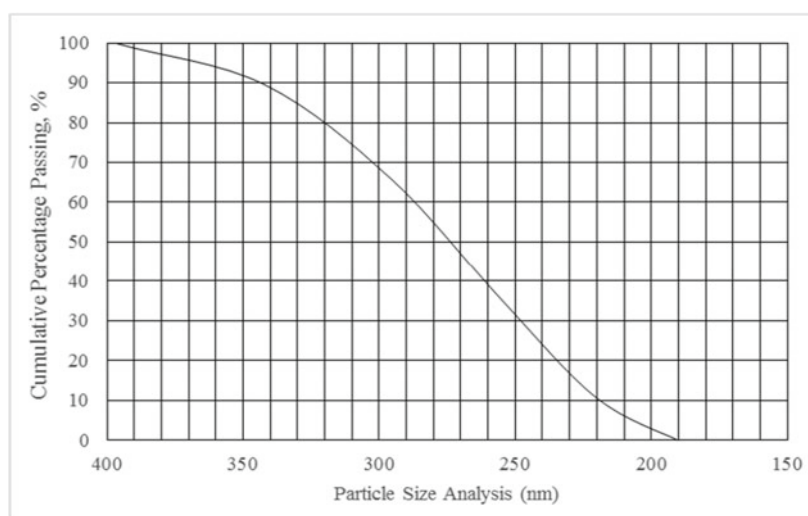

Fig. 1 Gradation of micro size eggshell powder

Table 2 The chemical compositions of ordinary Portland cement and eggshell powder

Oxide group	OPC (%)	Eggshell (%)
Calcium oxide	60.1	61.71
Silicon dioxide	21.8	0.06
Sulphur trioxide	2.5	0.82
Iron oxide	4.1	0.08
Magnesium oxide	0.5	0.34
Potassium oxide	0.25	0.05
Aluminium oxide	6.66	–

2.1.3 Water

The water used in this research is from the tap water supplied by Pengurusan Air Pahang Berhad (PAIP).

2.1.4 Fine Aggregate

Sand used throughout the research are washed river sand from Pahang River. Figure 2 shows the grading of this sand which meets the British Standard sieving test (BS812: Part103) [8].

2.2 Specimen Preparation

The specimen preparation throughout the study complied with ASTM C1329-05. The ratio between cement and sand is 1:2.75, while water/cement (w/c) ratio is 0.6. The cement was replaced by micro size eggshell powder according weight at the interval of 2.5% from 2.5 to 10%.
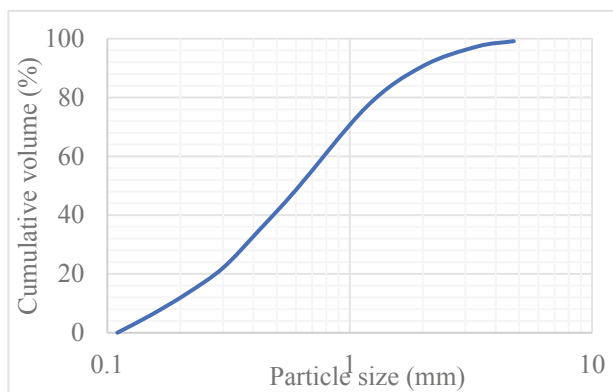

Fig. 2 Gradation of river sand

2.3   Test Method

Once the fresh mortar is prepared, the flow table test was carried out according to ASTM C1437-15 standard. For compressive strength test and flexural strength test, both were tested at the age of 1, 7, and 28 days according to BS EN 12390-3:2009 [6] and BS EN 12390-5:2009 [7] standard, respectively. The durability of mortar was tested with the same methods in the study of Tan et al. [18].

3   Result and Discussion

3.1   Workability

Workability is a parameter used to evaluate the concrete quality. Flow table test is considered as one of the standard methods to identify the characteristics of mortar which could measure the consistency of mortar. Figure 3 shows that the flow table value of mortar increases with the addition of micro size eggshell powder. This is due to the lower rate of water absorption of micro eggshell powder as compared to cement [18]. Compared with control mortar specimen with value of 105 mm, the highest flow table value could reach 120 mm with 10% replacement by eggshell powder. The result demonstrates that adding eggshell powder as supplementary cementitious material would not absorb water excessively, and it could improve the workability of mortar [18].

3.2   Mechanical Properties Test

3.2.1   Compressive Strength Test

For strength performance, all the specimens were cured in the water tank. Specimens are tested on 1, 7, and 28 days respectively to study strength of concrete with the age of concrete. Figure 4 shows the result of compressive strength of different mix designs with different age of concrete. From the result, the 1-day and 7-day compressive strength of eggshell with replacement of 7.5% and eggshell 10% are lower than that of others. Water curing promotes the formation of C-S-H gel during the hydration process which produces higher compressive strength [12]. For 28 days specimens, the compressive strength shows an increasing trend for eggshell powder replacement up to 5%. The improvement on strength is attributed from filler effect of micro size eggshell powder [18]. In some studies, the optimum for replacement has been observed to range from 7.5 to 15% [1, 5]. Furthermore, eggshell powder has similar chemical composition with limestone, forms calcium mono-carboaluminate hydrate phase through the reaction with alumina paste in the
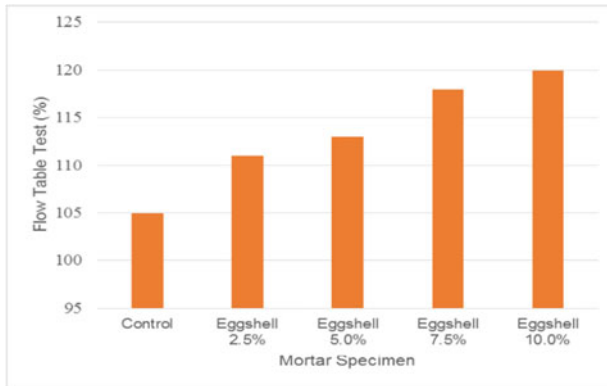
Fig. 3 Flow table result of different percentage of micro size eggshell replacement
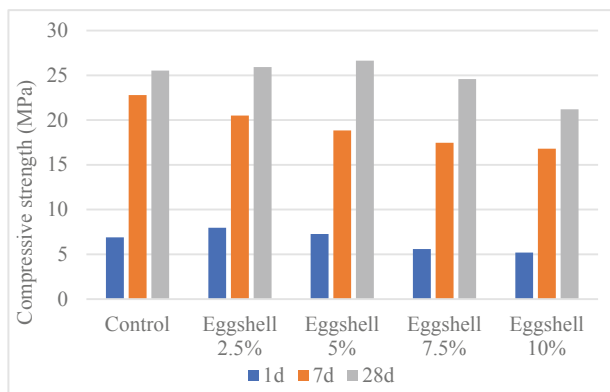

Fig. 4 The compressive strength of micro size eggshell mortar

cement [19]. As the eggshell power replacement exceeding 5%, the compressive strength of the mortar decreases, since excessive eggshell powder would weakened the bonding of the cement and aggregate [19].

3.2.2 Flexural Strength Test

Similar with the compressive strength test, the specimens for flexural strength test were also tested on 1, 7 and 28 days. Figure 5 shows the flexural behavior of specimens with different eggshell replacement. By referring to Fig. 5, 5% of cement replacement with eggshell powder has the highest strength compared to the other mix. The highest 28-day flexural strength could reach 6.17 MPa. However, the higher replacement percentage of eggshell makes the flexural strength of the
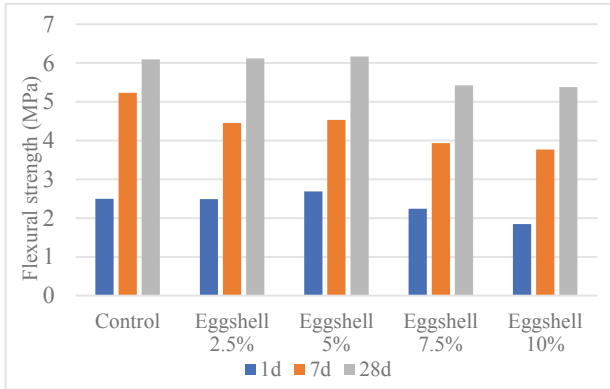
Fig. 5 The flexural strength of micro size eggshell mortar

eggshell mortar specimen decrease. It is because that excessive of eggshell powder may lead to reduction of the bonding properties between cement and aggregate. As the result, the optimum mix for the flexural strength is at 5% of cement replacement.

3.3 Durability Properties Test

3.3.1 Water Absorption Test

Figure 6 shows the result of water absorption for all the specimens. The addition of eggshell powder reduces the percentage of water absorption. According to Ing [13],
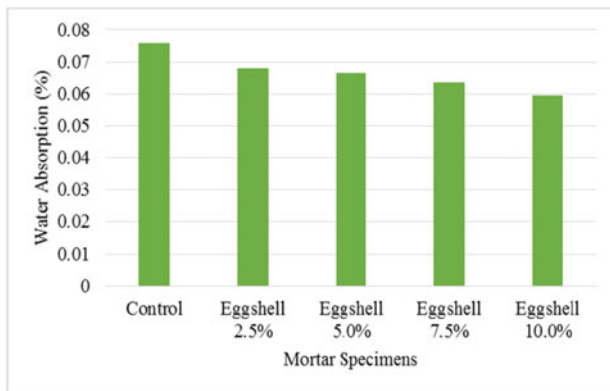

Fig. 6 Water absorption of micro size eggshell mortar

the eggshell acts as good filler to the internal voids thus producing denser cement matrix. A similar finding has been confirmed by Matschei et al. [15], revealed that micro size eggshell enhances the space filling properties of the paste.

3.3.2 Acid Attack

3.3.2.1 Residual Mass

Figure 7 show the mass loss of micro size eggshell mortar. It is observed that highest mass loss is not more than 1% of its original mass for all specimens. According to Zivica and Bajza [20], the gradually decrease of the weight which is one of the signs of the acid attack. The control and eggshell mortar specimens have lost some of the weight, as the calcium hydroxide is the first chemical compounds that attack by the sulphuric acid [11]. This chemical reaction forms calcium salts which are then leached away. The leaching cement compounds loosen the aggregate binding in mortar and consequently reduce the weight of mortar. Eggshell mortars which generally have higher calcium hydroxide as compared to control specimen show higher mass loss due to the reaction with the acidic environment. Thus, it indicates that eggshell mortar is not suitable for harsh acidic environment.

3.3.2.2 Compressive Strength Loss

Figure 8 shows the compressive strength loss for micro size eggshell powder immersed in the sulphuric acid solution for 28 days. It indicates that the compressive strength loss increases with the increase of cement replacement with eggshell powder. The control specimens show the lowest total compressive strength reduction compared to all the eggshell mortar. The mortar specimens experienced a gradual decrease in the compressive strength when the content of micro size eggshell powder increase. From the eggshell oxide content shown in Table 2, it indicates that eggshell has higher calcium oxide content and less silicon dioxide content compared with cement. During the hydration process, the silicon oxide reacts with
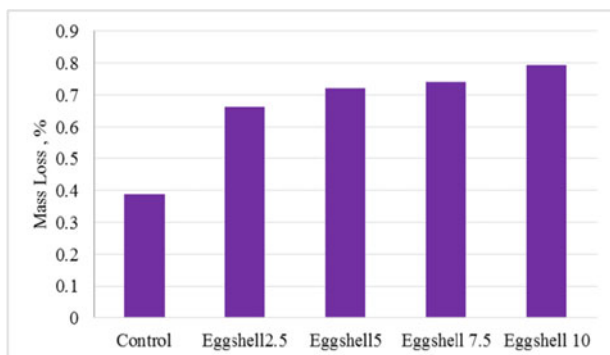

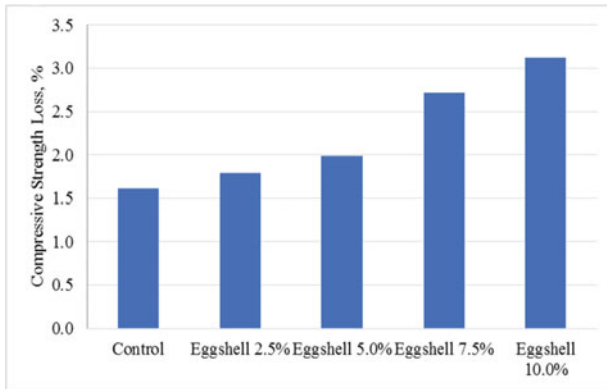**Fig. 7** Mass loss of micro size eggshell mortar

Fig. 8 Compressive strength loss of micro size eggshell mortar

the calcium hydroxide. However, for eggshell mortar, the content on silicon oxide is relatively low and generates lower amount of C-S-H gel. The excessive calcium hydroxide reacts with the aggressive solution thus reducing the compressive strength of the specimen. Therefore, the amount of the micro size eggshell used as partial replacement of cement should be consider carefully due to the low resistance of the mortar toward the acid attack.

4 Conclusion

Micro size eggshell powder was used as cementitious supplementary material for making mortar. Workability, mechanical properties and durability were discussed to evaluate the performance of micro size eggshell powder mortar. Based on the study, several conclusions could be drawn as follow:

1. The addition of eggshell powder could improve the workability of mortar which has a higher flow compared to control mix. The workability increases with the increase of eggshell replacement.
2. The 28-day compressive strength shows that a positive effect would occur when replacement percentage of eggshell powder is less than 5%, which was attributed to the filler function of micro size eggshell powder in mortar. However, when the replacement is exceeding 5%, the compressive strength reduces below the control specimen. This is due to the reduction of binding properties of the internal structure in mortar. The same phenomenon occurs for flexural strength of mortar. Therefore, optimum replacement percentage of cement by micro size eggshell powder should be 5%.

3. Water absorption and acid attack test were conducted to evaluate micro size eggshell powder mortar. The addition of eggshell powder in mortar reduces its water absorption. In acid environment, mortar was more vulnerable as the calcium oxide could react with acid solution, which resulted in mass loss and reduction of compressive strength of mortar.

References

1. Ansari MM, Kumar MD, Charles JM (2016) Replacement of cement using eggshell powder. SSRG Int J Civ Eng 3(3):1–3
2. Alengaram UJ, Al Muhit BA, bin Jumaat MZ (2013) Utilization of oil palm kernel shell as lightweight aggregate in concrete - a review. Constr Build Mater 38:161–172
3. ASTM C1329-05 (2016) Standard Specification for Mortar Cement. ASTM International, West Conshohocken, PA
4. ASTM C1437-15 (2015) Standard Test Method for Flow of Hydraulic Cement Mortar. ASTM International, West Conshohocken, PA
5. Bandhavya GB, Sandeep K, Bindhushree GB (2017) An experimental study on partial replacement of cement with egg shell powder in concrete. Int Res J Eng Technol 4(6):2318–2323
6. British Standard Institution (2009) Testing Hardened Concrete. Compressive strength of test specimens. London, BS EN 12390-3:2009
7. British Standard Institution (2009) Testing hardened concrete. Flexural strength of test specimens. London, BS EN 12390-5:2009
8. British Standard Institution (1985) Method for Determination of Particle Size Distribution. London, BS 812: Part 103
9. Choo CS, Ing DS, Yu TY (2017) The effect of different curing methods on the compressive strength of eggshell concrete. Indian J Sci Technol 10(6):1–4
10. Giergiczny Z (2019) Fly ash and slag. Cem Concr Res 124:15
11. Grubb JA, Limaye HS, Kakade AM (2007) Testing pH of concrete. Concr Int 29(4):78–83
12. Hiremath P, Shettar M, Shankar MCG (2018) Investigation on effect of egg shell powder on mechanical properties of GFRP composites. Mater Today-Proc 5(1):3014–3018
13. Ing DS (2014) The performance of eggshell as filler in concrete mixtures. In: Proceeding of the2014 international conference on industrial engineering and operations management, Bali, Indonesia, 7–9 January 2014
14. Jhatial AA, Sohu S, Memon MJ (2019) Eggshell powder as partial cement replacement and its effect on the workability and compressive strength of concrete. Int J Adv Appl Sci 6(9):71–75
15. Matschei T, Lothenbach B, Glasser FP (2007) The role of calcium carbonate in cement hydration. Cem Concr Res 37(4):551–558
16. Namoulniara K, Turcry P, Ait-Mokhtar A (2016) Measurement of CO_2 effective diffusion coefficient of cementitious materials. Eur J Environ Civ Eng 20(10):1183–1196
17. Rahman AF, Goh WI, Jhatial AA (2019) Flexural study of reinforced foamed concrete beam containing palm oil fuel ash (POFA) and eggshell powder (ESP) as partial cement replacement. Int J Sustain Constr Eng Technol 10(1):93–100
18. Tan YY, Doh SI, Chin SC (2018) Eggshell as a partial cement replacement in concrete development. Mag Concr Res 70(13):662–670

19. Yerramala A (2014) Properties of concrete with eggshell powder as cement replacement. Indian Concr J 88(10):94–105
20. Zivica VR, Bajza A (2001) Acidic attack of cement based materials—a review: Part 1. Principle of acidic attack. Constr Build Mater 15(8):331–340

Thermal Analysis and X-Ray Diffraction of Rice Husk Ash Blended Cement Under Sodium Sulfate with Wetting and Drying Cycles

P. J. Ramadhansyah, M. R. Hainin, O. Rokiah, R. Noram Irwan, W. I. Mohd Haziman, and S. A. Mangi

Abstract Sulfate attack is one of the most aggressive environmental deterioration affecting the durability of concrete structures. Thus, this study is to evaluate the effect of sodium sulfate (5% Na_2SO_4) solution on the performance of rice husk ash (RHA) blended cement under drying and wetting cycle, which is thought to simulate an aggressive environment in concrete. The RHA replacement level used was 10%. The performance of the specimen was evaluated by the differential thermal analysis (DTA), thermogravimetric analysis (TGA), and X-ray diffraction (XRD). The results showed that the replacement of ordinary Portland cement by 10% rice husk ash effectively improved the resistance of concrete due to sulfate attack. The result also indicate that the quantity of expansive gypsum formed by the reaction of calcium hydroxide will be less in RHA blended cement than in OPC specimen. In addition, RHA blended cement possibly reduced the potential of ettringite and gypsum formation due to the reduction in the quantity of calcium hydroxide, thus, improved the resistance of concrete to sulfate attack.

Keywords Sodium sulfate · RHA · XRD · Thermal · Wetting · Drying

P. J. Ramadhansyah (✉) · M. R. Hainin
Department of Civil Engineering, College of Engineering, Universiti Malaysia Pahang, 26300 Gambang, Pahang, Malaysia
e-mail: ramadhansyah@ump.edu.my

O. Rokiah · R. N. Irwan
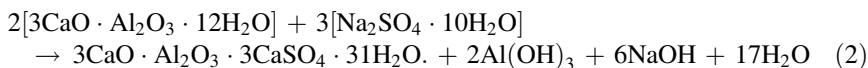Faculty of Civil Engineering Technology, Universiti Malaysia Pahang, 26300 Gambang, Pahang, Malaysia

W. I. M. Haziman
Faculty of Civil Engineering and Built Environment, Universiti Tun Hussein Onn Malaysia, Batu Pahat, 86400 Johor Bahru, Malaysia

S. A. Mangi
Department of Civil Engineering, Mehran University of Engineering and Technology, SZAB Campus Khairpur Mir's, Jamshoro 76060, Sindh, Pakistan

1 Introduction

Sulfate attack is one of the most important problems concerning the durability of concrete structures [7]. The effect of sodium sulfate attack on concrete can be divided into two principal reactions: the reaction of sodium sulfate (Na_2SO_4) and the reaction of magnesium sulfate ($MgSO_4$) with calcium hydroxide [$Ca(OH)_2$] to form gypsum [14]. The formed gypsum reacts with calcium aluminate hydrates to form ettringite [15]. These reactions result in a substantial increase in volume with subsequent cracking and peeling. Based on Santhanam et al. [15], the reactions can be represented as follows:

$$Ca(OH)_2 + Na_2SO_4.10H_2O \rightarrow CaSO_4.2H_2O + 2NaOH + 8H_2O \quad (1)$$

$$2[3CaO \cdot Al_2O_3 \cdot 12H_2O] + 3[Na_2SO_4 \cdot 10H_2O]$$
$$\rightarrow 3CaO \cdot Al_2O_3 \cdot 3CaSO_4 \cdot 31H_2O. + 2Al(OH)_3 + 6NaOH + 17H_2O \quad (2)$$

The reaction products are gypsum ($CaSO_4.2H_2O$) which leads to surface softening and loss of strength, and calcium sulphoaluminate ($3CaO.Al_2O_3.3CaSO_4.31H_2O$) known as ettringite which leads to considerable increase in volume [14]. According to Al-Akhras [2], the chemical interaction of sulfate attack is a complicated process and depends on many parameters including concentration of sulfate ions, ambient temperature, cement type and composition, water cement ratio, porosity and permeability of concrete, and the presence of supplementary cementitious materials. The exposure of concrete structures to the aggressive environments such as sulfate solution can lead to detrimental chemical, microstructural, and physical changes in the concrete matrix, resulting in serious deterioration [3]. It is generally accepted that exposure of concrete to a sulfate environment elicits two principal reactions: the reaction of sulfate ions and portlandite to form gypsum [18] and that of theresultant gypsum with calcium aluminate hydrates to form ettringite [11]. The effects of sulfate attack on the blended cement incorporating supplementary cementitious materials, such as fly ash, slag, metakaolin, and silica fume have been investigated [2, 7, 12, 13]. According to the available current literature, several researchers have confirmed that the incorporation of supplementary cementitious materials as partial replacement of OPC is a beneficial technique to improve the resistance of concrete to sulfate attack. For this reason, it is important to study the effect of RHA blended cement under sodium sulfate attack. In this investigation, thermal analysis and x-ray diffraction was used to evaluated the concrete containing 10% RHA replacement under sodium sulfate through wetting and drying cycles.

2 Materials and Methods

2.1 OPC

The ordinary Portland cement (OPC) used in this investigation satisfying the requirements of BS EN 197–1 [6] specification for ordinary and rapid-hardening Portland cement. The OPC was supplied in one batch for the entire study and kept in airtight containers to ensure consistent quality and properties. The chemical composition of the OPC used in this study was within the standard range of 70% CaO, 17.8% SiO_2, 3.9% Al_2O_3, 3.2% Fe_2O_3, 1.5% MgO, and 3.6% SO_3. The OPC also indicated a compound composition of 54.5% C_3S, 18.2% C_2S, 9.4% C_3A, and 10.5% C_4AF.

2.2 RHA

The rice husk ash (RHA) used in this study was ground using a laboratory ball mill with porcelain balls. Then, RHA was sieved to obtain ash of 9.52 μm. SiO_2 was identified as the main component of the RHA. In addition, SiO_2, Al_2O_3, and Fe_2O_3 comprised 92% of the material, in accordance with C618-12 [4] of the American Society for Testing and Materials (ASTM), which requires that these three main oxides should comprise no less than 70% of the pozzolanic material.

2.3 Aggregate

A single size (20 mm) of crushed granite was used as the coarse aggregate. The coarse and fine aggregates each had a specific gravity of 2.60 and 2.65, respectively. Where the water absorption rates of 0.47 and 0.85%, correspondingly.

2.4 Sample Preparation and Mix Design

A control mix was prepared using OPC. However, RHA replacement levels of 10% by weight of cement were applied through the study. At the laboratory, RHA was thoroughly mixed with OPC in blended cement, and water was added to the mixer. When the mixtures were prepared, the specimen was cured in water maintained at room temperature for a minimum of 28 days. Then, the specimens were subjected to 5% Na_2SO_4 solution with wetting–drying cycles. The sodium sulfate was prepared by mixing the chemical with distilled water at 5% by weight of volume. According to ACI 318–08 [1], 5% of Na_2SO_4 was representing extremely severe

sulfate exposure. At each cycle (wetting–drying), the solution was replaced by a freshly prepared one or based on the change in the pH of the solution.

2.5 Differential Thermal and Thermo Gravimetric Analysis Test

Differential thermal analysis is corresponding to the thermal decomposition of different phases in paste, whereas thermogravimetric analysis (TGA) measures weight loss caused by decomposition. On the specified day of testing, hardened cement paste samples were crushed into powder form with passing a 75 μm sieve. About 15–20 mg of sample was placed in a platinum pan and heated in a nitrogen atmosphere from 25 to 1000 °C at 10 °C/min. in addition, weight loss which occurs in hardened cement paste due to dehydration and decomposition of its components when heated gradually, was recorded at varying temperatures.

2.6 X-ray Diffraction Test

In accordance with BS EN 13925–1 [5], the samples were scanned in steps of 0.034 °C (2θ) with a fixed counting time of 1 s. The X-ray scan ranged from 2θ = 10 –90 °C using copper (KαCu) with a wavelength λ of 1.5406 nm as the X-ray source. EVA software was used to analyse the phase of the samples.

3 Results and Discussion

3.1 TGA/DTA Analysis

Vedalakshmi et al. [17] have reported that gypsum and ettringite existed in crystal form. In this study, the evidence on the formation of gypsum and ettringite was evaluated by TG–DTA. The graphical illustration representing the TG–DTA of specimens subjected to sodium sulfate solution with cyclic drying-wetting is presented in Fig. 1. The curve of the specimen showed four endothermic peaks. The first endothermic peak positioned between 94.99 and 137.95 °C, with a peak at 104.64 °C and a 5.48% loss of weight, resulted from the dehydration of ettringite and gypsum. According to Skaropoulou et al. [16], the dehydration of ettringite and gypsum from sodium sulfate solution takes place at around 80 and 130 °C. Based on the investigations conducted by Santhanam et al. [15], they found that incorporating pozzolanic material in cement pastes subjected to sulfate solution, the endothermic peak in the range of 80–100 °C is due to the dehydration of ettringite.
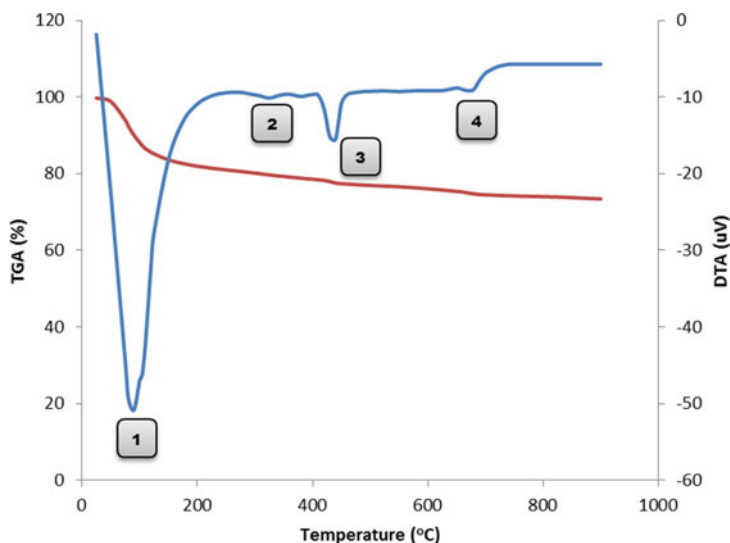
Fig. 1 TGA and DTA curve of RHA blended cement under sodium sulfate subjected to wetting–drying cyclic

The second endothermic peak, located between 277.43 and 357.88 °C, with a peak at 320.69 °C and loss of weight at 1.31%, corresponded to the decomposition of calcium aluminate silicate hydrate, calcium aluminate hydrate, and calcium chloroaluminate. Additionally, the specimen also contained a small peak of brucite, which was confirmed through XRD analysis (see Fig. 2). The endothermic peak at around 358.30 and 401.22 °C, with a peak at 379.16 °C and weight loss of 0.73% was resulted from brucite. The presence of brucite was probably due to the external sulfate attack. The third endothermic peak detected in the range of 410.28–494.15 °C, with a peak at 435.91 °C and weight loss of 1.82%, corresponded to the dehydration of calcium hydroxide. This finding is consistent with the results obtained by Gonçalves et al. [9] who have found that the endothermic peak between 400 and 460 °C is related to the dehydroxylation of the calcium hydroxide. Finally, the endothermic peaks appearing at 641.86 and 713.41 °C, with a peak at 672.78 °C and a 1.67% loss of weight, were associated with the decomposition of calcium carbonate.

3.2 Weight Loss

From the thermogravimetric analysis, the ettringite and gypsum formation were estimated quantitatively. The results are summarized in Table 1, which shows a trend for loss of weight with increasing ettringite and gypsum formation along with

Table 1 Thermo-gravimetric mass losses of cement pastes with different levels of RHA substitution, endothermic peak correspond to ettringite and gypsum

Type of mixes	Age (days)	Temp. range (°C)	Peak temp. (°C)	Weight loss (%)	Onset temp. (°C)	Final temp. (°C)
OPC	3	61.49–100.52	74.65	3.18	64.20	81.78
	7	61.52–119.61	92.50	5.37	78.21	100.28
	28	80.12–122.15	97.54	7.67	88.46	103.25
	56	75.89–130.37	90.49	8.62	84.74	104.06
	90	66.39–113.31	90.49	9.42	87.02	97.95
	180	91.36–137.94	103.61	10.47	96.57	112.24
RHA	3	79.37–126.75	85.74	2.74	79.40	91.07
	7	53.52–111.24	67.74	4.13	54.46	84.82
	28	94.99–137.95	104.64	5.48	87.86	113.58
	56	65.95–91.87	78.33	5.89	67.94	73.00
	90	89.71–130.76	101.50	6.22	95.94	110.76
	180	64.61–94.12	81.27	6.72	70.06	80.44

the increase of exposure period. The results also indicated that the weight losses of RHA blended cement were lower than those found in controlled specimen. This due to the pozzolanic reaction in RHA consumed the $Ca(OH)_2$, which the less amount of $Ca(OH)_2$ decreased the ettringite and gypsum formation. For instance, at early age (i.e. 28 days), the weight loss of the hydrated phases (ettringite and gypsum) was 5.48% (RHA blended cement) and 7.67% (OPC concrete). Based on Table 1, the trend is not consistent for all specimens. This can be explained due to severity of the drying and wetting cycles as used in the current study. Cyclic wetting and drying can increase the rate of corrosion in concrete as a result of two actions. First, cyclic wetting and drying concentrates ions, such as chloride, can increase the rate of corrosion by the evaporation of water during the drying phase [11]. Second, once chloride thresholds have been reached at the depth of cover, drying of the concrete increases the availability of oxygen required for corrosion, because oxygen has a substantially lower diffusion coefficient in saturated concrete [10]. Furthermore, the onset temperature values for the first endothermic peak and the end-set temperature value for the final endothermic peak were also investigated and the results are listed in Table 1.

3.3 XRD Analysis

The sulfate attack on concrete was due mostly to two main reactions: the reaction of Na_2SO_4 and $Ca(OH)_2$ to form gypsum and the reaction of the resulting gypsum with calcium aluminate hydrates to form ettringite. This explanation of the

mechanism of sulfate attack on concrete was confirmed through XRD analysis. The XRD trace indicates that gypsum, ettringite and $Ca(OH)_2$ were only crystalline phases present in the different depths of concrete in addition to quartz and calcium carbonate. Figures 2 and 3 show the XRD results for OPC and RHA blended cement subjected to 5% Na_2SO4 solution with drying-wetting cycles. The peak corresponding to the ettringite $(Ca_6Al_2(SO_4)_3(OH)_{12}\cdot26H_2O)$ was detected at around $16°2\theta$ and $21°2\theta$. Skaropoulou et al. [16] and Gao et al. [8] found that the peak in the regions from $16.2°2\theta$ to $22.9°2\theta$ was due to ettringite formation. However, a strong intensity peak corresponding to the gypsum $(CaSO_4\cdot2H_2O)$ still appeared at about $18°2\theta$. Gao et al. [8] reported that the maximum peak at $11.6°2\theta$ and $19.3°2\theta$ indicated the presence of gypsum. The presence of ettringite and gypsum in concrete subjected to sulfate solution showed that these parameters were the main corrosion products. On the other hand, a small amount of thaumasite $(Ca_3Si(OH)_6(CO_3)(SO_4)\cdot12H_2O)$ can be found in the XRD patterns of specimen exposed to Na_2SO_4 solutions. Ettringite and thaumasite have similar crystal structures [18], thus, their XRD patterns show similarities in intensity peaks. In this study, the corresponding peaks of thaumasite were observed at around $16.5°2\theta$. Finally, the corresponding peaks of calcium carbonate $(CaCO_3)$, calcium hydroxide $(Ca(OH)_2)$ and quartz (SiO_2) appeared at about $33°2\theta$, $34°2\theta$ and $47°2\theta$, respectively. The results also showed that the concentrations of ettringite and gypsum in RHA replacement cement were lower than that in the OPC specimen. This explains the trend exhibited in Figs. 2 and 3. It can be seen that the addition of RHA in blended cement reduced the deterioration of concrete caused by sulfate attack, which could be attributed to the pozzolanic reaction in rice husk ash. When RHA is mixed with cement in concrete, it combines with free lime during the hydration of
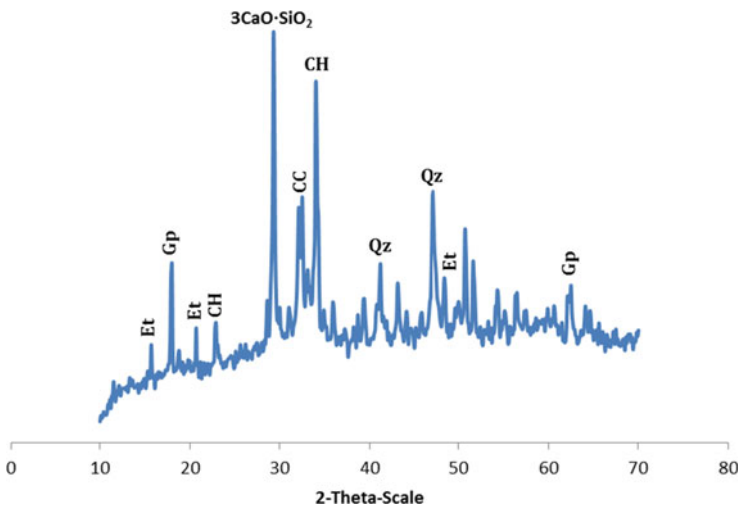

Fig. 2 XRD patterns of the ordinary Portland cement paste subjected to sodium sulfate solution with drying-wetting cycles
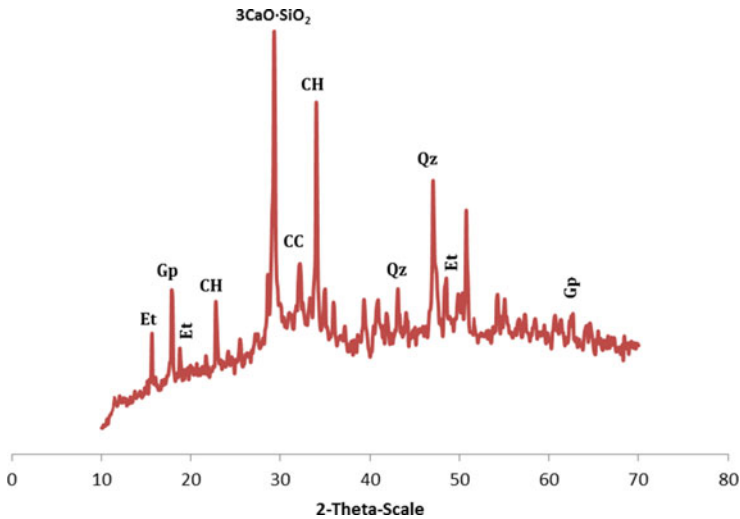
Fig. 3 XRD patterns of RHA blended cement paste subjected to sodium sulfate solution with drying-wetting cycles

cement in concrete to form calcium silicate hydrate (CSH). Similarly, the intensity peak of $Ca(OH)_2$ was found less than that of the OPC concrete due to the pozzolanic reaction. Because of the pozzolanic reaction, the specimen containing RHA had lower $Ca(OH)_2$ content than that of the OPC concrete. This lessened the amount of $Ca(OH)_2$ and subsequently decreased ettringite and gypsum formation. Cement replacement also reduced the overall amount of C_3A in the system and amount of ettringite and gypsum that formed upon sulfate attack.

4 Conclusions

The addition of RHA was found to decrease calcium hydroxide formation by hydration and, consequently, gypsum and ettringite were reduced during sulfate attack. The test results also demonstrated that the amount of calcium hydroxide in RHA blended cement was lower than that of Portland cement. This finding proposed that RHA could be used as an effective mineral addition in the design of durable concrete under sodium sulfate with drying-wetting cyclic condition. In addition, the cyclic exposure to sulfates attack increased the rate of deterioration of ordinary Portland cement which was confirmed by TGA, DTA and XRD analysis.

References

1. ACI 318-08 (2012) Building Code Requirements for Structural Concrete and Commentary. American Concrete Institute, Farmington Hills, USA
2. Al-Akhras NM (2006) Durability of metakaolin concrete to sulfate attack. Cem Concr Res 36:1727–1734
3. Al-Dulaijan SU, Maslehuddin M, Al-Zahrani MM, Sharif AM, Shameem M, Ibrahim M (2003) Sulfate resistance of plain and blended cements exposed to varying concentrations of sodium sulphate. Cement Concr Compos 25:429–437
4. ASTM C618–08 (2012) Standard Specification for Coal Fly Ash and Raw or Calcined Natural Pozzolan for Use in Concrete. American Society for Testing and Materials, West Conshohocken, PA 19428–2959, United States
5. BS EN 13925–1 (2003) Non-destructive testing. X-ray diffraction from polycrystalline and amorphous materials. General principles, British European Standard, London, United Kingdom
6. BS EN 197–1 (2000) Cement. Composition, Specifications and Conformity Criteria for Common Cements, British European Standard, London, United Kingdom
7. Chatveera B, Lertwattanaruk P (2009) Evaluation of sulfate resistance of cement mortars containing black rice husk ash. J Environ Manage 90:1435–1441
8. Gao X, Ma B, Yang Y, Su A (2008) Sulfate attack of cement-based material with limestone filler exposed to different environments. J Mater Eng Perform 17:543–549
9. Gonçalves JP, Toledo Filho RD, Fairbairn EMR (2008) Evaluation of magnesium sulphate attack in mortarmetakaolin system by thermal analysis. J Therm Anal Calorim 94:511–516
10. Macphee D, Diamond S (2003) Thaumasite in cementitious materials. Cement Concr Compos 25:805–807
11. Marchand J, Samson E, Maltais Y, Beaudoin JJ (2002) Theoretical analysis of the effect of weak sodium sulfate solutions on the durability of concrete. Cement Concr Compos 24:317–329
12. Najimi M, Sobhani J, Pourkhorshidi AR (2011) Durability of copper slag contained concrete exposed to sulfate attack. Constr Build Mater 25:1895–1905
13. Sahmaran M, Erdem TK, Yaman IO (2007) Sulfate resistance of plain and blended cements exposed to wetting–drying and heating–cooling environments. Constr Build Mater 21:1771–1778
14. Santhanam M, Cohen MD, Olek J (2001) Sulphate attack research-whiter now? Cem Concr Res 31:845–851
15. Santhanam M, Cohen MD, Olek J (2003) Mechanism of sulfate attack: a fresh look: Part 2. Proposed Mech Cement Concrete Res 33:341–346
16. Skaropoulou A, Kakali G, Tsivilis S (2006) A study on thaumasite form of sulfate attack (TSA) using XRD, TG and SEM. J Therm Anal Calorim 84:135–139
17. Vedalakshmi R, Sundara Raj A, Palaniswamy N (2008) Identification of various chemical phenomena in concrete using thermal analysis. Indian J Chem Technol 15:388–396
18. Zuquan J, Wei S, Yunsheng Z, Jinyang J, Jianzhong L (2007) Interaction between sulfate and chloride solution attack of concretes with and without fly ash. Cem Concr Res 37:1223–1232

Estimate the Durability of Rice Husk Ash Concrete Subjected to Sulfate Attack Through Wetting and Drying Cyclic

P. J. Ramadhansyah, M. R. Hainin, O. Rokiah, B. W. Chong, W. I. Mohd Haziman, and S. A. Mangi

Abstract It is well known that aggressive environments like the sulfate attack are the major factor affecting the durability of concrete. Thus, this research was carried out to estimate the durability of rice husk ash (RHA) concrete exposed to sodium sulfate attack through wetting and drying cyclic. Five levels of cement replacement namely 0, 10, 20, 30 and 40% (by weight) were studied. After being kept in the sodium sulfate solution for 3, 7, 28, 56, 90 and 180 days, the RHA concrete specimens were evaluated based on the rapid chloride permeability and its correlation. It was found that the total charge passed in Portland cement concrete was higher than that of RHA-blended cement concrete. However, it continued to decrease along with increasing levels of RHA replacement. In addition, the use of 40% RHA in the cement resulted in better resistance to sulfate attack when the concrete specimen was exposed to the wetting and drying cycles. It can be concluded that the use of 10 to 40% RHA effectively decreased the penetration depth (charge passed) in the concrete under sulfate attack.

Keywords Durability · Sulfate attack · RCPT · Wetting · Drying

P. J. Ramadhansyah (✉) · M. R. Hainin
Department of Civil Engineering, College of Engineering, Universiti Malaysia Pahang, 26300 Gambang, Pahang, Malaysia
e-mail: ramadhansyah@ump.edu.my

O. Rokiah · B. W. Chong
Faculty of Civil Engineering Technology, Universiti Malaysia Pahang, 26300 Gambang, Pahang, Malaysia

W. I. M. Haziman
Faculty of Civil Engineering and Built Environment, Universiti Tun Hussein Onn Malaysia, Batu Pahat, 86400 Johor Bahru, Malaysia

S. A. Mangi
Department of Civil Engineering, Mehran University of Engineering and Technology, SZAB, Campus Khairpur Mir's, Jamshoro 76060, Sindh, Pakistan

1 Introduction

RHA is known to be superior to other supplementary materials such as; slag, palm oil fuel ash (POFA), silica fume, and fly ash (FA). Due to its high pozzolanic activity, both strength and durability of concrete are improved [10]. During the past decades, extensive research has been carried out to investigate the performance of RHA in relation to the properties of concrete [5]. The use of RHA as a mineral admixture for concrete is not new and considerable amount of data has been published with regard to its influence on the behavior of concrete [2]. RHA, which is rich in silica, is obtained by burning rice husks to remove volatile carbons such as cellulose and lignin. Della et al. (2002) reported that for incineration temperatures of up to 700 °C for 6 h, 95% silica powder, predominantly in amorphous form, could be produced. It is generally agreed upon that the use of RHA whose main chemical composition of which is silica, helps to improve the durability of concrete especially when exposed to chloride and sulfate attacks [12, 15].

Pozzolanic materials such as fly ash (FA), silica fume, and RHA, which are mainly silicates when added to cement, react with $Ca(OH)_2$ to form additional calcium silicate hydrates in the hydrated cement matrix [13]. Romano et al. [16] reported that calcium silicates (Ca_3SiO_5) are the most important components of pozzolanic materials and are responsible for most of concrete properties such as the durability. Bui et al. [6] reported that the added pozzolanic materials, which are finer than cement particles, fill the pores and improve the particle packing of cement paste in the transition zone between aggregates and cement paste, leading to the reduction of permeability. When fine pozzolanic particles are dispersed in the paste, they generate a large number of nucleation sites for the precipitation of the hydration products. Thus, the addition of pozzolanic materials to Portland cement increases its durability when compared to the controlled specimen [11].

Cyclic wetting and drying process accelerate durability problem because it subjects the concrete to the movement and accumulation of harmful materials, such as sulfates, alkaline, acids, and chlorides. Sahmaran et al. [17] reported that continuous immersion of the specimens in chloride solution does not necessarily represent the field conditions. However, the specimens are subjected to aggressive environmental with wetting–drying cyclic and simulate in the laboratory are common methods of accelerating the tests [9, 18]. According to [8], continuous immersion of specimens does not necessarily represent the field conditions because generally, the concentration and pH of the site generally remains constant. Conversely, simulated field exposure conditions in the laboratory with the application of wetting and drying cycles are common methods of accelerating the tests [7, 14]. Based on the related literature presented, there are no information is available on the effect of RHA blended cement subjected to sulfate solution with wetting and drying cycles under laboratory simulation. Therefore, there is a need for further investigation on the durability of RHA concrete subjected to sulfate attack through wetting and drying cyclic.

2 Experimental Study

2.1 Raw Materials

Locally available ordinary Portland cement (OPC) used in this investigation was supplied in one batch for the entire study to ensure consistent quality and properties. It was revealed that the main constituents of cement were CaO (70%), SiO_2 (18%), Al_2O_3 (4%), Fe_2O_3 (3.2%), MgO (1.5%), and SO_3 (3.6%), respectively. Furthermore, RHA was produced by controlled burning of the Rice husk with the temperature of 700 °C (6 h). The ash was then ground using a laboratory ball mill with porcelain balls until it met the fineness as requirement by ASTM C 618. RHA used was mainly amorphous silica with main oxides namely SiO_2, Al_2O_3, and Fe_2O_3 comprised 92% which it met the standard of ASTM C 618 [4]. A coarse aggregate with a single size of 20 mm was used while local natural sand derived from granite was used as the fine aggregate in the concrete mixtures. The coarse and fine aggregates each had a specific gravity of 2.65, and water absorption rates of 0.47 and 0.85%, correspondingly.

2.2 Sodium Sulfate

Sodium sulfate is the sodium salt of sulfuric acid. It is a white crystalline solid of formula Na_2SO_4. At the laboratory, the sodium sulfate solution was prepared by mixing the chemical with distilled water at 5% (weight of volume) and it was used to represent extremely severe sulfate exposure as stated by ACI 318–08 [1]. At each cycle, the solution was replaced by a freshly prepared one or based on the change in the pH of the solution.

2.3 Concrete Mix Design

A control mix was prepared using OPC. RHA replacement levels of 10, 20, 30 and 40% by weight of cement were applied. These are referred to as RHA10, RHA20, RHA30 and RHA40, respectively. The RHA was thoroughly mixed with OPC in blended cement, and water was added to the mixer. Superplasticiser was added to the mix to maintain slump flow values. When the mixtures were prepared, the concrete was cured in water maintained at room temperature for a minimum of 28 days to achieve target strength of 40 MPa. After 28 days of curing under water, the specimens were subjected to sulfate solution via wetting–drying cycles. The tests were conducted at the ages of 3, 7, 28, 56, 90, and 180 days.

2.4 Wetting-Drying Cyclic Test

Cyclic wetting and drying is a main problem for concrete structure when exposed to sulfate attack. Cyclic tests were performed to obtain an understanding of the mechanisms causing the aggressive environment of concrete during the wetting and drying phases of the cycle. Wetting period with an average of 15 h was used throughout this investigation, followed by 9 h of drying per day. Time intervals of wetting and drying cycles were considered to simulate the Malaysian conditions of a tropical rainforest climate.

2.5 Rapid Chloride Permeability Test

The test was conducted according to the ASTM test method C1202 [3]. Concrete specimens of 100 mm diameter with 50 mm thickness were used. In the RCPT test, the concrete specimens were conditioned using a vacuum pressure of 1 mmHg (133 MPa) on the dry specimens and maintained for 3 h. The specimens were treated under vacuum saturation for a period of 1 h after adding water, and further soaking under water for a period of 18 h. The specimens were then placed into the RCPT instrument. Then, the current was measured and recorded at 5 min intervals with a data logger. The total charge passed through the specimen was computed, and the chloride ion penetrability was evaluated qualitatively.

3 Results and Discussion

3.1 Total Charge Passed

Generally, the total charge passed of RHA blended cement concrete continuously decrease with an up to 40% increase in RHA content as illustrated in Fig. 1. For instance, at 28 days of exposure, the total charge passed of 10% replacement RHA in cement was 1967 Coulombs (C), whereas at 20, 30, and 40% RHA, the corresponding total charge passed was 1054, 811 and 753 C, respectively. Hence, a 10% increase in RHA content can reduce of total charge passed in the range of 7.15 to 46.40%. At all RHA contents investigated, a 10% replacement was recorded as the highest charge passed, whereas 40% was recorded as the lowest total charge passed. This explains the trend exhibited in Fig. 1. On the other hand, the controlled concrete specimen presented the greatest average total charge passed compared with RHA cement concrete. For instance, at the age of 180 days, the average total charge passed in the OPC concrete was 51.78% more than that in the RHA10 concrete. It can be seen in Fig. 1, the rapid chloride permeability decreased with an
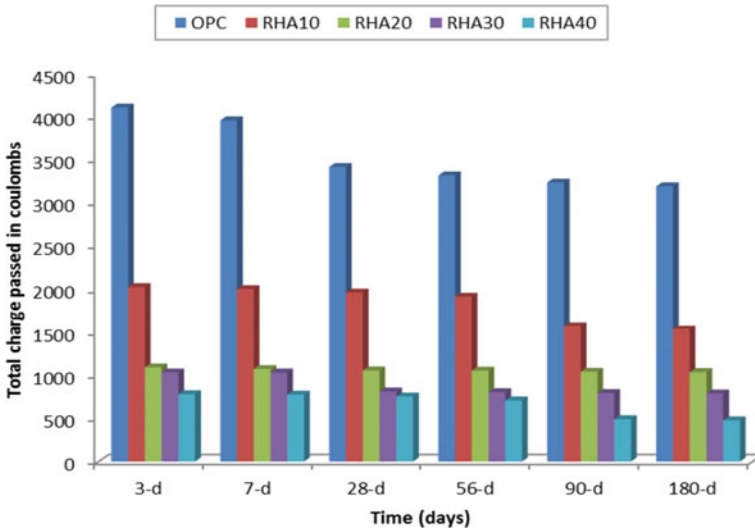
Fig. 1 Total charge passed of OPC and RHA blended cement concrete under sulfate attack via wetting–drying cyclic

increase in age. For example, for RHA10 concrete, the total charge passed was reduced from 2030 to 1538 C as the age increased from 3 to 180 days.

3.2 Classification of Charge Passed

According to the ASTM C1202-10 classification ranges, the chloride ion penetrability is considered "high" when the total charge passed is higher than 4000 C. When the total charge passed values are between 2000–4000, 1000–2000 and, 100–1000 C, as well as less than 100 C, concrete can be classified as "moderate", "low", "very low", and "negligible", respectively. It can be observed from the data presented in Table 1 that the charge passed of OPC concrete changed from "high" to "moderate" due to an increase in age ranging from 3 to 180 days. Conversely, replacing RHA reduced drastically the chloride ion penetrability of concrete from "moderate" to "very low" ratings from higher to lower replacement levels, respectively. For instance, at 20% replacement level, almost all the total charge passed was less than 2000 C, and chloride penetration was classified as "low". However, when the replacement level increased up to 40%, the total charge passed was lower than 1000 C, and concrete can be classified as "very low".

Table 1 Chloride permeability as per ASTM C 1202

RHA (%)	Total charge passed in coulombs					
	3-d	Risk of penetration	7-d	Risk of penetration	28-d	Risk of penetration
0	4101	High	3953	Moderate	3414	Moderate
10	2030	Moderate	2007	Moderate	1967	Low
20	1090	Low	1071	Low	1054	Low
30	1032	Low	1030	Low	811	Very low
40	778	Very low	774	Very Low	753	Very Low
RHA (%)	56-d	Risk of penetration	90-d	Risk of penetration	180-d	Risk of penetration
0	3315	Moderate	3234	Moderate	3189	Moderate
10	1920	Low	1575	Low	1538	Low
20	1052	Low	1040	Low	1035	Low
30	802	Very low	792	Very low	788	Very low
40	707	Very low	490	Very low	477	Very low

3.3 Correlation Between Charge Passed, Current and Temperature

The curves in Fig. 2 illustrate the relationship between current rate and time for all mixes, showing a consistent trend for majority of the mixes. However, using RHA blended cement showed the positive effect of decreasing current rate, which resulted in reduced total charge passed. Generally, by adding up to 40% of RHA, the specimen exhibited the lowest current rate compared with other mixes. On the other hand, increasing current rate was obtained for all concrete specimens as the time increased. The average current of OPC concrete was 1.25, 20.08, 34.19%, and 40.80% higher than those of RHA10, RHA20, RHA30 and RHA40 cement concrete, respectively. As such, the added RHA in the cement concrete reduced the current rate of specimens even when subjected to sulfate solution with drying-wetting rotations.

3.4 Correlation Between Charge Passed, Current and Time

Clearly, the total charge passed of OPC and RHA cement concrete increased proportionally over time as show in Fig. 3. The rate of increase in total charge passed with respect to time of OPC concrete was also higher than that of the other concrete specimens. Among the replacement levels, the RHA40 blended cement concrete exhibited the lowest rate of increase, followed by RHA30, RHA20, and RHA10. From the slope of the graph shown in Table 2, the total charge passed and
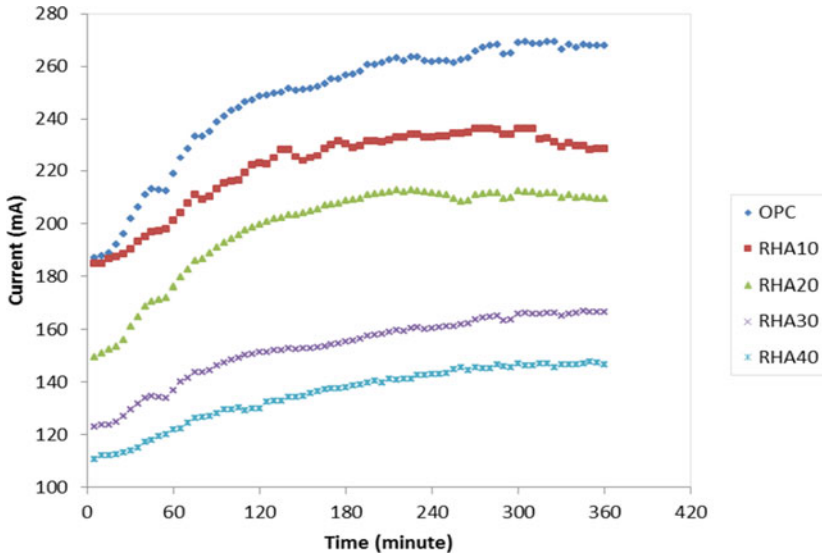
Fig. 2 Relationship between current and time of OPC and RHA blended cement concrete under sulfate attack via wetting–drying cyclic
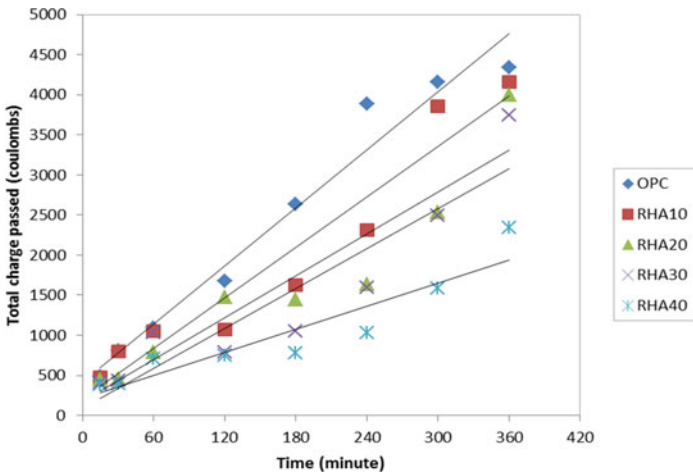

Fig. 3 Relationship between total charge passed and time of OPC and RHA blended cement concrete under sulfate attack via wetting–drying cyclic

Table 2 Coefficients of the linear relationship between total charge passed and time

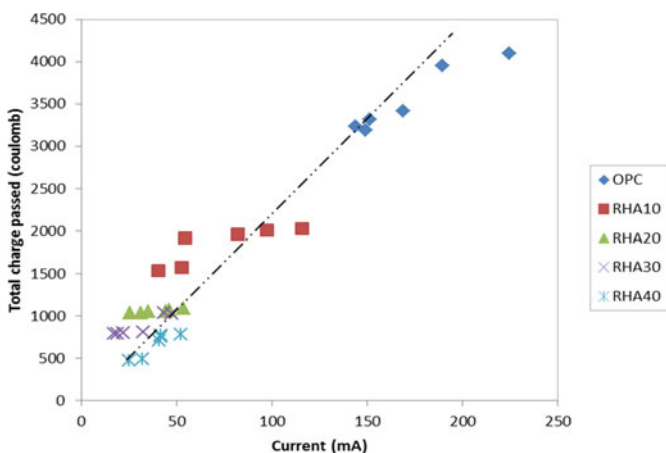| Mixture type	Independent variable, x	Dependent variable, y	Constant		R^2
			c	m	
OPC	Time	Total charge passed	411.91	12.09	0.97
RHA10			202.93	10.52	0.92
RHA20			169.66	8.73	0.89
RHA30			91.92	8.29	0.86
RHA40			212.61	4.81	0.86

Fig. 4 Relationship between total charge passed and current of OPC and RHA blended cement concrete under sulfate attack via wetting–drying cyclic

time were linearly correlated with R-Square values exceeding 0.86. In addition, the effect of RHA on chloride ion permeability was significant. In order to illustrate the relationship between the total charge passed and current based on the experimental data, the total charge passed was graphically correlated with the current as presented in Fig. 4. Table 3 shows the linear regression parameters linking total charge passed and current. The different percentages of the RHA mixes showed R-Square values beyond 0.85, which also showed other parameters of the linear equation.

Table 3 Coefficients of the linear relationship between total charge passed and current

Mixture type	Independent variable, x	Dependent variable, y	Constant		R^2
			c	m	
OPC	Current	Total charge passed	1462	12.1	0.92
RHA10			1378	6.24	0.88
RHA20			985	1.84	0.89
RHA30			138	13.51	0.85
RHA40			613	8.7	0.87

4 Conclusions

Rice husk ask proved to be a suitable replacement material for cement, and helped to reduce the total charge passed and increased the durability of concrete under sulfate attack through wetting and drying cyclic. A higher RHA replacement level as the results decreased the total charge passed, thus enhancing the resistance of concrete to sulfate attack. The increase of RHA replacement in concrete from 10 to 40% have the positive effect of decreasing current rate, which resulted in reduced total charge passed.

References

1. ACI 318-08 (2012) Building Code Requirements for Structural Concrete and Commentary. American Concrete Institute, Farmington Hills, USA
2. Al-Ahdal BMS, Li X, Tufail RF (2018) Mechanical properties of concrete containing waste glass powder and rice husk ash. Biosys Eng 4:1019–1033
3. ASTM C1202 (2019) Standard Test Method for Electrical Indication of Concrete's Ability to Resist Chloride Ion Penetration. American Society for Testing and Materials, West Conshohocken, PA 19428–2959, United States
4. ASTM C618–08 (2012) Standard Specification for Coal Fly Ash and Raw or Calcined Natural Pozzolan for Use in Concrete. American Society for Testing and Materials, West Conshohocken, PA 19428–2959, United States
5. Bheel N, Meghwar SL, Sohu S, Khoso AR, Kumar A, Shaikh ZH (2018) Experimental study on recycled concrete aggregates with rice husk ash as partial cement replacement. Civil Eng J 4:2305–2314
6. Bui DD, Hu J, Stroeven P (2005) Particle size effect on the strength of rice husk ash blended gap-graded Portland cement concrete. Cement Concr Compos 27:357–366
7. Fan YF, Zhang SY, Wang Q, Shah SP (2016) The effects of nano-calcined kaolinite clay on cement mortar exposed to acid deposits. Constr Build Mater 102:486–495
8. Ganjian E, Pouya HS (2009) The effect of Persian Gulf tidal zone exposure on durability of mixes containing silica fume and blast furnace slag. Constr Build Mater 23:644–652

9. Hekal EE, Kisharb E, Mostafab H (2002) Magnesium sulfate attack on hardened blended cement pastes under different circumstances. Cem Concr Res 32:1421–1427

10. Hu L, Zhen H, Shipeng Z (2020) Sustainable use of rice husk ash in cement-based materials: environmental evaluation and performance improvement. J Cleaner Prod 264:1–14

11. Jittin V, Bahurudeen A, Ajinkya SD (2020) Utilisation of rice husk ash for cleaner production of different construction products. J Cleaner Prod 263:2–27

12. Koushkbaghi M, Mahyar JK, Mosavi H, Ehsan M (2019) Acid resistance and durability properties of steel fiber-reinforced concrete incorporating rice husk ash and recycled aggregate. Constr Build Mater 202:266–275

13. Le HT, Ludwig H-M (2020) Alkali silica reactivity of rice husk ash in cement paste. Constr Build Mater 243:1–12

14. Mahdikhani M, Bamshad O, Shirvani MF (2018) Mechanical properties and durability of concrete specimens containing nano silica in sulfuric acid rain condition. Constr Build Mater 167:929–935

15. Olutoge FA, Peter AA (2019) Effects of rice husk ash prepared from charcoal-powered incinerator on the strength and durability properties of concrete. Constr Build Mater 196:386–394

16. Romano JS, Marcato PD, Rodrigues FA (2007) Synthesis and characterization of manganese oxide-doped dicalcium silicates obtained from rice hull ash. Powder Technol 178:5–9

17. Sahmaran M, Erdem TK, Yaman IO (2007) Sulfate resistance of plain and blended cements exposed to wetting–drying and heating–cooling environments. Constr Build Mater 21:1771–1778

18. Zhou C, Zheming Z, Aijun Z, Lei Z, Yong F, Lin L (2019) Deterioration of mode II fracture toughness, compressive strength and elastic modulus of concrete under the environment of acid rain and cyclic wetting-drying. Constr Build Mater 228:1–11

Non-destructive and Flexural Testing of Multilayer Bamboo Hollow-Core Reinforced Composite Bridges

Nawir Rasidi, Taufiq Rochman, Eva Arifi, Evi Nur Cahya, and Sri Wiwoho Mudjanarko

Abstract Bamboo is an orthotropic material with high strength along and low strength transversal to its fibers. In the construction field, Bamboo is an environmentally friendly material and has been widely used as a construction material due to its excellent mechanical behavior. Fast growing and renewal capabilities characteristics have also been studied. Based on that, the application of a composite slabs system between concrete and multilayer bamboo which is arranged in a cross-section, without steel reinforcement on a short span bridge is the topic in this paper. This composite system using hollow-core system due to the presence of whole bamboo, therefore this model is named Mulbamcomphol (multilayer cross-ply bamboo composite hollow-core). Full-scale flexural behavior will be examined in non-destructive tests under the actual load of trucks with rocks, sand, gravel and agricultural products. The analysis uses FEM (thick shell and solid element) based programs, due to exact the results are difficult to obtain and tend to be far from the results of flexural testing in the laboratory. Bamboo slabs on a weak axis restrain a smaller load than conventional slabs, but it has deflection that is 81% smaller than conventional slabs at the equal load of 21 kN. Meanwhile, if tested on a strong axis, bamboo slabs restrain 52% greater load and produce 73% less deflection than conventional slabs. In the other hand Bridges with cross-arranged bamboo composite concrete slab systems called Mulbamcomphol have a good performance in resisting flexural loads in terms of ductility and maximum load that can be carried both visually and in analysis and experimental testing

N. Rasidi (✉) · T. Rochman
Civil Engineering Department, State Polytechnics of Malang, Jl. Soekarno Hatta No. 9, Malang 65141, East Java, Indonesia
e-mail: nawir.rasidi@polinema.ac.id

E. Arifi · E. N. Cahya
Faculty of Engineering, Brawijaya University, Jl. MT. Haryono 167, Malang 65145, Indonesia

S. W. Mudjanarko
Department of Civil Engineering, Narotama University, Jl. Arief Rahman Hakim 51, Surabaya 60117, Indonesia

1 Introduction

Nowadays construction technology is more developed, especially in the case of bridges. Starting from conventional reinforced concrete T girders, then prestressed concrete I girder, precast and cast in situ girder box bridges, both in constant depth simple span and variable depth balanced cantilever types, arch bridges, cable stayed bridges and suspension bridges. Material nonlinearities start to be more complex, ranging from steel, concrete, strands and tendons of high-quality steel, and FRP (fiber reinforced polymer) composite fibers from carbon, glass, Kevlar and others. This is a concern and encouragement to make the bridge research based on traditional materials which is very easy to obtain and is a renewable natural resource but is actually very sophisticated because the composite material used is the creation of God which is complex and multi-nonlinear, namely bamboo.

Bamboo as a functionally graded composite-bamboos are giant grass-like plants and not trees as commonly believed, belonging to the family of the *Bambusoideae*. The bamboo culm, in general, is a cylindrical shell, divided by transversal diaphragms at the nodes. Bamboo is an orthotropic material with high strength along and low strength transversal to its fibers (Xiao et al. [1]. In the construction field, Bamboo is an environmentally friendly material and has been widely used as a construction material due to its excellent mechanical behavior [2, 3]. Fast growing and renewal capabilities characteristics have also been studied (Li et al. 2018).

In terms of strength, bamboo has a higher resistance compared to conventional construction materials such as concrete, steel, and aluminum alloys [5] especially in short spans [6], more than 200 four-point bending tests has carried out on *Guadua angustifolia Kunth* (bamboo) culm for which numerous mechanical and physical properties were measured [7], in the other hand Bamboo composite behavior through the rule of mix and a concise summary regarding bamboo reinforced concrete beams, permanent shutter concrete slabs and columns has discussed [8].

Based on that, the application of a composite slabs system between concrete and multilayer bamboo which is arranged in a cross-section, without steel reinforcement on a short span bridge is the topic in this paper. This composite system using hollow-core system due to the presence of whole bamboo, therefore this model is named *Mulbamcomphol* (multilayer cross-ply bamboo composite hollow-core). Full-scale flexural behavior will be examined in non-destructive tests under the actual load of trucks with rocks, sand, gravel and agricultural products. The analysis uses FEM [9] (thick shell and solid element) based programs, due to exact the results are difficult to obtain and tend to be far from the results of flexural testing in the laboratory.

2 Characteristics and Biomechanical Properties of Bamboo

Bamboo in South and Southeast Asia is about 80% of the total in the world. The genus *Bambusa* has the highest number of species, and is especially abundant in the tropics, including Indonesia. Figure 1 shows the parts and segments of bamboo [8].

There are three important physical characteristics of bamboo: the first wettability or the ability of a liquid to maintain contact with a solid surface, and it is controlled by the balance between the intermolecular interactions of adhesive type (liquid to surface) and cohesive type (liquid to liquid), and the wettability of bamboo has studied [10, 11], the second is water content, water content is an important physical property of bamboo because it affects the mechanical properties of bamboo. The last is density, the density of bamboo varies from 500 to 800 kg/m^3 [1].

The mechanical characteristics of bamboo are inseparable from the micro structure of the bamboo plant, both of the position or location of the fiber, the density of the fiber, the direction of the fiber in its longitudinal and radial direction [12]. Figure 2 shows the roots and segments of bamboo *Phyllostachys Edulis* species. The natural distribution of the composite fibers shows the nonlinearity of the composite material as well as the geometrical nonlinearity of bamboo.

Bamboo parts in the form of segments and stems and enlarged bamboo cell micro structure are shown in Fig. 3. The density of these cells depends on the elevation of the cross section of the bamboo being reviewed, the age of the bamboo and the type of bamboo and the radial direction of the bamboo.

The radial direction of bamboo also determines the density of bamboo fibers. Figure 4a shown an example of a box-type *Phyllostachys* bamboo, the concave part (middle) tighter than the convex one (corner), and the orthogonal direction of the
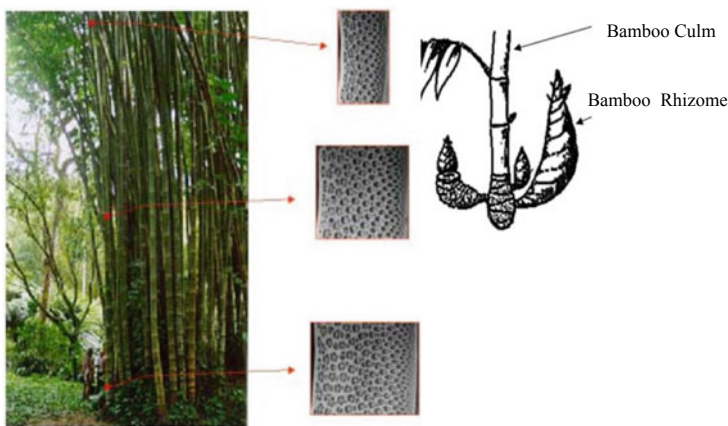

Fig. 1 The structure of *Dendrocalamus Giganteus* bamboo plants and fiber density characteristics in three different cross sections parts and segments of bamboo
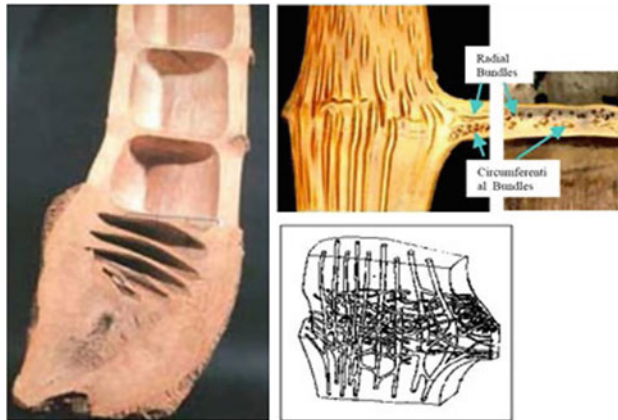
Fig. 2 The roots and segments of bamboo *Phyllostachys Edulis*
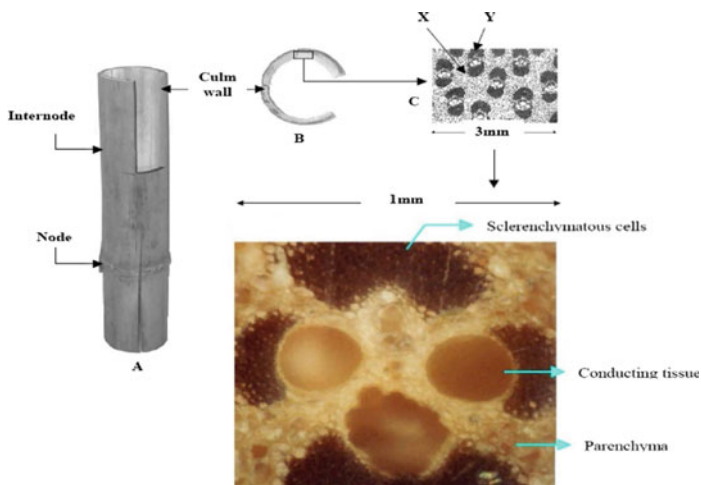

Fig. 3 Micro structure of bamboo

bamboo fiber is shown in Fig. 4b the bamboo stiffness observed in parallel with the bamboo longitudinal direction is better than tangential or radial stiffness.

3 Experimental

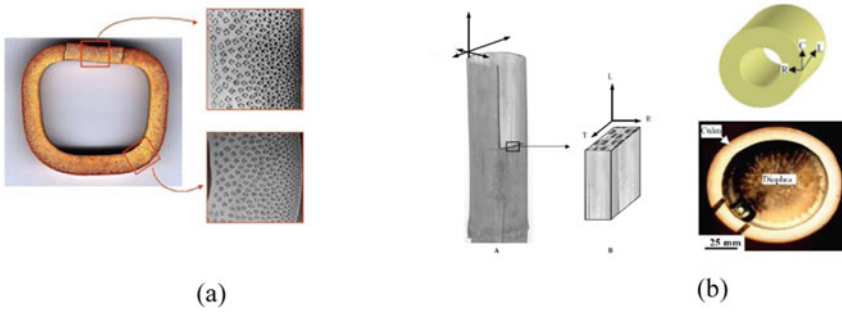The analysis and experimental path of this study are presented in the Fig. 5 as follows:

Fig. 4 (**a**) *Phyllostachys* bamboo box-type in radial direction. (**b**) the orthogonal direction of the bamboo fiber
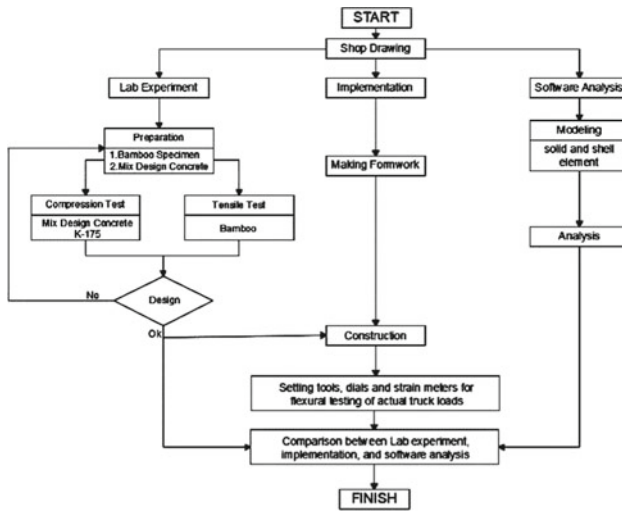

Fig. 5 Research experimental flow chart

3.1 Material

The raw bamboo material is Indonesian local bamboo, namely "Ori" bamboo species. Research of "Ori" bamboo and "Petung" bamboo have also been studied [13] using the Universal Testing Machine with a tensile capacity of 13.6 tons. The testing machine is equipped with a computer that present stress–strain diagrams outputs as shown in Fig. 6.
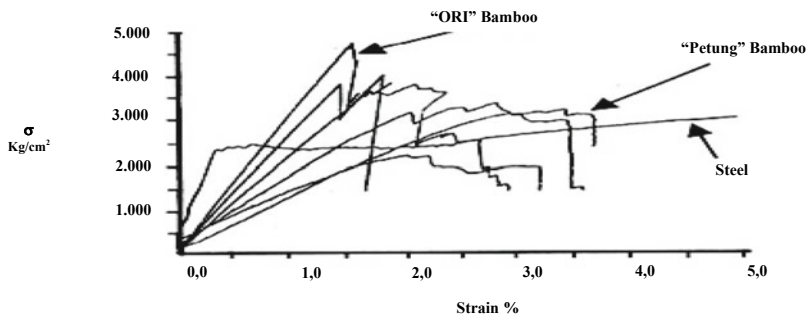
Fig. 6 Stress–strain outputs diagrams

3.2 Tensile Test

The bamboo culms test consists of three specimens with measuring 210 mm 40 mm with a notched center of up to 10 mm that presented in Fig. 7.

Bamboo tensile testing is executed in Mechanical Engineering laboratory State Polytechnic of Malang used UTM (Uniaxial Tensile Machine) that shown in Fig. 8.

3.3 Flexural Test

Composite slabs consisting of concrete and bamboo as reinforcement with measuring 1000 mm × 1000 mm and 250 mm thickness is described in Fig. 9.

Flexural test specimens are implemented on the weak axis (Fig. 10) and strong axis (Fig. 11) for composite plates and conventional plate.

Schematic loading is described in Fig. 12 and flexural testing is carried out in the structure laboratory of the Civil Engineering Department of the State Polytechnic of Malang with a Hydraulic Hand Pump Jack with Pressure Gauge as shown in Fig. 13.
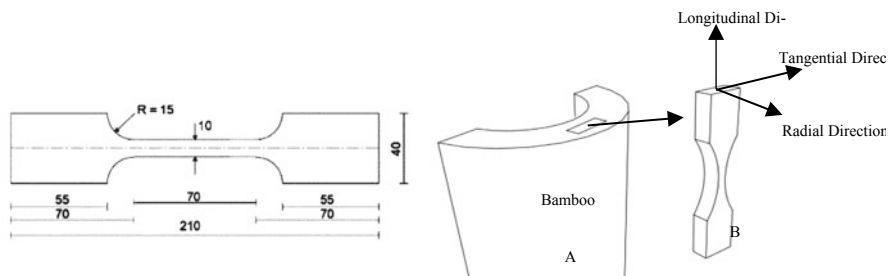

Fig. 7 Specimen bamboo for tensile test
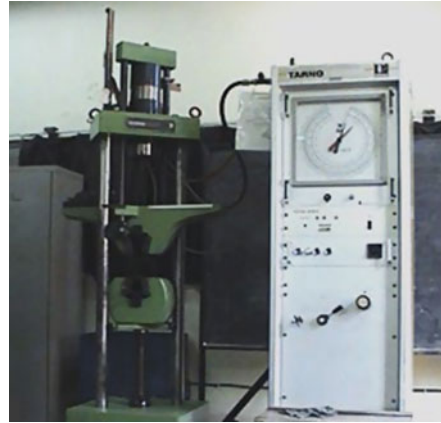
Fig. 8 Uniaxial tensile machine

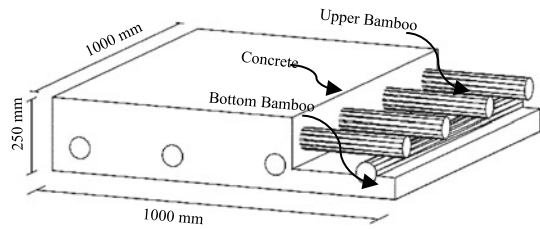**Fig. 9** Composite slab specimen concept

Fig. 10 Sketch of weak axis specimen
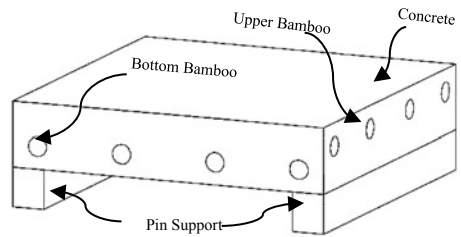
Fig. 11 Sketch of strong axis specimen
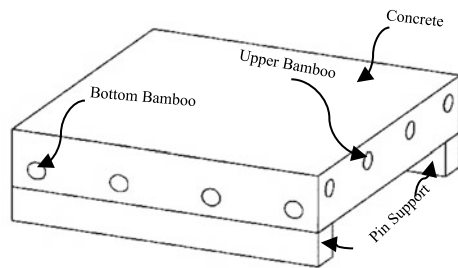
Fig. 12 Schematic loading
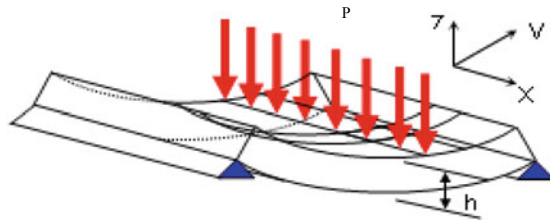
Fig. 13 Flexural weak axis testing of hollow-core slab

3.4 Multilayer Bamboo Composite Bridge

3.4.1 The Construction

Multilayer bamboo is implemented on the actual bridge as shown in Fig. 14 where Fig. 14a show the multilayer bamboo reinforcement and multilayer bamboo hollow-core reinforced composite bridges is represent in Fig. 14b

a

b

Fig. 14. a). Multilayer bamboo reinforcement **b)**. Multilayer bamboo hollow-core reinforced composite bridges.

3.4.2 The Field-Full Scaled Test Using Truck Loading

Full scale flexural and non-destructive testing process by attaching strain gauge to the bottom of bridges (Fig. 15) and connecting to the strain meter (Fig. 16) as follow:

Actual load truck with various axle variations are performed in bridge testing (Fig. 17) to obtain the load combination that gives the greatest strain results.

4 Test Results and Discussion

4.1 *Bamboo Tensile Test*

The results of stress and strain bamboo tensile test is presented in the Fig. 18.

Vertical axis values represent the stress (σ), while values on the horizontal axis is present the strain (ε) which is defined $\varepsilon = \frac{\Delta L}{L}$. Based on Fig. 18. The maximum

Fig. 15 Attaching strain gauge to the bottom of bridges

Fig. 16 Connecting strain gauge to the strain meter

Fig. 17 Full scaled test using truck loading

Fig. 18. Stress and strain of bamboo tensile test.

tensile stress value of bamboo for each specimen are 242.5 N/mm^2, 255 N/mm^2, and 257.5 N/mm^2 with an average value of 251.67 N/mm^2.

4.2 Laboratory Slab Testing

Tests carried out for slabs are deflection tests and flexural tests. Slab test is divided into three specimens based on the pin support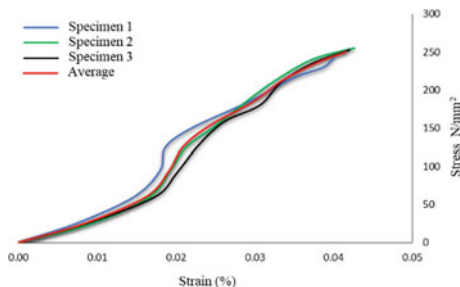 on the weak axis as specimen 1, the strong axis as specimen 2, and the conventional plates as specimen 3. The results of laboratory deflection slab testing are shown in Fig. 19 and Fig. 20 show the results of laboratory flexural slab testing as follow:

Based on Fig. 19 and Fig. 20 the deflection values for each specimen are 0.16 mm, 1.67 mm, and 1.33 mm with the maximum Mn values for each specimen are 8.55 kN.m, 17.32 kN.m, and 9.91 kN.m, while the maximum load that can restrain by specimens 1,2,3 is 21 kN, 55 kN, and 26 kN. Observation of specimen 1 and specimen 2 cracks did not occur at all. It is estimated that there is a slip between bamboo and concrete (bonding) on bamboo.
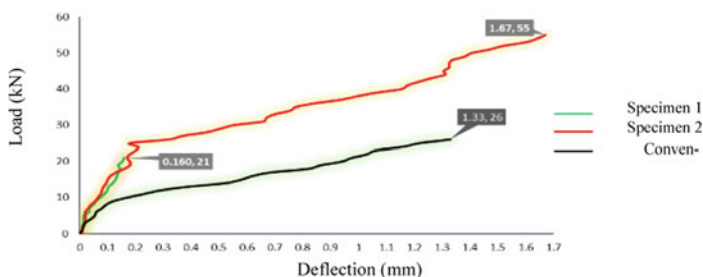

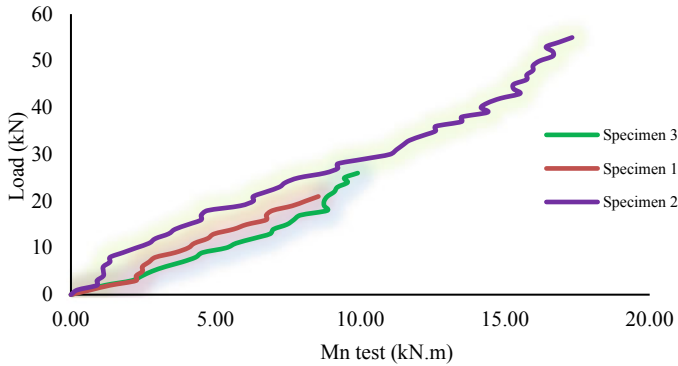**Fig. 19** Load - deflection of slabs test

Fig. 20 Load versus moment of flexural slabs test

4.3 The Field-Full Scaled Test

The results of strain on the load that has been processed at four different strain gauge locations at a number of combinations of axial axis variations, hereinafter referred to as cyclical loads 1 to cyclical loads 14. The strain pattern trends are shown in Fig. 21.

Based on Fig. 21a1. The strain value at location 1 is very small, this occurs because the first location range is shorter and the load suffered is a front axle load with a maximum load of 10 t, while the tendency for strain to increase with repetition is increasingly shown in Fig. 21a2 this strain pattern is thought to be caused by a small slip on the concrete-bamboo surface, but a larger slip is restrained by a sliding connector (cross bamboo, cross section and concrete wire).

Figure 21b1 shows that the strain at location 2 is slightly larger than location 1 due to the location span 2 is longer than location 1 and the load received is the rear axle load with a maximum load of 20 t. The pattern of stretch increase is also shown in Fig. 21b2. However, small slips on the bamboo-concrete surface tend to shrink and produce a constant bond so that it is predicted that this increase in strain will be smaller and more asymptotically at infinite load repetition.

Figure 21c1 shows that the strain at location 3 is very small but slightly larger than location 1 due to the load received is the rear axle load with a maximum load of 20 t. The equal trend is shown by Fig. 21c2 with a tendency to increase the strain that is getting smaller and asymptotically at infinite load repetition.

Figure 21d1 shows the strain at location 4 is also slightly larger due to the span of location 4 is longer than location 3 and the load received is the rear axle load with a maximum load of 20 t. The equal trend is shown by Fig. 21d2 with a tendency to increase the strain that is getting smaller and asymptotically at infinite load repetition.
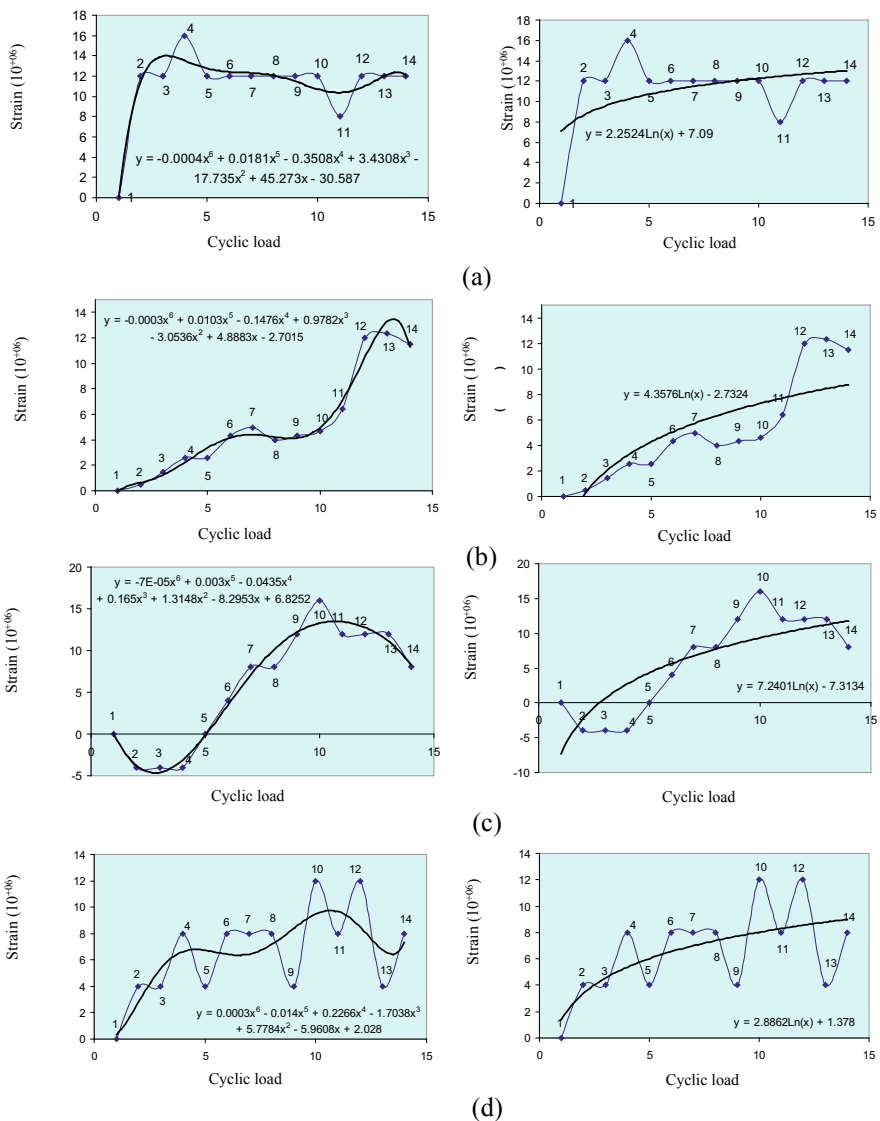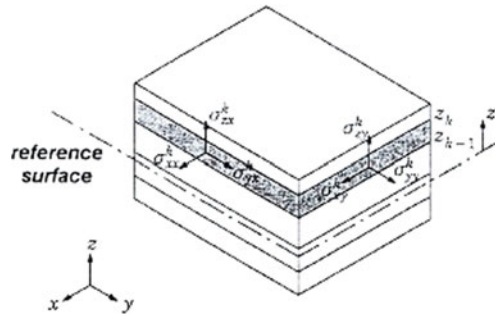
Fig. 21 **a** strain pattern trends at location 1. **b** strain pattern trends at location 2. **c** strain pattern trends at location 3. **d** strain pattern trends at location 4

Fig. 22 Tractions acting on the laminated plate [14]

5 Analytical Models

5.1 Slabs Modeling

The *Mulbamcomphol* slab is modeled with the following idealization:

Stress resultants are defined to represent the forces and moments produced by these tractions. the shaded area is the depressed element that is being reviewed. The notation σ_x is the normal stress that occurs in the x direction while the σ_y notation is the stress that occurs in the y direction. z_k notation is the thickness of the stress area. By integrating the stresses over the cross-section, the force and moment resultants per unit length of reference surface based on first-order shear deformation theory are defined Eq. 1–3 [14] as follow:

$$\{N\} = \begin{Bmatrix} N_x \\ N_y \\ N_{xy} \end{Bmatrix} = \int_h \begin{Bmatrix} \sigma_x \\ \sigma_y \\ \tau_{xy} \end{Bmatrix} dz = \sum_{k=1}^{n} \int_{z_{k-1}}^{z_k} \begin{Bmatrix} \sigma_x \\ \sigma_y \\ \tau_{xy} \end{Bmatrix} dz \qquad (1)$$

$$\{M\} = \begin{Bmatrix} M_x \\ M_y \\ M_{xy} \end{Bmatrix} = \int_h \begin{Bmatrix} \sigma_x \\ \sigma_y \\ \tau_{xy} \end{Bmatrix} zdz = \sum_{k=1}^{n} \int_{z_{k-1}}^{z_k} \begin{Bmatrix} \sigma_x \\ \sigma_y \\ \tau_{xy} \end{Bmatrix} zdz \qquad (2)$$

$$\{Q\} = \begin{Bmatrix} Q_y \\ Q_x \end{Bmatrix} = \int_h \begin{Bmatrix} \tau_{yz} \\ \tau_{xz} \end{Bmatrix} dz = K \sum_{k=1}^{n} \int_{z_{k-1}}^{z_k} \begin{Bmatrix} \tau_{yz} \\ \tau_{xz} \end{Bmatrix} dz \qquad (3)$$

Idealization of the cross-section of the slab is shown in Fig. 23. The cross-section of x direction shows the strong axis on the slab. The weak axis is shown in the y direction. While the idealization of local shells and the global coordinate system used for composite bamboo are shown in Fig. 24 with ideal concrete as solid elements (3D solid) and bamboo layers idealized as shell elements.

Based on that idealization. The *Mulbamcomphol* actual bridge is modeled in MIDAS/Civil 7.0.1 is shown in Fig. 25. The bridge is modeled with 7497 nodal points, the bamboo culms are modeled with 2500 beam elements and the bridge

Concrete (solid shell)

Bamboo (shell)

Core concrete (solid shell)
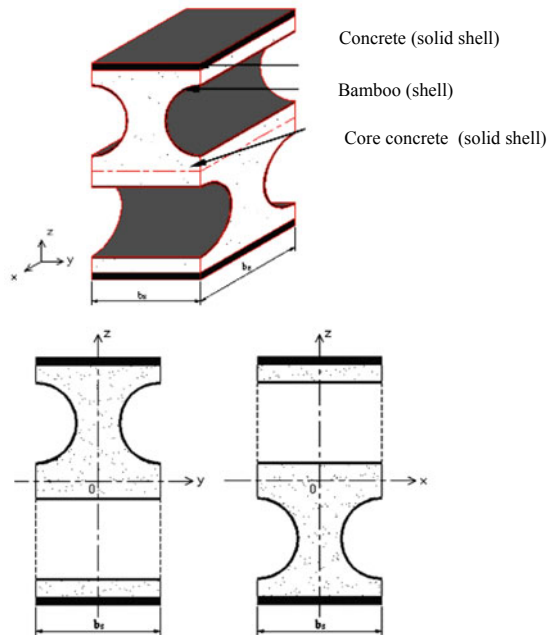
Fig. 23 Representative element of the two-way
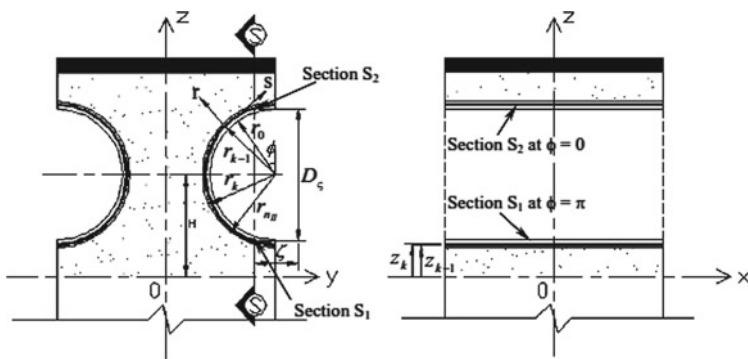
Fig. 24 The idealization of local shells and the global coordinate system used for composite bamboo

slabs is modeled with 6000 shell elements. The bridge is supported by a simple roller-joint placement, and loading with an even load of 2.2 tons/m^2, i.e. "D" load and "P" line load of 12 tons/m. While *Mulbamcomphol* modeling for laboratory testing uses STAAD.pro with a measure of 1000 $\times$ 1000 mm and a thickness of
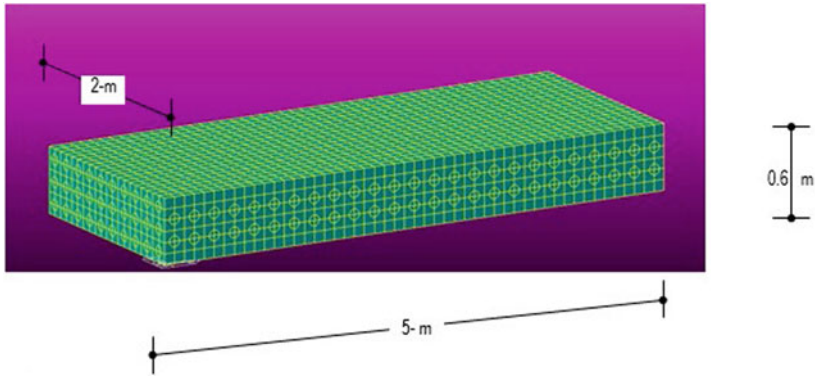
Fig. 25 Mulbamcomphol full bridge modeling in MIDAS/Civil

(a)   (b)
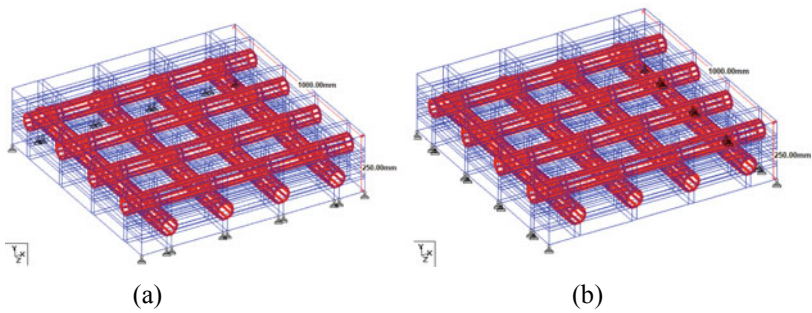
Fig. 26 **a** Strong axis slab modeling in STAAD.Pro. **b** weak axis slab modeling in STAAD.Pro

250 mm is shown in Fig. 26. Figure 26a shows the modeling of the strong axis slab while Fig. 26b for the weak axis slab.

5.2 Software Analysis Results

5.2.1 MIDAS/Civil

Figure 27 Indicates the part of the bridge that has maximum deflection in the middle of the bridge with maximum deflection values are 1.689 mm. Axial forces are shown in Fig. 28

The results of deflection value are shown in Fig. 27 as follow:
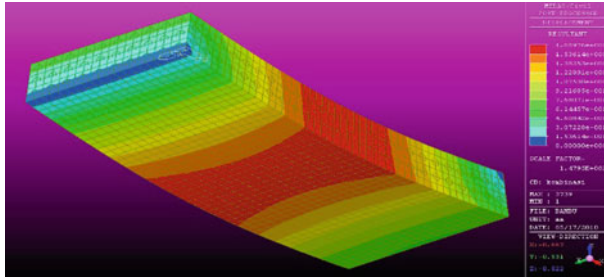
Fig. 27 Deflection contours for each element

Figure 28 shows the maximum axial force for upper and bottom section bridge are 4.1549 N, and 4.2068 N. While the stress of the *Mulbamcomphol* bridge are presented in Fig. 29.

Based on Fig. 29. The maximum axial stress σx of bamboo culms is 1.48786 N/mm^2, the maximum effective stress σx of solid concrete is 5,707 N/mm^2, the maximum axial stress σx of concrete for upper and bottom bridge are 3.4184 N/mm^2, 3.37327 N/mm^2.

5.2.2 STAAD.Pro

The stress results of bamboo and concrete analysis are presented in Fig. 30. Figure 30a illustrates the stress of the bamboo culms on the weak axis, Fig. 30b illustrates the stress of the concrete on the weak axis, Fig. 30c shows the bamboo culms stress on the strong axis, and Fig. 30d shows the stress of the concrete on the strong shaft as follows.

Figure 30 shows the maximum stress value of bamboo on the weak and strong axis are 0.027 N/mm^2 and 0.054 N/mm^2. This value is used to compute the Moments (MFEM) by multiplying the total maximum stress value by the moment arm. The bamboo stress graph shown in Fig. 31.
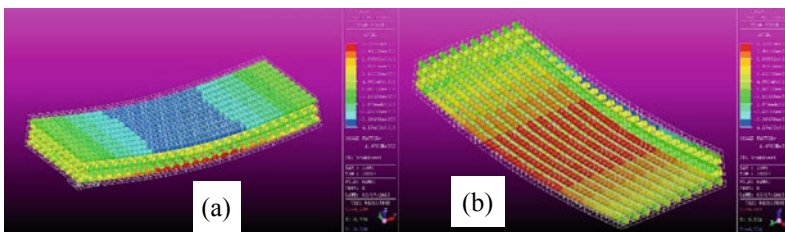
Fig. 28 **a** Axial force "Fx" with contours (upper bridge). **b** Axial force "Fx" with contours (bottom bridge)
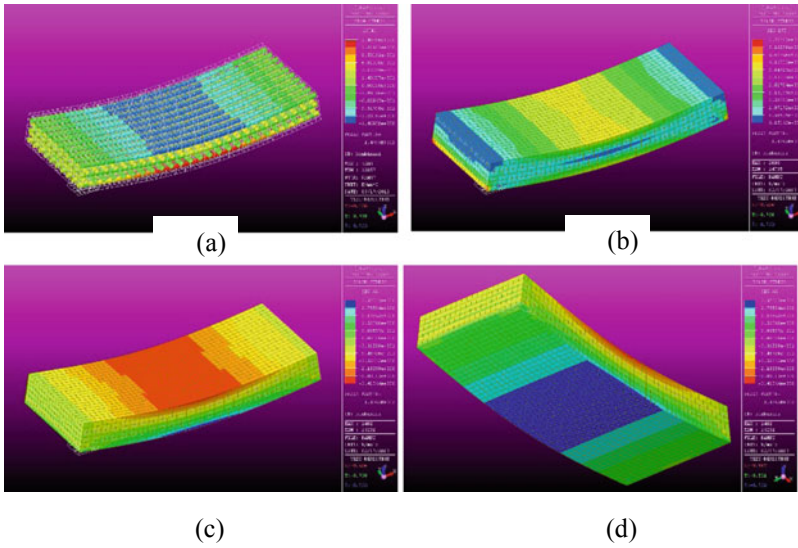
Fig. 29 **a** axial stress σx of bamboo culms. **b** effective stress σx of solid concrete. **c** axial stress σx of concrete (upper bridge). **d** axial stress σx of concrete (bottom bridge)
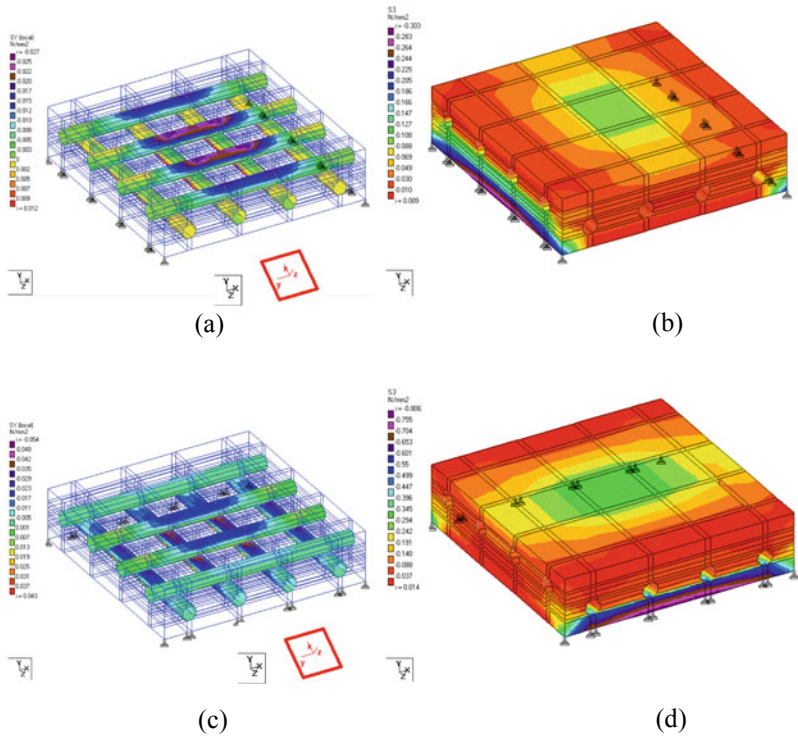
Fig. 30 **a** Stress of bamboo culms on the weak axis. **b** stress of concrete on the weak axis **c** Stress of bamboo culms on the strong axis. **d** stress of concrete on the strong axis.

(a)

(b)

(c)

(d)
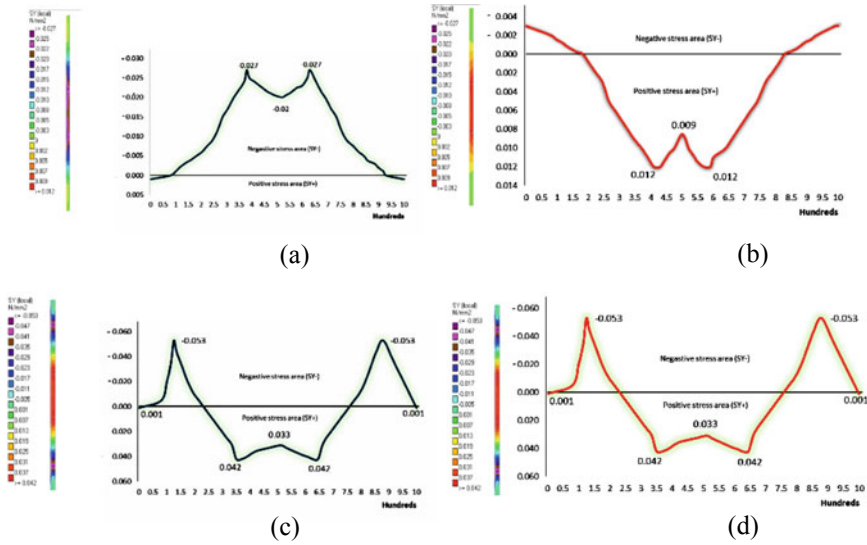
Fig. 31 **a** compressive stress (Sy) of bamboo culms on the weak axis **b** tensile stress (Sy) of bamboo culms on the weak axis. **c** compressive stress (Sy) of bamboo culms on the strong axis. **d** tensile stress (Sy) of bamboo culms on the strong axis.

(a)

(b)
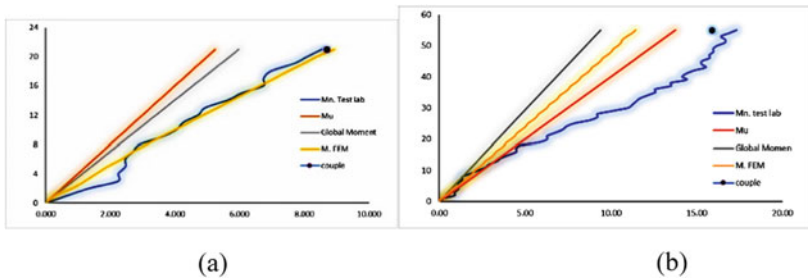
Fig. 32 **a** load versus moment comparison on the weak axis. **b** load versus moment comparison on the strong axis

The maximum stress values obtained is then compared with the moment of the experimental results and manual calculations as shown in Fig. 32.

Figure 32 shows the load versus moment correlation for laboratory testing on software analysis and manual computation.

6   Conclusions

Bamboo slabs on a weak axis restrain a smaller load than conventional slabs, but it has deflection that is 81% smaller than conventional slabs at the equal load of 21 kN. Meanwhile, if tested on a strong axis, bamboo slabs restrain 52% greater load and produce 73% less deflection than conventional slabs. In the other hand Bridges with cross-arranged bamboo composite concrete slab systems called Mulbamcomphol have a good performance in resisting flexural loads in terms of ductility and maximum load that can be carried both visually and in analysis and experimental testing.

Strain tends to be small but increases slightly with the frequency of repetitive loads, but this increase tends to be smaller and asymptotically so that it will have a strain that is not much different and do not fluctuate in service loads. It is estimated that there is a small slip on the concrete-bamboo surface, but the shear connector on the Mulbamcomphol slabs system is sufficient to restrain the larger slips, and The Mulbamcomphol Bridge is easy to implement, inexpensive, does not require highly skilled human resources, and belongs to the category of fast/rapid construction.

References

1. Xiao Y, Inoue M, Paudel SK (2007) Modern bamboo structures. In: First International Conference on Modern Bamboo Structures (ICBS-2007), Changsha, China, October 2007. CRC Press 2008
2. Ahmad M, Kamke FA (2011) Properties of parallel strand lumber from Calcutta bamboo (Dendrocalamus strictus). Wood Sci Technol 45:63–72
3. Li H, Wu G, Xiong Z, Corbi I, Corbi O, Xiong X (2019) Length and orientation direction effect on static bending properties of laminated Moso bamboo. Eur J Wood Wood Prod 77:547–557. https://doi.org/10.1007/s00107-019-01419-6
4. Li H, Wu G, Zhang Q, Deeks AJ, Su J (2017) Ultimate bending capacity evaluation of laminated bamboo lumber beams. Constr Build Mater 160:365–375. https://doi.org/10.1016/j.conbuildmat.2017.11.058
5. Li HT, Chen G, Zhang Q, Ashraf M, Xu B, Li Y (2016) Mechanical properties of laminated bamboo lumber column under radial eccentric compression. Constr Build Mater 121:644–652. https://doi.org/10.1016/j.conbuildmat.2016.06.031
6. Tan C, Li H, Wei D, Lorenzo R, Yuan C (2020) Mechanical performance of parallel bamboo strand lumber columns under axial compression: Experimental and numerical investigation. Constr Build Mater 231. https://doi.org/10.1016/j.conbuildmat.2019.117168
7. Trujillo D, Jangra S, Gibson JM (2017) Flexural properties as a basis for bamboo strength grading. Proc Inst Civ Eng Struct Build 170:284–294. https://doi.org/10.1680/jstbu.16.00084
8. Ghavami K (2004) Bamboo as reinforcement in structural concrete elements. Cem Concr Compos 27:637–649. https://doi.org/10.1016/j.cemconcomp.2004.06.002
9. Klein B (2012). Grundgleichungen der linearen Finite-Element-Methode. FEM, Wiesbaden: Vieweg+Teubner Verlag pp 16–33. https://doi.org/10.1007/978-3-8348-2134-8_3.
10. Moldoveanu SC, David V (2017) RP-HPLC Analytical Columns. Sel. HPLC Method Chem. Anal. Elsevier, p 279–328. https://doi.org/10.1016/b978-0-12-803684-6.00007-x.

11. Ahmad M, Kamke FA (2003) Analysis of Calcutta bamboo for structural composite materials: surface characteristics. Wood Sci Technol 37:233–240. https://doi.org/10.1007/s00226-003-0172-x
12. Mansur A (2006) Analysis of Calcutta Bamboo for Structural Composite Materials. Universiti Teknologi Malaysia 2006
13. Morisco (1999) Rekayasa Bambu, Jakarta: Nafiri Offset
14. Huang D (2004) Structural Behaviour of Two-Way Fibre Reinforced Composite Slabs. University of Southern Queensland

Compressive Strength of Concrete Containing Plastic Waste as Fine Aggregate

Sri Wiwoho Mudjanarko, Nawir Rasidi, and Mohd Haziman Wan Ibrahim

Abstract Plastics and plastic goods are increasing following the development of technology, industry, and population in Indonesia. Plastic has advantages over other materials. It is more robust, lighter, more flexible, anti-rust, sturdier, easy to color and work with. Also, it can act as a heat and electricity insulator. The study uses plastic waste as an additive or component mixing fine aggregate. The research investigates how strong the concrete is due to its compressive strength combined with crushed plastic waste as a substitute for fine aggregate with a variation of 5, 10 and 15%, concerning standard strength concrete of fc 25. From the compressive strength test with design variations, it is found that the compressive strength of regular concrete decreases from 18.68 to 16.44 MPa. While for concrete with a mixture of 5%, the compressive strength drops from 16.54 to 14.56 MPa. Lastly, regular concrete's compressive strength with a mix of 10 and 15% decrease from 14.41 to 12.68 MPa and from 15 to 14.41 MPa, respectively. The results above do not match our expectations. The casting process, the mixing process between the aggregate and the added material, and the concrete topping that does not contain sulfur-like materials can cause the cracks in the concrete uneven's compressive strength.

Keywords HDPE · Garbage · Concrete compressive strength

S. W. Mudjanarko (✉)
Department of Civil Engineering, Narotama University, Surabaya 60117,
East Java, Indonesia
e-mail: sri.wiwoho@narotama.ac.id

N. Rasidi
Department of Civil Engineering, Politeknik Negeri Malang, Malang, East Java, Indonesia

M. H. W. Ibrahim
Faculty of Civil Engineering and Built Environment, Universiti Tun Hussein Onn Malaysia,
Batu Pahat, 86400 Johor Bahru, Malaysia

1   Introduction

Plastic has advantages over other materials. It is more robust, lighter, more flexible, anti-rust, sturdier, easy to color and work with. Also, it can act as a heat and electricity insulator. However, in the end, plastic will become garbage that harms the environment. It is because they do not biodegrade quickly and can reduce soil fertility. On the other hand, plastic waste has been used as a substitution in various constrtion materials in civil engineerings, such as concrete aggregate and highway materials.

As a material, many categories of plastic have been used based on their purposes. One of the plastic variety used in the research is High-density Polyethylene (HDPE). HDPE is a polyethylene thermoplastic processed from crude oil. In pipe production, it is called acanthine or polythene." HDPE is used to produce the plastic bottle, corrosion-resist pipe, geodetics membrane, and plastic wood because of its high-density strength-ratio characteristic. HDPE is recyclable and coded with the number of "2" as its resin identification (Suprayitno et al. 2019).

However, regarding its potentials, HDPE used is still in developing stages that encourage many new types of research within this field and civil engineering studies. Therefore, the research investigates whether the use of HDPE as a concrete mixture will affect essential qualities. The research examines the concrete strength resulted from the variation substitution percentages of recycled HDPE.

2   Literature Review

Concrete is a mixture of some materials. The main component consists of a mix of cement, fine aggregate, coarse aggregate, water, and other added components with a specific ratio. Because concrete is a composite, then the concrete's quality is highly dependent on the quality of each material forming (Tjokrodimulyo 2007).

A concrete mix design with a different composition will produce extra strength. Concrete with an aggregate mixture of processed plastic waste will produce other concrete with different characteristics and strengths. Therefore, the research investigates numbers of recycled HDPE composition variations as a partial replacement of fine aggregate to uphold concrete compressive strength.

2.1   Aggregate

Aggregate is a natural grain mineral that serves as a concrete filler. Ideally, concrete contains approximately 70–80% of aggregates. (Gencel et al. 2010). Moreover, the grain size determines the aggregate type. The biggest aggregate size is the coarse aggregate with a minimum of 4,75–4,80 mm in diameter, while any other type of aggregate smaller than 4,80 mm is named fine aggregate.

2.2 Cement

There are two kinds of cement, hydraulic cement, and non-hydraulic cement. Hydraulic cement is the cement that reacts to water and having characteristics of resistance to water penetration and stability in the water after its hardened process (Nugraha et al. 2007). Moreover, Portland cement is a hydraulic cement formed by producing clinker. Its central element consists of calcium silicates, which are hydraulically cast as the added material.

Based on the intended use of Portland cement in Indonesia, there are five types of Portland cement, as described in Table 1 below.

2.3 Water

Concrete needs water for its chemical process. Water will react to the cement within the concrete mixture for the hardened process. Furthermore, water acts as the adhesive for the grains and cement paste aggregates. The water content also makes concrete paste workable. The needed water in mixing the concrete is often called a cement water factor (FAS).

Water required for cement mixing is only about 25–30% by cement weight; however, it will be challenging to stir if the cement water factor is less than 35%. Yet, the amount of lubricant in the concrete mixture should not be too much; it can affect the concrete strength (Tjokrodimuljo 2007).

2.4 Plastic

Plastic is a polymer that has unique properties and exceptional. The polymer is a substance consisting of molecular units called monomers (Mujiarto 2005).

Table 1 The types of portland cement

Type of cement	General characteristics
Type I	It is for general use, which does not require any special requirement
Type II	It is for sulfate resistance to heat of hydration medium
Type III	It is for high initial strength requirements after bonding
Type IV	It is for a low hydration heat demanded
Type V	It is highly resistant to sulfate

Source: Kardiono 1996

Plastics have a variety of useful properties, including (Azizah 2009):

1. Mild strength.
2. Chemically stable (does not react with air, water, acids, alkalis, and other chemical substances).
3. An excellent electrical insulator.
4. Easy to set up, especially heated.
5. Usually transparent and clear.
6. Flexible / plastic.
7. The price is relatively low.

In general, there are two classifications of plastic, namely thermoplastic and thermoset plastics. Thermoplastic is plastic that can be printed repeatedly, for example, PP (polypropylene), PE, ABS (Acrylonitrile Styrene Butadiene), nylon, PET (Polyethylene Terephthalate), CPM, Polyacetal (POM), PC, etc. Whereas thermosets plastics are plastics, which in certain conditions cannot be reprinted anymore, for example, PU (Poly Urethane), UF (Urea Formaldehyde), MF (Melamine Formaldehyde), polyester, epoxy, etc.

2.5 Compressive Strength

Concrete compressive strength is the ability of solid concrete to endure compressive force in its square unit. Pressure (P) is defined as the force (F) per unit area (A), is expressed by the equation:

$$P = F/A \tag{1}$$

There is a number factor affecting the compressive strength of concrete, namely;

1. Water factor; the lower the water-cement factor (FAS), the higher the concrete's compressive strength. However, if the FAS is too low, it would be hard to compact concrete.
2. Cement density; density of the concrete significantly affects the compressive strength of concrete after hardening.
3. Age of concrete; concrete strength increase with the age of the concrete.
4. The type of cement used in the manufacture of concrete must be fit for purpose and use.
5. The aggregate nature; the aggregate nature that affects concrete strength is the surface hardness and size. The use of grain aggregates that are too large will reduce the concrete's strength so that the granular aggregate's adhesion is less intense.

3　Research Methods

The research uses the experimental method of concrete compressive strength by using the CTM method with a toughness of 2,000 Kn. The study modifies a concrete mixture using plastic bottle waste. The research is divided into stages, namely the preparation of materials, the manufacture of test specimens, maintenance, and testing (Table 2).

4　Process of Substance Test

4.1　Casting

Casting is a process of pouring fresh concrete into a mold of the structural element by variations in the mix of flakes of waste plastics. The process serves to mix all aggregate into a specimen container to obtain forms to suit the wishes. The image below shows the process (Fig. 1).

Table 2 The result of regular concrete material

Name	Volume	Unit
Water	181	kg
Add mixture (Supplement)	51	kg
Cement	287	kg
Coarse aggregates	971	kg
Fine aggregate	710	kg
Total	2,200	kg

Fig. 1 Concrete mixture with plastic material

4.2 Concrete Containing Plastic Waste

The stage comes after the casting stage. Concrete is poured into the specimen tube with variations and the desired size to obtain the expected dimensions (Fig. 2).

4.3 Slump Test

The slump test is an empirical test/method used to determine the consistency/stiffness (workable or not) of the concrete mix (fresh concrete) to assess its workability level (Fig. 3).

Fig. 2 Normal concrete

Fig. 3 Slump test

4.4 Weighing

Before conducting the compressive strength test, it is necessary to weigh the testing material. For relatively small tested material, it can be done using weight measures or devices. Yet, it also can be done by measuring the height and diameter of the object (Fig. 4).

4.5 Concrete Compressive Strength

The tested object is placed vertically on the compression test unit with a 2000 Kn scale of accuracy. The manometer's needles guide of the compressive strength test unit should be at zero. The needle of the manometer will indicate the equivalent working compression force when the test machine starts. When it exceeds the specimen's maximum load capability, the sample will break. The red needle will remain at the maximum load rating, while the black one will move down back at the position (zero) (Fig. 5).

Fig. 4 Weighing

Fig. 5 Concrete compressive strength

4.6   Compressive Strength of Concrete

See Tables 3, 4, 5, 6.

Table 3 The results of normal strength concrete compressive strength

Age Day	Mass off the test object, kg	Dimension		Broad field (mm2)	Compressive force (kN)	Compressive strength (N/mm²)	Crushed voltage (kg/cm²)	Corrected compressive strength (MPa)	Estimate compressive strength (MPa)	Information
		Ø (mm)	H (mm)							
		A	B	C = A × B	D	E = [P*1000C]	F = [E*1009.81]	G = [F × 0.83 × 9.81/100]	H = G0.88	
14	11,918	150	300	17,671	350	19,81	202	16,44	18,68	Normal
14	11,858	150	300	17,671	345	19,52	199	16,20	18,41	Normal

Table 4 The results of compressive strength of normal concrete mix of plastic waste flakes 5%

Age Day	Mass off the test object, kg	Dimension		Broad field (mm2)	Compressive force (kN)	Compressive strength (N/mm²)	Crushed voltage (kg/cm²)	Corrected compressive strength (MPa)	Estimate compressive strength (MPa)	Information
		Ø (mm)	H (mm)							
		A	B	C = A × B	D	E = [P*1000C]	F = [E*1009.81]	G = [F × 0.83 × 9.81/100]	H = G0.88	
14	11,430	150	300	17,671	290	16,41	167	13,62	15,48	5%
14	11,482	150	300	17,671	310	17,54	179	14,56	16,54	5%

Table 5 The results of compressive strength of normal concrete mix flakes of plastic waste 10%

Age Day	Mass off the test object, kg	Dimension Ø (mm)	H (mm)	Broad field (mm2)	Compressive force (kN)	Compressive strength (N/mm²)	Crushed voltage (kg/cm²)	Corrected compressive strength (MPa)	Estimate compressive strength (MPa)	Information
		A	B	$C = (A \times B)$	D	$E = [P*1000C]$	$F = [E*1009.81]$	$G = [F \times 0.83 \times 9.81/100]$	$H = G0.88$	
14	11,613	150	300	17,671	335	18,96	193	15,73	17,88	10%
14	11,594	150	300	17,671	270	15,28	156	12,68	14,41	10%

Table 6 The results of compressive strength of normal concrete mix flakes of plastic waste 15%

Age Day	Mass off the test object, kg	Dimension Ø (mm)	H (mm)	Broad field (mm2)	Compressive force (kN)	Compressive strength (N/mm²)	Crushed voltage (kg/cm²)	Corrected compressive strength (MPa)	Estimate compressive strength (MPa)	Information
		A	B	$C = (A \times B)$	D	$E = [P*1000C]$	$F = [E*1009.81]$	$G = [F \times 0.83 \times 9.81/100]$	$H = G0.88$	
14	11,660	150	300	17,671	270	15,28	156	12,68	14,41	15%
14	11,685	150	300	17,671	285	16,13	164	13,39	15,21	15%

5 Conclusions

The results show variations in the addition of concrete to waste plastic flakes with variations of 0, 5, 10 and 15% of the mass of Portland cement type 1. From the compressive strength test with design variations, it is found that the compressive strength of regular concrete decreases from 18.68 to 16.44 MPa. While for concrete with a mixture of 5%, the compressive strength drops from 16.54 to 14.56 MPa. Lastly, regular concrete's compressive strength with a mix of 10 and 15% decrease from 14.41 to 12.68 MPa and from 14.4 to 12.68 MPa, respectively.

Therefore, it can be concluded the results do not match our expectations. The casting process, the mixing process between the aggregate with the added material, and the concrete topping that does not contain sulfur-like materials can cause the cracks in the concrete uneven's compressive strength. For further research, the required quality of waste and the plastic volume percentage is more suitable for maximum results.

References

Azizah U (2009) Polimer Berdasarkan Sifat Thermalnya. Chem-is-Try.Org. J Int 16(3)

Gencel O et al (2010) Concretes Containing Hematit for Use AS Shielding Barriers

Mujiarto I (2005) Sifat dan Karakteristik Material Plastik dan Bahan Aditif, Staf Pengajar AMNI Semarang

Nugraha P, Antoni (2007) Teknologi Beton. Yogyakarta: Penerbit Andi

Suprayitno SWM, Koepiadi ADL (2019) The study of mineral plastic used HDPE type as asphalts mixture for Asphalt Concrete Wearing Course. Paduraksa Journal, vol 8, no 2

Tjokrodimuljo (2007) Teknologi Beton. Biro penerbit: Yogyakarta

Tjokrodimulyo K (1996) Teknologi Beton, Yogyakarta

Performance of Pre-fabricated Frame Scaffolds Falsework

Balya Mulkan Wijaya Mohammad Yusuf, Ezzarhan Abdullah, and Intan Fadhlina Mohamed

Abstract Scaffolds and falsework have been used widely in building constructions. Their function as supporting structure plays an important role during initial construction of a building. In this paper, some requirements for steel scaffolds and falsework are presented to highlight the factors that influence the performance of both scaffolds and falsework. The leading factors that are discussed in this paper are bracing force, joint, fittings, loading condition and structural element. Emphasis is given to the use of falsework according to the standards in some countries. Performance test conducted on 3×3 bay frame scaffolds falsework system in a local engineering lab was discussed. The result shows that the bracing and joint has significant effect on scaffolds falsework capacity. In addition, this paper presented few case studies and ability of finite element models that showing the significant of joint failure in the use of scaffolds.

1 Introduction

The impact of building industry is indisputable to the economic sector of a country [9]. However, according to occupational health and safety data in Malaysia, this industry is among major contribution of high accident rates. Most of the total fatal accidents in Malaysia takes place in this construction industry. Thus, this confirms on how important it is to concern and improve the safety conditions of height-related temporary work structures used in construction sites.

B. M. W. M. Yusuf (✉) · E. Abdullah
Forensic Engineering Division, Department of Occupational Safety and Health,
Ministry of Human Resource, 62530 Putrajaya, Malaysia
e-mail: balya@mohr.gov.my

I. F. Mohamed
Department of Mechanical and Manufacturing Engineering, Faculty of Engineering and Built
Environment, Universiti Kebangsaan Malaysia (UKM), 43600 Bangi, Selangor, Malaysia

Scaffolds and falsework are among temporary work structures that have been used widely in building constructions. Their function as supporting structure plays and important role during initial construction of a building. Scaffolding and falsework are two different things. Scaffolding is a system for access working platform while falsework is a system for structural support. Falsework is a temporary structure used to support permanent structure so as it remains in place until it is strong enough to become self-supporting. Both systems require different requirements from different standard and regulations. Although their usage is only in short term during construction period, however their function is important as permanent structure and can cause catastrophic collapse if they're not properly managed. In fact, scaffold component can be used for both scaffolding and falsework system. An example of the use of pre-fabricated frame scaffold component in a falsework is shown in Fig. 1 where a falsework consists of scaffold and steel hollow section supporting a timber formwork.

Frame scaffolds falsework system is used to support heavy dead and live loads typically during the construction of building structures. As well as the requirement for vertical support, these scaffolds falsework system also require lateral support in the form of diagonal bracing. These diagonal braces maintain the stability of the system and reduce the effective length of the vertical standards [11]. As for vertical member, the common method for connecting the columns or normally called standards, is using a joint pin. The joint pin consists of smaller diameter tube which slide into the larger diameter tube to provide a safe connection under gravity load [11]. General concept of bracing and joint, considerations that need to be given into account in the design and the elements that influence the capacity of the falsework will be presented herein.

There are many code standards that can be referred, in the United Kingdom the standards used for construction of falsework is British Standard [4]. Scopes covered
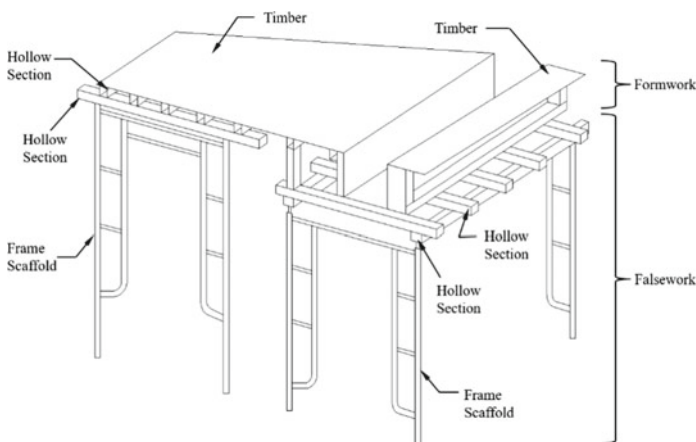

Fig. 1 Frame scaffolds falsework

in the standards are design, specification, construction, the use and dismantling of falsework. Other notable standards are American Concrete Institute [2] and Australian Standard [3]. In Malaysia, requirements for falsework mentioned in Factory and Machinery (Building Operations and Works of Engineering Construction) (Safety) Regulations (BOWEC) [8] and as for pre-fabricated scaffold components, the reference is Malaysia Standard [14]. Although the scope standard is only for scaffolding erected as access working platform, the specifications of pre-fabricated scaffold component is based on this standard. Guidelines for false-work has been drafted by a committee set up under Department of Occupational Safety and Health.

2   Design Standards and Regulations

Regulation 30(1), BOWEC [8] requires horizontal and diagonal bracing shall be provided in both longitudinal and transverse directions, as may be necessary to provide structural stability. Shores shall be properly seated top and bottom, and shall be secured in place. It means falsework used for structural support must be equipped with necessary components to ensure their stability.

Clause 19.2.9.2, [4] mentioned, within falsework structures the effective lengths of members, as struts, may be reduced by introducing points of restraint within the length of the strut. A point of restraint will normally be achieved where there is lacing or bracing in two directions to that point, usually called a node point. Each level of lacing and associated diagonal bracing should be capable of resisting a notional force, denoted by NH, of 2.5% of the vertical load in the strut(s).

[3] requires that each restraining element be designed to transfer a transverse load equal to the sum of 0.025 times the axial force in the compression member at the location of the restraint, and an additional load equal to half that value for each additional compression member being restrained, up to a maximum of seven members (shores).

[2] simply requires that formwork be designed to transfer all horizontal loads to the ground and to complete construction in such a manner as to ensure safety at all times. The standard requires that diagonal bracing be provided in vertical and horizontal planes, where required, to resist lateral loads and to prevent instability of individual members.

3   Calculation of Bracing Force

[4] mentioned to ensure the lateral stability of general falsework structures, including beam grillages, they should be designed to be able to resist, at each phase of construction, the applied vertical loads (W) and a horizontal disturbing force F_H which is the greater of:

Fig. 2 Bracing force
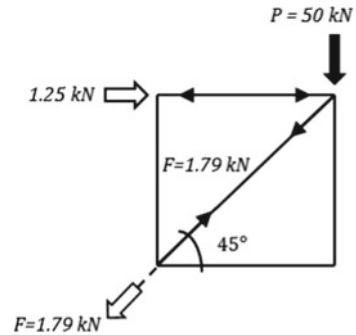
a) 2.5% of the applied vertical loads (i.e. 2.5% W) considered as acting at the points of contact between the vertical loads and the supporting falsework; or
b) The forces that can result from erection tolerances (normally taken as 1% of the applied vertical load (i.e. 1% W) plus the sum of other imposed loads, including wind, out of vertical by design, concrete pressures, water and waves, dynamic and impact forces, and the forces generated by the permanent works.

Lateral load will be considered based on vertical load value and for that case, value 2.5% in option (a) will be used in the calculation.

Diagonal member forces can be calculated when the force from supported structure acts on the same axis of the standard. Considering lateral force is 2.5% of the vertical force, if P is the vertical force acting on the scaffold falsework, the bracing force F is (P/40) sec α where α is the angle of the diagonal member. If the diagonal member is assembled at an angle of $\alpha = 45°$, F is P/28. For example, for a vertical load of 50 kN, the lateral load is 1.25 kN and the required bracing force is $50/28 = 1.79$ kN as shown in Fig. 2 [11]. In condition, diagonal member must be connected rigidly with standard and ledger.

4   Joint

Joint between the scaffold standards is important in determining the capacity of the scaffold falsework since the scaffold component is connected vertically to several units to reach required height and the most common method used for connecting the pre-fabricated scaffold component is to use a joint pin or sometimes called spigot joint. The 2D sketches and component descriptions of the scaffold supporting the mold box are as shown in Fig. 3. The mounting support starts at the top and ends at the bottom using the top jack (U-head) and bottom jack (jack base). The extension of these two components can be adjusted depending on the height of the mold box from the surface level.

A model of a scaffold vertical member is shown in Fig. 3 of particular importance are the top and bottom sections (called "top jack" and "base jack"). These
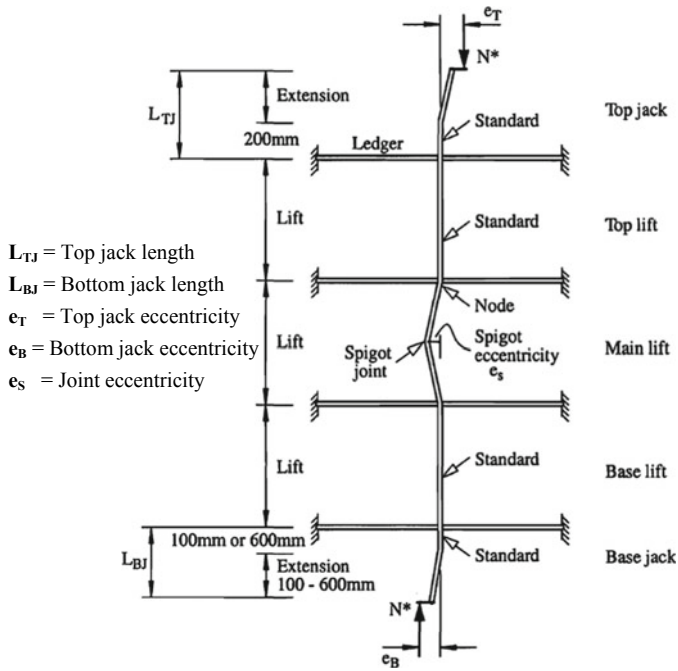
Fig. 3 Model of vertical member [12]

sections are variable in length depending upon the unevenness of the ground on which the structure sits and the variable height of the timber formwork at the top. They are also loaded eccentrically at the top depending upon the arrangement of the timber formwork support. They are often loaded eccentrically at the bottom depending upon the base plate and its location on ground [11]. Other connection is joint pin connecting between the standards.

Connection using joint pin is a moveable point due to the difference between pin and standard diameter. On manufacturing point, there are tolerances in fabricating scaffold components, so there is a small gap between joint pin and standard that used either for scaffolding or falsework. It is believed that the lateral displacement which is a result of this could have a significant effect on the strength and stability of a frame incorporating joints. Specifically, the difference between the outside diameter of the joint pin and the inside diameter of the standards allows some horizontal movement in the joint, which translates into an eccentricity in the vertical standards [12]. The nature of the joint pin is such that all axial load is transmitted through the standards and not the pin. This means that, in theory, the pins do not carry any load under normal service conditions. This is achieved by ensuring that the holes for the pins are large enough so that at no stage does the loading cause the pins to bear on any of the elements. Instead, axial load is transmitted by the upper standard bearing directly on the lower standard.

According to a study by John et al. [12], taking the joint out of a standard increases the load capacity by 3.13%, with no significant change in deflections. The joint was known to cause failure in eight of fifteen (62%) full scale tests performed at the University of Sydney, Centre for Advanced Structural Engineering [5].

5 Finite Element Analysis

Analysis was carried out by James et al. [11] using finite element method with Strand7 software (2009) to see the significance of joint in scaffold system. Figure 4 gives a good visual representation of failure occurring at the joint. In (a), it is evident that failure occurs in one plane at the joints in the top lift of the system. In (b), the extra capacity that the system has available being joint-less is utilized and an extra 8 kN of ultimate strength is achieved. In this case the vertical standard can cope with the higher load, it is the large 600 mm jack extension that initiates and causes failure of the system.

6 Case Study

Case study 1 by Radin and Balya [15]: Falsework collapsed during a concrete casting work at the construction site in Petaling Jaya, Selangor. The erection consists of prefabricated steel frame scaffold components and steel hollow sections supporting timber made formwork. Dimension of scaffold components in average is
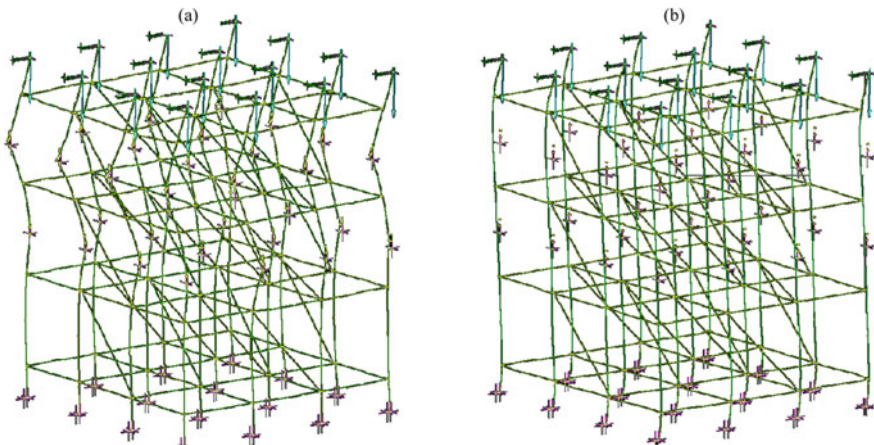

Fig. 4 Buckling failure mode for 2.0 m lift 600 mm extension, 3×3 bay system with **a** with joint **b** without joint

1700 mm (height) × 1219 mm (width), 42.2 mm (diameter) and 2.19 mm (thickness). Falsework erected with 3 lift vertically with extension of 600 mm adjustable plate and U-head fitting 6.4 m floor to floor height. Cross brace used as bracing member and tubular pipe assembled acting as horizontal tie. Other permanent structure ties not found. The fame scaffold falsework was designed to support 67.24 kN per frame, equivalent to 33.62 kN or 3.362 tonne load per standard. The structure collapsed when they pouring 92 m^3 out of 103 m^3 (intended) fresh concrete. It means the scaffold falsework have not carrying full load yet before they collapsed.

Case study 2 by Ezzarhan and Balya [7]: Falsework collapsed at the construction site in Putra Height, Selangor. Dimension of scaffold components in is 1700 mm (height) × 1219 mm (width), 42.2 mm (diameter) and 2.19 mm (thickness). Falsework erected with 4 lift vertically with extension of 300 mm adjustable plate and U-head fitting 7.5 m floor to floor height. Cross brace used as bracing member and tubular pipe assembled acting as horizontal tie. Other permanent structure ties not found. The fame scaffold falsework was designed to support 11 kN per frame, equivalent to 5.5 kN or 0.55 tonne load per standard. Contractor was planning to pour 120 m^3 fresh concrete and collapsed happened when concreting is almost 90% completed.

Case study 3 by Abdul and Balya [1]: Falsework collapsed at the construction site in Kuala Lumpur. Dimension of scaffold components in is 1700 mm (height) × 1219 mm (width), 42.22 mm (diameter) and 1.6 mm (thickness). Falsework erected with 4 lift vertically with extension of 300 mm adjustable plate and U-head fitting 9.2 m floor to floor height. Cross brace used as bracing member and tubular pipe assembled acting as horizontal tie. Other permanent structure ties not found. The fame scaffold falsework was designed to support 11 kN per frame, equivalent to 7.5 kN or 0.75 tonne load per standard. Contractor was planning to pour 20 m^3 fresh concrete and collapsed happened when concreting is almost 15 m^3 or 75% completed (Fig. 5).

Fig. 5 Frame scaffold erection **a** Case 1 [15] **b** Case 2 [7] **c** Case 3 [1]

7 Performance Test of Frame Scaffolds Falsework

Background

Steel frame scaffolds falsework system performance test have been conducted in the Construction Research Institute of Malaysia (CREAM). The tests were conducted on two frame scaffolds samples from construction site. Method of testing is according to MS 1462–1 [14], where three bay by three lift scaffolding was erected. Additional tubular bracings and wall ties were provided to ensure that the loading jack and frame scaffolds remained at their position during load increment. There were six points for deflection gauge to measure displacement in direction of transverse (X-dir), longitudinal (Y-dir) and vertical (Z-dir). Load is applied to all frame scaffold standards, with reduction due to position, to simulate the behavior of falsework during carrying the loads.

Dimension

Samples for dimension test were randomly selected in accordance with ISO 2859–1 [10] Table 2-A – Single Sampling Plan for normal inspection. Three (3) readings were recorded and average value was reported. The dimensional tolerance for frame scaffolding is given in Table 1 and 2 of MS 1462–1 [14]. There are few dimension that is out of tolerance as shown in Tables 1 and 2.

Table 1 Dimension scaffold sample 1

Tubular	Average height (mm)	Average width (mm)	Average outer diameter (mm)	Average thickness (mm)	Tolerance (mm)			
					Height	Width	Outer diameter	Thickness
Frame_1	1700	1220	42.44	2.63	0	+1	−0.26	+0.13
Frame_2	1699	1219	42.23	2.50	−1	0	−0.47	0.00
Frame_3	1700	1219	42.32	2.77	0	0	−0.38	+0.27
Frame_4	1700	1218	42.30	2.54	0	−1	−0.40	+0.04

Table 2 Dimension scaffold sample 2

Tubular	Average height (mm)	Average width (mm)	Average outer diameter (mm)	Average thickness (mm)	Tolerance (mm)			
					Height	Width	Outer diameter	Thickness
Frame_1	1700	1220	42.18	2.49	0	+1	−0.52	−0.01
Frame_2	1700	1219	42.30	2.61	0	0	−0.40	+0.11
Frame_3	1699	1219	42.38	2.53	−1	0	−0.32	+0.03
Frame_4	1699	1218	42.41	2.57	−1	−1	−0.29	+0.07

Load Test

The setup based on MS 1462–1 [14] method consists of one (1) number of Hydraulic Loading Jack 300 kN, One (1) number of Load Cell 500 kN, four (4) numbers of Linear Variable Displacement Transducer (LVDT) 100 mm, two (2) numbers of Linear Variable Displacement Transducer (LVDT) 50 mm, one (1) number of Data Logger. Four (4) numbers of tubular pipe were tied from joints to adjacent RC wall and six (6) numbers of tubular pipes were assembled at middle lift of scaffolds erection acting as diagonal bracing. One (1) tubular pipe tied horizontally at the bottom (Figs. 6 and 7).
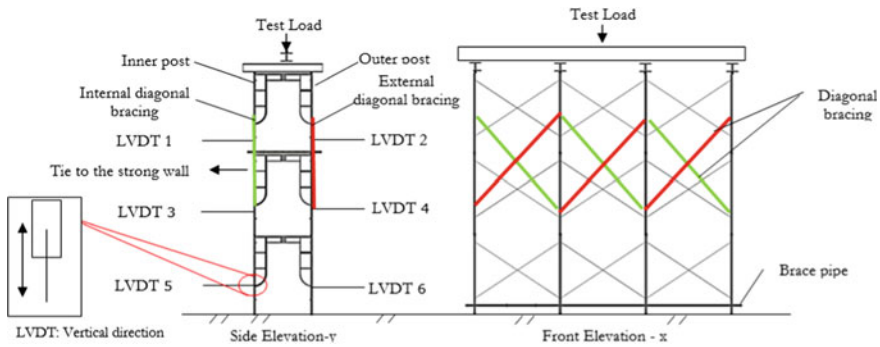

Fig. 6 Test setup for load test on a 3-bay × 3 lift steel frame scaffolds falsework

Ultimate load test was carried out on both samples. The ultimate load is when excessive buckling observed and tubular wall tie fitting starts to break. The ultimate load for sample for sample 1 is 250 kN and for sample 2 is 249 kN, converting capacity per individual frame is 75 and 74.7 kN, distributed to each standard 37.5 and 37.35 kN (Figs. 8 and 9, Tables 3 and 4).

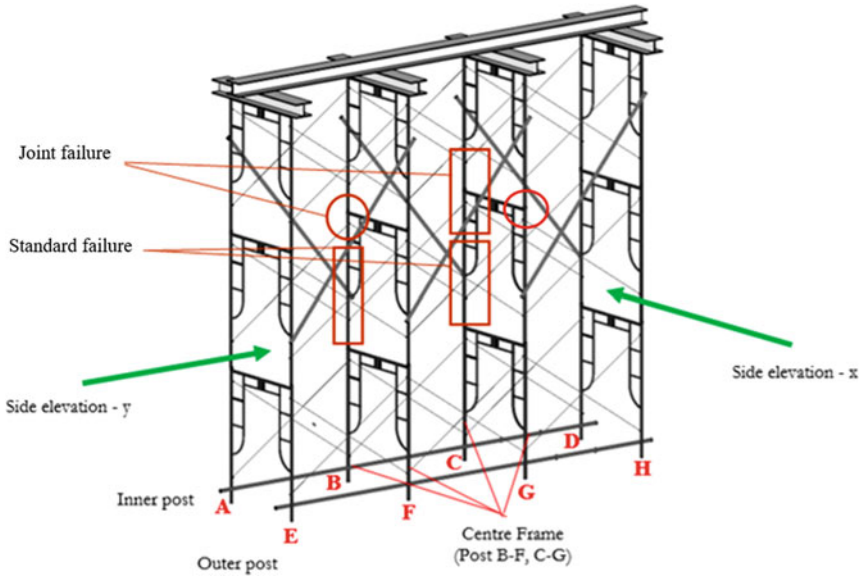**Fig. 7** Frame scaffold erection on test equipment

Fig. 8 Location of failure combine for both samples

Falsework Sample 1

(a)

Falsework Sample 2

(b)
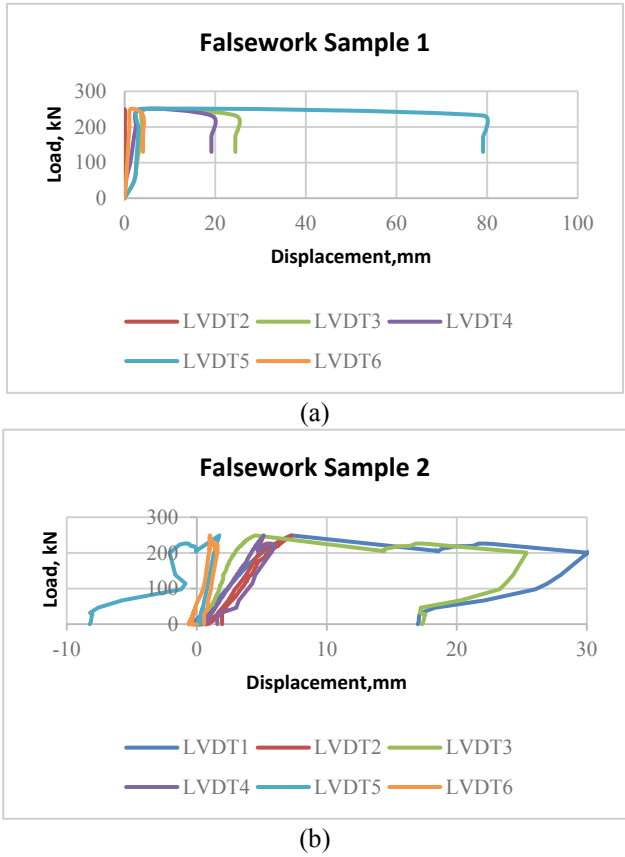
Fig. 9 Load (kN) vs displacement (mm) **a** Sample 1 **b** Sample 2

Table 3 Deflection after ultimate load **a** Sample 1 **b** Sample 2

(a)			(b)		
Max Load (kN)	Displacement transducer	Maximum Deflection (mm)	Max Load (kN)	Displacement transducer	Maximum Deflection (mm)
250	LVDT1	0.00	250	LVDT1	7.3
250	LVDT2	0.00	250	LVDT2	7.3
250	LVDT3	24.44	250	LVDT3	4.52
250	LVDT4	19.14	250	LVDT4	5.14
250	LVDT5	79.11	250	LVDT5	1.73
250	LVDT6	4.07	250	LVDT6	1.01

Table 4 Test result summary

	Sample 1		Sample 2	
Max load (kN)	250		249	
Distributed load to each frame (kN)	Centre frame	Side frame	Centre frame	Side frame
	75	50	74.7	49.8
Distributed load to each standard (kN)	37.5	25.0	37.35	24.9
Maximum post deflection (mm)	76 (Post B, x – elevation)	18 (Post D, y – elevation)	19 (Post G, x – elevation)	18 (Post H, y – elevation)

8   Conclusions

Basic considerations for design of steel frame scaffold falsework and test on frame scaffolds have been presented. Test load was distributed using single beam and every standard received different percentage of load. The maximum deflection of sample 1 is at inner frame at x–direction, while sample 2 was occurred at inner frame y–direction. It should be noted that for both center frame, the failure occurs when the load applied exceed the design load for three collapsed cases. It is believed because of wall tie and diagonal member increased the capacity due to the stiffness of the joints and bracing members. It is recommended that all party in construction industry whether clients, designers or contractors to consider this factors during design and construction.

References

1. Abdul HI, Balya MWMY (2017) Laporan Kejuruteraan Forensik Kes Runtuhan Penyangga Sementara di Kuala Lumpur
2. American Concrete Institute (2004) Guide to formwork for concrete (ACI347)
3. Australian Standard (2018) Concrete formwork specifications (AS3610)
4. British Standard (2019) Code of practice for temporary works procedures and the permissible stress design of falsework (BS 5975)
5. CASE (2006) Tests of formwork subassemblies and components. Investigation Report No. S1499. Centre for Advanced Structural Engineering, School of Civil Engineering, University of Sydney
6. Construction Research Institute of Malaysia (CREAM) - Test on Steel Frame Scaffolding Report
7. Ezzarhan A, Balya MWMY (2015) Laporan Kejuruteraan Forensik Kes Runtuhan Penyangga Sementara di Selangor
8. Factory and Machinery Act (1986) Building Operations and Works of Engineering Construction (Safety) Regulations (BOWEC)
9. Gyi DE, Gibb AGF, Haslam RA (1999) The quality of accident and health data in the construction industry: interviews with senior managers. Construct Manage Econom 17:197–204

10. International Organization for Standardization (1999) Sampling procedures for inspection by attributes-Part 1: Sampling schemes indexed by acceptance quality limit (AQL) for lot-by-lot inspection (ISO 2859–1)
11. James R, Kim Jr R, Hao Z (2013) Optimisation of Scaffolding Systems, Research Report R942
12. John E, Robert H, Gregory JH (2000) Structural stability of braced scaffolding and formwork with spigot joints
13. Osman MH et al (1998) Design and performance of tubular steel scaffold. Journal of Civil Engineering, vol 11, no 1
14. Malaysian Standard (2012) Prefabricated scaffolds - Specification for steel frame scaffolding (MS 1462 – 1)
15. Radin HRH, Balya MWMY (2016) Laporan Kejuruteraan Forensik Kes Runtuhan Penyangga Sementara di Selangor

Comparison Between Predicted and Experimental Strength for Concrete via Compression and Non-destructive Method

Mustaqqim Abdul Rahim, Lee Choon Onn, Adib Fikri Abdul Manaf, Shahiron Shahidan, Sharifah Salwa Mohd Zuki, Mohamad Azim Mohammad Azmi, and Nor Hazurina Othman

Abstract Rebound hammer and ultrasonic pulse velocity are preferred as non-destructive testing methods whereas compression test is a type of destructive test. A general series of rebound hammer, ultrasonic pulse velocity and compression tests were carried out at a heavy concrete laboratory to obtain the necessary parameters and to develop correlation and calibration between the tests. A set of 36 concrete cubes measuring $100 \times 100 \times 100$ mm were cast and subjected to water curing for periods lasting 7, 14, 21 and 28 days to obtain cube strength, rebound number, pulse velocity and pulse wave transmission period. Ultrasonic pulse velocity and rebound hammer tests were initially done before the compression test. The results showed that the differences between predicted strength and experimental strength (compression test) were 1.6 and 6.38% for the rebound hammer test and the ultrasonic pulse velocity test, respectively. This indicated that rebound hammer testing managed to predict strength more accurately compared to ultrasonic pulse velocity testing. Both non-destructive tests showed a margin of less than 10% error compared to destructive tests.

Keywords Rebound Hammer · Ultrasonic pulse velocity · Strength prediction · Experimental strength

M. A. Rahim (✉)
School of Environmental Engineering, University Malaysia Perlis, 02600 Arau, Perlis, Malaysia
e-mail: mustaqqim@unimap.edu.my

L. C. Onn
Poh Cheong (Malaysia) Sdn Bhd, Lot 1250/1251 Jalan Seelong, 81400 Mukim Senai, Johor, Malaysia

A. F. A. Manaf · S. Shahidan · S. S. M. Zuki · N. H. Othman
Faculty of Civil Engineering and Built Enviroment, Universiti Tun Hussein Onn, Batu Pahat, 86400 Parit Raja, Johor, Malaysia

M. A. M. Azmi
Departments of Civil Engineering, Center for Diploma Studies, Universiti Tun Hussein Onn Malaysia, Education Hub Pagoh, 84600 Muar, Johor, Malaysia

1   Introduction

It is important to test concrete structures after concrete has solidified to determine whether a particular structure is in the desired condition and suitable for its purpose without interrupting its properties. There are quite a number of parameters that can be determined by non-destructive tests such as density, modulus of elasticity, strength, surface hardness and surface absorption as well as reinforcement location, size and distance from the surface. At the same time, non-destructive tests are also used for maintenance work on existing building structures such as void detection, cracking and delamination [1].

Rebound hammer testing is an inexpensive method that can be used to determine the properties of concrete. It does not require any current but instead utilises springs to gain rebound energy. In addition, a rebound hammer can be reused, hence incurring low maintenance costs [2]. When the plunger of a rebound hammer is pressed to the top of a concrete surface, a spring-controlled mass with constant energy is made to hit the concrete surface and rebound. The distance of rebound for measuring the surface hardness is carried out using a graduated scale. The test surface can be horizontal or vertical but the instrument must be calibrated in a fixed position before the test begins. The value obtained from the graduated scale is known as a Rebound Number (rebound index). Several readings are required to ensure the accuracy of the rebound hammer and compressive strength values. Concrete with higher strength and stiffness will absorb less energy which results in a higher rebound value [2]. Meanwhile, the ultrasonic pulse velocity method involves longitudinal ultrasonic waves converted by mechanical energy passing through a concrete structure. The ultrasonic wave generated by a transducer penetrates through the concrete structure on one end of its surface. The wave then travels through the concrete structure and is converted to electrical signals received by another transducer on the opposite surface [3]. There are plenty of functions for ultrasonic wave velocity on concrete structures such as strength testing, homogeneity, trapped air, internal flaws, cracks, segregation, honeycombing, compaction, workmanship, durability and so on [4]. A compression test is categorised as a destructive test in accordance with BS EN 12390-3:200 [5]. A non-stop compressive load is usually applied to the specimen until the ultimate capacity is reached. The aim of this research is to develop the relationship between non-destructive and destructive tests on concrete.

2   Materials and Methods

2.1   Preparation of Materials

Concrete mixing is a process where Ordinary Portland cement (OPC), aggregate, sand (fine aggregate) and water are mixed uniformly and hardened to become

concrete. Design grade concrete, namely M20, M25 and M30 were used in this research. According to JKR 20,800 Standard Specification for Building Works (JKR Standards [6]), grade M20, M25 and M30 concrete mixes require a cement, sand and aggregate ratio of 1:2:4, 1:1:5 and 1:1:2, respectively. Overall, 3 sets of 12 concrete test cubes were cast and used for the tests. Cube moulds measuring $100 \times 100 \times 100$ mm were used to cast the specimens according to BS EN 12390-1:200 [7] (Fig. 1).

According to BS EN 1881: Part 203 [8], a flat ground location is recommended to ensure that the rebound hammer equipment is not positioned at an inclined angle. From Fig. 2, the plunger of the rebound hammer was pressed onto the surface center of the concrete cube specimens and held vertically downward at a right angle to the concrete specimens. Figure 5 shows the application of the rebound hammer at the centre of the concrete cube surface.

The ultrasonic pulse velocity method involves propagating ultrasonic waves generated through electric current in concrete and measuring the time taken for waves to propagate from one point to another. This method was conducted in accordance with BS EN 12504-4:2004 [9]. The equipment or generator of pulse waves called PUNDIT Lab consists of 2 transducers for wave transmission and reception purposes (Fig. 3).
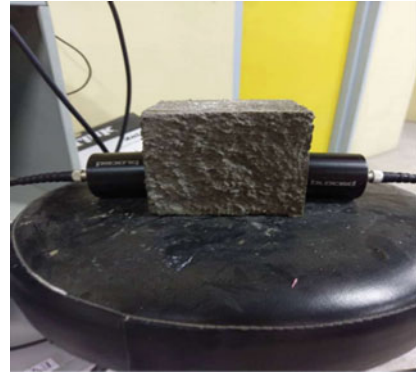

(a)   (b)

Fig. 1 Concrete specimen: **a** Cube specimen, **b** Curing process

Fig. 2 Rebound hammer on concrete surface

Fig. 3 Direct method of
ultrasonic pulse velocity

3 Results and Discussions

From Fig. 4, higher initial experimental strength compared to the other two
non-destructive tests can be observed. Afterwards, the lowest readings of experi-
mental strength were recorded after a curing period of 14 and 21 days. The highest
experimental strength was finally obtained after a curing period of 28 days.

From Fig. 5, only a small difference between the experimental strength and
predicted strength was observed. The experimental strength and predicted strength
were very close and concentrated. This indicates that the prediction of compressive
strength from non-destructive testing is very accurate and close to the actual
compressive strength prediction via destructive tests.

From Fig. 6, the results after a curing period of 7 and 14 days were unstable and
not concentrated. The lowest experimental strength was recorded on the initial day
of curing while the highest was recorded on day 14. After 14 days of curing, a
stable and concentrated relationship between experimental strength and predicted
strength was obtained.

From Table 1, the overall variation between experimental strength and predicted
strength of the rebound hammer test lies in the range of −4.5 to 8.2%, with an
average value of 1.6%. Meanwhile, the overall variation between experimental
strength and predicted strength of the ultrasonic pulse velocity test lies in the range
of 4.62 to 7.29%, with an average value of 6.38%. Finally, the overall difference
between experimental strength and predicted strength through the ultrasonic pulse
velocity test lies in the range of 4.2to 7.87%, with an average value of 6.62%. To
sum up, the relationship between non-destructive and non-destructive tests of
concrete can be developed through correlation between actual compressive strength
of concrete test specimens with different concrete mix designs and curing periods.
Actual compressive strength can be obtained from compression tests whereas the
predicted strength can be obtained from rebound hammer and ultrasonic pulse
velocity tests. From the results, both non-destructive tests show a margin of less
than 10% error compared to the destructive test. Thus, non-destructive tests are
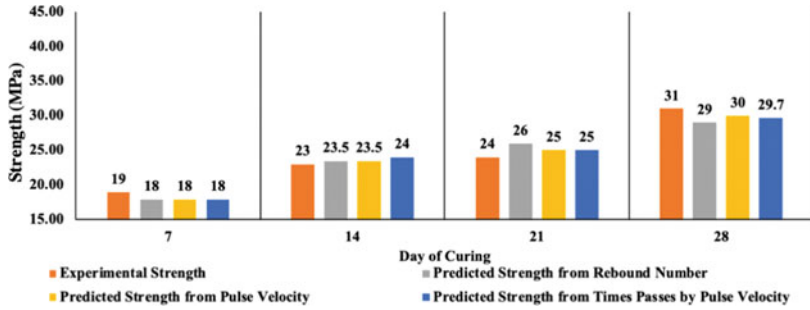
Fig. 4 The comparison between the predicted strength and experimental strength of grade M20 test specimens against day of curing
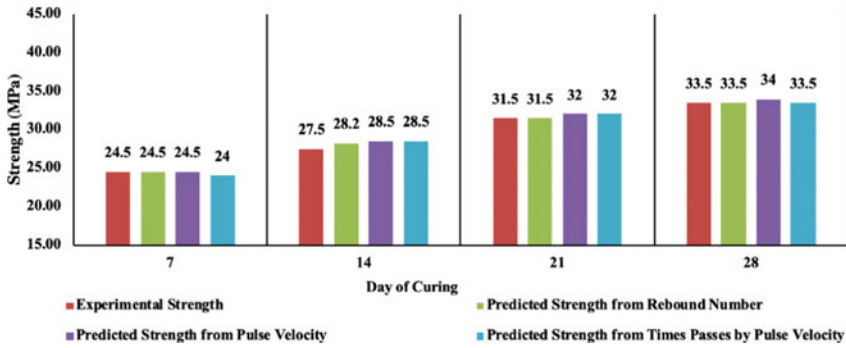

Fig. 5 The comparison between the predicted strength and experimental strength of grade M25 test specimens against day of curing
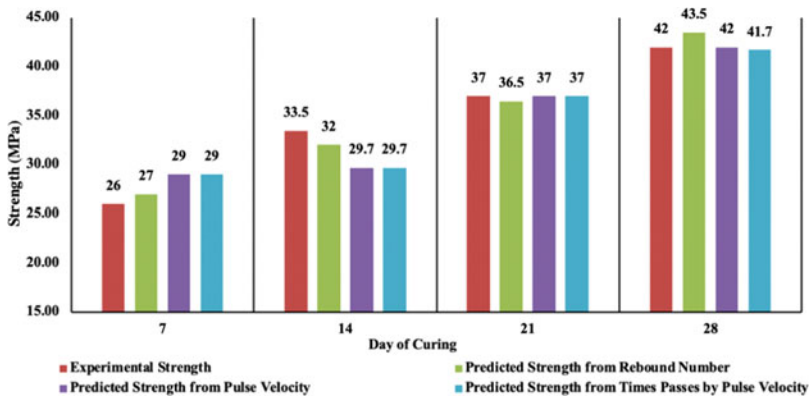

Fig. 6 The comparison between the predicted strength and experimental strength of grade M30 test specimens against day of curing

Table 1 The variation and average between experimental strength and predicted strength of concrete

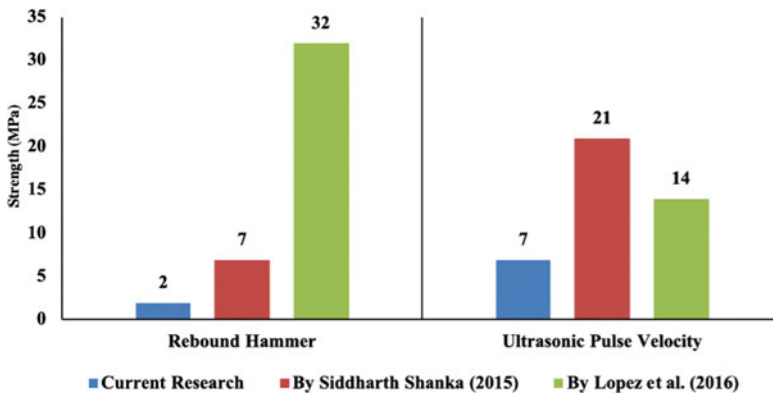| Grade of test specimens	Overall variation between experimental strength and predicted strength by rebound hammer (%)	Overall variation between experimental strength and predicted strength by using pulse velocity (%)	Overall variation between experimental strength and predicted strength by using time passes through the specimens (%)
M20	8.20	7.22	7.8
M25	1.10	4.62	4.20
M30	-4.50	7.29	7.87
Average	1.6	6.38	6.62

Fig. 7 The comparison between the predicted strength and experimental strength of grade M30 test specimens against day of curing

more suitable for predicting concrete strength as it does not affect the arrangement of inner particles and the life span of concrete.

In Fig. 7, it can be seen that this study obtained a lower average variation between experimental strength and predicted strength compared to two other studies. The regression equation developed by Siddharth and Joshi [10] was found to be acceptable and was integrated into this research for both non-destructive methods. The regression equation for the rebound hammer test developed by Lopez et al. [11] was less appropriate for this research. This may be due to several

conditions, such as different practice codes, limited applications of the regression equation and strength or type of trendline during the development of the regression equation.

4   Conclusion

From the results, it is evident that the higher the rebound number, the higher the predicted strength. For the ultrasonic pulse velocity test, a direct method was applied to obtain 2 parameters namely, pulse velocity and pulse wave transmission period through the test specimens. Correlation graphs were plotted to obtain predicted concrete strength. Unlike the rebound hammer test, a positive linear correlation graph was obtained for the pulse velocity test whereas a negative linear was obtained for pulse wave transmission period. The exponential form for ultrasonic pulse velocity was found to be unsuitable since the coefficient of determination for both parameters was less than 50%. This indicates that the predicted strength was inaccurate. Meanwhile, the linear form for ultrasonic pulse velocity showed a relatively high coefficient of determination and was thus chosen to deduce the predicted strength of concrete.

From the ultrasonic pulse velocity test results, it can be concluded that the higher the pulse velocity, the higher the predicted strength. This is because the shorter the time needed for a pulse to be transmitted to a receiving transducer, the denser a material is, thus indicating that the material possesses high strength. The relationship of pulse velocity and time passes by pulse wave was inversely proportional. When the results of the rebound hammer test and the ultrasonic pulse velocity test were compared, it was found that the rebound hammer test has a higher coefficient of determination than the ultrasonic pulse velocity test. This suggests that the rebound hammer test shows greater accuracy for predicting concrete strength.

References

1. Suryakanta (2015). What is the importance of non-destructive testing of concrete structures. civilblog.org
2. Gopal Mishra (2017). Non-Destructive Testing of Concrete and its Method. The Constructor Civil Engineering Home.
3. Chai Peng How (2015). Ultrasonic pulse velocity (UPV) test on concrete under compression. A study on effect of aspect ratio' FYP from Faculty of Engineering, UniMAS
4. Helal P, Mendis MS (2015) Non-destructive testing of concrete: a review of methods. Special Issue: Electron J Struct Eng 14(1):2015

5. BS EN 12390-3 (2002) Testing Hardened Concrete—Part 3: Compressive Strength of Test Specimens
6. JKR Standard. Proportions and strength requirements for prescribed mixes by volume batching. Standard Specifications for Building Works 2005.
7. BS EN 12390-1 (2000) British Standard for Testing Hardened Concrete—Part 1: Shape. Dimensions and Other Requirements for Specimens and Moulds, BSI, London
8. BS EN 1881: Part 203 (1986) Testing Hardened Concrete: Recommendations for Surface Hardness Testing by Rebound Hammer.
9. BS EN 12504-4 (2004) Testing Harden Concrete: Determination of Ultrasonic Pulse Velocity.
10. Siddharth S, Joshi H (2015) Comparison of Concrete Properties determined by Destructive and Non-Destructive Tests. J Inst Eng **10**(1):130–139
11. Abdullah N, Yahaya MP, Hudi NS (2008) Implementation and Use of Lightning Detection Network in Malaysia. In: Power and Energy, pp 383–386
12. Lopez YD, Vanalli L, Ferrari VJ (2016) Concrete compressive strength estimation by means of nondestructive testing: a case study. Open J. Civil Eng. 6:503–515

Properties of Concrete Containing Recycled Polyethylene Terephthalate (PET) Fibre

Adib Fikri Abdul Manaf, Shahiron Shahidan, Shamrul-Mar Shamsuddin, Najamuddin Falakh Sharif, Sharifah Salwa Mohd Zuki, Siti Radziah Abdullah, Faisal Sheikh Khalid, and Mohamad Azim Mohammad Azmi

Abstract As Malaysia's population increases rapidly, so has the demand for different types of materials. There are several types of fibres which can cause serious environmental problems. Many methods for improving the quality of concrete make use of waste materials produced by different industries. Concrete mixes containing fibres normally demonstrate better performance compared to standard concrete because of the positive sewing effect that fibres have on concrete crack. The main objectives of this study are to determine the compressive and splitting tensile strength of concrete specimens containing different percentages of recycled plastic bottle fibre (PET) (0, 0.5, 1.0, 1.5 and 2.0%.) and to evaluate the optimum percentage of PET fibres in concrete. The tests conducted to obtain the workability and strength of concrete included slump tests, compression tests and tensile tests. The results indicate that the addition of 1% PET recycled fibre to concrete showed the best value in terms of strength. As for the splitting tensile strength test, the addition of 1% PET fibre also resulted in the highest value compared to the other mixes.

A. F. Abdul Manaf · S. Shahidan (✉) · S.-M. Shamsuddin · N. F. Sharif · S. S. Mohd Zuki · S. R. Abdullah · F. S. Khalid · M. A. Mohammad Azmi
Faculty of Civil Engineering and Built Environment, Universiti Tun Hussein Onn, 86400 Batu Pahat, Johor, Malaysia
e-mail: shahiron@uthm.edu.my

A. F. Abdul Manaf · S. Shahidan · S.-M. Shamsuddin · N. F. Sharif · S. S. Mohd Zuki · S. R. Abdullah · F. S. Khalid · M. A. Mohammad Azmi
Departments of Civil Engineering, Center for Diploma Studies, Universiti Tun Hussein Onn Malaysia, Education Hub Pagoh, 84600 Muar, Johor, Malaysia

1 Introduction

Concrete is commonly used in the development of infrastructure worldwide. The materials used to produce concrete are gravel, sand and water. Due to its performance and economic cost (Kim et al. [1]), it is used globally. Concrete shows good compression strength (Foti [2]).

As Malaysia's population increases rapidly, so has the demand for different types of materials. There are several types of fibres which pose serious environmental problems (Foti [3], Irwan Juki et al. [4]. Many methods for improving the quality of concrete make use of waste materials produced by different industries. Fibre concrete is usually more superior than normal concrete because of the sewing effect fibres have on concrete cracks. Therefore, the addition of fibres to concrete mixes are especially beneficial for structures with low reliability levels such as concrete slabs and walls.

These benefits have a positive effect on the application of fibers in structures, especially those with low reliability levels such as slabs on grade, walls, and foundation.

These days, there is an increasing amount of plastic in the environment caused by the disposal of solid waste. Polyethylene (PET) is the second highest category of plastic waste being produced today. However, incorporating PET into concrete mixtures may help alleviate environmental pollution.

The use of recycled PET in concrete has been widely applied in the field of civil engineering. The efficiency of recycled PET waste in concrete is largely determined by the shape of the plastic fibre. For instance, using 30 mm long PET fibres can increase the tensile strength up to 1.5% more compared to 20 mm long fibres (Irwan Juki et al. [4]). The ductility of concrete can be improved depending on the shape of the PET fibre used.

This study uses lamellar-shaped recycled PET fibres with rigid length and width in the concrete mix. The incorporation of PET fibre into concrete was conducted. In addition, the optimal quantity of recycled PET fibre to be added to concrete was also determined (Frigione [5]).

Due to the rapid growth in population, fibre waste generated by domestic households is the main factor which has contributed to environmental pollution. According to Borg et al. [6], 20 mm long PET fibres were not suitable but the use of 30 mm long fibres with a volume replacement of up to 1.5% made a positive change by increasing the tensile strength of concrete. This is because long fibres have the ability to form a tighter aggregate interlock in concrete.

Fibre waste is a serious problem as plastic waste is not degradable and harms the environment. The mismanagement of various types of wastes, limited landfills and the increase in production costs have lead to the search for alternative solutions such as the use of fibre waste in concrete mixes (Ochi et al. [7], Ramadevi et al. [8]).

Ramadevi et al. [8], found that compressive strength went up when 2% of cement content was replaced with PET fibres. As the fibre content increases, concrete strength also increases. Irwan et al. [9] used a waste bottle with irregularly

shaped PET fibres. The authors claimed that the concrete mixture was not the only factor that contributed to the improvement of the compressive strength of fibre concrete. The fibre size and shape are also important for preventing fibre from slipping out at high stress loads to exhibit FC performance.

Due to lack of research work on PET fibres, this study sets out to evaluate the influence of PET length on concrete strength. The main goal of this research is to investigate the influence of recycled PET fibres on concrete strength. To achieve the above goal, the following specific objectives are outlined as follows: 1) To determine the compressive strength and splitting tensile strength of different percentages of recycled PET plastic bottle fibre (0, 0.5, 1.0, 1.5 and 2.0%.) in concrete specimens measuring 25 mm long and 5 mm wide, and 2) To evaluate the optimum percentage of recycled PET fibres in concrete.

The use of recycled PET fibres in a concrete mix can help reduce environmental issues by reducing the growing amount of PET plastics bottles thrown into landfills. Therefore, it is important to study the optimum amount of recycled PET fibres which can be added to a concrete mix so that it would be suitable for use in the construction industry.

2 Materials and Methods

2.1 Preparation of Materials

The materials used in this research included Ordinary Portland Cement Type 1 (OPC: TYPE 1) grade 42.5 (according to MS EN 197-1: 2014), fine aggregate measuring 0.075–5 mm, coarse aggregate measuring 5–20 mm, water and recycled PET fibres measuring 25 mm long and 5 mm wide. The preparation of materials and recycled PET fibres is shown in Fig. 1.

Polyethylene terephthalate (PET) plastic bottles were collected and cleaned before being cut into fibre form. The recycled PET plastic bottles were collected from areas around Universiti Tun Hussein Onn Malaysia and residential colleges located at Taman Universiti. The process of collecting all the plastic bottles took around four months. After the bottles were collected, they were cleaned and dried to get rid of any impurities. Next, the recycled PET bottles were cut into smaller pieces to make the next process easier. Finally, the recycled PET pieces were cut into the desired size, namely 25 mm long and 5 mm wide. The process of processing PET fibre is shown in Fig. 2.

Mix design is a process conducted to select the most suitable materials for producing concrete and to determine their relative quantities to achieve desired strength. In this study, the concrete proportioning was designed using the trial mix. Table 1 shows the proportion of the materials needed in this study based on the DOE method.

Fig. 1 Preparation of materials: **a** Cement, **b** Fine aggregate, **c** Coarse aggregate, **d** PET fibre

Fig. 2 The preparation of recycled PET fibres: **a** Collecting recycled PET plastic bottles, **b** Cleaning and drying recycled PET plastic bottles, **c** Cut recycled PET pieces into desired size and shape (25 mm long, 5 mm wide)

Table 1 Mix design of concrete

Quantities	Cement (kg)	Water (kg)	Fine aggregate (kg)	Coarse aggregates (kg)	PET fibres (kg)
Per m^3	500.00	225.00	505.00	1175.00	420.00
0.049 m^3	34	15.3	34.34	79.9	28.50
Total	**170**	**76.5**	**171.7**	**399.5**	**1.47**

A total of 60 specimens were prepared in this research. This included 30 cube specimens measuring $150 \times 150 \times 150$ mm and 30 cylindrical specimens measuring 150 in diameter and 300 mm in height. Five types of mixes were prepared where the control specimens were prepared with 0% of fibre, followed by specimens containing 0.5, 1.0, 1.5 and 2.0% of recycled PET fibres. The concrete properties were tested after a curing period of 7 days and 28 days. A compressive test was conducted as specified in the test method BS 1881-116:1983, Part 116: Method for the determination of compressive strength of concrete cubes. Meanwhile, the splitting tensile strength test was conducted based on BS EN12390-6:2000, Part 6: Tensile splitting strength of test specimens.

3 Results and Discussions

The analysis of the results obtained from the data collected from the laboratory tests is discussed here. The analysis was done according to the parameters used for controlling the effect of the percentages of recycled PET fibres in concrete under curing conditions lasting 7 days and 28 days. This section consists of the results for slump tests, compressive strength tests and splitting tensile strength tests carried out in this study.

Figure 3 shows that a decrease of workability was recorded when PET fibre was added to the concrete mix. Based on the concrete mix design according to the DOE (Department of Environmental) method, the slump range target of this mixture should be between 60 to 180 mm. The slump of normal concrete was 101 mm which is between the target slump range of 60 mm to 180 mm. The slump kept decreasing with the addition of fibre into concrete mixtures. The reason behind this decrease is due to the presence of PET fibres in concrete which causes more friction between the particles. This leads to less workability in the mixtures. Besides, the high content and large surface area of the fibres can easily absorb the cement paste, thereby increasing the viscosity of the concrete mixture. As the PET content increases, the plasticity and consistency of fresh concrete will decrease.

Figure 4 shows the compressive strength values of the control specimen and specimens containing different percentages of PET fibre. The target strength of the concrete specimen is 35 N/mm^2. However, as the percentage of PET fibres increases, the compressive strength value of concrete containing recycled PET fibres decreases.
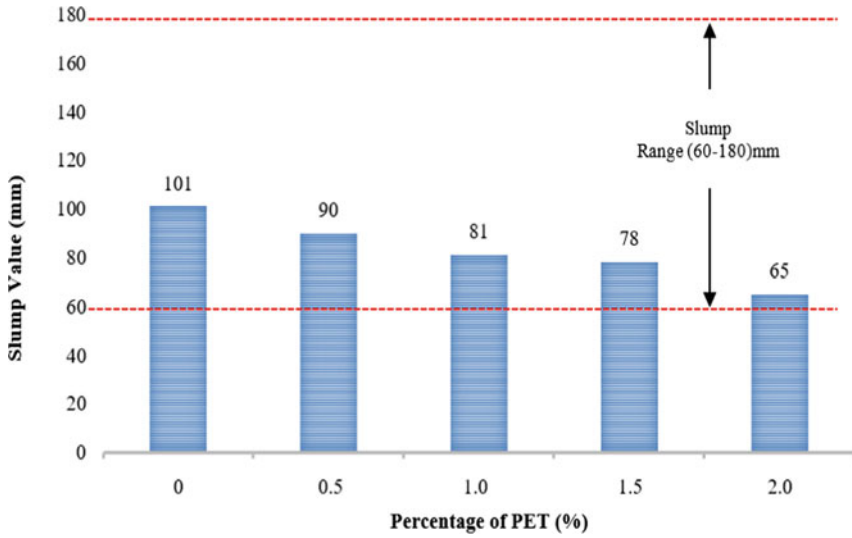
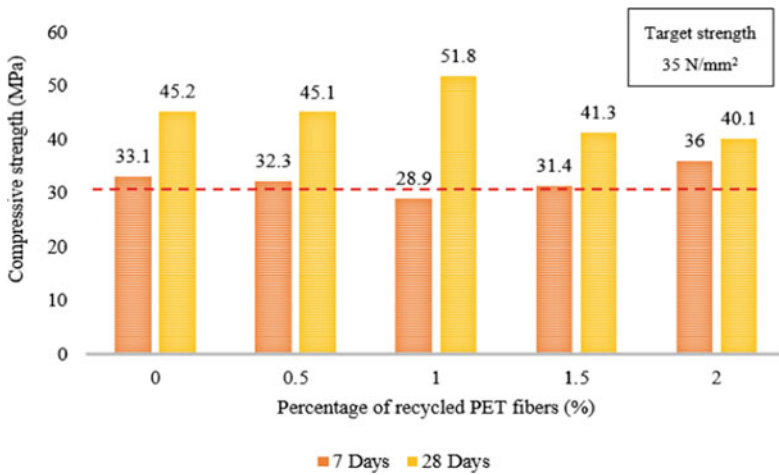**Fig. 3** Slump versus the volumetric content of fibre (%)

Fig. 4 Compressive strength versus percentages of PET fibres

1.0% PET fibre concrete showed the best fibre distribution among other fibre concrete specimens. The addition of fibres tends to cause bundling during mixing and pouring, also known as fibre balling. Fibre balling weakens the concrete due to the high possibility of fibre surfaces coming in contact with one another. The area between fibre surfaces is the weakest point in concrete; microcracks and macrocracks caused by compression loading easily appear in this area (Yin et al. [10]).
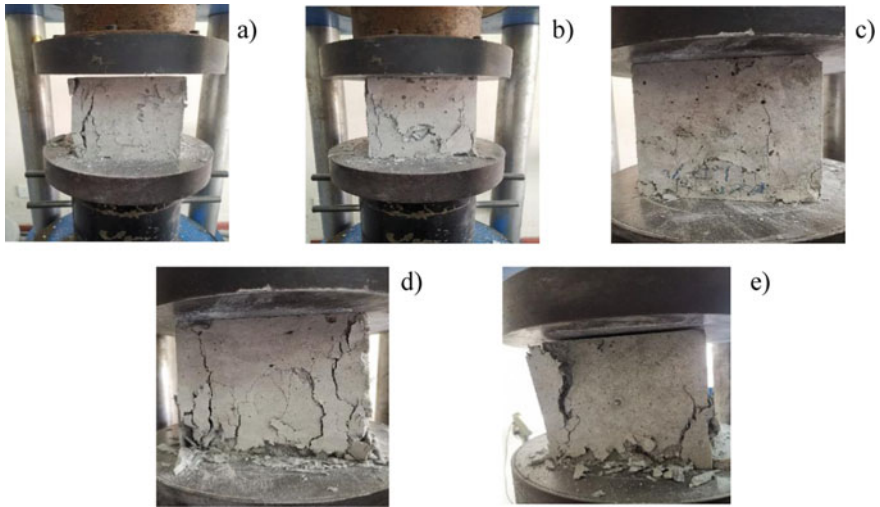
Fig. 5 Real observation of cube specimens: **a** 0% PET fibre, **b** 0.5% PET fibre, **c** 1.0% PET fibre, **d** 1.5% PET fibre, **e** 2.0% PET fibre

However, 1.0% PET fibre concrete showed the best fibre distribution among other fibre concrete specimens. Hence, 1.0% PET fibre concrete produced the highest value in terms of compressive strength. The area between fibre surfaces is the weakest point in concrete; microcracks and macrocracks caused by compression loading easily appear in this area. In general, the rate of reduction in strength was found to decrease with the increase in the percentage of recycled PET fibres and also the length of PET fibres (Fig. 5).

Figure 6 presents the pattern of splitting tensile strength values of all the concrete specimens. According to the results, the splitting tensile strength increased only with the addition of fibres up to about 1.0% after which, the tensile strength decreases with the addition of more fibres. Both of the tests for the specimens aged 7 days and 28 days showed that the splitting tensile strength increases only up to 1.0% addition of PET fibres in the concrete specimens. The outcomes indicate that the fibres must be uniformly distributed in the mixture. Besides, the fibre proportions must be carefully selected. The splitting tensile strength increases by about 10% with the addition of 1.0% PET fibre in concrete compared to normal concrete.
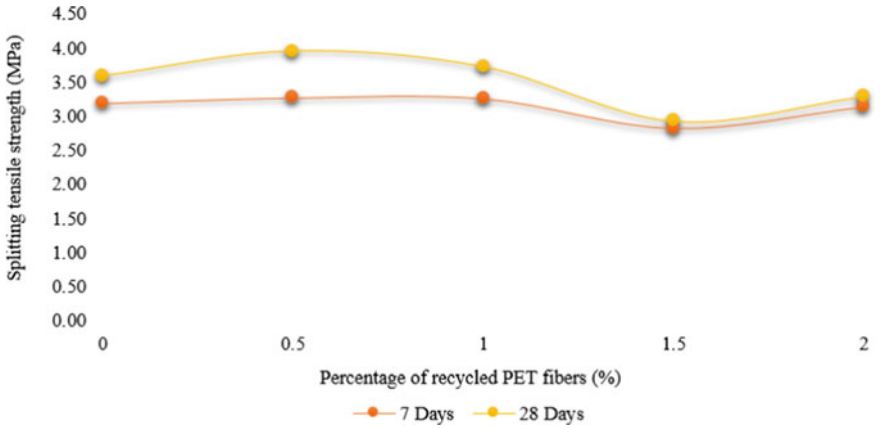
Fig. 6 Splitting tensile strength versus percentage of PET fibres

The outcomes indicated that the fibres must be uniformly distributed in the mixture and that the fibre proportions must be carefully selected. The splitting tensile strength increased with the addition of 0.5% PET fibre in concrete compared to normal concrete. The splitting tensile strength increased due to the bridging mechanism of recycled PET fibres and after certain rations, it reduced the bond strength between concrete materials (Choi et al. [11]). Referring to Faisal et al. [12] studied the splitting tensile strength of concrete incorporated with polyethylene terephthalate (PET) bottles as lightweight aggregates (WPLA). It can be concluded that the splitting tensile strength of concrete mixtures decreases with an increase in PET aggregate content and increases when there is a reduction in water-cement ratio (Fig. 7).
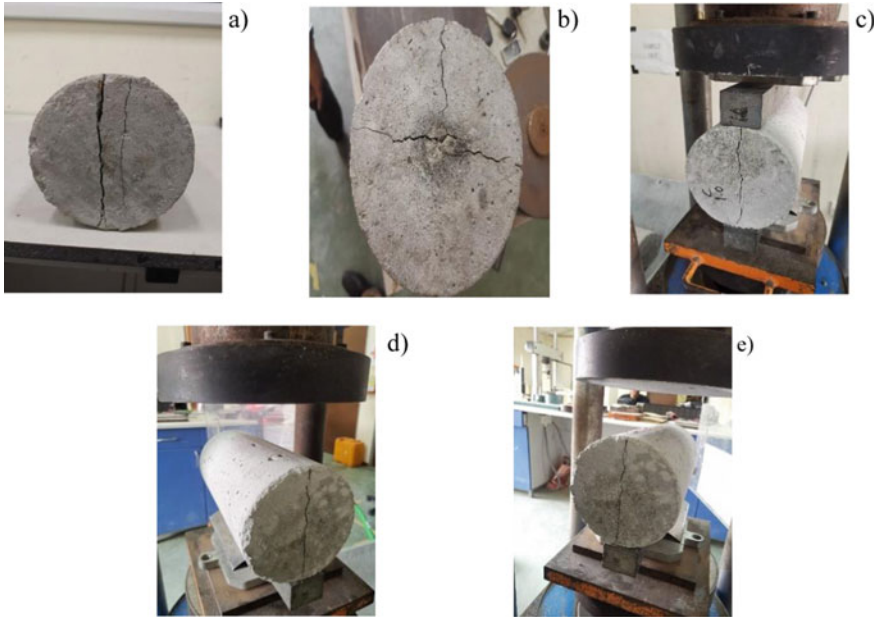
Fig. 7 Real observation of cylindrical specimens: **a** 0% PET fibre, **b** 0.5% PET fibre, **c** 1.0% PET fibre, **d** 1.5% PET fibre, **e** 2.0% PET fibre

4 Conclusion

From the analysed data, it can be concluded that the optimum percentage of recycled PET fibres to be added to concrete was 1% to achieve the highest compressive strength. Even though the slump test showed a decrease while the compressive strength test showed some fluctuation, the addition of 1% of PET recycled fibre into concrete showed the best value in terms of strength. As for the splitting tensile strength test, the addition of 1% PET fibre also resulted in the highest value compared to other concrete mixes.

References

1. Kim SB, Yi NH, Kim HY, Kim JHJ, Song YC (2010) Material and structural performance evaluation of recycled PET fibre reinforced concrete. Cem Concr Compos 32(3):232–240
2. Foti D (2013) Use of recycled waste pet bottles fibres for the reinforcement of concrete. Compos Struct 96:396–404
3. Foti D (2011) Preliminary analysis of concrete reinforced with waste bottles PET fibres. Constr Build Mater 25(4):1906–1915
4. Irwan Juki M, et al. (2013) Development of concrete mix design nomograph containing Polyethylene Terephthalate (PET) as fine aggregate. Adv Mater Res 701:12–16
5. Frigione M (2010) Recycling of PET bottles as fine aggregate in concrete. Waste Manag 30 (6):1101–1106
6. Borg RP, Baldacchino O, Ferrara L (2016) Early age performance and mechanical characteristics of recycled PET fibre reinforced concrete. Constr Build Mater 108:29–47
7. Ochi T, Okubo S, Fukui K (2007) Development of recycled PET fibre and its application as concrete-reinforcing fibre. Cem Concr Compos 29(6):448–455
8. Ramadevi K, Manju R (2012) Experimental investigation on the properties of concrete with plastic PET (bottle) fibres as fine aggregates. J Emerg Technol Adv Eng 2(6):42–46
9. Irwan JM, Faisal SK, Othman N, Wan IMH, Asyraf RM, Annas MMK (2013) Performance of concrete using light waste PET fibre. Adv Mater Res 795:352–355
10. Yin S, Tuladhar R, Shi F, Combe M, Collister T, Sivakugan N (2015) Use of macro plastic fibres in concrete: a review. Constr Build Mater 93:180–188
11. Choi OC, Lee C (2003) Flexural performance of ring-type steel fibre-reinforced concrete. Cem Concr Res 33(6):841–849
12. Faisal SK (2015) Engineering properties of ring shaped polyethylene terephthalate (RPET) fibre self-compacting concrete. Universiti Tun Hussein Onn

Effectiveness of Different Curing Media in Self-healing Process Monitored by Compressive Strength and Water Absorption of Cement Mortar

Norfaniza Mokhtar, Wan Amizah Wan Jusoh, and Muhammad Fitri Mah Hassan

Abstract The root cause of the majority of structural failure is attributed to cracking, there is a compelling economic incentive to develop concrete that can treat and repair the damage by itself. Even though some research has been carried out in this area a breakthrough in method to supply nutrient for effective healing are yet to materialise. For the present study, *Bacillus sphaericus* with diatomaceous earth as a protective vehicle was selected to determine the best performance with different curing media as an alternative method to supply a nutrient. For the growth of the bacterial, the nutrients are supplied using three different curing media which is deposition medium (controlled nutrients), runoff water (uncontrolled nutrients) and also distilled water. The performance of Bio-based cement mortar (BBCM) was evaluated by comparing the influence on compressive strength and water absorption subjected to different curing media. BBCM cured in run-off water had the best compressive strength with increment of 39.04% compared to others curing media. Also, with its great dispersal characteristics, denser BBCM with a reduction of water absorption. BBCM cured in run-off water had a 40% improvement in strength compared to normal curing. As a conclusion, run-off water is highly promising in supplying sufficient nutrients to bacteria for the biomineralization process to produce $CaCO_3$. This work also aims to apply this approach in the field especially in sewerage and drainage system.

Keywords Bacillus sphaericus · MICP · Run-off water · Diatomaceous Earth

N. Mokhtar (✉) · M. F. M. Hassan
Faculty of Civil Engineering and Built Environment, University Tun Hussein Onn Malaysia, Parit Raja, 86400 Batu Pahat, Johor, Malaysia
e-mail: norfaniza@uthm.edu.my

W. A. W. Jusoh
Faculty of Engineering Technology, University Tun Hussein Onn Malaysia, Pagoh, 84600 Panchor, Johor, Malaysia

247

1 Introduction

Nowadays an extensive study of modern and innovative developments in concrete technology focused on the principle of 'intrinsic self-healing' has created a kind of concrete which is able to cure itself by inserting spore-forming microorganisms into concrete called microbial concrete with autonomous healing. Autonomous healing may be described as a normal form of hydration without overt operations with unreactive brick, brick/mortar, laundry, and burned (Rooij *et al.* [17]) cover and near cracks that named as Microbiologically induced calcite precipitation (MICP) which happen during the precipitation phase. The MICP strengthens the overall properties of concrete by calcium precipitation, filling the voids within cement matrixes and leading as an independent self-healing mechanism to enhance the durability of concrete. This approach is pollution-free and sustainable as there is no shortage of natural resources because it quickly replicates the bacteria by cultivation (June *et al.* [13]).

Previous research indicated that the incorporation of bacteria into the concrete matrix will accomplish self-healing activities (Wang *et al*. [23]; Wang *et al*. [25]; Gilford [10]; Jonkers and Schlangen [11]; Rao *et al*. [15]; Jonkers *et al*. [12]; Thao *et al.* [20]; Van Tittelboom *et al.* [21]; Schlangen and Jonkers [18]; Vekariya and Pitroda [22]). In brief, it was believed that latent but viable bacterial spores are metabolically involved in the concrete matrix once moist reaches into newly produced cracks. Such breaks would instead be repaired by precipitation of microbial calcite, avoiding more water and other chemicals. The key to concrete qualities is their compressive strength and durability. It is important to determine the effect of biomineralization on certain attributes.

Crack, pore density, and its application have a detrimental effect on concrete and resulting structural property of concrete systems. The durability of concrete stated by Pacheco-Torgal and Labrincha in [14] can be improved as main mechanisms for transportation to fluid and gases, via reductions in absorption, permeability, and diffusion. Six times decreasing permeability occurred to sample with polyurethane immobilized bacteria due to the carbonate precipitation via the integration of cells. In addition, the effectiveness of the *Bacillus sphaericus* immobilised in diatomaceous earth was reported on water absorption. Tests also have shown that 50% of these studies without bacteria have been consumed with water-based immobilised bacteria (Wang *et al.* [24]). The application of Bacillus sphaericus has resulted in watertight concrete 6 times below 168 h relative to water absorption coefficient control experiments, Achal *et al.* [2]. Incapsulated *Bacillus sphaericus* was recorded to result in a 15 to 34% reduction in compressive strength (Wang *et al.* [26]) and compression intensity improved by 7 to 28 days with *Bacillus sphaericus* in cubic mortar, Achal *et al.* [1]. While the compressive strength effect of 5×10^6 cells/mm^3 cells has been favorable to the bio-based product, the compression intensity of the mortar has decreased in the large cell concentration (5×10^8 cells/mm^3). Bang *et al.* [6] investigated the 7-day and 28-day impact that cell concentration enhancement would have on mortar specimens, which would dramatically

raise compressive intensity from 24% from 6.1×10^7 cells/cm^3 to 3.1×10^9 cells/cm^3 *Sporosarcina pastorii*. In addition, the symptoms of immobilised ureolytic and denitrifying bacteria in defensive materials are reported by Erşan *et al.* [9]. Their analysis showed that 63 and 60% respectively decreased compressive strength by adding *Bacillus sphaericus* in concrete at 7 and 28 days. While the ingestion of denitrifying bacterium (*Diaphorobacter nitroréducens*) decreased the compressive strength in expanded clay and granular active carbon for both 7 and 28 days, the immobilisation of *Diaphorobacter nitroreducens* increased marginally the compressive strength. The metacaolin and zeolite immobilisation of *Bacillus sphaericus* adversely affected strain.

In this sense, understanding the mechanism of microbial induced calcite precipitation process is very important. Thus, the effect of microbial activity of *Bacillus sphaericus* to produce CaCO$_3$ and the capability to seal cracks and fill pore should be studied to set these products as a self-healing product and the influence of nutrients should be investigated to check their efficiency for self-healing indicated by precipitation of CaCO$_3$ and the subsequent improvement in strength and water absorption of cement mortar. Considering the above current issue, it is concluded that there is a need to study the effectiveness of different curing media in self-healing process monitored by compressive strength and water absorption of cement mortar in various media such as distilled water, deposition medium and runoff water and use them to explain some aspects of the observed engineering behaviour in a well-controlled laboratory condition. In this thesis, an attempt has been made to evaluate the effect of microbial activity of *Bacillus sphaericus* on the properties of Portland cement mortar.

2 Methodology

2.1 Cement Mortar Specimen Preparations

As per ASTM 403 (ASTM [4]), two series of cement mortar, consisting of bio-based cement mortar (BBCM) and control cement mortar (CCM) were cast. It is prepared in a ratio of 0.5 of water to cement and 0.333 of cement to sand. Three minimum samples of BBCM and CCM cement mortar replicates were prepared. Cement and sand were dry for a very slow 30 s, then the mixing water was partially dissolved before being thoroughly mixed with 80% of the entire immobilised bacteria culture at moderate speed with a concentration of 0.25, 2.5 and 5% of cement mass, in part with the mixing water. The mixer's sides stopped and shelved and then blended again for 30 s. The remaining 20% of immobilised bacterial cultures were then inserted and further blended for another 60 s and the mortar mixture was eventually blended for 30 s at a faster pace before being poured into the respective moulds depending on a specific examination. For BBCM series 45 g of Diatomaceous Earth (DE) and 225 g bacterial solution (BS) was added. To

Table 1 Proportions of cement mortar specimens for the different mixtures

Mixture	Cement (g)	Sand (g)	Water (g)	DE (g)	BS (g)	Nutrients (g)
CCM	900	2700	450	0	0	0
BBCM	900	2700	225	45	225	69.75
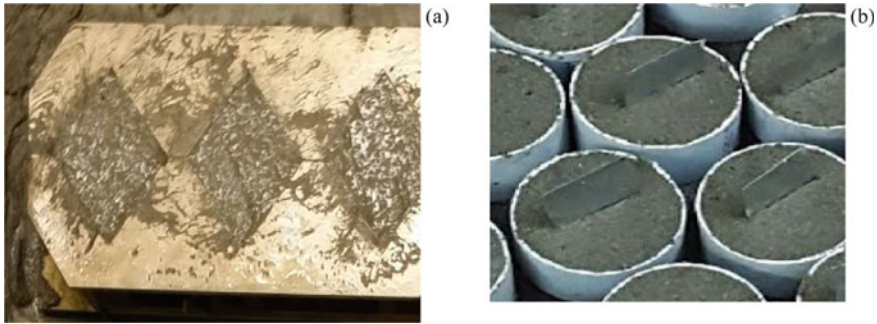
**Fig. 1** Mortar samples **a** sample for compressive strength **b** sample for water absorption test

extract compressed dust, a vibrating table compacted the samples for 60 s and finished the surface stage. Figure 1 illustrated the mortar samples for compressive strength and water absorption test. Table 1 lists the test elements.

2.2 Curing

Specimens were cured into 3 different curing media such as run-off water (RW), distilled water (DW), and deposition medium (DM) for 3, 7, 28, 56, and 90 days in closed containers and maintained temperature at 25 ± 2 °C. Cure media were sterilised at 120 °C for 20 min prior to the treatment phase in order to ensure that the *Bacillus sphaericus* and no externalisation bacteria were involved in the MICP phase (Fig. 2).

2.3 Compressive Strength Test

The compressive power of CCM and BBCM cubic specimens with measurements $50 \times 50 \times 50$ mm has been carried out in compliance with the ASTM C109 (ASTM [5]) standard. Cubes have been cast and compacted in a vibrational system. The cure was conducted at the periods of 3, 7, 28, 6, and 90 days after removal of the sample in a regulated temperature room of 25 ± 2 °C in specific curing media. A compressive strength check has been carried out using a standardized test tool.

Fig. 2 Curing process
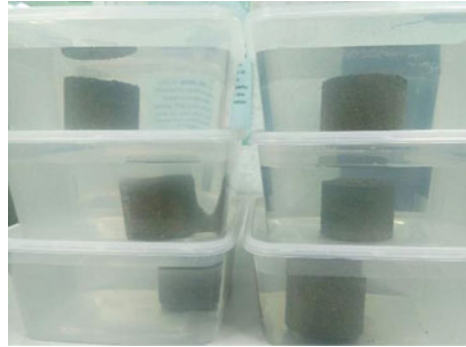
2.4 Water Absorption

The water absorption research was conducted using the vacuum saturation apparatus (RILEM, 1984) on 55 mm diameter × 40 mm thick mortary samples. The specimens have been dried in an electrical oven at 105 °C for 24 h. The weight of dry specimens (W4) was then calculated. The tests also took place for 3 h at a vacuum pressure of one bar. While the sample was still in vacuum, water was added. The experiments were immersed in a centimeter of water to cover the surface of the experiments. The vacuum state was preserved for a further 3 h following the injection of liquids. After three hours the vacuum state was released and kept in water for another 1 h to reach maximum saturation. The specimens were then separated from the water and the sample surfaces were wiped with the dried fabric. In the air (W2) and in the water (W3), the weight was then calculated. Of every sequence, monitoring was conducted at age 3, 7, 28, 56, and 90 days. The water (A) consumed by the following Eq. 1 was determined;

$$A(\%) = \frac{W_2 - W_4}{W_4} \times 100 \tag{1}$$

3 Results and Discussions

3.1 Effect of BBCM on Compressive Strength on Different Curing Media

The compressive intensity of CCM and BBCM was found to be an alternate mechanism for supplying nutrients to the healing agent and any variations in pressure were detected solely because of microbial interaction at various exposures to healing material. The outcome in Fig. 3 indicates that for the CCM series, the strength for all different curing media is almost the same for all series. It does,
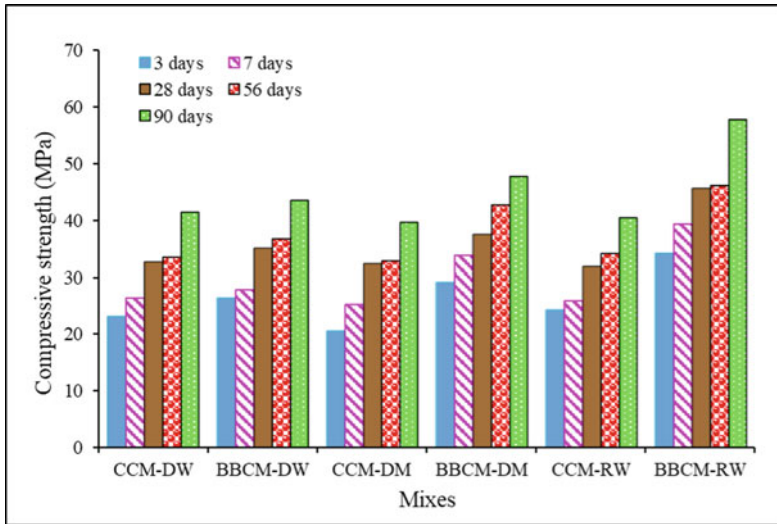
Fig. 3 Compressive strength of cement mortar cubes under different curing media

however, from 3rd to 28th day show increase in strength but for all healing media, it becomes almost stagnant up to 56 days. The reality that there might be insufficient nutrients but a sharp growth in intensity of BBCM-DM and BBCM-RW after 56 days cannot be ascribed to any major changes in CCM-DW or BBCM-DW after 28 days due to no significant improvement of strength. Beside that at this stage the Bacillus *sphaericus* still in the log phase that represents a period of time of bacteria to adapt a new environment which during this stage the number of cell changes very little and population growth during this period is very close to zero but the cells are not dormant. The gradually increased availability of nutrients to *Bacillus sphaericus*, contributing to CaCO$_3$ persistent precipitation, is possibly attributed to the steady increase for BBCM-DM by around 38% over 90-day duration.

Bacillus sphaericus growth phase is reflected by BBCM-RW's strength improvement as recorded by Zwietering *et al.* [27] and Skarstad *et al.* [19], due to significant log-phase bacterial activity, the gradual strength increases from 3 to 28 days. Nevertheless, there is a small change in the stationary period following 28 days up to 56 days. The rapid spike in intensity after 56 days can be correlated with the growth process of *Bacillus sphaericus*, which has significantly enhanced cell size as a consequence of the maximum bacterial development during the exponential period. The increase in intensity in 28 to 56 days is not so significant. This may be attributed to inadequate survival nutrition because the bacteria have rapidly spread and the *Bacillus sphaericus* begins to die. Later on, if the percentage of *Bacillus sphaericus* declines to a point that every other *Bacillus sphaericus* receives adequate nutrients. The explanation for the increase in intensity again is 56 to 90 days.

In contrast to BBCM-DM and BBCM-RW, the performance increase in the specimens of BBCM-RW is significantly greater than that of BBCM-DM. The primary explanation is the existence of rainwater of an abundant supply of nutrients. The properties of run-off water have been studied by way of chemical analysis in order to validate this assertion. An important factor in bacterial survival by supplying sufficient nutrients during the MICP cycle is the availability of total suspended solids and total dissolved solids in flowing water. Low COD means that oxygen demands on the components of the oxidation are smaller, thus making more oxygen accessible in the mortar for bacteria. The findings indicate significant truths that bacteria are provided sufficient nutrients for MICP activity due to the existence of rich nutrient sources in runoff water, which is why it contributes to a higher intensity.

3.2 Water Absorption

The pore structure of BBCM has been studied to analyse the results of various cure and treatment outlets. Figure 4 showed specifically that decreased water absorption from BBCM in contrast with CCM was largely due to the healing time factor and adequate nutrient of precipitate pores or vacuum during bacterial metabolic operation, to $CaCO_3$. When neutral materials such as $CaCO_3$ obstruct the openings, the vapour, air and pollutant passage is sealed to which the permeation of vapour and chloride through the mortar. The most pronounced reduction in water absorption was for specimens cured in RW and DM that are provided with nutrients for bacteria to complete the metabolic activity to produce more $CaCO_3$ which ends up going to fill the pore compared to DW.
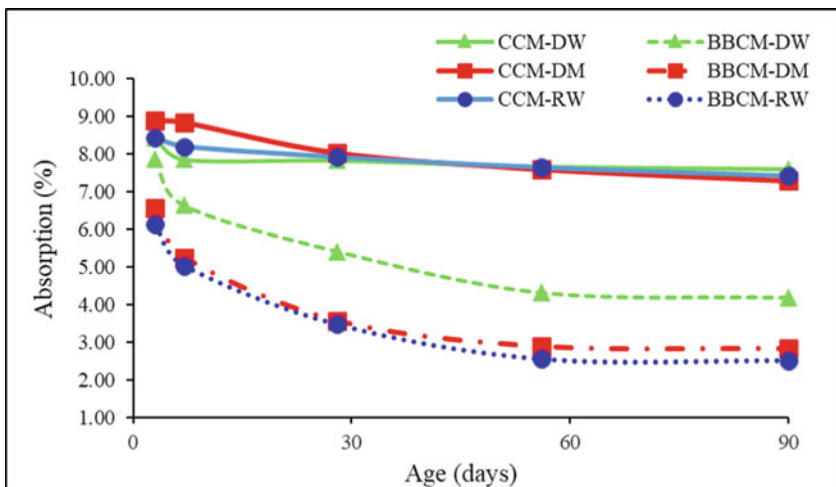

Fig. 4 Water absorption of CCM and BBCM in different curing media

Similar findings were published on the bacterial surface activity of carbonate crystal compounds, by Achal *et al.* [2], Wang, *et al.* [24], Chahal and Siddique [7], which enhanced the calcite deposits as important factors in raising the resistance of concrete frameworks et cement-built content to decay. Similar findings were published on the soil. Precipitation of carbonate in Bacillus cells impacting the surface of nutrient uptake, undermining proton energy, and eventually contributing to the death of the cell. This may be due to the decline in BBCM-DM in accordance with BBCM-RW. The reduction of the cell counts allows ureolytic function to decrease. However, there is a small rise in the number of cells attributable to development attributable to nutrients other than urea in the DM relative to RW being neither adequate nor inadequate. De Muynck *et al.* [8] and Achal *et al.* [3] have reported that the intake of water in contrast with control conditions in the presence of bacteria has been greatly decreased. The porosity of toxic compounds with precipitated calcite-crystals that enhance mortar longevity is lowered as hypothesised by Van Tittelboom *et al.* [21]. Such findings appear to suggest that bacterial $CaCO_3$ precipitation substantially affects the moving processes of mortar fluids. The bacterial mediation of calcite deposition culminated intolerance to water absorption. *Bacillus Sphaericus* helped block pores to provide a promising solution for the durability of the mortar.

3.3 Correlation Between Compressive Strength and Water Absorption

BBCM's water absorption was investigated to understand the compressive strength effect of pore formation based on different curing media and prolonged period as shown in Fig. 5(a–c). As the water absorption of BBCM reduced, BBCM improved its compressive power, and this also relied on the treatment medium. From the third days of healing until the 56 days of healing, the water absorption of BBCM fell significantly but stayed stable afterward because of an improvement of the cure duration. The relation between compressive strength and the water absorption capability of BBCM is nevertheless high. One point to remember is that the water absorption of bio-based cement mortar slowly declined as the curing time went up. In Fig. 5 BBCM-RW indicates the association between compressive intensity and water absorption and porosity and proceeded to demonstrate a good connection between compressive resistance and water absorption and porosity. The Fig. 5(d) indicates a negative linear relationship with a strong regression association, R2, with compressive intensity and water absorption and BBCM-RW porosity. The compressive intensity of BBCM-RW was observed to slowly decrease with absorption and porosity.
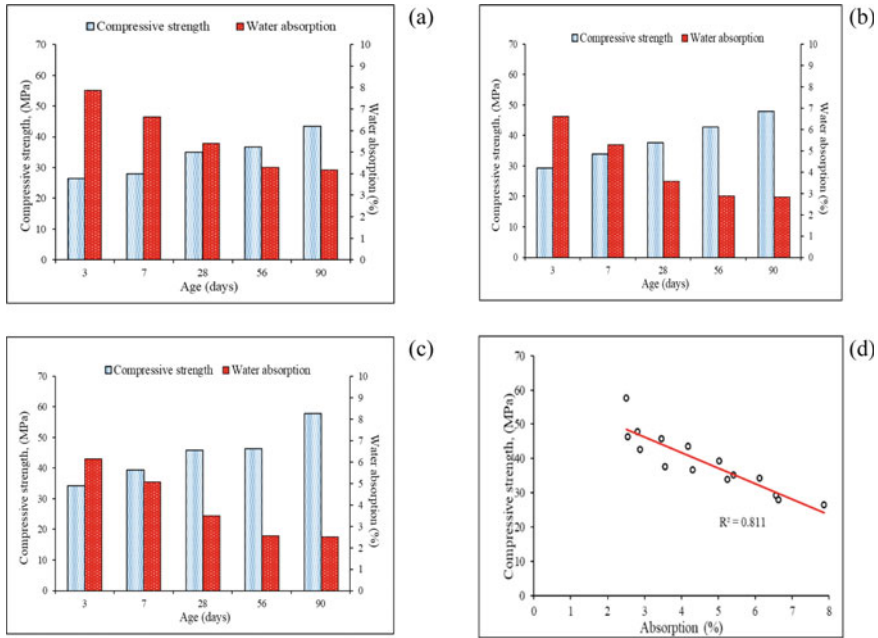
Fig. 5 Effect of curing media and curing period on compressive strength and water absorption **a** distilled water **b** deposition medium **c** run-off water **d** correlation between compressive strength and water absorption

4 Conclusions

The new theoretical process for enhancing cement mortar longevity was the microbial mediated deposition of calcite. The present paper deals with the various media, which are essential criteria in affecting the survival of bacteria as an alternate nutrient supply system by calculating a fixed period, compressive power, water absorption, and permeability. The microbial calcite precipitation technique with media cured with sufficient nutrient promising substantial strength improvement and improved water permeability. This method, as a novel biological metabolic product that can be added to the wastewater and drainage system, is very exciting as this research has demonstrated that runoff water can provide adequate nutrients to the cycle of biomineralisation to generate $CaCO_3$. The maintenance and rehabilitation costs may be reduced at once.

References

1. Achal V, Mukerjee A, Sudhakara Reddy M (2013) Biogenic treatment improves the durability and remediates the cracks of concrete structures. Constr Build Mater 48:1–5

2. Achal V, Mukherjee A, Reddy MS (2011) Microbial concrete: way to enhance the durability of building structures. J Mater Civ Eng 23(6):730–734

3. Achal V, Mukherjee A, Reddy MS (2010) Biocalcification by sporosarcina pasteurii using corn steep liquor as nutrient source. J Ind Biotechnol 6:170–174

4. ASTM (2008) Standard Test Method for Time of Setting of Concrete Mixtures by Penetration Resistance. ASTM C403/C403M-08, 100 Barr Harbor Drive, West Conshohocken, 7

5. ASTM (2013) Standard Test Method for COmpressive Strength of Hydraulic Cement Mortar (Using 2-in or [50-mm] Cube Specimens. ASTM C109/C109M-13, 100 Barr Harbor Drive, West Conshohocken, 10

6. Bang SS, Lippert JJ, Yerra U, Mulukutla S, Ramakrishnan V (2010) Microbial calcite, a bio-based smart nanomaterial in concrete remediation. Int J Smart Nano Mater 1:28–39

7. Chahal N, Siddique R (2013) Permeation properties of concrete made with fly ash and silica fume: Influence of ureolytic bacteria. Constr Build Mater 49:161–174

8. De Muynck W, Debrouwer D, De Belie N, Verstraete W (2008) Bacterial carbonate precipitation improves the durability of cementitious materials. Cem Concr Res 38(7):1005–1014

9. Ersan YC, de Belie N, Boon N (2015) Microbially induced $CaCO_3$ precipitation through denitrification: an optimization study in minimal nutrient environment. Biochem Eng J 101:108–118

10. Gilford J (2012) Microencapsulation of Self-Healing Concrete Properties. Ph.D. thesis. Louisiana State University

11. Jonkers HM, Schlangen E (2007) Self-healing of cracked concrete: a bacterial approach. In: 6th International Conference on Fracture Mechanics of Concrete and Concrete Structures, vol 3, pp 1821–1826

12. Jonkers HM, Thijssen A, Muyzer G, Copuroglu O, Schlangen E (2010) Application of bacteria as self-healing agent for the development of sustainable concrete. Ecol Eng 36 (2):230–235

13. Wang JY, Van Tittelboom K, De Belie N, Verstraete W (2010) Potential of applying bacteria to heal cracks in concrete. In: 2nd International Conference on Sustainable Construction Materials and Technologies, pp 1–12

14. Pacheco-Torgal F, Labrincha JA (2013) Biotech cementitious materials: some aspects of an innovative approach for concrete with enhanced durability. Constr Build Mater 40:1136–1141

15. Rao MVS, Reddy VS, Hafsa M, Veena P, Anusha P (2013) Bioengineered concrete - a sustainable self-healing construction material. Res. J Eng Sci 2(6):45–51

16. RILEM TC 14-CPC (1984) 11.3. Absorption of water by immersion under vacuum. Mater Struct 17(101):391–394

17. de Rooij M, Van Tittelboom K, De Belie N, Schlangen E (eds) (2013) Self-healing Phenomena in Cement-Based Materials. Springer, Dordrecht

18. Schlangen E, Jonkers H (2008) A two component bacteria-based self-healing concrete. Concr Repair Rehabil Retrofitting II:119–120

19. Skarstad K, Steen HB, Boye E (1983) Cell cycle parameters of slowly growing Escherichia coli B. J Bacteriol 154(2):656–662

20. Thao TDP, Johnson TJS, Tong QS, Dai PS (2009) Implementation of self-healing in concrete – proof of concept. IES J Part A Civ Struct Eng 2(2):116–125

21. Van Tittelboom K, De Belie N, De Muynck W, Verstraete W (2010) Use of bacteria to repair cracks in concrete. Cem Concr Res 40(1):157–166

22. Vekariya MS, Pitroda J (2013) Bacterial concrete: new era for construction industry. Int J Eng Trends Technol 4(9):4128–4137

23. Wang J, Van Tittelboom K, De Belie N, Verstraete W (2012) Use of silica gel or polyurethane immobilized bacteria for self-healing concrete. Constr Build Mater 26(1):532–540

24. Wang JY, De Belie N, Verstraete W (2012) Diatomaceous earth as a protective vehicle for bacteria applied for self-healing concrete. J Ind Microbiol Biotechnol 39(4):567–577

25. Wang JY, Snoeck D, Van Vlierberghe S, Verstraete W, De Belie N (2014) Application of hydrogel encapsulated carbonate precipitating bacteria for approaching a realistic self-healing in concrete. Constr Build Mater 68:110–119
26. Wang JY, Soens H, Verstraete W, De Belie N (2014) Self-healing concrete by use of microencapsulated bacterial spores. Cem Concr Res 56:139–152
27. Zwietering MH (1990) Modeling of the bacterial growth curve. Appl Environ Microbiol J 56 (6):1875–1881

Mechanical Properties of Concrete Containing Untreated Palm Oil Fuel Ash and Egg Shell Powder

Fatin Shafirah Abdul Ghaffar, S. S. Mohd Zuki, S. Shahidan, Fadzli Mohamed Nazri, Mustaqqim Abdul Rahim, Mohamad Azim Mohammad Azmi, Norashidah Abdul Rahman, and M. H. W. Ibrahim

Abstract This study aims to use two (2) waste products, namely Palm Oil Fuel Ash (POFA) and Egg Shell Powder (ESP) as cement replacement in concrete. This is because the properties of POFA and ESP are similar to the properties of cement. The objective of this study is to determine the mechanical properties (compressive strength and tensile strength) of concrete containing POFA and ESP as cement replacement. With both properties known, the optimum percentage of POFA and ESP as cement replacement can then be determined. The percentage of replacement of POFA was fixed at 20%, however the percentages of ESP varied from 0 to 20%. Six $100 \times 100 \times 100$ mm cubes and six 100×200 mm cylinders were prepared for each variation of percentages. The cubes and cylinders were tested for compressive and tensile strength after 7 and 28 days of water curing. Generally, as the percentages of ESP increased, the workability, compressive strength and tensile strength of the concrete sample decreased. In conclusion, the combination of POFA and ESP as cement replacement in concrete is only able to achieved 76% of targeted strength.

Keywords Palm oil fuel ash · Egg shell powder · Green concrete · Sustainable concrete

F. S. A. Ghaffar · S. S. Mohd Zuki (✉) · S. Shahidan · N. Abdul Rahman · M. H. W. Ibrahim
Department of Civil Engineering, Faculty of Civil Engineering and Built Environment, Universiti Tun Hussein Onn Malaysia, Parit Raja, 86400 Batu Pahat, Johor, Malaysia
e-mail: sharifahs@uthm.edu.my

F. Mohamed Nazri
School of Civil Engineering, Universiti Sains Malaysia, Engineering Campus, 14300 Nibong Tebal, Pulau Pinang, Malaysia

M. Abdul Rahim
School of Environmental Engineering, Universiti Malaysia Perlis, 02600 Arau, Perlis, Malaysia

M. A. Mohammad Azmi
Department of Civil Engineering, Center for Diploma Studies, Universiti Tun Hussein Onn Malaysia, Education Hub Pagoh, 86400 Muar, Johor, Malaysia

1 Introduction

Few researchers (Alyousef et al. [4]; Hamada et al. [9]; Hamideh and Akbar [10]; Prakash and Satyanarayanan [16]; Premalatha et al. [17]) have attempted to utilise waste materials to improve the mechanical properties of cement and to solve issues associated with waste transfer. Waste materials such as Palm Oil Fuel Ash (POFA), silica fume, quartz sand, egg shell powder (ESP) and others have been used in the production of concrete. Previous researchers have utilised a wide range of cementitious materials and solid waste items. Using waste materials helps reduce the use of cement in concrete and offers a way to make use of waste materials. In addition, using these materials in practical development applications will help decrease landfill costs, spare vitality assets and shield the earth from any conceivable contamination effects. Many analysts have contemplated the use of POFA and eggshell in normal concrete, high quality concrete and lightweight concrete, including foam concrete. In this study, two major types of agricultural waste (ESP and POFA) are used as cement replacement. According to Raji and Samuel [22] eggshell waste could cause ecological problems because of its accessibility and compound piece. Hence, legitimate administration and treatment are required. Nowadays, chicken eggshells have been recorded worldwide as one of the most noticeably serious environmental problems, causing bad odours which can be a discomfort to humans (Raji and Samuel [22]).

Malaysia is the largest exporter of palm oil. Disposing of POFA has been a problem for many years. Through public concern and research efforts, agricultural waste has the potential to be utilised as construction material to replace conventional cement (Tambichik et al. [18]). Generally, waste from the palm oil industry is becoming a major problem because palm oil waste is not being reused or recycled in any way. POFA refers to ash created by incinerating palm oil shell and husk as fuel in a palm oil factory heater so as to deliver steam to produce power for the palm oil extraction process. This perilous material is typically sent to landfills. If POFA is just left in landfills, it can cause environmental pollution (Hamada et al. [9]). To solve this problem, a few specialists had endeavoured to reuse POFA sustainably. It was discovered that POFA has pozzolanic properties that makes it suitable as a replacement of cement in concrete. Specifically, it can be used as structure development material. Due to all the problems mentioned above, this research employs POFA and ESP as partial cement replacement (Ansari et al. [15]). Both physical properties and chemical analysis indicated that POFA is a pozzolanic material (Abdullah et al. [14]). As in ASTMC618-92a, POFA is grouped between Class C and Class F. POFA is moderately rich in silica content while its lime content is very low compared to OPC (Awal and Hussin [23]). However, the chemical composition of POFA is depending on the operating system in palm oil mills.

Eggshell is a bio-material with a chemical composition similar to that of limestone (Yerramala et al. [21]). Eggshell is considered an important constituent of pure calcium carbonate source, which exists in the form of the calcite phase. The chemical composition of eggshell matter is as follows: calcium carbonate 94 wt%, organic

compound 4 wt%, calcium phosphate 1 wt% and magnesium carbonate 1 wt% (Ansari et al. [15]; Hamideh and Akbar. [10]). The density of waste eggshell samples is about 2.47 g/cm^3, which is within the range of calcium carbonate materials.

Therefore, the main objectives of this study is to determine the mechanical properties (compressive and tensile strength) of concrete containing POFA and ESP as cement replacement.

1.1 POFA as Cement Replacement

Premalatha et al. [17] used POFA as partial substitute for cement. The percentages of POFA used are 10, 20 and 30%. Both compressive strength and tensile strength of concrete containing POFA and normal concrete were investigated and the results were compared. Figure 1 shows the compressive strength of the samples tested. The notation CC stands for normal concrete whereas PAC stands for concrete with POFA as cement substitute. The results showed that the sample containing 20% of POFA achieved the highest compressive strength. The presence of POFA in concrete reduced the overall density and simultaneously increased the acid resistance of concrete. 20% of cement replacement seems to be the optimum replacement percentage since it leads to the highest concrete compressive strength. In addition, it is even worth mentioning that at 30% of cement replacement, the compressive strength of concrete containing POFA is still higher than that of normal concrete. A similar trend can be found in terms of the tensile strength of POFA concrete as shown in Fig. 2.
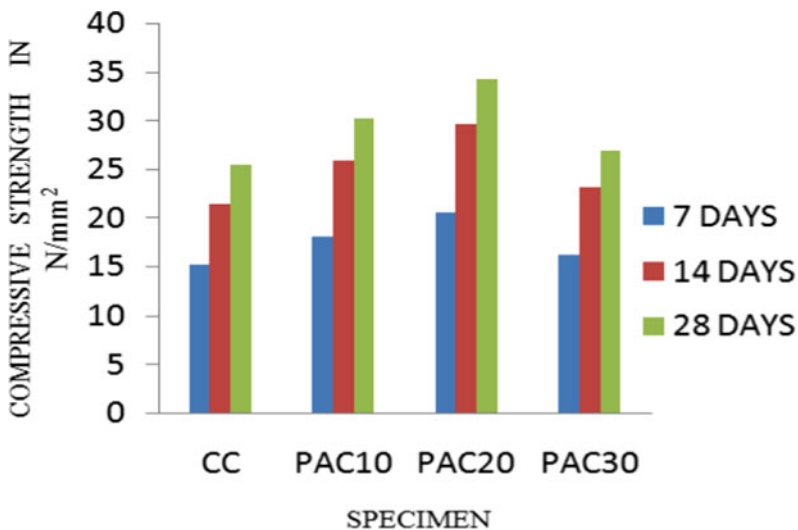

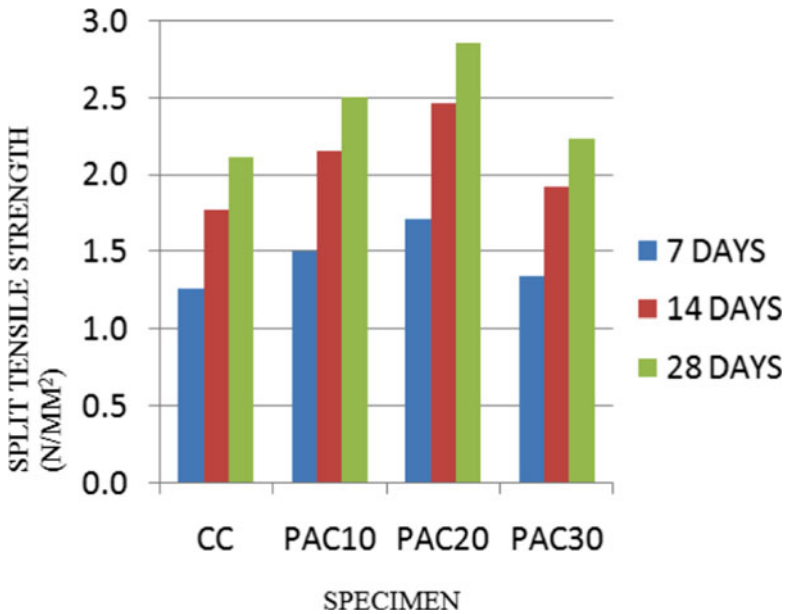Fig. 1 Compressive strength (Premalatha et al. [17])

Fig. 2 Split tensile strength (Premalatha et al. [17])

According to Hamada et al. [9], concrete containing POFA has better compressive strength, durability, flexural strength and split tensile strength. In addition, the use of POFA in concrete helps minimise the emission of CO^2 gas, thus improving environmental conditions. In terms of percentage of replacement, Hamada et al. [9] reviewed that 10 to 20% of POFA as cement replacement proved to be optimum percentages for enhancing the compressive strength of concrete. Other than that, the incorporation of 10 to 20% of POFA as a filler in lightweight foamed concrete has also been observed to improve compressive, flexural and tensile strength compared to lightweight foamed concrete containing sand only.

1.2 ESP as Cement Replacement

Prakash and Satyanarayanan [16] investigated the partial replacement of cement with ESP. ESP is replaced in percentages of 5, 10 and 15% in addition to silica fume in percentages of 2.5, 5 and 7.5% of the weight of cement. The samples were subjected to split tensile strength, compressive strength and flexural strength tests. Figure 3 shows the compressive strength of concrete containing ESP after 28 days of curing. After 28 days, the compressive strength of normal concrete (denoted by the blue bar graph in Fig. 3) is 31 N/mm^2. Meanwhile, concrete with 5% of ESP
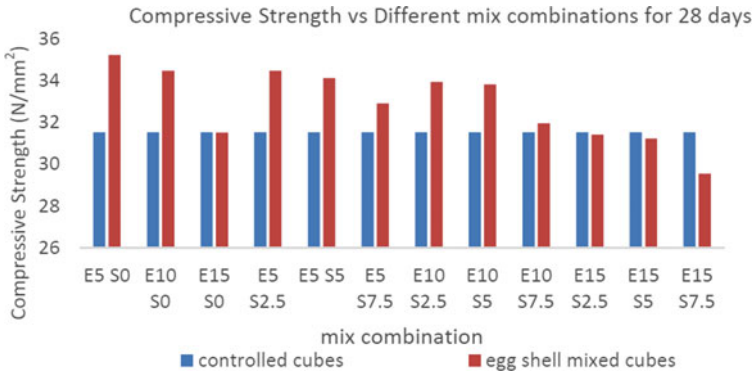
Fig. 3 Compressive strength at 28 days (Prakash and Satyanarayanan [16])
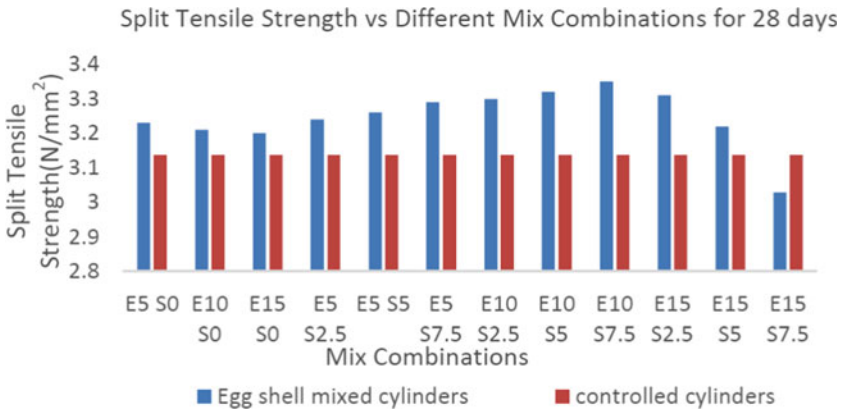

Fig. 4 Split tensile strength at 28 days (Prakash and Satyanarayanan [16])

(without silica fume, E5 S0) gained the maximum compressive strength of 35 N/mm^2 after 28 days. In Fig. 3, it can be clearly seen that the addition of silica fume failed to increase the strength of the concrete specimens. Therefore, it can be concluded that the addition of silica fume had an insignificant effect on the compressive strength of concrete with ESP. In addition, it is worth noting that the strength of the concrete decreases as the percentages of ESP increases. Figure 4 shows the split tensile strength result on day 28. The maximum strength achieved by the specimen containing 10% of ESP and 7.5% of silica fume is 3.3 N/mm^2. From the compressive and tensile strength results, it was found that the optimum percentage of ESP as partial cement replacement lies between 5 to 10%. Beyond this range, the strength of concrete will decrease.

Anand Babu et al. [2] replaced 5 to 25% of cement in concrete with ESP. The results indicated that ESP can successfully be used as a partial replacement of cement in concrete. The result indicated that the optimum ESP percentage is 20%

which achieved a value of 19.5 MPa at 28 days. This result is almost similar to the control sample which achieved a value of 19.7 MPa at 28 days. Similarly, the highest tensile strength was achieved by the sample containing 20% of ESP replacement (5.16 MPa). This value is only slightly lower than the control sample which had a tensile strength of 5.35 MPa.

2 Methodology

2.1 Preparation of Specimens

Table 1 shows the total number of samples used in this study. The notation S1 until S6 refers to variation of percentages of POFA and ESP in the concrete mixes (shown in the first column of Table 1). POFA was collected from Ban Dung Palm Oil Industries Sdn Bhd located in Parit Sulong, Batu Pahat, Johor. POFA was dried in an oven at a temperature of 105 °C for 24 h. Then, POFA was sieved using a 150 μm sieve and retained on a 75 μm sieve. This was intended to remove large particles, reduce carbon content and to avoid crystallisation which may affect the pozzolanic feature. After the sieving process, POFA will be kept in a container to maintain its moisture. Whereas, egg shell were collected from restaurant in Parit Raja, Johor. After the eggshells were collected, they were rinsed and cleaned with water to remove any residue. After that, the eggshells were sun dried for 24 h. After 24 h, the eggshells were ground using a ball mill machine for 2 h and then sieve using a 150 μm sieve.

Table 1 Total number of samples

Main composition (%)	Compression test		Tensile test		Total samples
	Concrete age		Concrete age		
	7	28	7	28	
S1 Normal concrete	3	3	3	3	12
S2 POFA 20% + ESP 0%	3	3	3	3	12
S3 POFA 20% + ESP5%	3	3	3	3	12
S4 POFA 20% + ESP 10%	3	3	3	3	12
S5 POFA 20% + ESP15%	3	3	3	3	12
S6 POFA 20% + ESP20%	3	3	3	3	12
					72

Table 2 Concrete Mix Design

Quantities/ samples	Cement (kg)	Water (kg)	Fine aggregates (kg)	Coarse aggregates (kg)	ESP (kg)	POFA (kg)
Per kg^3	320	160	462	1383	760	420
0.0221 kg^3	7.51	3.54	10.21	30.56	16.80	9.28
S1	7.07	3.54	10.21	30.56	-	-
S2	5.66	3.54	10.21	30.56	-	1.86
S3	5.3	3.54	10.21	30.56	0.8	1.86
S4	5	3.54	10.21	30.56	1.68	1.86
S5	4.5	3.54	10.21	30.56	2.5	1.86
S6	4.2	3.54	10.21	30.56	3.36	1.86
Total	**31.73**	**21.24**	**61.26**	**183.36**	**8.34**	**9.3**

The preparation of concrete cubes was done in accordance with BS EN 12,390-1:2000 while the preparation of concrete cylinders was done in accordance with BS EN 12,390-1:2000. The cubes and cylinders were placed in a closed container in the laboratory. The samples then underwent a water curing process for 7 and 28 days. The mixes were designed using the Department of Environment's Design Method (DOE) as shown in Table 2. The targeted design strength is 25 MPa. In this study, the percentage of POFA used was fixed at 20% based on suggestions by previous researchers. However, the percentage of ESP used varied between 5 to 20% with 5% increment of ESP for every mixes.

2.2 Experimental Test

In this study, the samples were tested in terms of workability (slump test) and strength (compressive test and tensile test). The slump test was done in accordance to BS EN 12,350-2:2009. The aim of conducting the slump test is to obtain the true slump which ranges between 30 to 60 mm. The compressive strength of concrete was tested using concrete cubes measuring $100 \times 100 \times 100$ mm. The concrete mix was poured into moulds. After 24 h, the hardened samples were removed from the moulds and the curing process was carried out. 30 samples were prepared and tested on day 7 and day 28. The test was performed using a universal testing machine (UTM) shown in Fig. 5. The tensile test was conducted on cylinder samples measuring 100 mm in diameter with a height of 200 mm until failure occurred. The tensile force was applied to the samples indirectly so that they split into two. In this study, the determination of tensile strength test was done in accordance with BS EN 12,390-6:2009.
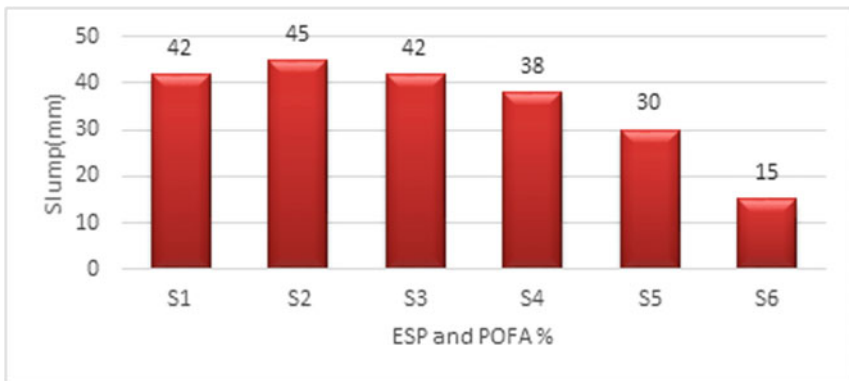
Fig. 5 Universal testing machine

Fig. 6 The relationship between concrete slump and ESP and POFA replacement

3 Results and Discussion

3.1 Workability of Concrete

All the measured slumps in this test were true slumps. Considering the design of the concrete mix, the targeted slump lies between 30 and 60 mm. Figure 6 shows the slumps of all samples. The slump value slightly increased when POFA was added (S2). However, the slump value decreased as the percentages of ESP increased (S3, S4, S5 and S6). This is related to the calcium carbonate that presence in ESP. According to Jaber et al. [12], Calcium Carbonate can affect the cement hydration process both chemically and physically. In addition, Calcium Carbonate accelerated the formation of calcium silicate hydrate or also known as C-S-H gel. This accelerated formation can reduce the pore in concrete hence decreased the water absorption capabilities of the concrete. Thus resulting in low value of slump.

3.2 Compressive Strength

Figure 7 shows the compressive strength of concrete samples containing different percentages of ESP and POFA as cement replacement for 7 and 28 days. It was observed that compressive strength increases with increasing curing age. This is a good indication of the development of strength as a result of cement hydration. The maximum compressive strength at 28 days obtained was 18.9 MPa (S2) by the concrete sample with only 20% of POFA and 0% of ESP as cement replacement. Several researchers have examined the use of POFA as cement replacement (Hamada et al. [9]; Premalatha et al. [17]) and concluded that 10 to 20% of POFA as cement replacement enhanced the compressive strength of concrete. This is because POFA is a pozzolanic material that possesses the same physical and chemical properties as OPC (Abdullah et al. [14]). Hence, it is expected that the use of POFA as cement replacement alone can potentially enhance the compressive strength of concrete. However, the strength gained after 28 days was still far from the control samples (S1). According to Alyousef et al. [4], it is known that longer curing periods enhance the strength of POFA concrete due to the pozzolanic behaviour of POFA, in addition to the formation of additional calcium silicate hydrate gel during the hydration process. Therefore, it is suggested (for future research) that the curing period of the samples are increased to 56 and 90 days.

The maximum strength achieved by concrete samples containing both POFA and ESP as cement replacement at 28 days was 17.9 MPa (S4) which is just slightly lower than the value obtained for S2. The chemical composition of ESP mainly consists of calcium carbonate which is also the main component in OPC (Ansari et al. [15]). Another chemical composition that exists in eggshell is Calcium Oxide
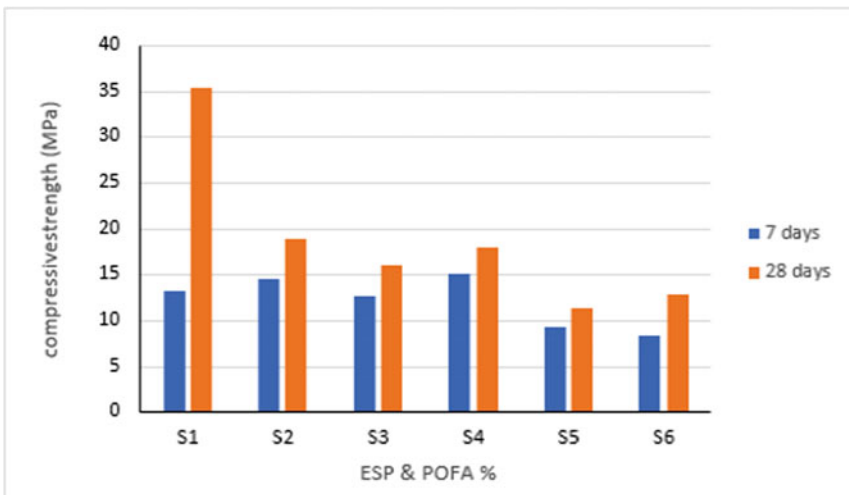

Fig. 7 Compressive strength of tested samples

(CaO). According to Ansari et al. [15], CaO is known to delay the setting time of concrete. Hence, if the test is done after 28 days, the compressive strength of S4 might be similar to S2.

3.3   Tensile Strength

Figure 8 shows the tensile strength of the concrete samples containing different percentages of ESP and POFA as cement replacement for 7 and 28 days. It was observed that the tensile strength increases with increasing age. This was a good indication of the development of strength as a result of cement hydration. The highest tensile strength obtained after 28 days was 1.53 MPa (S4). The second highest tensile strength was achieved by S2, which is concrete with only 20% of POFA as cement replacement. Generally, the results obtained were in agreement with the results of the compression test. It can be concluded that 20% of POFA and 10% of ESP as cement replacement are the optimum percentages for cement replacement in concrete. However, the strength achieved was only 76% of targeted strength.
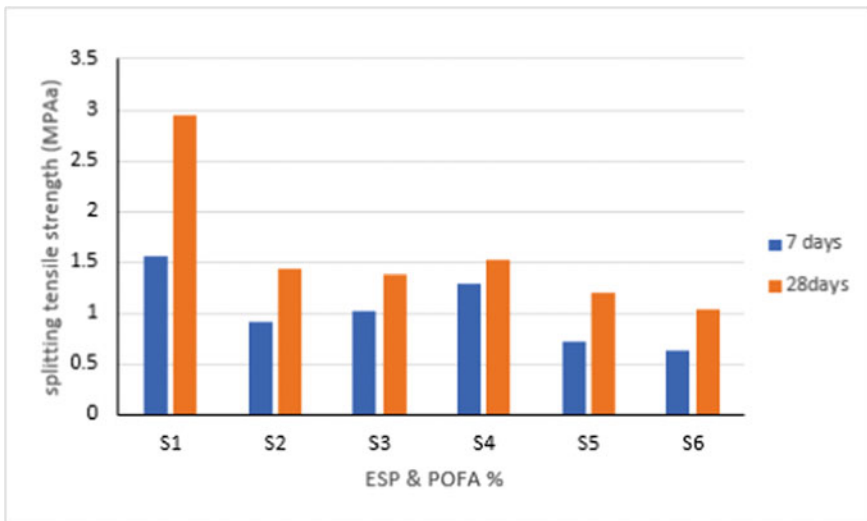

Fig. 8 Tensile strength of tested samples

4   Conclusion

Based on the results of the slump test, compressive test and tensile strength test, the following conclusions can be drawn;

I. The workability of the concrete with POFA and ESP decreased as the percentages of ESP increased. This is due to the presence of calcium carbonate in ESP.

II. Since the compressive strength of the optimum percentages is only 76% of targeted strength, it is suggested that the curing ages increased to 56 and 90 days. Prolonging the curing stages help with hydration process of the silicate.

References

1. Ash A (2018) Palm oil fuel ash as a cement replacement in concrete. Mod Approaches Mater Sci 1(1):4–8
2. Anand Babu A, Ramprasant AA, Shanmugavadivu VA (2017) Experimental investigation on partial replacement of eggshell powder in conventional concrete. Int J ChemTech Res 10 (8):453–457
3. Ahmadi R, Saiful MS, Zawawi DF, Rahaman SZA, Ismail I, Mannan MA, Nazri FM (2018) Evaluation of microfine palm oil fuel ash (POFA) as cement partial replacement material for mitigation of chloride attack. Int J Eng Technol 7(318):58
4. Alyousef R, Mohammadhosseini H, Tahir MM, Alabduljabbar H (2020) Green concrete composite production comprising metalized plastic waste fibers and palm oil fuel ash. Mater Today Proc 39:911–916
5. BS EN 12390-3 (2002) Testing Hardened Concrete—Part 3, Compressive Strength of Test Specimens
6. BS EN 12390-6 (2009) British Standard Institution Testing Hardened Concrete. Tensile Splitting Strength of Test Specimens
7. BS EN 12390-1 (2000) British Standard for Testing Hardened Concrete – Part 1: Shape, Dimensions and other Requirements for Specimens and Moulds. BSI, London
8. BS EN 12350-2 (2009) British Standard for Testing Fresh Concrete. Slump Test
9. Hamada HM, Jokhio GA, Yahaya FM, Humada AM, Gul Y (2018) The present state of the use of palm oil fuel ash (POFA) in concrete. Constr Build Mater 175:26–40
10. Hamideh F, Akbar A (2018) Application of eggshell wastes as valuable and utilizable products: a review. Res Agric Eng 64(2):104–114
11. Hamada HM, Al-Attar AAA, Yahaya FM, Muthusamy K, Tayeh BA, Humada AM (2020) Effect of high-volume ultrafine palm oil fuel ash on the engineering and transport properties of concrete. Case Stud Constr Mater 12:e00318
12. Jaber HA, Mahdi RS, Hassan AK (2020) Influence of eggshell powder on the Portland cement mortar properties. Mater Today Proc 20:391–296

13. Megat Johari MA, Zeyad AM, Muhamad Bunnori N, Ariffin KS (2012) Engineering and transport properties of high-strength green concrete containing high volume of ultrafine palm oil fuel ash. Constr Build Mater 30:281–288

14. Abdullah, K., Hussin, M.W., Zakaria, F., Muhamad, R., Hamid, Z. (2006) A potential partial cement replacement material in aerated concrete. In: 6th Asia Pacific Structural Engineering and Construction, APSEC 2006, 5–6 September

15. Mohamed Ansari M, Dinesh Kumar M, Milan Charles J, Vani G (2016) Replacement of cement using eggshell powder. SSRG Int J Civ Eng (SSRG-IJCE) 3(3):1–2

16. Prakash M, Satyanarayanan KS (2017) Experimental study on partial replacement of cement with eggshell powder and silica fume. Rasayan J Chem 10(2):442–449

17. Premalatha P, Vinodh K, Anto L, Nithiya R, (2016) Properties of palm ash concrete. Int. J Eng Sci Invention 5(8)

18. Tambichik MA, Mohamad N, Samad AAA, Bosro MZM, Iman MA (2018) Utilization of construction and agricultural waste in Malaysia for development of green concrete: a review. IOP Conf Ser Earth Environ Sci 140:012134

19. Tasnim S, Rahman ME, Ahmadi RB (2018) Mechanical performance of modified cement paste made with micro-fine POFA in ammonium nitrate environment. Constr Build Mater 162:534–542

20. Tangchirapat W, Jaturapitakkul C, Chindaprasirt P (2009) Use of palm oil fuel ash as a supplementary cementitious material for producing high-strength concrete. Constr Build Mater 23(7):2641–2646

21. Yerramala A (2014) Properties of concrete with eggshell powder as cement replacement. Indian Concr J 88(10):94–102

22. Raji SA, Samuel AT (2015) Egg shell as a fine aggregate in concrete for sustainable construction. Int J Sci Technol Res 9:8–13

23. Awal ASMA, Hussin MW (1997) Palm oil fuel ash - a potential pozzolanic material in concrete construction. J Ferrocem 27:321–327